Multi-Sensor Systems for VOC: Recalibration and Coating Procedures

Multisensorsysteme für VOC: Rekalibrierung und Beschichtungstechniken

DISSERTATION

der Fakultät für Chemie und Pharmazie
der Eberhard-Karls-Universität Tübingen

zur Erlangung des Grades eines Doktors
der Naturwissenschaften

2001

vorgelegt von
MICHAEL FRANK

Tag der mündlichen Prüfung: 02. Mai 2001

Dekan: Prof. Dr. H. Probst

1. Berichterstatter: Prof. Dr. C. Ziegler

2. Berichterstatter: Prof. Dr. H. Baltes

Voll Ernst das Spiel und heiter alle Arbeit.

Friedrich Hölderlin

Meinen Eltern

CONTENTS

ABSTRACT

Although in industry a very large number of potential applications of "electronic noses" exists, these systems could not meet one's expectations in many cases. One of the reasons can certainly be attributed to the fact that for a long time their use was focussed on case studies, real-life applications have been rarely considered. It would be of course enjoyable to distinguish between apples and pears with the help of gas sensors, but this is far away from the actual problems related to industrial processes.

A crucial prerequisite for the successful use of sensor systems is the long-term stability of the sensors. Since drift or response fluctuations are unavoidable, appropriate strategies for re-calibration have to be applied. In order to be able to use data banks which are based on preliminary calibrations these two aforementioned criteria have to be fulfilled. The procedures carried out for re-calibration must be adapted to the corresponding application which is especially important for quantitative predictions.

The first part of this work deals with samples originating from the food industry. In one case the ageing process of corn oil was monitored with gas sensor systems and subsequently the age / quality of independent test samples was determined. In parallel, GC/MS measurements were carried out to identify the volatile compounds being relevant for the oil's flavour.

It could be demonstrated that even for rather short time periods in the range of a few months re-calibrations were already essential. In addition, the composition of the standards used for re-calibration had to be adjusted to the varying constitution of the samples measured. Therefore, the monitoring of dynamic processes requires the appliance of different standards.

The second kind of investigation related to foodstuff comprised the correlation between human sensory evaluations and corresponding data derived from gas sensor systems. Again, GC/MS served as a complementary method for the interpretation of the sensor data.

Within extensive studies sensor systems at different locations were trained for the recognition of packaging materials. The materials were based on plastics and cardboard. These calibrations showed that human and technical odour (intensity) measurements can be correlated successfully.

In comparison with human assessments, the electronic counterpart turned out to have an equal performance. Even months later, within the testing phase, the prediction ability of the sensor system was still very convincing. This achievement is certainly a consequence of the re-calibration used, being adapted to the packaging material problem.

Furthermore, mathematical algorithms for the analysis of time series were applied to sensor data obtained over a period of up to one year in order to search for the reasons of the response fluctuations. Besides the intrinsic changes of a sensor (e.g. ageing of the sensitive layer), faulty sample preparation and improper sampling played an important role. The latter was the dominating effect causing the response fluctuations of the quartz crystal microbalances. In the cases of the metal oxide sensors intrinsic and extrinsic changes had almost the same impact. The most efficient methods to describe and to detect such phenomena are cross-correlations.

Based on the experiences which have been obtained with well established, commercially available sensor systems, the second part of this work reports on the development of a miniaturised, portable gas sensor device. The main task was the coating of already bonded and housed CMOS-microsensors with polymers. The major requirement consisted in the achievement of homogeneous films with reproducible layer heights.

Two coating techniques are presented here, which differ fundamentally from all current procedures. One of them uses CNC machined tools in the µm-range which enable the transportation of smallest amounts of polymers. This method convinces by its high lateral precision, the excellent reproducibility of the layers and the possibility for automation.

The second technique uses glass micropipettes through which small polymer droplets can be deposited on several sensor structures.

In total 16 polymers were investigated to check their wetting abilities towards silicon substrates. Additional gas tests provided partition coefficients of the corresponding chemically sensitive materials.

ZUSAMMENFASSUNG

Obwohl es eine sehr große Zahl an industriellen Anwendungen gibt, in denen sogenannte „Elektronische Nasen" eingesetzt werden könnten, ist deren Leistungsfähigkeit den oftmals hochgesteckten Erwartungen nicht gerecht geworden. Die Gründe hierfür sind vielschichtig, wobei eines der Hauptprobleme sicherlich darin besteht, daß trotz beinahe unzähliger Fallstudien wenig an sogenannten „Real-life"-Anwendungen gearbeitet wurde. Äpfel von Birnen unterscheiden zu können, mag erfreuen, von den Aufgabenstellungen mit industrieller Relevanz ist man damit jedoch weit entfernt.

Eine der Grundvoraussetzungen für den erfolgreichen Einsatz von Sensorsystemen, ist die Langzeitstabilität der Sensoren bzw. die Möglichkeit, zeitlich veränderliche Sensorantworten durch geeignete Rekalibrierungsverfahren zu kompensieren. Beide Punkte haben zum Ziel, anfangs durchgeführte Kalibrationen der Systeme und die darauf basierenden Datenbanken über längere Zeiträume (Monate, Jahre) sinnvoll nutzen zu können. Da vor allem quantitative Aussagen über die untersuchten Proben von großem Interesse sind, müssen die Verfahren zur Rekalibrierung den entsprechenden Anwendungsgebieten angepaßt werden.

Der erste Teil dieser Arbeit ist Untersuchungen an Proben aus der Lebensmittelindustrie gewidmet. Hierbei ging es zunächst darum, den Alterungsprozeß von Maiskeimöl mit einem Gassensorsystem zu verfolgen und daraufhin das Alter bzw. die Qualität von unabhängigen Testproben bestimmen zu können. Als analytisch-chemisches Verfahren wurden parallel dazu GC/MS-Messungen zur Identifizierung der flüchtigen, qualitätsbeeinflussenden Bestandteile durchgeführt. Es konnte gezeigt werden, daß auch für relativ kurze Zeiträume von wenigen Monaten Rekalibrierungen unerläßlich sind. Darüber hinaus müssen die zur Rekalibration eingesetzten Standards den sich ändernden Zusammensetzungen des Dampfraumes der Proben angepaßt werden. Dies bedeutet, daß zur Überwachung eines dynamischen Prozesses, unterschiedliche Standards zum Einsatz kommen müssen.

Das zweite Einsatzgebiet im Rahmen der Lebensmittelindustrie beschäftigte sich mit der Korrelation von humansensorischen Geruchsbeurteilungen und den entsprechenden Meßergebnissen eines Sensorsystems. Auch in diesem Fall diente die GC/MS als komplementäre Methode zur Interpretation der Sensordaten.

In umfangreichen Studien wurden an verschiedenen Standorten Sensorsysteme auf die Erkennung von Verpackungsmaterialien trainiert, die sowohl aus Kunststoffen, als auch aus Papier bestanden. Anhand dieser Kalibrationsmessungen konnte demonstriert werden, daß es möglich ist,

menschliche und technische Geruchsmessungen in quantitativer Form miteinander zu kombinieren.

In unabhängigen Testmessungen, die Monate nach der Trainingsphase durchgeführt wurden, war die Vorhersagegenauigkeit des Sensorsystems so gut wie diejenige der menschlichen Beurteilungen. Eine entscheidende Voraussetzung hierfür lag in der angewandten Rekalibration, die nun auf Verpackungsmaterialien abgestimmt war.

Aus den vorliegenden Sensordaten, die sich auf Zeiträume von bis zu einem Jahr erstreckten, wurde mit Hilfe von mathematischen Algorithmen zur Analyse von Zeitreihen nach den Gründen für das sich zeitlich verändernde Sensorverhalten gesucht. Es stellte sich dabei heraus, daß neben dem „Eigenleben" der Sensoren, auch –zum Teil unvermeidbare- Fehler verursacht durch die Probenvorbereitung und die Probenahme zu Fluktuationen der Sensorantworten geführt haben. Vor allem bei polymerbeschichteten Schwingquarzsensoren hatten diese Fehler einen Hauptanteil. Bedingt durch den anderen Betriebsmodus der Metalloxidsensoren hielten sich hier der Einfluß durch Probenahmefehler und Veränderungen des Sensors (z.B. seiner sensitiven Schicht) die Waage. Zur Beschreibung solcher Phänomene erwiesen sich vor allem Kreuzkorrelationen als effiziente Methoden.

Basierend auf den Erfahrungen, die durch die Anwendung etablierter, kommerziell erhältlicher Sensorsysteme gewonnen werden konnten, zielte der zweite Teil dieser Arbeit auf die Entwicklung eines miniaturisierten, portablen Gassensorsystems. Im speziellen ging es um die Frage, in wieweit mikrostrukturierte CMOS-Sensoren, die bereits „gebondet" und gehäust sind, mit unterschiedlichsten Polymeren beschichtet werden können. Zentrale Anforderungen an diese Schichten waren Homogenität und kontrollierte Schichtdicke.

Die beiden im Rahmen dieser Arbeit vorgestellten Beschichtungsmethoden unterscheiden sich fundamental von allen gängigen Verfahren. Ein Ansatz beruht darauf, durch CNC-gefertigte Mikrowerkzeuge kleinste Mengen an Polymeren zu transportieren. Diese Methode ist durch ihre hohe laterale Ortsgenauigkeit, die große Reproduzierbarkeit der erhaltenen Schichten, sowie die Automatisierbarkeit charakterisiert. Das zweite Verfahren bedient sich Glasmikropipetten, mit deren Hilfe kleinste Polymertropfen auf verschiedene Strukturen appliziert werden können.

Insgesamt wurden sechzehn Polymere auf ihre Benetzungseigenschaften gegenüber Silizium untersucht. Parallel durchgeführte Gasmessungen zur Bestimmung der Verteilungskoeffizienten lieferten weitere Ergebnisse zur Selektion sensitiver Schichten.

1 INTRODUCTION

Over the years, the challenge to mimic human senses by technical solutions has in some cases been very successful. Cameras and microphones are well known in replacing the senses of sight and sound. Robots are able to grope for objects lying in front of them. However, still the senses of taste and smell, being somehow related (e.g. retro-nasal smelling), are rather poorly understood [*Lai 91*]. For a long time olfactory research was motivated by the following questions [*Ros 96*]:

- How do we recognise and discriminate between thousands of odours?
- Which molecular properties determine the smell of a compound?
- Why, in some cases, do compounds which are completely different in structure have similar odours (and conversely)?

These questions give evidence of the complexity of natural scent and they show how ambitious it is to imitate this sense by technical approaches. Although the basic "architecture" of the olfactory system in mammals and its technical counterpart reveals similarities [*Goe 98, Pea 97ᵃ, Pea 97ᵇ*], there still exist many differences (e.g. odour thresholds vs. limits of detection). Therefore, the established term "Electronic Nose" (EN) is for several reasons misleading, because it implies that such systems are generally applicable and that their performance is comparable with the sensing system in mammals. Even though there is increasing interest in their use as tools for the qualitative and quantitative analysis of volatile compounds produced from materials [*Kal 00, Apa 00, Gua 00ᵃ*], the philosophy behind ENs is not to replace well established techniques such as sensory panels or gas chromatography / mass spectrometry (GC/MS). Neither are they able to describe an odour by certain attributes (e.g. fruity, green, rancid etc), nor can they give the composition of the evaluated odour. Instead, gas sensor arrays have to be recognised as complementary tools for particular practical applications which allow rapid screening and which are normally easy to handle. The transducers and their sensitive layers can be selected according to the application. In all cases, an accurate optimisation of the measurement conditions (sample up-take, temperature and humidity control, working conditions of the sensors) as well as an extensive calibration phase for the collection of training data are crucial points. In addition, an appropriate re-calibration procedure has to be developed to assure the comparability of temporally different data since sensor long-term drifts or fluctuations are still an unavoidable problem if using sensor systems over a longer period [*Hau 00*]. For all these reasons the term "Application-Specific Sensor System" (ASSS) should replace the notion of an "Electronic Nose" [*Hie 00*].

Having these considerations in mind, the present work focuses on the use of gas sensor arrays as a tool for quality control in selected fields of the food industry. Together with industrial partners, the performance of such a system was extensively tested in order to assess the spoilage state of corn oil and to predict the quality of packaging materials on the basis of their volatile organic compounds (VOCs). In both cases GC/MS measurements were carried out in parallel. In addition, a comparison of sensory evaluations with gas sensor data was performed on the packing materials.

The second part presents the very recent development of a hand-held device which is the result of a common project with the ETH Zurich (Prof. H. Baltes Group), the University of Bologna (Prof. M. Rudan Group) and the University of Tübingen (Prof. W. Göpel and Dr. U. Weimar Group). The work proposal was awarded in 1998 by the Körber European Science Award. In particular, new coating techniques for micro-structured CMOS-sensors and the characterisation of these layers by scanning electron microscopy as well as by a surface profilometer were to be reported.

1.1 Vegetable Oil

The first applications of gas sensor systems used for the examination of foodstuffs date back to the early 1990s [*Ais 91*, *Ste 93*, *Win 93*]. The monitoring of the reduction in quality of vegetable oils caused by degradation products (mainly originating from unsaturated fatty acids) was a main topic already from the very beginning. Most of the publications describe the ability of sensor arrays to differentiate between varieties or brands of oil [e.g. *Gon 99*, *Gua 00*[b]]. These investigations are useful case studies showing that gas sensors have the potential to trace certain differences in the samples' headspaces, but very often a clear correlation between the VOCs present in the headspace and the oil's quality is missing. Moreover, the discrimination of different brands only has a very low industrial interest and thus, systems which are able to monitor the quality of a particular product on a long-term basis are in great demand. The latter requires stable sensors or -since temporal response changes are usually unavoidable-appropriate re-calibration methods to compensate for these changes.

Based on this knowledge, the selection of a re-calibration standard became a crucial point. To find the best strategy, the following considerations had to be taken into account. Firstly, the headspace composition of the re-calibration sample should be very similar to that of the samples to be investigated. The reason for this prerequisite originates from the concentration dependency of the sensor responses. Assuming a linear behaviour as is generally the case for QCMs

[*Gra 00*], a "wrong" headspace concentration can be treated mathematically by linearisation of the obtained sensor value. Looking at MOXs whose responses in general follow a power law [*Bâr 99*], deviations become much more difficult to handle. As a consequence not only the compounds but also their concentrations should be almost the same. The qualitative and quantitative determination of the headspace includes GC/MS investigations. Without this information, the search for convenient re-calibration samples is random. However, even if the question about the headspace composition is answered, there still persists the problem of artificially producing a standard with the needed requirements. Since the headspace of the re-calibration sample should be a "mirror image", the nature of its matrix[1] is less important, unless of course calibration samples for quantification purposes in headspace gas chromatography are being used. Then, matrix effects play an important role [*Kol 97*]. Very suitable are liquid matrices consisting of molecules with high molecular masses, e.g. polyethylene glycol (PEG) or paraffin oil. Liquid matrices can be easily handled with pipettes and the homogenous dilution of chemical substances chosen for the imitation of the "real" headspace is guaranteed.

Secondly, the spoilage of vegetable oil is a dynamic process, i.e. the composition of the headspace changes constantly. Depending on the experimental conditions, the artificially speeded up spoilage can be in the range of a few months (under "household" conditions the shelf life is at least one year). Therefore, the re-calibration sample has to be adapted according to the actual stage within the degradation cycle. For the spoilage of corn oil, two different re-calibration samples were selected: a.) unspoiled, fresh corn oil kept in a freezer at –20° C and b.) a dilution of 100 ppm pentanal in fresh corn oil. Indeed, fresh corn oil has almost no compounds in the headspace. The oil is odourless because before filling all volatile compounds are removed under vacuum. Hence, corn oil unlike olive oil, has no characteristic odour[2]. In addition, its use as an indifferent matrix is rather simple, since the preparation of artificial re-calibration samples can be carried out with high reproducibility; all preparative steps can be carried out with pipette systems. According to the literature [*Ull 87*], pentanal and the other analogous linear aldehydes appear in the degradation process of unsaturated fatty acids, although hexanal is normally the dominating compound. From the chemical point of view (e.g. concerning reactivity, functional groups), there is hardly any difference between pentanal and hexanal; except the molecular weight. That is

---

[1] Definiton of matrix [*Kol 97*]: The matrix is the bulk of the sample that contains the volatile compounds to be measured.

[2] The compounds being relevant for the odour of olive oil are described in e.g. [*Gut 91, Ang 97, Ang 98, Mor 95*].

why both substances have nearly the same impact on a set of sensors if they are applied with an identical concentration. In other words, a particular concentration of pentanal leads to a response pattern which is the same for the hexanal.

1.2 Packaging Materials

The quality of packaging material, especially with respect to out-gassing organic compounds has a great effect on the food quality itself. Packaging is implicated in more than 50% of consumer complaints dealing with off-flavours. The most important problems encountered in practice may be divided into three categories:

- Migration of odorous substances from package to food and package headspace
- Inadequate protection of food from environmental influences
- Reaction of packaging substances with food components

In order to guarantee a standard of raw materials as well as final products these factors become increasingly important. Often, the products do not only get spoiled due to natural ageing but also due to faulty packaging. Therefore, a fast, cheap and reliable method is needed to control the wrapping material before it gets into contact with foodstuff. The potential sources of off-odours are various; they depend largely on the manufacturing process of the foils, the composition of the printing colours and adhesives. For this reason, "classical" organic solvents like cyclohexane, toluene, propan-2-ol (isopropanol) and ethyl acetate are common as well as aldehydic compounds, e.g. hexanal, which derive from the printing inks at higher temperatures during processing.

Since many different types of contamination are possible in food, specific and accurate descriptors are needed for characterising the problem with precision at an early stage in the production.

The procedure to control the sensory quality of food packaging materials is based on two tests:

- Olfactory check: this check is applied to detect any odour (solvent, ink, monomer, slip agents or other additives) released by flexible packaging materials (paper, plastics).
- "Robinson" taint transfer test: this test is applied to paper and cardboard materials with offset/lithography printing, excluding any other type of support or print.

The critical level of substances likely to affect the quality of products must be in agreement with the recommended composition limits in packaging materials and

with the specific migration limits in food. A listing of the specifications of the most common odorous substances is displayed in chapter 2.1.2.1 *Printing Inks and Adhesives*.

One main interest in the use of gas sensor arrays is their possible employment as easy to handle on-line instrumentation. Nowadays, the arrays are mainly used in quality assurance laboratories as complementary tools to GC/MS [*Hus 97*, *Mis 97*, *Wam 97*], Near Infrared Spectroscopy (NIR) [*Kaw 95*] and human sensory panels [*Fli 93*]. Compared with these "classical" odour evaluation techniques, sensor systems have certain drawbacks like sensitivity (at least for some analytes) or the missing "taint description". Therefore, their future use is seen in fast on-line checks indicating problems during the packaging process, i.e. ASSS should be able to monitor deviations of a particular product and its reference standard. This would offer a way from spot checks to real process control if sensor systems are also used as actuators (at this stage an identification of the compounds responsible for the quality changes is of secondary importance). Until today, these spot checks are performed by the reference methods mentioned above, whereas human sensory panels still have a unique advantage; they can describe an (off-) odour. For this reason, it would be very profitable if an odour intensity attributed by panels and represented by a numerical value could be correlated with the output of sensor arrays evaluating the same sample.

Often, within the production of packaging materials the quality variations are rather low, i.e. samples with extremely bad and unacceptable quality are rare. As a consequence, chemical sensors should be able to discriminate between small fluctuations around a "quality mean value". Related to this requirement, a successful re-calibration of whole sensor arrays becomes even more important, and in order to monitor small changes also more demanding.

1.3 Miniaturised Gas Sensor System

The miniaturisation of gas sensors came along with the increasing importance of microelectronics and their fabrication techniques (e.g. CMOS fabrication and subsequent micromachining). Besides the steadily improving sensitivity of a microsensor, their small size opens up a completely new area of sensor systems; portable, hand-held devices. Naturally, such systems focus on different applications like common, already existing apparatus' (a listing can be found under [*Nos 01*]) which have to be considered as laboratory tools.

Portable systems as they are available today, are (or will be) used in field surveys for such purposes as leakage detection, in the control of industrial emissions (e.g. exhaust or fume gases) and in the monitoring of the release of agricultural biogases.

However, the concept of hand-held devices involves particular precautions to ensure a reliable usage:

- Stable temperature and humidity control
- Provision of reference gas (for practical reasons the use of synthetic air is excluded)
- Standardised sample up-take
- Low power consumption

The approach chosen by the consortium from Zurich, Bologna and Tübingen is based on an established CMOS-microsensor production [*Hie 00, Kol 00, Lan 01*]. Thus, the integration of several transducers[3] with individual signal conditioning and processing circuitry on a single chip can be realised. For the hand-held system, three transducer types are located on one single chip: a cantilever, a thermopile and an interdigital capacitive structure. The whole system will consist of nine chips each of them having a chemically different layer on the sensing areas.

The miniaturisation of sensors entails among other things the search for new coating techniques for the deposition of sensitive layers on considerably small areas. Taking in particular the specification that the sensors will be coated at a very late stage of the whole fabrication process into account, simple, universal and accurate methods were tested. Moreover, these techniques had to result in very smooth and thick layers (5-10 µm). In total, 16 different sensitive layers were screened, their ability to form a closed and homogeneous film being the most relevant requirement.

---

[3] The advantageous, simultaneous use of different transducers (so-called hybrid systems) is discussed in [*Mit 98, Hie 00*].

Most of the preliminary tests were performed utilising silicon wafers with a thin, native SiO_2 layer, before using already bonded and working sensors. Their performance in the detection of VOCs was characterised by exposing them to ten different organic solvents. The influence of the polymer placements on other substrates was also examined.

1.4 References

[*Ais 91*]: T. Aishima, Discrimination of liqueur aromas by pattern recognition analysis of responses from semiconductor gas sensor array, J. Agric. Food Chem. 39 (1991) 752-756.

[*Ang 97*]: F. Angerosa, L. Di Giacinto, N. d'Alessandro, Quantification of some flavour components responsible for the "green" attributes in virgin olive oils, J. High Resol. Chromatogr. 20 (1997) 507-510.

[*Ang 98*]: F. Angerosa, L. Camera, N. d'Alessandro, G. Mellerio, Characterisation of seven new hydrocarbon compounds present in the aroma of virgin olive oils, J. Agric. Food Chem. 2 (1998) 648-653.

[*Apa 00*]: R. Aparicio, S.M. Rocha, I. Delgadillo, M.T. Morales, Detection of rancid defect in virgin olive oil by the electronic nose, J. Agric. Food Chem 48 (2000) 853-860.

[*Bâr 99*]: N. Bârsan, J.R. Stetter, M. Findlay Jr., W. Göpel, High-performance gas sensing of CO: comparative tests for semiconducting SnO_2-based and for amperometric gas sensors, Anal. Chem. 71 (1999) 2512-2517.

[*Fli 93*]: I. Fliedner, F. Wilhelmi, Grundlagen und Prüfverfahren der Lebens-mittelsensorik, B. Behr's Verlag GmbH & Co, Hamburg, 1993.

[*Fra 98*]: M. Frank, Vergleichende Messungen an Lebensmittelproben mit Verfahren der Analytischen Chemie und der Gassensorik, Diploma Thesis, University of Tübingen, 1998.

[*Goe 98*]: W. Göpel, Chemical imaging: I: Concepts and visions for electronic and bioelectronic noses, Sens. Actuators B 52 (1998) 125-142.

[*Gon 99*]: Y. Gonzáles, J.L. Pérez, B. Moreno, C. Garća, Classification of vegetable oils by linear discriminant analysis of electronic nose data, Anal. Chim. Acta 384 (1999) 83-94.

[*Gra 00*]: J.W. Grate, Acoustic wave microsensor arrays for vapour sensing, Chem. Rev. 100 (2000) 2627-2648.

[*Gua 00[a]*]: A. Guadarrama, J.A. Fernández, M.Í ñiguez, J. Souto, J.A. de Saja, Array of conducting polymer sensors for the characterisation of wines, Anal. Chim. Acta 411 (2000) 193-200.

[*Gua 00[b]*]: A. Guadarrama, M.L. Rodŕiguez-Méndez, J.A. de Saja, J.L. Ríos, J.M. Oĺas, Array of sensors based on conducting polymers for the quality control of aroma of the virgin olive oil, Sensors and Actuators B 69 (2000) 276-282.

[*Gut 91*]: H. Guth, W. Grosch, A comparative study of the potent odorants of different virgin olive oils, Fat. Sci. Technol. 93 (1991) 335-339.

[*Hau 00*]: J.E. Haugen, O. Tomic, K. Kvaal, A calibration method for handling the temporal drift of solid state gas-sensors, Anal. Chim. Acta 407 (2000) 23-39.

[*Hie 00*]: A. Hierlemann, D. Lange, C. Hagleitner, N. Kerness, A Koll, O. Brand, H. Baltes, Application-specific sensor systems based on CMOS chemical microsensors, Sens. Actuators B 70 (2000) 2-11.

[*Hus 97*]: C.K. Huston, Ion trap mass spectrometry for food aroma analysis, in: Techniques for analysing food aroma, R. Marsili (Ed.), Marcel Dekker, Inc., New York, 1997, pp. 209-235.

[*Kal 00*]: E.-L. Kalmann, A. Löfvendahl, F. Winquist, I. Lundström, Classification of complex gas mixtures from automotive leather using an electronic nose, Anal. Chim. Acta 403 (2000) 31-38.

[*Kaw 95*]: S. Kawano, Progress in application of NIR and FT-IR in food characterisation, in: Characterisation of food – emerging methods, A.G. Gaonkar (Ed.), Elsevier, Amsterdam, 1995, pp. 185-199.

[*Kol 97*]: B. Kolb, L.S. Ettre, Static headspace gas chromatography – theory and practice, Wiley-VCH, New York, 1997.

[*Kol 00*]: A. Koll, CMOS capacitive chemical micorsystems for volatile organic compounds, Ph.D. thesis No. 13460, ETH Zurich, Zurich, 2000.

[*Lai 91*]: D.G. Laing, R.L. Doty, W. Breipohl (Eds.), The human sense of smell, Springer-Verlag, Berlin, 1991.

[*Lan 01*]: D. Lange, Ph.D. thesis in compilation, ETH Zurich, Zurich, 2001.

[*Mis 97*]: B.S. Mistry, T. Reineccius, L.K. Olson, Gas chromatography – olfactometry for the detection of key odorants in foods, in: Techniques for analysing food aroma, R. Marsili (Ed.), Marcel Dekker, Inc., New York, 1997, pp. 265-292.

[*Mit 98*]: J. Mitrovics, H. Ulmer, U. Weimar, W. Göpel, Modular sensor system for gas sensing and odour monitoring: the MOSES concept, Acc. Chem. Res. 31 (1998) 307-315.

[*Mor 95*]: M.T. Morales, M.V. Alonso, J.J. Rios, R. Aparicio, Virgin olive oil aroma: relationship between volatile compounds and sensory attributes by chemometrics, J. Agric. Food Chem. 43 (1995) 2925-2931.

[*Nos 01*]: Web-page of the European Network of Excellence on Artificial Olfactory Sensing, "NOSE", address: http://nose.uia.ac.be/review/

[*Pea 97[a]*]: T.C. Pearce, Computational parallels between the biological olfactory pathway and its analogue "The Electronic Nose": Part I. Biological olfaction, BioSystems 41 (1997) 43-67.

[*Pea 97[b]*]: T.C. Pearce, Computational parallels between the biological olfactory pathway and its analogue "The Electronic Nose": Part I. Sensor-based machine olfaction, BioSystems 41 (1997) 69-90.

[*Ros 96*]: K. J. Rossiter, Structure-Odor Relationships, Chem. Rev. 96 (1996) 3201-3240.

[*Ste 93*]: J.R. Stetter, M.W. Findlay Jr., K.M. Schroeder, C. Yue, W.R. Penrose, Quality classification of grain using a sensor array and pattern recognition, Anal. Chim. Acta 284 (1993) 1-11.

[*Ull 87*]: F. Ullrich, W. Grosch, Identification of the most intense volatile flavour compounds formed during autoxidation of linoleic acid, Z. Lebensm. Unters. Forsch 184 (1987) 277-282.

[*Wam 97*]: T.P. Wampler, Analysis of food volatiles using headspace-gas chromatographic techniques, in: Techniques for analysing food aroma, R. Marsili (Ed.), Marcel Dekker, Inc., New York, 1997, pp. 27-58.

[*Win 93*]: F. Winquist, E.G. Hornsten, H. Sundgren, I. Lundström, Performance of an electronic nose for quality estimation of ground meat, Measur. Sci. Technol. 4 (1993) 1493-1500.

2 BASICS AND SURVEY

2.1 Taints and Off-flavours

Foodstuff can in general be characterised by texture, colour and flavour. The latter is a combination of taste and smell. A smell impression originates from volatile compounds coming into contact with the "regio olfactoria" [*Ohl 90*] which is part of the smelling system in mammals. The acceptance of a product by a consumer is strongly affected by the aroma active compounds released from food or packaging. Although the definitions of "taint" and "off-flavour" are different[1] both terms will be used synonymously.

Quantitative descriptions of taints by humans are expressed by several terms:

- *Threshold:* Lowest, but still perceptible concentration of a substance.
- *Detection threshold:* Perceptible concentration difference of a dissolved compound compared with the pure solvent.
- *Recognition threshold:* Concentration at which the odour quality of a compound can clearly be assessed.

Both detection and recognition thresholds depend largely on the solvent. Usually the term threshold is used to describe the lowest limit of detection of an odorous compound.

In common with other human sensory perception, the perceived intensity of an odour is not completely linearly related to its concentration [*Gar 99*]. Typically there is a sigmoidal relationship of the type shown in Fig. 2.1.1, where there is a threshold below which the odour is not detected and where above a certain concentration the perception of the odour intensity levels off (saturation region).

---

[1] Definition of "taint": Unpleasant odour or flavour imparted to food through *external sources*.
Definition of "off-flavour": Unpleasant odour or flavour imparted to food through *internal deteriorative change*.
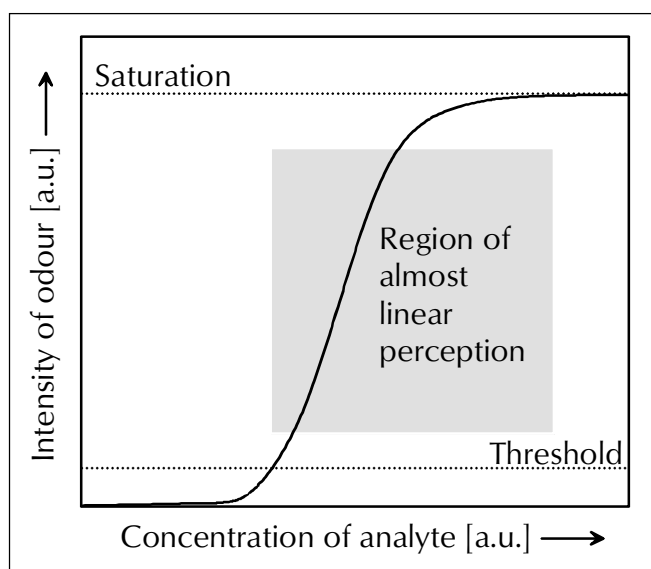
Fig. 2.1.1: General form of the sigmoidal relationship between the perceived intensity of an odour and its concentration [Gar 99].

Of all the substances which can be identified in the headspace of a particular sample, only a few might actually be involved in the sample's aroma [*Gut 91*]. A further term to quantify the odour impact of a compound is the <u>o</u>dour <u>a</u>ctivity <u>v</u>alue (OAV). It is defined as the ratio of the concentration to the component's threshold. After determining the concentrations of components present in the headspace and knowing the corresponding threshold[2], the major contributors to an off-flavour can be established.

2.1.1 Vegetable Oil – Formation of Off-flavours

The main components of food oils and fats are triglycerides (triesters of fatty acids and glycerol). Additionally, a lot of minor compounds are present; free fatty acids, hydrocarbons, sterols, triterpenes, alcohols, anitoxidants, trace metals etc. [*Bel 87*]. Refining procedures carried out during the processing of the oils normally remove these unwanted minor components. Hence, freshly refined and deodorised oils have gentle flavours but these can be transformed into off-flavours on storage. The degeneration of fat-containing foodstuff is based on the breakdown of lipids caused by enzymatic and / or oxidative mechanisms. The latter is also called oxidative rancidity and is one of the major causes of food spoilage.
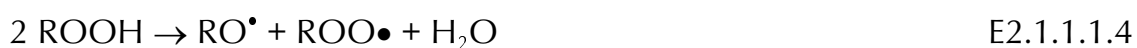
---

[2] An extensive study of aliphatic and alicyclic compounds with oxygen-containing functional groups is presented in [*Sch 88*]. The thresholds of prominent odorous compounds can be found in papers dealing with more specific topics (e.g. [*Ott 97, Mil 97*]).

2.1.1.1 Unsaturated Lipids as Off-flavour Precursors

A detailed description of possible steps occurring on the way from the lipid to the off-flavour is given in [*Koc 96*]. In the following paragraph only the theoretical background relevant to the interpretation of the results of this study will be presented.

The formation of hydroperoxides, the off-flavour precursors, is a free radical process and can be formally divided into three stages:

- *Initiation:*

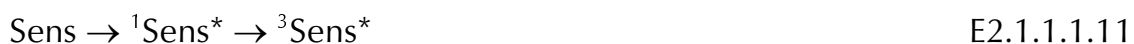|	
$RH \rightarrow R^{\bullet} + H^{\bullet}$ (free radicals formed due to heat, light, metals)	E2.1.1.1.1
$ROOH + M^{3+} \rightarrow ROO^{\bullet} + H^{\bullet} + M^{3+}$	E2.1.1.1.2
$ROOH + M^{2+} \rightarrow RO^{\bullet} + {}^{\bullet}OH + M^{2+}$	E2.1.1.1.3
$2\ ROOH \rightarrow RO^{\bullet} + ROO\bullet + H_2O$	E2.1.1.1.4

- *Propagation:*

$R^{\bullet} + O_2 \rightarrow ROO^{\bullet}$	E2.1.1.1.5
$ROO^{\bullet} + RH \rightarrow ROOH + R^{\bullet}$	E2.1.1.1.6
$RO^{\bullet} + RH \rightarrow ROH + R^{\bullet}$	E2.1.1.1.7

- *Termination:*

$R^{\bullet} + R^{\bullet} \rightarrow 2\ R$	E2.1.1.1.8
$R^{\bullet} + ROO^{\bullet} \rightarrow ROOR$	E2.1.1.1.9
$ROO^{\bullet} + ROO^{\bullet} \rightarrow ROOR + O_2$	E2.1.1.1.10

With RH = unsaturated fatty acid or ester with H- atom attached to allylic carbon atom, $R^{\bullet}$ = alkyl radical, $RO^{\bullet}$ = alkoxy radical, $ROO^{\bullet}$ = peroxyl radical, ROOH = hydroperoxide, M = transition metal.

The formation of free radicals ($RO^{\bullet}$, $ROO^{\bullet}$) in the initiation stage can take place by thermal or photo-decomposition of hydroperoxides, by metal catalysis and / or by ultraviolet irradiation (see Eqs. E2.1.1.1.2 and E2.1.1.1.4). A concurrent reaction is represented by Eq. E2.1.1.1.1, where a hydrogen radical is separated from a carbon atom in the α-position relative to the double bond. This process can also be induced by heat or light and it results in the formation of lipid or alkyl radicals. According to Eq. E2.1.1.1.5, these radicals react with oxygen molecules to generate peroxy radicals ($ROO^{\bullet}$). The $ROO^{\bullet}$ removes a hydrogen atom from the α-CH_2 group of another unsaturated lipid molecule leading to a hydroperoxide (see Eq. E2.1.1.1.7). This reaction is the slowest and thus, is the rate-determining oxidation step at room temperature. The whole process is

terminated by re-combination reactions forming non-radical, stable products (Eqs. E2.1.1.1.9 - E2.1.1.1.10).

The reaction between unsaturated fatty acids and oxygen is thermodynamically unfavourable (the activation energy is about 144 kJ/mol). Therefore, an initiation reaction can arise through photo-sensitised oxidation. This reaction is characterised by the following steps:

$$Sens \rightarrow {}^1Sens^* \rightarrow {}^3Sens^* \qquad\qquad E2.1.1.1.11$$

$$^1Sens^* + {}^3O_2 \rightarrow {}^3Sens^* + {}^1O_2^* \qquad\qquad E2.1.1.1.12$$

$$^1O_2^* + RH \rightarrow ROOH \qquad\qquad E2.1.1.1.13$$

With Sens = sensitiser (basic state, excited singlet and excited triplet state, respectively). An excited singlet oxygen ($^1O_2^*$) is produced from ordinary triplet oxygen ($^3O_2$) by radiation (visible, ultraviolet or x-ray) in the presence of a sensitiser such as chlorophyll, pheophytin, myoglobin and / or erythrosin [Cha 77]. The $^1O_2^*$ generated is highly reactive, and reacts with methyl linoleate 10^3 to 10^4 times faster than the normal oxygen. Since natural photosensitisers are usually removed by refining and bleaching procedures, the deterioration by singlet oxygen is reduced.

Besides the aforementioned reaction there are also other factors which influence the rate of lipid oxidation:

- *Fatty acid composition:* Unsaturated fatty acids are chemically more reactive than the corresponding saturated species with the same number of C-atoms. This behaviour is based on H- atoms neighbouring a double bond showing an increased acidity higher acidity, thus facilitating the removal of a hydrogen atom.

- *Free fatty acids:* Free fatty acids oxidise at a slightly higher rate than when they are esterified to the glycerol moiety. The presence of relatively high amounts of free fatty acids in oils can increase the uptake of catalytic trace metals from storage equipment and hence enhance the rate of oil oxidation.

- *Oxygen concentration:* At high oxygen pressure (in a first approximation O_2 of an unlimited amount) the oxidation rate is almost independent of the O_2-pressure. In contrast, at low oxygen pressures the oxidation is directly proportional to the pressure.

Further factors playing only a minor role in our investigations are mentioned for completeness; surface area, temperature, moisture, pro-oxidants, haematin compounds, enzymes and antioxidants.

Formation of monohydroperoxides produced by photoxidation ($^1O_2$):

It has to be stressed that the formation of hydroperoxides can proceed according to the free radical mechanism and / or the photosensitised oxidation. The oxidation induced by $^1O_2$ is most probably the dominating mechanism taking the experimental conditions of the artificial spoiling of corn oil into account which will be mentioned later on (see chapters *Experimental* and *Results and Discussion*). The photooxidation can be described by a concerted cycloaddition (involving six electrons) between the oxygen double bond, the double bond(s) of the unsaturated fatty acid and an α-C-H-bond. The reaction schemes for the formation of isomeric hydroperoxides of oleate (Fig. 2.1.1.1.1) and linoleate (Fig. 2.1.1.1.2) are shown below.
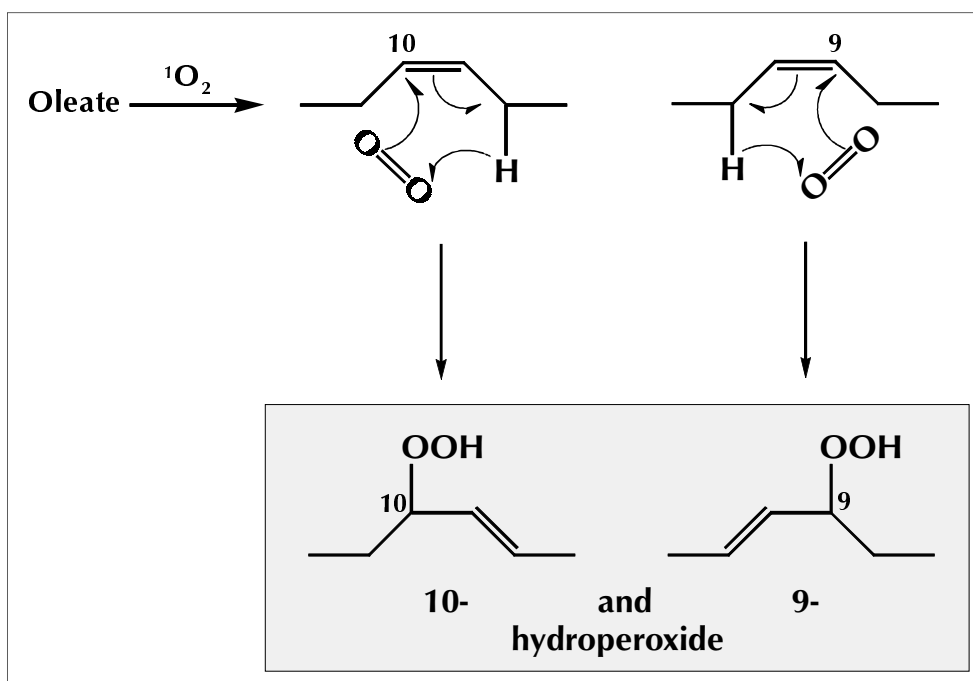
Fig. 2.1.1.1.1: Photooxidation of oleate induced by $^1O_2$ [Koc 96].

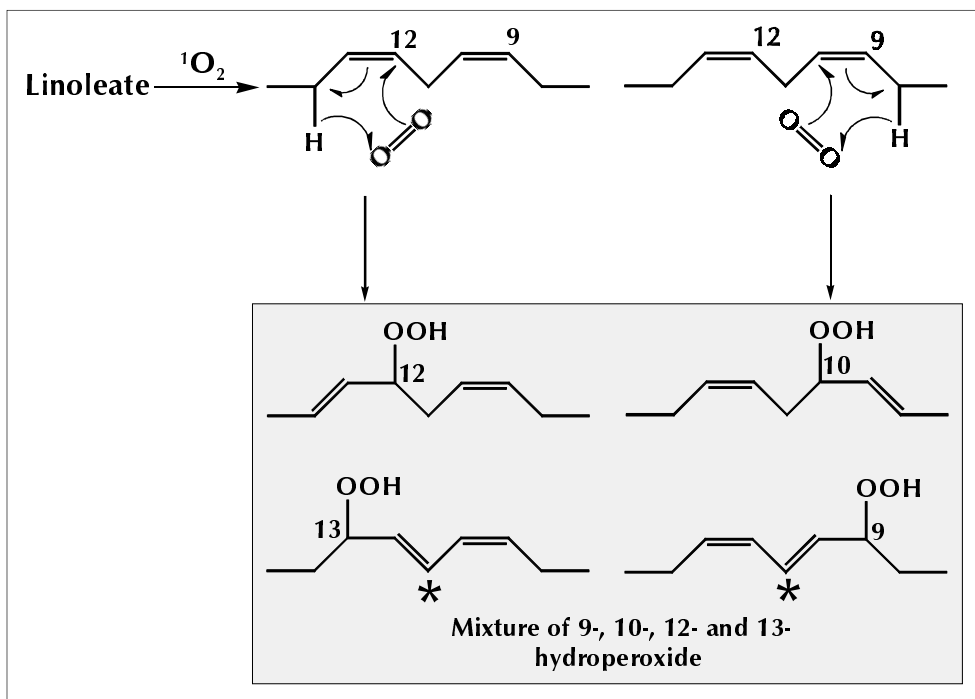*Fig. 2.1.1.1.2: Photooxidation of linoleate induced by $^1O_2$ [Koc 96]. (At the position marked * the valence angle is in fact 120° due to the sp^2- hybridized C- atom).*

The monohydroperoxides formed as a result of the aforementioned oxidation reaction are very unstable and decompose easily into a variety of products, such as aldehydes, ketones, alcohols, acids, hydrocarbons, lactones, furans and esters.

As previously shown by *Grosch* [*Gro 87*], the decomposition of hydroperoxides starts with homolytic cleavage of the HOO- group, forming an alkoxy and a hydroxy radical. The alkoxy radical can undergo β-scission of the C-C bond, with the formation of an unsaturated aldehyde and an alkyl radical (scission I), or a saturated aldehyde and a vinyl radical (scission II). Further secondary reactions are displayed in Fig. 2.1.1.1.3. The proportions of the final products formed are dependent on reaction parameters like temperature, solvent etc.
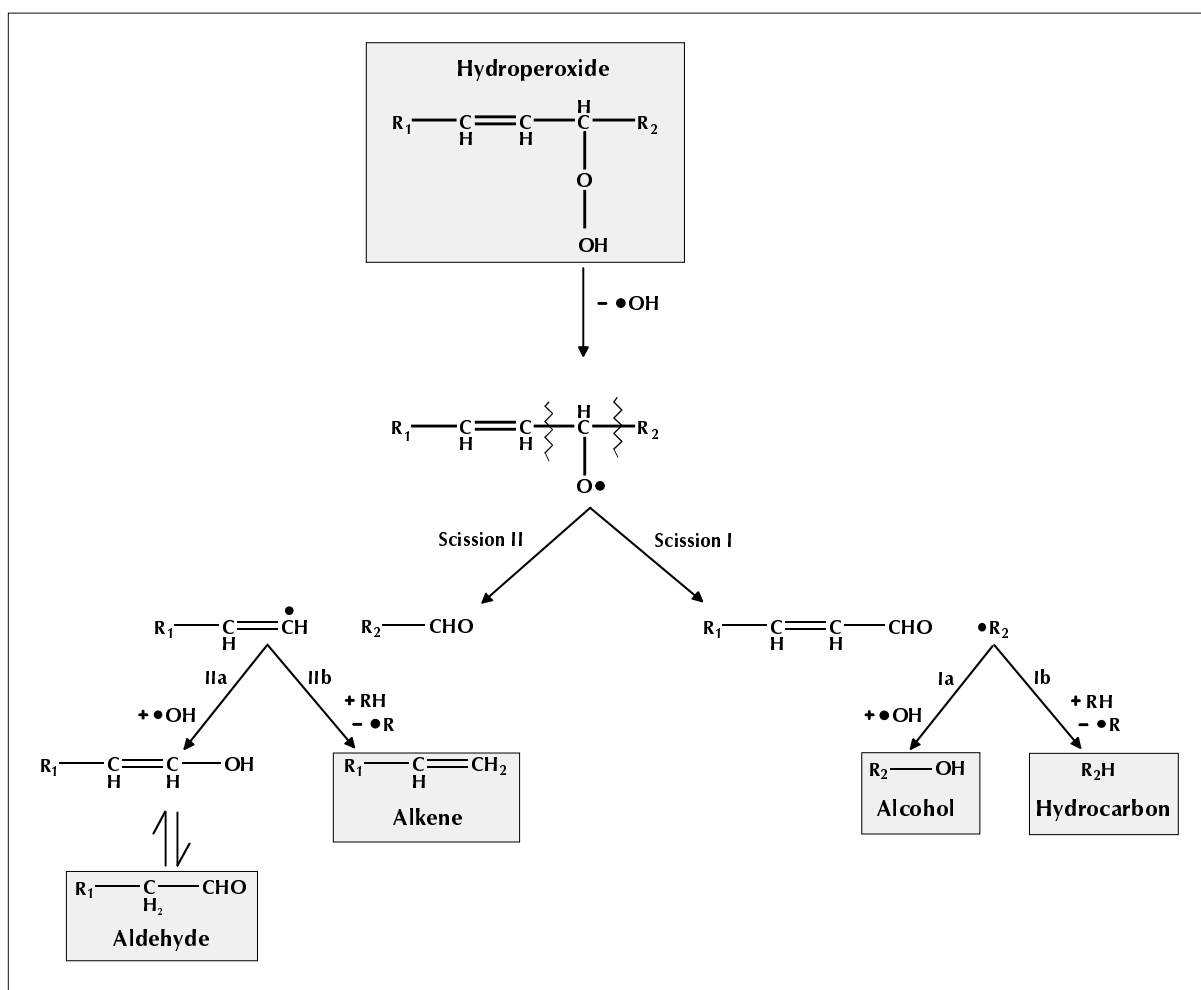
Fig. 2.1.1.1.3: Reaction pathway for the homolytic cleavage of monohydroperoxides of unsaturated acids [Koc 96].

2.1.2 Packaging Materials – Formation of Off-Flavours

Food packaging is manufactured from a variety of materials including metal, glass, cardboard, paper and a wide range of plastics. Besides the original function of packaging materials (the protection of foodstuff against external contamination), they themselves can be a source of odorous substances. The food spoilage can occur simply by vapour transfer or, if the foodstuff is in direct contact with the packaging, by migration. In general, direct migration happens more readily with lipid-containing foods. Fats and oils can penetrate the surface of particular packaging materials, thus promoting migration into the product.

One of the main problems in carrying out odour sensing tests on packaging materials using a panel of testers, is obtaining comparable descriptions from the individual panel members on the nature of any odours detected. Various difficulties arise in classifying or describing an odour, especially if the taint is based on several substances [*Kos 86*]. Potential sources of off-odours are:

- Main components of the packaging material
- Impurities
- Reaction products formed during manufacture
- Environmental contamination

Although GC/MS is *the* analytical tool to identify VOCs released from packaging material, it is very likely that if a consumer detected a strong odour when the package was opened, the food would be rejected without tasting it.

2.1.2.1   Printing Inks and Adhesives

The printing of packaging material has great importance with respect to sales appeal and product information. Most forms of printing use inks that consist of pigments and resins dissolved or dispersed in solvents (typical organic solvents like ethanol, isopropanol, ethyl acetate or water). Since most of the solvents employed are relatively volatile, the drying of the print is rather fast. However, sometimes a small portion of a slow-drying solvent is added to control the evaporation and to give the required print quality. Both types of solvents can often be detected in headspace analyses. The numerous adhesives can be roughly classified according to the following listing:

- Water-based solvents with dextrins, starch and vinyl acetate
- Organic solvent-based adhesives used for laminating plastic layers together
- Hot melt adhesives
- Cold seal adhesives (the bond between different packaging layers is simply achieved by pressure)

Particular printing ink and varnish formulations depend largely on the method of printing employed.

Lithographic inks: The solvents are principally petroleum distillates (i.e. hydrocarbons, HC). Usually, "low odour" petroleum distillates are selected having very low concentrations of aromatic HCs. Resins used in lithographic inks are of the alkyd type, which oxidise in the drying process and can liberate odorous by-products, such as aldehydes and ketones.

Flexographic inks: The organic solvents these inks are based on span a wide range; ethanol, isopropyl alcohol, n-propyl alcohol, ethyl acetate, isopropyl acetate, n-propyl acetate etc. The resins include polyamides, cellulose nitrate and acrylics. Commonly, acetate esters give the flexographic printed packaging materials an unacceptable odour, being unusual for the resin to cause taint problems.

There are no generally agreed on maximum levels for residual solvents in food packaging. This is because a number of factors determine whether remaining solvents will produce an unacceptable odour. These factors include:

- Nature of the food
- Storage time and temperature
- Packaging substrate material

As a general guide, the total level of residual solvents should normally not exceed 30 mg/m^2, whereas for some more odorous solvents, such as isopropyl acetate, the individual levels should be less than 5 mg/m^2. Here, the particular odour thresholds, which span a range from ppm to ppt, also have to be taken into account. Nestlé's policy to ensure the quality of their products is described in the following listing which presents the specifications of the most common substances:

Residual solvents: Food packaging must not contain residual solvents in a quantity exceeding:

- 20 mg/m^2 for total amount
- 7 mg/m^2 for total amount of combined ketones, acetate and toluene
- 2 mg/m^2 for toluene

Styrene monomer: Polystyrene for food packaging must not contain styrene monomer in a quantity exceeding 500 mg/kg. Foodstuffs must not contain styrene monomer in a quantity exceeding 0.3 mg/kg.

Chlorophenols / Chloroanisoles: All materials used in packaging (paper or jute, adhesive, barrier ply, etc.) or in transport (pallet, container, warehouse, etc.) must not contain chlorophenols above analytically detectable limits or chloroanisoles above the sensory threshold.

2.1.2.2 Paper Packaging

Paper used for packaging is made from pulp, which in turn is made from wood. In general, two different pulps can be differentiated:

- Mechanical pulp, where the cellulose fibres are prepared by mechanical processes on the wood; it still contains lignin, resins and inorganics.
- Chemical pulp, where the cellulose fibres are isolated by means of chemical treatment of the wood.

Often chocolates are packaged in glassine being a paper manufactured by a process similar to greaseproof paper. In addition, glassine is supercalendered

resulting in a glossy surface. Modern paper-based packaging frequently consists of multilayers to give strength, barrier properties, easy sealing and good printability. A typical multilayer structure comprises paper laminated to one or more plastic layers with a foil intermediate. Adhesives are used to glue the layers together. Plastic / cardboard composites are now commonly used for liquid packaging, such as for milk. The plastic layer is usually polyethylene (PE). They also contain an aluminium foil layer; this provides a barrier to oxygen permeation through the food (the Al-foil is found between the board and the food). *Donetzhuber* [*Don 82*] has attributed certain odours to substances arising from bacteria, autoxidation of residual resins and degradation of processing chemicals. Metallic ions, such as iron and copper, in the inorganic residues left in the pulp, can catalyse the oxidation of lipids. He listed more than 200 volatiles which have been identified in the gas phases from pulp, paper and cardboard samples[3]. They belong to the subsequent main classes:

- n-alkanes, up to C_{15}
- branched alkanes, up to C_{13}
- alkenes, up to C_{13}
- aldehydes
- ketones
- alcohols
- esters
- heterocyclics (especially furan derivatives)
- aromatics (benzene and its substituted derivatives)
- alkyl sulphides
- terpene hydrocarbons

The odour of some substances is not categorically unpleasant; this applies for instance to the "green-grassy" odour of hexanal which is, compared with other aldehydes, often present in rather high concentrations. Its smell is accepted as "mild, natural". The presence of hexanal will be discussed in chapter 4.2.2 *GC/MS Investigations* in more detail.

In contrast to many packaging materials like printed plastics, some paper / cardboard materials have emerged to become more odorous on storage. Usually, one would expect that after manufacture a release of residual solvents takes place (which is most probably the case), but the quality of paper and cardboard can be negatively affected by degradation processes induced by catalytic metal ions liberating aldehydic compounds. To overcome this difficulty

---

[3] Other very similar results are presented in [*Sod 85*].

complexing agents such as ethylene diamine tetraacetic acid (EDTA) are added to the pulp.

Alkyl substituted benzenes can originate from a filler (containing synthetic resin binders) utilised as paper / cardboard surface coatings.

2.1.2.3   Plastic Packaging

The range of plastic packaging used spans a wide range due to the great variety of polymers which can be produced today. Therefore, these materials are used to wrap foodstuff (e.g. cheeses, meats, biscuits, dry foods, fats, ready-meals) and to bottle beverages, oils and sauces. Their use within these different applications can only be fulfilled if the packaging materials are especially "designed" for a particular requirement. Necessarily, this leads to rather complex and sophisticated plastics often consisting of multiple layers (and also paper, cardboard or thin metal films like aluminium).

One potential source of taints results from the monomer units, the basic starting materials for all plastics. During polymerisation these monomers form the final product and usually, low quantities of unreacted monomers left in the polymer's bulk. The remaining monomers, being relatively volatile and some of them having low odour threshold values, can be liberated by heating the polymer material to elevated temperatures in an air stream. Except for a few examples[4], this is the most common procedure for eliminating unwanted monomers.

Although the concentration of a certain monomer in plastic packaging itself might be below a specified maximum, investigations on the migration of these compounds confirm their enrichment in food. In particular, fat- and lipid-containing food products have a higher potential to accumulate residual monomer since in most cases they are shown to be lipophilic [*Gil 83*, *Pas 83*].

Polyolefin plastics, such as polyethylene (PE) and polypropylene (PP), are the most common of all the plastics used for food packaging as wrapping films, containers and bottles. Off-odours liberated from PE and PP are not usually caused by remaining monomers. Due to the nature of the substance class the two polymers belong to, mainly aliphatic hydrocarbons (HCs) can be identified in the headspace. As these HCs often have relatively high odour thresholds, they may not be detected sensorially, even though their concentration is not negligible.

The main source of taint in PE and PP can be attributed to carbonyl compounds, especially conjugated unsaturated species, like 2-nonenal or 1-hepten-3-one. The aldehydes and ketones are formed by oxidation (induced thermally, by light or ionising radiation). So far, the oxidation pathways are not

---

[4] Styrene is one of the exceptions, being reformed from polystyrene under excessive heat.

entirely clear. Since these compounds (above all the "1-en-3-ones") are already perceivable at very low concentrations, trace amounts can contribute to the overall odour. The detection by GC/MS is difficult and often only GC/olfactometry techniques, such as <u>a</u>roma <u>e</u>xtract <u>d</u>ilution <u>a</u>nalysis (AEDA) or <u>c</u>ombined <u>h</u>edonic <u>a</u>roma <u>r</u>esponse <u>m</u>easurement (CHARM) [*Sch 95*] give information on their odour impact. Nevertheless, it turned out that not a single compound was predominantly responsible for the taint of oxidised PE or PP films being described by the terms "waxy" and/or "burnt plastic".

Remark: Although all plastic packaging materials examined within the frame of this thesis by different kinds of analysis (sensory panel, GC/MS and sensor array system) were not in contact with foodstuff before the measurements, for completeness it has to be mentioned that substances from the food product can also migrate into the packaging. This results in changes in the organoleptic properties of both, food and packaging (for more details see [*Tic 96*]).

2.1.2.4   State of the Art in Analysing Packaging Materials

Today the most appropriate analytical technique for the analyses of volatiles released from packaging materials is GC/MS. Although the limit of detection for MS in the total ion scan mode is typically a few nanograms (also depending on the range of scanned masses), sometimes more sophisticated procedures have to be applied in order to achieve higher sensitivity.

One of them would be to use the MS in the <u>s</u>elected <u>i</u>on <u>m</u>onitoring (SIM) mode on condition that the substances to be traced are already identified; otherwise an unequivocal identification based on only a few m/z-peaks is impossible.

All kinds of techniques dealing with enrichment represent further ways to enhance sensitivity. The most prominent approach is dynamic headspace coupled with thermodesorption. With this technique a certain amount of packaging material is placed in a sealed vessel. Then, the vessel is purged for a period of time with a constant flow of an inert gas removing volatiles from the sample which are subsequently collected and concentrated ("trapped") on a porous polymer. Brand names for these polymers are Tenax™, Porapak Q™, and Porapak R™. Finally, the trap is heated to elevated temperatures liberating the particular compounds (solvent elution and injection as a solution is also possible). Other techniques are based on steam distillation, solvent extraction or solid phase isolation [*Sha 83*].

The identification of a substance does not necessarily involve information on its odour characteristics. To obtain this information a sniffing port is connected to a split at the end of the GC-column.

The use of <u>F</u>ourier <u>t</u>ransform <u>infra</u>red (FTIR) spectrometry as an alternative or in addition to MS for the identification of VOCs has increased over the last years [*Kaw 95*]. FTIR is a well known tool for detecting chemical functional groups, such as carbonyls or amines. However, even more important is the information provided on molecular geometry, which helps to distinguish between isomers. The latter is a clear drawback of MS because very often the fragmentation patterns of isomers are hardly differentiable.

2.2 Pattern Recognition, Multivariate Calibration and Prediction

2.2.1 Principal Component Analysis (PCA) [Bee 98, Ein 97, Jur 00, Ott 99]

Principal component analysis is a mathematical manipulation of a data matrix where the goal is to represent the variation present in many variables using a small number of "factors". A new row space is constructed in which to plot the samples by redefining the axes using factors rather than the original measurement variables. These new axes, referred to as factors or principal components (PCs), allow the analyst to probe matrices with many variables (here sensor responses) and view the true multivariate nature of the data in a relatively small number of dimensions.

All principal components have the following properties:

- The first PC explains the maximum amount of variation possible in the data set in one direction. Stated another way, it is the direction that describes the maximum spread of data points; the second axis shows the second largest variance, and so on. Furthermore, the percentage of the total variation in the data set described by any PC can be precisely calculated. PCs are orthogonal to each other.

- Just as the sample has co-ordinates in the original row space (defined by the original variables), it also has co-ordinates with respect to the new PC axes; the latter are typically termed "scores".

- Each PC is constructed from combinations of the original measurement variables. The extent to which such a variable contributes to a PC depends on the relative orientation in the space of the PC and variable axes. For interpretation, it is useful to know which variables contribute most significantly to the individual PCs. These are the axes that are potentially the best discriminating between samples. The cosine values of the angle between the variable and the PC axis are often called "loadings", and can range from –1 to 1.

Scores plot: The scores are the co-ordinates of the samples in the new co-ordinate system where the axes are defined by the PCs. These axes are used to view the relevant variation in the data set in a smaller number of dimensions. The plot reveals how the samples are related to each other given the measurements that have been made. Samples that are close to each other in a given scores plot are similar with respect to the original measurements provided the plot displays a sufficient amount of the total variation. This mathematical proximity translates to chemical similarity if meaningful measurements have been made.

PCA is an unsupervised orthogonal projection algorithm which means that no input from the operator is needed beyond the raw sensor data.

2.2.2 Calibration and Prediction

In order to predict information Y from measurements X, the prediction formula $\hat{Y} = f(X)$ must first be determined. For complex analytical problems with noise inherent in the system the parameters must be estimated statistically, based on realistic, empirical measurements from representative calibration samples.

Multivariate calibration involves models at several levels. Most fundamental is the "mental model" of how it is thought that the different variables in X and Y are phenomenologically related. At an intermediate level some "abstract mathematical model" is chosen to represent the phenomena expected to be found between X-and Y-variables. The regression model y = X·b + f is an example of this. The mathematical calibration model has unknown coefficients (model parameters like b and f). During calibration these unknown parameters are then estimated from calibration data, yielding the calibration model. The latter contains the desired prediction function $\hat{Y} = f(X)$. Finally, the calibration model is used in prediction, and it is implicitly assumed that the prediction objects obey the same model structure as those used in calibration.

The phenomena which can affect the quality of a calibration equation and the subsequent prediction are the following:

- *Model errors*: If the model used represents a bad fit to the data, the calibration equation will never have the possibility of giving precise results.
- *Lack of representativity*: This error source arises when the calibration set does not cover the total range of variability in the population of future objects. In such cases one is in danger of bad prediction ability for objects outside the calibration range.
- *Random noise in calibration and prediction data*: Multivariate calibration can cancel out much of the random noise in the data used for calibration when

the number of objects (i.e. individual measurements) is high relative to the number of independent calibration parameters to be estimated. However, the noise in the individual future X-data (test data) constitutes an intrinsic limitation in the analytical method.

There are several ways in estimating the prediction ability of a model. In practice one of the best descriptors is the root mean square error (RMSE). It is best estimated by direct comparison of "true" and "predicted" values for a representative series of objects, either the calibration objects or a new set of independent test objects. The RMSE is computed according to the following equation:

$$RMSE = \sqrt{\frac{1}{n} \sum_{i=1}^{n} (\hat{y}_i - y_i)^2}$$ E2.2.2.1

$\hat{y}_i$ = predicted value, y_i = measured value ("true"),

n = number of data points used for the linear fit

Assuming that the test objects are representative for the future unknown objects, it is important to find the correct model complexity; modelling too few X-phenomena gives under-fitting, whereas too many phenomena leads to over-fitting. Both resulting in bad predictive ability [*Mar 93*].

The major drawback of such external prediction testing is that large and representative sets of test objects are required. In order to circumvent this (expensive) disadvantage internal validation methods can be used. They concern validation from the calibration data themselves and an assessment based on internal validation is not the same as prediction testing! Ideally, the predictive ability can only be determined by testing on new, independent objects. In some cases, however, cross-validation and leverage correction give also sensible results with high information about the prediction ability [*Sne 76*]. To estimate the error in the model without using independent test samples the so-called "leave-one-product-out" cross-validation is a very valuable tool. The method involves leaving out samples from the calibration data set and calibrating the model based on the remaining data points, then predicting the values for the left-out samples and computing the prediction residuals. This procedure is repeated until every sample has been left out once; then all prediction residuals are combined to compute the validation residual variance (VRV) and the root mean square error of prediction (RMSEP). The cross-validation was carried out automatically processing each individual data set with the software package used in the investigations.

2.2.3 Principal Component Regression (PCR) [Bee 98, Ein 97, Jur 00, Ott 99]

Principal component regression is one of the most widely used multivariate calibration method in chemometrics. Multivariate calibration is applied not only for the determination of the concentration of substances, but also for the direct determination of certain quality parameters. For instance, the sensory tenderness of beef was determined by PCR using near-infrared spectra as the manifest data [*Hil 94*].

PCR is based on PCA but comprises a significant additional step and also needs additional input. After the determination of the PCs, a regression of the reference method on the scores is performed based on the correlation of quantities, e.g. concentrations and measurement data. Or in other terms, it provides a link between the matrix $\mathbf{X}$[5] of response information and the matrix $\mathbf{C}$ of concentration information. The matrix $\mathbf{C}$ is $m \times s$, where s denotes the number of analytes. The matrices are related by $\mathbf{C} = \mathbf{XP}$, where $\mathbf{P}$ is the $n \times s$ matrix of regression coefficients.

The calibration information in $\mathbf{C}$ and $\mathbf{X}$ can be used to find an approximation to the regression coefficients. The true regression coefficients cannot be calculated exactly due to the unavoidable presence of experimental error. By using a subset of the available PCs, only the systematic variance in the data is taken into account, which is introducing a small systematic error but which also improves the robustness of the prediction for generalisation [*Ulm 99*]. The subset of data used is obtained by cross-validation, which means that the data set is split into two subsets, i.e. one for building the model and one for testing it. With the resulting matrix $\mathbf{P}$, quantitative estimates for unknown concentrations of species in mixtures, which are present in known amounts in the reference data, can be obtained. Note, that the PCs are determined without regard to the predicted property.

PCR as linear technique will be most successful if sensor responses are linear. However, it will produce overly optimistic results if the prediction accuracy is based only on data used to generate the PCs and not independent data. PCR is a supervised technique as for the prediction the known concentrations of the reference sample are required as input.

---

[5] The matrix $\mathbf{X}$ shows in general collinearity, i.e. $\mathbf{X}$ has dominating types of variability that carry most of the available information. The purpose of PCA is then to express the main information in the variables $\mathbf{X} = \{\mathbf{x}_k, k = 1, 2,...\}$ by a lower number of variables, the so-called principal components of $\mathbf{X}$.

2.2.4 Correlation between Sensory and Instrumental Data

The objective of relating sensory to instrumental measurements is twofold. A first objective can be that it may help a better understanding of the sensory attributes. A second goal is that instrumental measurements may eventually replace the sensory panel. So far not much success has been scored in this area due to the complexity of human sensory perception. When relating instrumental measurements to sensory data one should focus on quantitative descriptive analysis (QDA) data. Hedonic scores are generally not well suited for comparisons with instrumental results, since there usually will not be a linear relationship.

QDA is quantitative in the sense that reproducible scores for sensory attributes can be obtained that are useful in describing the samples tested. In principle, the scores of individual panellists are not of the most interest. Moreover, the panel scores as a whole is of importance, hence the mean score of the panel is taken as the reading of the sensory "instrument". It should be stressed that a QDA panel records, it gives no judgement on the acceptability of a product. In many ways one may consider a well-trained QDA panel as an analytical instrument that measures the intensity of certain attributes. A common way to record the intensity is by marking an unstructured line segment that has a left anchor ("absent") and right anchor ("very strong").

In order to correlate the scores of the sensory panel with the instrumental (here sensor system) data, a PCR is carried out relating the individual sensory scores with the corresponding values of the sensor responses upon exposure to the same sample.

2.3 Sensor Drift - Evaluation and Compensation

First two different terms describing temporal changes of sensor responses have to be clearly distinguished. In most of the publications addressing this very important issue, the term "drift" is used in any case where a change in the sensor response could be monitored. The following examples illustrate the difficulties in finding an unequivocal definition for "drift":

- "A gradual change in any quantitative characteristic that is supposed to remain constant" (Webster's 7th New Collegiate Dictionary).
- "Non-cumulative drifts denote statistical variations of the sensor signal. Cumulative drifts lead to irreversible changes of the calibration curves.... Long-term drifts are usually related to the stability of the zero level or the base line" ([*Goe 91*]).

- "Drift is defined as the temporal shift of sensor response under constant physical and chemical conditions" ([*Hol 97*]).
- "Drift is typically characterised by a relatively slow, monotonic, temporal change..." ([*Jam 98*]).
- "Low-frequency noise is often called drift – a slowly varying change in instrument background or sensitivity" ([*Sal 98*]).

The general problem caused by drift is the decreased precision of an analytical experiment, i.e. it is not only related to measurements where chemical sensors are involved. Each discipline in analytical chemistry has to cope with this phenomenon e.g. pyrolysis mass spectrometry [*Goo 96*].

However, there are same crucial, experimental requirements which have to be considered when inspecting sensor data for drift; poisoning or ageing of the sensors (e.g. change in the grains of the nanocrystalline SnO_2- particles or shrinkage of a polymer's bulk), temperature and pressure variations, changes in the background gas, memory effects caused by condensation of VOCs etc.

In practice, the treatment of drift is most often performed by periodic reestablishment of the relationship between a measured signal and a particular, known concentration of a chemical compound. In this relation, a short-term drift, for instance throughout a measurement sequence, is distinguished from a long-term drift (recorded over weeks or months). Usually, the latter has a much greater impact on the precision of the prediction of a sample's quality or the concentration of emitted volatiles.

According to *Salit et al.* [*Sal 98*] a measured signal can formally be composed of:

$$S_{measured} = S_{truth} + \varepsilon_{drift} + \varepsilon_{noise} \qquad E2.3.1$$

$S_{measured}$ denotes the observed signal, S_{truth} is the true signal, ε_{noise} represents noise that leads to a poor signal-to-noise ratio for the measurement of a given sample and ε_{drift} expresses noise that results in a poor signal-to-noise ratio for repeated measurements of a given sample. A drifting system is characterised by $\varepsilon_{drift} > \varepsilon_{noise}$. In addition other criteria related to ε_{drift} have to be recognised:

- ε_{drift} is a relatively smooth function of time being independent of the samples to be measured.
- ε_{drift} can be independent of the signal level, i.e. the drift is additive or ε_{drift} depends on the signal level which might be the case for sensors with a non-linear calibration curve.

As already mentioned in chapter 1.1 *Vegetable Oil*, the samples used for re-calibration have to meet the following requirements:

- Reproducible preparation (involving stable chemical substances).
- Easy handling, e.g. standards in common headspace vials (if performing a headspace analysis using an autosampler).
- High correlation between the headspace compositions of the real samples and the standards applied for re-calibration, i.e. the volatiles presented in the headspace and their concentrations should ideally be the same. Thus, the response patterns of the sensors for both should be as similar as possible.

Looking at response changes of individual sensors, it is important to determine whether all sensors behave in the same manner (indicating a common source of their behaviour) or if each of them behaves uniquely, being not correlated with the other. To give an estimate of the relationship between two variables (here sensor responses) chemometric analysis can provide useful methods. The aim of correlation analysis is to compare one or more functions and to calculate their relationship with respect to a change of τ (so-called lag) in time or distance [*Cha 89*]. In this way, memory effects within the time curve or between two curves can be revealed. Correlation within a time series is described in terms of autocorrelation [*Ein 97, Ott 99, Mas 97*]. Two different time series are characterised by the cross-correlation. Another common descriptor is the covariance which also indicates the linear relationship between two variables. It is given on a scale which is a function of the scales of two variables, and may not be easy to interpret. Therefore, it is usually simpler to study the correlation itself. Typical information to be derived from such models provides information about:

- Drift ($\equiv \varepsilon_{drift}$)
- Statistical fluctuations
- Noise ($\equiv \varepsilon_{noise}$)
- Forecasting (prediction) of future values on the basis of the series history.

The correlation within a measurement series should decrease while simultaneously the time lag increases; this behaviour would indicate that no periodicities or drift phenomena are present. Applying an empirical autocorrelation, the amount of correlation can be calculated. For this purpose, the empirical autocorrelation, $r(\tau)$, for a time lag τ and n data points is defined by:

$$r_{yy}(\tau) = \frac{\sum\limits_{t=1}^{n-\tau}(y_t - \bar{y})(y_{t+\tau} - \bar{y})}{\sum\limits_{t=1}^{n}(y_t - \bar{y})^2}$$

E2.3.2

$\bar{y}$ is the arithmetic mean and the denominator is a measure of the variance, s^2.

The evaluation of all possible autocorrelations is done by plotting r(τ) against the time lag τ in a correlogram, or in other terms, an autocorrelation function. Data being uncorrelated show a statistical distribution in their autocorrelation function. Whereas for correlated data several behaviour of the r(τ)-values can be observed:

An exponential decay: In many cases the slopes of the autocorrelograms show a stepwise change at $\tau = 1$. The initially steep drop of the value of the autocorrelation from 1 at $\tau = 0$ to a significantly lower value at $\tau = 1$ is followed by a less steep exponential decay. This is a typical shape for processes with two time constants. The first part of the correlogram describes a fast process with a small time constant, whereas the second part represents the slower part of the process. This situation may occur if the noise (or other source of variation) of the measuring device contributes substantially to the measured process variations. Because noise is a fast process compared to the signal two time constants are usually found. In some instances it is even possible to derive the relative contribution of measurement noise to the observed process fluctuations.

Drift of the mean: Drift of the mean introduces a positive (or negative) correlation with respect to the overall mean of the process. This is reflected in the correlogram by the fact that the values do not asymptotically approach the zero correlation line, but some other value. Because for large τ-values noise is uncorrelated, small drifts are more easily detected from the autocorrelation function than from the original data.

Periodicity: Periodicity of process values introduces a periodic correlogram. For the same reason as explained for drift, periodicities are more easily detected in the correlogram than in the original process values.

To express the correlation of two different time series, x(t) and y(t), the empirical cross-correlation for a time lag τ is calculated according to the following equation:

$$r_{xy}(\tau) = \frac{\sum\limits_{t=1}^{n-|\tau|}x_t y_{t+\tau}}{\sqrt{\sum\limits_{t=1}^{n}x_t^2 \sum\limits_{t=1}^{n}y_t^2}}$$

E2.3.3

In general, correlation coefficients r are dimensionless measures of the degree of linear relationship between two variables (in our case two independent sensors); they vary from -1 to $+1$.

A positive cross-correlation coefficient $r_{xy}(\tau)$ indicates a positive relation between the two variables, i.e. when one increases, the other also has a tendency to increase. The closer to $+1$, the stronger is this relation. Negative correlation indicates a negative relation between the two variables (sensors), i.e. when one increases the other has a tendency to decrease. The closer to -1, the stronger is this relation.

In order to monitor the relationship between the responses of two sensors, the cross-correlation coefficient is a very useful tool. If $r_{xy}(\tau)$ is in the region of $+1$ this is a clear indication that both sensors are influenced by a sample measured in the same manner. Moreover, a high value of $r_{xy}(\tau)$ (of almost $+1$) proves the stable relationship between the sensors in the time period being considered. In contrast, negative values of $r_{xy}(\tau)$ would signify that two sensors are influenced upon exposure to a particular sample in a different way. This in turn, might already be a hint for a drifting / fluctuating sensor. The "analytical value" of the cross-correlation coefficient is schematically displayed in Fig. 2.3.1. The evaluation of the sensor data is presented in chapter 4.2.4 *Long-term Investigations, Sensor Response Fluctuations and Re-calibration.*

Observation:
Non-stable sensor response over time
(although the concentration of the
exposed analyte should be the same)

Reasons:

**Analyte concentration
is not constant**
(due to faulty sample preparation,
errors in the sampling system etc.)

**Sensor shows drift
or fluctuations**
(due to ageing, poisoning,
change in the carrier gas etc.)

**Cross-correlation
coefficient**:

$$r_{xy}(\tau) = 1 \qquad\qquad r_{xy}(\tau) \ll 1$$

Optimisation of:

**Sampling,
sample preparation**

**Sensor
performance**
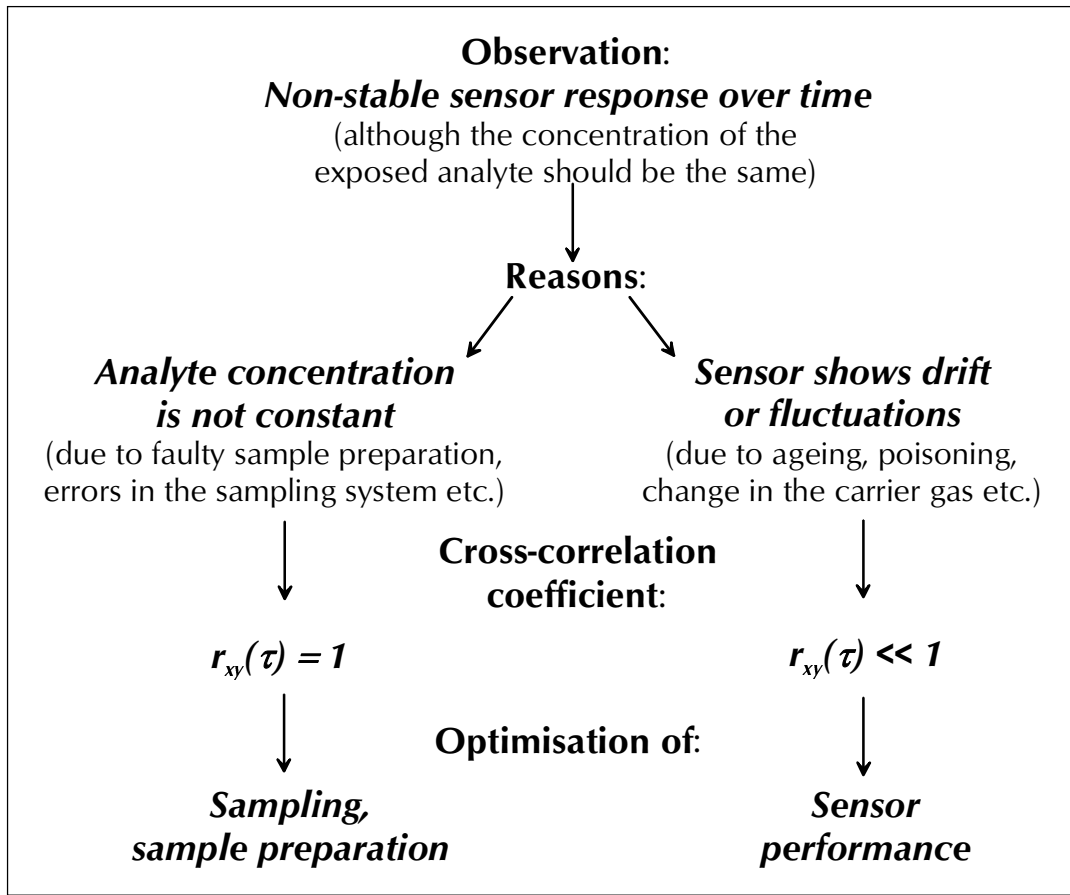
Fig. 2.3.1: Scheme demonstrating the "analytical value" of $r_{xy}(\tau)$.

2.4 Miniaturised Gas Sensor System

As part of the miniaturisation of the gas sensor system one part of the work was focussed on the sensitive layers being used for three different kinds of transducers located on one single chip; a mass-sensitive cantilever [*Lan 98, Mau 99, Lan 99, Bet 00, Hie 00*], a calorimetric microsensor [*Kol 99, Ler 99, Ker 00*] and an interdigitated capacitive microsensor [*Kum 99, Kra 00, Kol 00*].

The production of the aforementioned microsensors is based on industrial CMOS technology combined with post-CMOS micromachining and thin film deposition. The following descriptions are summarised from [*Hie 00* and *Kol 00*].

After the CMOS processing, membrane-type structures are obtained by anisotropic etching from the back of the wafer by applying KOH_{aq}. A planar and defect-free back face of the entirely processed wafer is necessary to provide good etching results. In order to define etch windows, a silicon nitride layer is deposited and patterned. The etching step only affects the wafer's rear side.

If all the bulk silicon of the CMOS wafer is etched through, membranes consisting of the dielectric CMOS layers immediately above the silicon substrate are accessed. These membrane structures are used for sensors requiring excellent

thermal insulation, such as calorimetric chemical sensors. Thermopiles and heating resistors can be created by incorporating polysilicon and metal structures in between the dielectric layers. The combination of bulk micromachining processes and reactive-ion-etching (RIE) leads to bridge structures and cantilevers.

2.4.1 Resonating Cantilever

Although micro-machined cantilevers were originally used in atomic force microscopy (AFM), they also proved to be a new type of mass-sensitive transducer. The cantilever is a layered structure composed of the dielectric layers of a standard CMOS process, silicon and metallizations. A schematic drawing and a microscope picture are shown in Figs. 2.4.1.1 and 2.4.1.2, respectively. The cantilever structures are released by anisotropic etching with an electrochemical etch-stop technique and two additional RIE steps (for details see [*Hie 00*] and [*Lan 01*]). One side of the cantilever beam is firmly connected to the silicon support. The unattached end is covered with a polymeric, chemically sensitive layer; it is bent depending on the added mass of the coating material and on the amount of analyte molecules being absorbed in this material. The layer's thickness is typically in the µm-range (see chapter 4.3.5 *Topography Investigations*). The beam consists of the silicon n-well covered by the dielectric layers of the CMOS process. The polymer film can be deposited by spray-coating (air-brush technique) or, as shown later, by means of micro-mechanical tools which will be discussed in detail.

The cantilever mainly consists of silicon and SiO_2. Due to the different thermal expansion coefficients of both materials, cantilever vibrations can be initiated by periodically applying heating pulses to the embedded resistors. The vibrations are detected using piezoresistors. In contrast to AFM where the beam deflection is recorded optically, the use of piezoresistors enables a fully integrated device. They are arranged in a Wheatstone bridge arrangement. The output signal of this bridge is finally amplified.
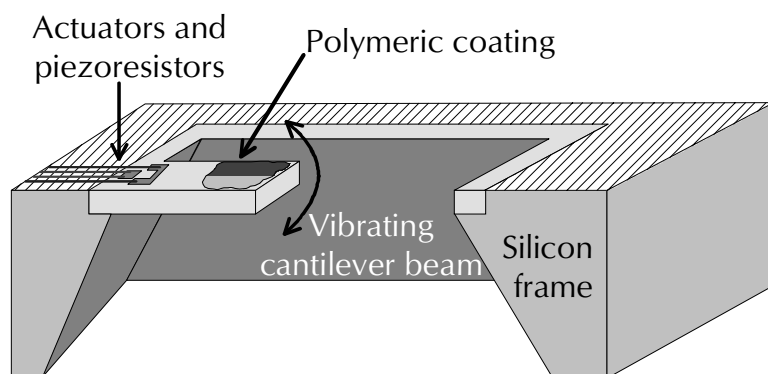
Fig. 2.4.1.1: Scheme of a resonating cantilever [Lan 99b].
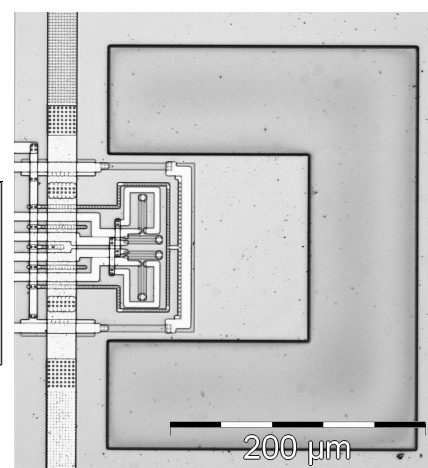
Fig. 2.4.1.2: Light microscope picture of a cantilever (without polymeric coating). Only parts of the whole circuitry are shown.

For analyte detection, the cantilever is excited in its fundamental mode (fundamental resonance frequency $f_0 \approx 350$ kHz) and the change in resonance frequency upon analyte absorption is finally measured. In order to achieve high operation frequencies rather short (typically 150 µm) and stiff cantilevers are required. Moreover, this approach is advantageous (e.g. compared with the so-called static mode[6]) taking the integration of electronics and the simplicity of the whole set-up into account.

In comparison with QCMs, cantilevers also show a linear response behaviour upon exposure to varying VOC concentrations. Therefore, almost the same theoretical considerations explaining the change in the resonance frequency of a cantilever can be applied. According to Eq. E2.4.1.1, the frequency shift Δf [Hz] is directly proportional to the analyte concentration change Δc [mol/m^3]:

$$\Delta f = G \cdot M \cdot K \cdot \Delta c \qquad \text{E2.4.1.1}$$

G is a cantilever-specific figure, depending on its geometric dimensions and the material; it is called the gravimetric sensitivity with units [Hz·m^3/kg]. The analyte molecular weight is represented by M [kg/mol] and K denotes the thermodynamic partition coefficient, which is dimensionless and characteristic of the particular polymer-analyte combinations (for details see [*Hie 96*] and [*Bod 97*]). Depending on M and K, limits of detection (LOD) are in the lower

---

[6] In the static mode the cantilever deflection upon loading a mass is measured by e.g. means of a laser [*Kim 00*].

ppm-range; for example: $LOD_{Ethanol/PEUT} \approx 70$ ppm, $LOD_{Toluene/PEUT} \approx 10$ ppm (see [*Lan 01*]).

The elastic modulus of the polymers used as coating materials is rather small in comparison with those of the cantilevers. Moreover, in most cases changes in the polymer's elastic modulus and swelling effects can be neglected.

2.4.2 Thermoelectric Microsensor

The fundamental measurement principle of a calorimetric sensor is based on enthalpy changes caused by the chemical to be detected [*Wal 91*]. The physisorption process of a volatile chemical compound on or into a polymeric layer leads to a release or absorption of heat (ΔH) from the surroundings. With regard to other physical parameters like the mass m or the relative dielectric constant ε_r, phenomena related to heat changes are quite different; heat is non-specific and flows spontaneously from a warmer to a colder part of the system [*Jan 89*]. For the latter reason, heat shows a transient, i.e. non-equilibrium, behaviour which means that a temperature change can be detected only as long as a reaction proceeds. In contrast to almost all other chemical sensors, at thermodynamic equilibrium ($\Delta G = 0$) no heat production and therefore no measurable signal is observed. This results in the typical measurement curves of a calorimetric sensor upon exposure to a VOC (condensation heat) and the subsequent purge step (i.e. desorption with the corresponding vaporisation heat) which are exemplarily depicted in [*Fra 01, Ker 00, Ler 96*].

The sensor response curve expresses an overall process which can formally be divided into four principal steps [*Hee 94*]:

- Absorption and partitioning of the analyte, leading to
- Generation of heat, which results in
- Temperatures changes, that are transformed into
- Thermovoltage changes

To a first approximation, the integrated peak area of the sensor signal is proportional to the enthalpy change. In addition, calibration is necessary measuring a known heating power provided by a polysilicon heater on the membrane (for details see below). The thermovoltage change ΔU [V] is proportional to the derivative of the analyte activity (or concentration) as a function of time (da/dt):

$$\Delta U_{thermo} = A \cdot B \cdot V_{poly} \cdot \Delta H \cdot K \cdot (da/dt) \qquad \text{E2.4.2.1}$$

The device- and coating-specific constants A [K•s/J] and B [V/K] describe the translation of a generated molar absorption enthalpy ΔH [J/mol] via a temperature change into a thermovoltage. The sensitive polymer volume is expressed by V_{poly} and K denotes the partition coefficient.

The aforementioned phenomena lead to the following, contradictory prerequisites of a thermal sensor; the sensor has to allow the interaction between the sensitive layer and the analytes to be detected (representing a thermodynamically open system) and simultaneously, the sensing area has to be as thermally isolated as possible.

In general, CMOS calorimetric sensor systems consist of two dielectric, thermally isolated membranes (of several hundred μm in length), one of them coated with the chemically sensitive polymer, the uncoated one serving as a reference [*Kol 99*]. They are produced according to post-CMOS anisotropic KOH back etching processes from dielectric CMOS layers.

Polysilicon / aluminium thermopiles are sandwiched in between the dielectric membrane layers to record the temperature variations caused by the absorption and desorption of VOCs into the polymer. The hot junctions of the thermopiles are placed on the membrane (thermally isolated) which is covered with the sensitive layer. The cold junctions are attached to the bulk wafer (a good thermal conductor). The resulting temperature gradient between hot and cold junctions finally generates a thermovoltage. This sensing principal is based on the so-called *Seebeck*-effect; if two different metals or semiconductors are connected at a hot junction and a temperature difference is maintained between this hot junction and a colder part, then an open circuit voltage develops between the wires at the cold point. This thermovoltage is proportional to the difference in the temperature dependent *Galvani*-potentials at the two temperatures and hence, proportional to the temperature difference itself. The limits of detection for ethanol and toluene are approximately 80 ppm [*Fra 01*].

A schematic drawing as well as the microscope picture of an uncoated calorimetric sensor are shown in Figs. 2.4.2.1 and 2.4.2.2.
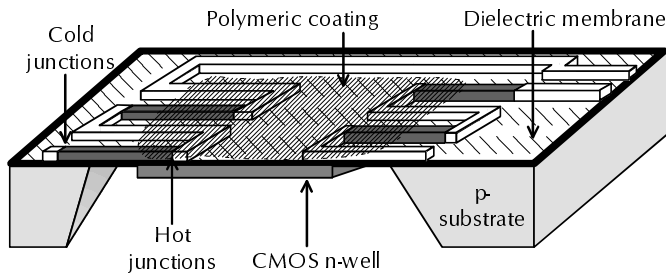
Fig. 2.4.2.1: Scheme of a calorimetric micro-sensor [Kol 99].
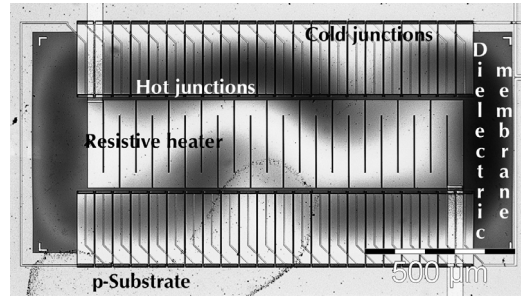
Fig. 2.4.2.2: Microscope picture of a microcalorimeter (top view); the meandric shadow indicates the tension of the membrane.

2.4.3 Capacitive Microsensor

The measurement principle of this kind of microsensor is based on the detection of capacitance changes. In practice, the relative changes of a sensing capacitor and a reference capacitor are determined. The reference capacitor is covered with a passivation layer of Si_3N_4[7]. The set-up consists of an interdigitated structure using the two metal layers of the CMOS process. Fig. 2.4.3.1 shows a cross-section of a interdigitated, two-metal-based sensor:
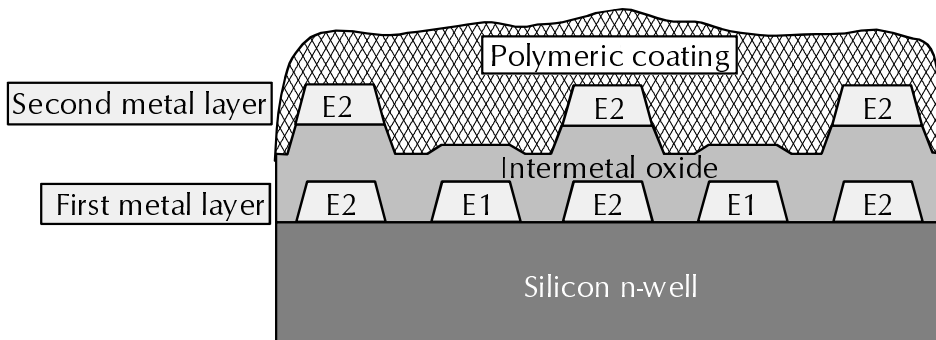
Fig. 2.4.3.1: Cross-section of a interdigitated capacitive sensor with two metal layers; E1 and E2 denote the electrodes 1 and 2 [Hag 99].

Electrode E1 is made out of the first metal layer, whereas electrode E2 comprises both metal layers. The "three-dimensional" design aims at increasing the number of electric field lines within the polymer and enhancing the sensitivity of the micorsensors towards changes in dielectric properties.

The electrode width and the spacing is 1.6 µm with a periodicity of 6.4 µm. Typical interdigitated capacitors consist of 130 and 128 fingers of electrode E1 and E2, respectively. The length of each is 800 µm.

---

[7] Due to the high dielectric constant of Si_3N_4 ($\varepsilon_r \approx 7.9$) almost all the electric field lines are confined within this passivation layer.

The readout circuitry is integrated on a chip; this requires the conversion of the difference between the polymer coated sensing and the reference capacitor already in the first stage of a fully differential second order $\Sigma\Delta$-modulator (for details see [*Hag 99, Kol 00*]).

The resulting sensor responses can be attributed to two effects which change the capacitance of the sensitive layer upon absorption of an analyte:

- Swelling, i.e. increase in the polymer's volume caused by the incorporation of analyte molecules.
- Capacitance change of the polymer/analyte system initiated by different dielectric properties of the analyte in comparison with the polymer.

By varying the polymer and its layer thickness, one effect can be more preferential than the other and thus, a "fine-tuning" towards a particular VOC to be detected with the capacitor is possible.

As a basic requirement, the thickness of the polymer coating has to be high enough to cover the top of the upper electrodes. Otherwise, if the layer height is less than half the electrode's periodicity, the swelling of the polymer upon analyte absorption leads to an increase in capacitance, regardless of the ε_r of the VOC. This effect originates from the increased polymer/analyte volume being penetrated by the field lines. Since air with a lower dielectric constant ($\varepsilon_r \approx 1$) is replaced by the swelling layer, an increased capacitance can be observed. For a layer of thickness larger than half the periodicity, another effect determines the capacitance change. Here, the ratio of the dielectric constants of both analyte and polymer ($\varepsilon_{r,analyte} / \varepsilon_{r,polymer}$) plays the dominating role. Two cases can be distinguished:

1. $\varepsilon_{r,analyte} / \varepsilon_{r,polymer} > 1 \Rightarrow$ capacitance is increased
2. $\varepsilon_{r,analyte} / \varepsilon_{r,polymer} < 1 \Rightarrow$ capacitance is decreased

An earlier publication [*Ste 95*] describes the aforementioned effects influencing the sensor capacitance and it gives the following formulae Eqs. E2.4.3.1 and E2.4.3.2 which allow calculation of the observed changes:

$$\varepsilon_{eff} = \varepsilon_{poly} \cdot (1 - VF_a \cdot c_a) + \varepsilon_a \cdot VF_a \cdot c_a \qquad \text{E2.4.3.1}$$

$$h_{eff} = h \cdot (1 + S_a \cdot c_a) \qquad \text{E2.4.3.2}$$

ε_{eff} = resulting effective dielectric constant of the polymer/analyte system

ε_{poly} = dielectric constant of the polymer

c_a = concentration of the analyte in the gaseous phase

$VF_a{}^{8}$ = volume fraction experimentally determined for every polymer/analyte-
combination

h_{eff} = resulting effective polymer thickness after analyte absorption

$S_a{}^{8}$ = experimental swelling coefficient of the polymer for the respective analyte

The equations indicate that the LODs of particular analytes depend on several parameters; typically the LODs are in the lower ppm-range, e.g. $LOD_{Toluene/PEUT} \approx 8$ ppm and $LOD_{Ethanol/PEUT} \approx 5$ ppm, both determined at 301 K [*Kol 00*].

2.4.4 Surface Wetting

The term "wetting" can be regarded as a contact angle and / or a capillary action phenomenon [*Ada 97*]. For the coating purposes both have to be considered.

Usually wetting means that the contact angle between a liquid and a solid is zero or so close to zero that the liquid spreads over the solid easily. Conversely, non-wetting means that the angle is greater than 90° and as a consequence the liquid tends to ball up and run off the surface easily. The central relationship of a contact angle situation is expressed by the *Young* equation [for details see *Ada 97*]. Fig. 2.4.4.2 illustrates the definition of contact angle:
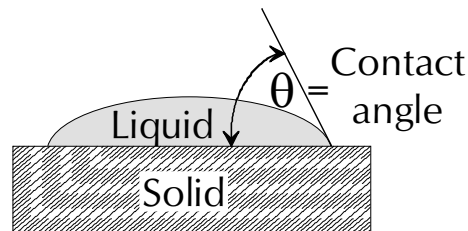
Fig. 2.4.4.2: Schematic drawing of the contact angle situation.

---

[8] VF_a and S_a are constants (applying Henry's law); their determination can be accomplished by mass sensitive or optical measurements.

The contact angle is dependent on the cohesive forces on the surface of the drop (surface tension) and the adhesive forces between the liquid and the solid. The larger are the adhesive forces the smaller is the contact angle. If the surface tension of the liquid is high the contact angle can be either large or small depending on the adhesive forces. However if the surface tension is low the contact angle is usually small since the adhesive forces always overcome the cohesive forces.

The thermodynamics of the wetting transition for polymer solutions are discussed by *Nakanishi et al.* [*Nak 83*], whereas *Schlangen et al.* investigated the influence of vapour adsorption on wetting [*Sch 94*]. The boundary surface tension between two coexisting surface phases was studied by *Perkovic et al.* applying a model with a van-der-Waals like theory [*Per 95*]. With regard to the importance of a precursor film on the wetting behaviour of pure liquids and solutions, in 1980 *Marmur et al.* reported in their discovery of the dependence of spreading rates on the size of the solid surface [*Mar 80*].

Besides the contact angle, the capillary action is an additional basic mechanism of the wetting phenomenon. This holds for all structured surfaces (including e.g. dust) because capillarity, i.e. the pressure difference across the curved surface, is the driving force. A detailed discussion is given in [*Ada 97*]. However, about the spreading behaviour of polymer solutions on Si wafers or even microsensors no relevant publication could be found.

2.5 References

[*Ada 97*]: A.W. Adamson, A.P. Gast, Physical chemistry of surfaces, John Wiley & Sons, Inc., New York, 1997.

[*Bee 98*]: K.R. Beebe, R.J. Pell, M.B. Seasholtz, Chemometrics: a practical guide, John Wiley & Sons, Inc., New York, 1998.

[*Bel 87*]: H.-D. Belitz, W. Grosch (Eds.), Food chemistry, Springer-Verlag, Berlin, 1987, pp. 128-200.

[*Bet 00*]: T.A. Betts, C.A. Tipple, M.J. Sepaniak, P.G. Datskos, Selectivity of chemical sensors based on micro-cantilevers coated with thin polymer films, Anal. Chim. Acta 422 (2000) 89-99.

[*Bod 97*]: K. Bodenhöfer, Chirale Erkennung mit Schwingquarzen, Ph.D. thesis, University of Tübingen, Tübingen (1997).

[*Cha 77*]: H.W.-S. Chan, Photo-sensitised oxidation of unsaturated fatty acid methyl esters. The identification of different pathways, J. Am. Oil Chem. Soc. 54 (1977) 100-104.

[*Cha 89*]: C. Chatfield, The analysis of time series: an introduction, 4th Ed., Chapmann and Hall, London, 1989.

[*Don 82*]: A. Donetzhuber, Characterisation of pulp and paper with respect to odour, Conference Proceedings of the International Symposium on Wood and Pulping Chemistry, The Ekman Dags, Vol. 4, 1982, pp. 136-138.

[*Ein 97*]: J.W. Einax, H.W. Zwanziger, S. Geiß, Chemometrics in environmental analysis, Wiley-VCH, Weinheim, 1997.

[*Fra 01*]: M. Frank, N. Kerness, S. Raible, C. Hagleitner, U. Weimar, H. Baltes, New coating procedure for CMOS chemical microsensors, ISOEN 01, Washington, 2001, accepted.

[*Gar 99*]: J.W. Gardner, P.N. Bartlett, Electronic noses – Principles and applications, Oxford University Press, Inc., New York, 1999, pp. 22-53.

[*Gil 83*]: J. Gilbert, J.R. Startin, A survey of styrene monomer levels in food and plastic packaging by coupled mass spectrometry-automatic headspace gas chromatography, J Food Sci. Agr. 34 (1983) 647-652.

[*Goe 91*]: W. Göpel, K.-D. Schierbaum, Definitions and typical examples, in: Chemical and biochemical sensors, part I, Sensors - a comprehensive survey, Vol. 2, VCH Weinheim, 1991, pp. 1-27.

[*Goo 96*]: R. Goodacre, D.B. Kell, Correction of mass spectral drift using artificial neural networks, Anal. Chem. 68 (1996) 271-280.

[*Gro 87*]: W. Grosch, Reactions of hydroperoxides – products of low molecular weight, in: Autoxidation of unsaturated lipids, H.W.-S. Chan (Ed.), Academic Press, London, 1987, pp. 95-139.

[*Gut 91*]: H. Guth, W. Grosch, A comparative study of the potent odorants of different virgin olive oils, Fat Sci. Technol. 9 (1991) 335-339.

[*Hag 99*]: C. Hagleitner, A. Koll, R. Vogt, O. Brand, H. Baltes, CMOS capacitance chemical microsystem with active temperature control for discrimination of organic vapours, Proc. of Transducers 99, Sendai, Japan (1999) 1012-1015.

[*Hee 94*]: A.W. van Heerwarden, P.M. Sarro, J.W. Gardner, P. Bataillard, Liquid and gas micro-calorimeters for (bio)chemical measurements, Sens. Actuators A 43 (1994) 24-30.

[*Hie 96*]: A. Hierlemann, Massensensitive Detektion flüchtiger organischer Substanzen mit modifizierten Polysiloxanen, Ph.D. thesis, University of Tübingen, Tübingen (1996).

[*Hie 00*]: A. Hierlemann, D. Lange, C. Hagleitner, N. Kerness, A. Koll, O. Brand, H. Baltes, Application-specific sensor systems based on CMOS chemical microsensors, Sens. Actuators B 70 (2000) 2-11.

[*Hil 94*]: K.I. Hildrum, B.N. Nilsen, M. Mielnick, T. Naes, Prediction of sensory characteristics of beef by near-infrared spectroscopy, Meat. Sci. 38 (1994) 67-80.

[*Hol 97*]: M. Holmberg, F.A.M. Davide, C. Di Natale, A. D'Amico, F. Winquist, I. Lundström, Drift counteraction in odour recognition applications: lifelong calibration method, Sens. Actuators B 42 (1997) 185-194.

[*Jam 98*]: S. Jamasb, S. Collins, R.L. Smith, A physical model for drift in pH ISFETs, Sens. Actuators B 49 (1998) 146-155.

[*Jan 89*]: J. Janata, Principles of chemical sensors, Plenum Press, New York, 1989, pp. 39-53.

[*Jur 00*]: P.C. Jurs, G.A. Bakken, H.E. McClelland, Computational methods for the analysis of chemical sensor array data from volatile analytes, Chem. Rev. 100 (2000) 2649-2678.

[*Kaw 95*]: S. Kawano, Progress in application of NIR and FT-IR in food characterization, in: Characterization of food – emerging methods, A.G. Gaonkar (Ed.), Elsevier Science B.V., Amsterdam, 1995, pp. 185-199.

[*Ker 00*]: N. Kerness, C. Hagleitner, A. Koll, A. Hierlemann, O. Brand, H. Baltes, CMOS calorimetric chemical gas sensors, Book of abstracts, IMCS 00 (2000) 201.

[*Kim 00*]: B.H. Kim, F.E. Prins, D.P. Kern, S. Raible, U. Weimar, Multicomponent analysis and prediction with a cantilever array based gas sensor, Proc. of EUROSENSORS XIV, Copenhagen, (2000) 699-702.

[*Koc 96*]: S.P. Kochhar, Oxidative pathways to the formation of off-flavours, in: Food taints and off-flavours, M.J. Saxby (Ed.), Blackie Academic & Professional (Chapman & Hall), London, 1996, pp. 168-225.

[*Kol 99*]: A. Koll, A. Schaufelbühl, N. Schneeberger, U. Münch, O. Brand, H. Baltes, C. Menolfi, Q. Huang, Micromachined CMOS calorimetric chemical sensor with on-chip low noise amplifier, Proc. of MEMS 99 (1999) 547-551.

[*Kol 00*]: A. Koll, CMOS capacitive chemical micorsystems for volatile organic compounds, Ph.D. thesis No. 13460, ETH Zurich, Zurich, 2000.

[*Kos 86*]: J. Koszinowski, O. Piringer, Evaluation of off-odours in food packaging – The role of conjugated unsaturated carbonyl compounds, J. Plastic Films and Sheeting 2 (1986) 40-50.

[*Kra 00*]: G. Krause, Charakterisierung integrierter, kapazitiver CMOS-Sensoren in Mikrosystemtechnik zur Gasanalyse, Diploma thesis, University of Tübingen, Tübingen, 2000.

[*Kum 99*]: A. Kummer, Charakterisierung kapazitiver chemischer Mikrosensoren, Diploma thesis, ETH Zurich, Zurich (1999).

[*Lan 01*]: D. Lange, Ph.D. thesis in compilation, ETH Zurich, Zurich, 2001.

[*Lan 99[a]*]: H.P. Lang, M.K. Baller, R. Berger, C. Gerber, J.K. Gimzewski, F.M. Battiston, P. Fornaro, J.P. Ramseyer, E. Meyer, H.J. Güntherodt, An artificial nose based on a micromechanical cantilever array, Anal. Chim. Acta 393 (1999) 59-65.

[*Lan 99[b]*]: D. Lange, C. Hagleitner, O. Brand, H. Baltes, CMOS resonant beam gas sensor with integrated preamplifier, Proc. Transducers 99, Sendai, Japan, (1999) 1020-1023.

[*Lan 98*]: D. Lange, A. Koll, O. Brand, H. Baltes, CMOS chemical microsensors based on resonant cantilever beams, Proc. Of SPIE Smart Structures and Materials 3328 (1998) 233-243.

[*Ler 96*]: J. Lerchner, J. Seidel, G. Wolf, E. Weber, Calorimetric detection of organic vapours using inclusion reactions with organic materials, Sens. Actuators B 32 (1996) 71-75.

[*Ler 99*]: J. Lerchner, A. Wolf, G. Wolf, Recent developments in integrated circuit calorimetry, J. Therm. Anal. 55 (1999) 212-223.

[*Mar 80*]: A. Marmur, M.D. Lelah, The dependence of drop spreading on the size of the solid surface, J. Colloid Interface Sci. 78 (1980) 262-265.

[*Mar 93*]: H. Martens, T. Næs, Multivariate calibration, John Wiley & Sons, Chichester, 1993, pp. 237-260.

[*Mas 97*]: D.L. Massart, B.G.M. Vandeginste, L.M.C. Buydens, S. de Jong, P.J. Lewi, J. Smeyers-Verbeke, Handbook of chemometrics and qualimetrics: Part A, Elsevier Science B.V., Amsterdam, 1997, pp. 593-601.

[*Mau 99*]: M. Maute, S. Raible, F.E. Prins, D.P. Kern, H. Ulmer, U. Weimar, W. Göpel, Detection of volatile organic compounds (VOCs) with polymer-coated cantilevers, Sens. Actuators B 58 (1999) 505-511.

[*Mil 97*]: C. Milo, G.A. Reineccius, Identification and quantification of potent odorants in regular-fat and low-fat mild Cheddar cheese, J. Agric. Food Chem., 45 (1997) 3590-3600.

[*Nak 83*]: H. Nakanishi, P. Pincus, Surface spinodals and extended wetting in fluids and polymer solutions, J. Chem. Phys. 79 (1983) 997-1003.

[*Ohl 90*]: G. Ohloff, Riechstoffe und Geruchssinn – Die molekulare Welt der Düfte, Springer-Verlag, Berlin, 1990.

[*Ott 97*]: A. Ott, L.B. Fay, A. Chaintreau, Determination and origin of the aroma impact compounds of yoghurt flavour, J. Agric. Food Chem. 45 (1997) 850-858.

[*Ott 99*]: M. Otto, Chemometrics – Statistics and computer application in analytical chemistry, Wiley-VCH, Weinheim, 1999.

[*Pas 83*]: N. Passy, Off-flavours from packaging materials in food products, in: Instrumental analysis of foods, Vol. 1, Academic Press, Inc., New York, 1983, pp 413-421.

[*Per 95*]: S. Perkovic, E.M. Blockhuis, E. Tessler, B. Widom, Boundary tension: from wetting transition to pre-wetting critical point, J. Chem. Phys. 102 (1995) 7584-7594.

[*Sal 98*]: M.L. Salit, G.C. Turk, A drift correction procedure, Anal. Chem. 70 (1998) 3184-3190.

[*Sch 88*]: K.O. Schnabel, H.-D. Belitz, C. von Ranson, Investigations on the structure-activity-relationship of odorous substances. Communication I. Detection thresholds and odour qualities of aliphatic and alicyclic compounds containing oxygen functions, Z. Lebensm. Unters. Forsch. 187 (1988) 215-223.

[*Sch 94*]: L.J.M. Schlangen, L.K. Koopal, M.A. Cohen Stuart, J. Lykluma, Wettability: thermodynamic relationships between vapour adsorption and wetting, Colloids and Surfaces A: Physicochem. Eng. Aspects 89 (1994) 157-167.

[*Sch 95*]: P. Schieberle, New developments in methods for analysis of volatile flavor compounds and their precursors, in: Characterization of food – emerging methods, A.G. Gaonkar (Ed.), Elsevier Science B.V., Amsterdam, 1995, pp. 403-431.

[*Sha 83*]: S. Shang-zhi, G. Stanley, High-performance liquid chromatographic analysis of chlorophenols in cardboard food containers and related materials, J. Chromatogr. 267 (1983) 183-189.

[*Sne 76*]: R.D. Snee, Validation of regression models: Methods and examples, Technometrics 19 (1976) 415-428.

[*Sod 85*]: L. Soderhjelm, S. Eskelinen, Characterisation of packaging materials with respect to taint and odour, Appita 38 (1985) 205-209.

[*Ste 95*]: F.P. Steiner, A. Hierlemann, C. Cornila, G. Noetzel, M. Bächtold, J.G. Korvink, W. Göpel, H. Baltes, Polymer coated capacitive microintegrated gas sensor, Proc. of Transducers 95, Stockholm, Vol. 2 (1995) 814-817.

[*Tic 96*]: P. Tice, Packaging materials as a source of taints, in: Food taints and off-flavours, M.J. Saxby (Ed.), Blackie Academic & Professional (Chapman & Hall), London, 1996, pp. 226-263.

[*Ulm 99*]: H.E. Ulmer, Hybride modulare Sensorsysteme für die Gasanalytik und Olfaktometrie, Ph.D. thesis, University of Tübingen, Tübingen (1999).

[*Wal 91*]: P.T. Walsh, T.A. Jones, Calorimetric chemical sensors, in: Sensors, Chemical and biochemical sensors, Vol. 2, Part I, W. Göpel, M. Kleitz, I. Lundström, T. Seiyama (Eds.), VCH Weinheim, Germany, 1991, pp. 529-574.

3 EXPERIMENTAL

3.1 Studies between GC/MS-Coupling, Gas Sensor Arrays and Sensory Panels

3.1.1 The Hybrid Modular Sensor System (MOSES II)

Parts of the investigations on gas sensor arrays were carried out with the hybrid Modular Sensor System (MOSES II) [*Mit 98*] which consists of two modules with different transducer principles. The quartz crystal microbalance (QCM)- module comprises eight individual sensors with varying polymer coatings. The QCMs are coated by an air-brush technique, with the polymers appropriate to suit their specific applications. The individual coatings are described in [*Ulm 99*] pp. 49 - 52. The second module contains eight commercially available metal oxide-based semiconductor gas sensors (MOXs) which were selected due to their individual sensitivity and selectivity (see also [*Ulm 99*] p. 46). A schematic overview of the whole system including electronics and data processing is shown in Fig. 3.1.1.1. The sample's headspace was carried through the measurement chambers of the modules sequentially.
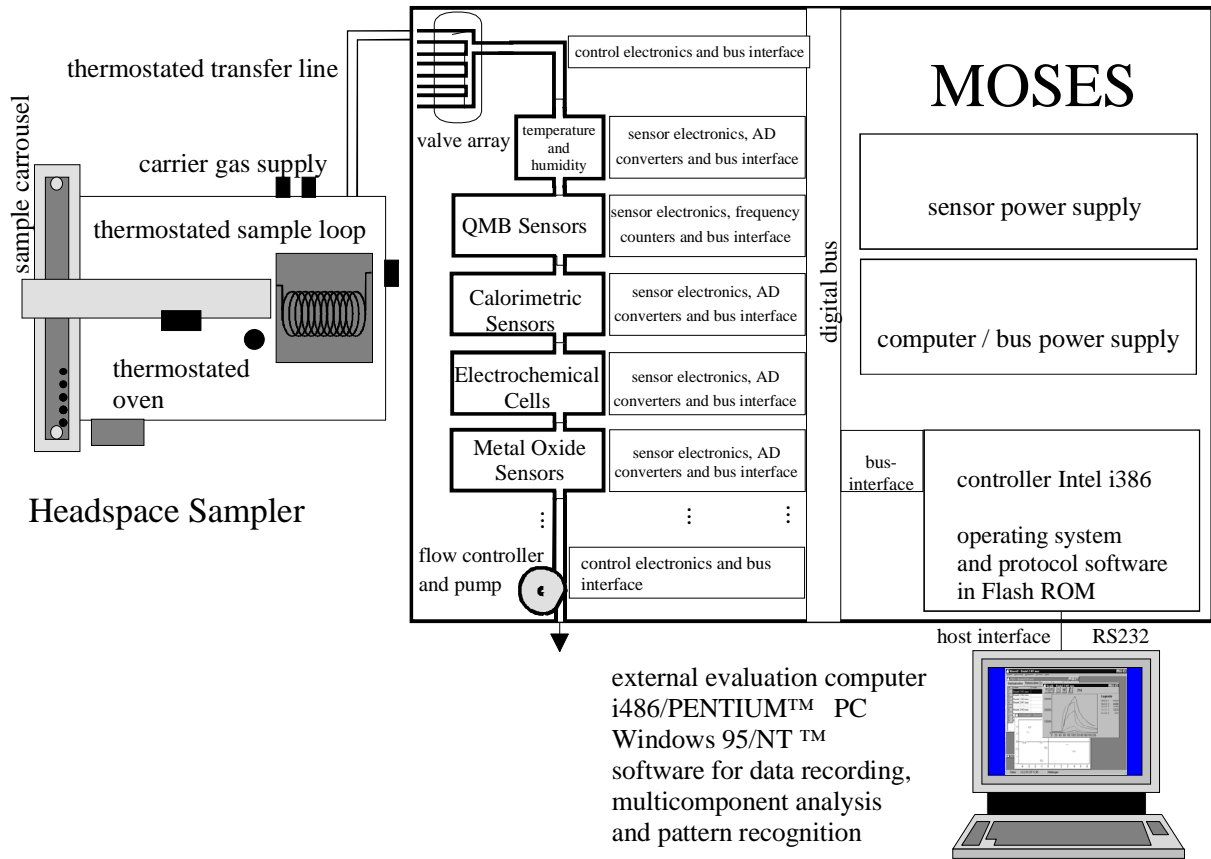
Fig. 3.1.1.1: General MOSES layout: Independent modules communicate with the system controller via a digital bus. Several alternative input units may be chosen. Our investigations were carried out using the QCM- and MOX- modules (for details see [Mit 98]).

The measurements with the sensor array were carried out according to the specific application with the following set of parameters.

Parameter	Application	
	Vegetable oil	*Packaging materials*
Headspace sampler		
Temperatures [°C]:		
Oven	90	85
Sampling loop	130	110
Transfer line	160	120
Time intervals [min]:		
Sample equilibration	20	60
Pressurisation	0.5	1
Vent	0.3	0.5
Vent equilibration	0.05	0.05
Injection (GC/MS // Sensor Array)	2.5 // 1	2.5 // 1
Pressures [bar]:		
Auxiliary pressure on headspace	0.3	0.5
Flows [ml/min]:		
Total flow through the system	1.5 // 20	1.5 // 15
Sensor array		
Temperatures [°C]:		
QCM chamber	25	25
Time intervals [s]:		
Sampling rate ("tick rate")	1.2	1.2
Measurement cycle	360	360
Gate frequency counter	1	1
Voltages [mV]:		
MOX potentials	1000	102
Heater voltage	4700	4700

Table 3.1.1.1: Measurement parameters of the headspace autosampler and the MOSES-system for the investigations of vegetable oil and packaging materials.

3.1.2 The Gas Chromatography / Mass Spectrometry System

The gas chromatography/mass-spectrometry (GC/MS) investigations were performed using a Hewlett-Packard gas chromatograph (HP 6890 GC) and a Hewlett-Packard mass selective detector (HP 5973 MSD). The capillary column was 0.32-mm-i.d. with an intermediate polarity polysiloxane phase (HP-VOC, Hewlett-Packard). The stationary-phase film thickness was 1.8 µm, and the column's length was 60 m. Helium (purity 6.0, Messer-Griesheim, Germany) was used as the carrier gas. The GC/MS system was coupled to a Hewlett-Packard headspace auto-sampler (HP 7694 HSS). The fully automated and reproducible sample uptake is maintained by the carrier gas supply through a thermostated injection needle, sample loop and transfer-line to the GC inlet.

For the investigations of the packaging materials the following sample conditioning (for headspace parameters see Table 3.1.1.1) and chromatographic procedure were carried out (see Table 3.1.2.1):

Parameter	Application	
	Vegetable oil	*Packaging materials*
Gas chromatograph (GC)		
Temperatures [°C]:		
Injector inlet	200	200
Oven	40 for 6 min, ramp of 7/min to 230, 230 for 6 min	40 for 6 min, ramp of 7/min to 230, 230 for 6 min, ramp of 10/min to 250, 250 for 5 min
GC/MS interface	270	270
Flows [ml/min]:		
Total flow through the system	1.5	1.5
Mass selective detector (MSD)		
Temperatures [°C]:		
Ion source	230	
Quadrupole	150	
Acquisition:		
Scan mode	33-220 amu[1]	

Table 3.1.2.1: Measurement parameters of the GC/MS system for the investigations of vegetable oil and packaging materials.

3.1.3 Sensory Panel (for packaging materials only)

To assess the quality of wrapping foils a sniff test [*Nes 98*] was performed by a sensory panel of the Nestlé Research Centre in Vers-chez-les-Blanc. The sniff test belongs to the group of quantitative descriptive analyses. This means that normally only the evaluation of one type of product is asked for (the panel members are trained in using the particular product or material involved), the tests are repeated and the results undergo statistical analysis. The sensory panel (6-12 members) was especially trained for the evaluation of packaging materials. The panel has classified the global odour of the samples on a scale of 0 to 4:

---

[1] amu = atomic mass unit

0 ≡ no difference to a given reference

1 ≡ hardly perceptible difference (not definable)

2 ≡ slight difference (just definable)

3 ≡ large difference (clearly definable)

4 ≡ very large difference to the reference

The limiting odour score value is 2.5 (median score); only packaging materials with lower odour values are permitted to wrap the foodstuff. For the sniff test, 1000 cm^2 of the packaging material are stored at 40° C for one hour in a glass jar. Subsequently, the jar is opened and the headspace is evaluated by the panel member.

3.1.4 Artificial Ageing of Vegetable Oil

The corn oil[2] used for the ageing experiment was delivered directly by the co-operation partner. On arrival 3 l of the oil were stored in a freezer at –20° C. Vials for re-calibration (pure, fresh oil as well as pentanal-doped oil) were filled from this source. Another 2 l underwent daily irradiation with a UV-Lamp (power: 12W, λ = 254nm, Heraeus, Germany). The irradiation time was 30 min per day (except weekends). The 2 l- flask was wrapped in aluminium foil in order to protect the oil from ordinary daylight.

In varying intervals the samples were taken for both investigations by the sensor array and the GC/MS. Especially at the beginning and the end of the investigation, the intervals became rather short (less than one week). For the GC/MS measurements, three samples of the artificially aged oil were used. The chromatograms obtained were then compared to check for outliers / anomalies. If no significant deviations for a particular compound could be found, the areas under a peak (integration results) were averaged over the three individual samples. The identification was achieved by comparison with library spectra included in the GC/MS software package or in ambiguous cases, the retention time of the pure substances was additionally determined (see chapters 4.1.1 *GC/MS Investigations* and 4.1.2. *Sensor Array Investigations*).

For the MOSES- system measurements four aged samples were immediately analysed. The sum of all the data from the samples investigated at this stage built the training data set. In addition, four oil samples from each ageing stage were kept in the freezer until the whole experiment finished after three months. Then, these samples were also measured; they represented the test data whose age was finally predicted on the basis of the training model. The whole procedure of the

---

[2] The brand name is "Mazola – Maiskeimöl"

data analyses is described in detail later on, together with the investigations of the packaging materials.

3.1.5 Sample Preparation of the Packaging Materials

The variety of packaging materials covers nearly all the needs of food manufacturers. In most cases wrapping foils have a complex structure consisting of different kinds of layers. A selection of all the packaging materials investigated in the course of this work is given in Tables 3.1.5.1 and 3.1.5.2.

Sample set 1	
Packaging material no.	*Specification*
1	Slip agent / print / met OPP / nitrocellulose lacquer
2	OPP / print / OPP / cold seal
3	OPP / print / OPP / cold seal
4	Slip agent / print / OPP / cold seal
5	Slip agent / print / met OPP / nitrocellulose lacquer
6	Slip agent / print / met OPP / nitrocellulose lacquer
7	OPP / print / OPP / cold seal
8	Slip agent / print / met OPP / cold seal

Table 3.1.5.1: Listing of packaging materials belonging to sample set 1. Although they have in some cases the same specification, the printing was always different. OPP = oriented polypropylene, met = metalized.

Normally, packaging material producers provide the food industry with wrapping rolled up on big reels. For outgassing off-odours the materials are re-worked and re-evaluated. This procedure is often quite simple; the packaging is rolled off again, it is aerated in an air stream and finally rolled up once more. This ventilation process enables the packaging supplier to ameliorate the product's quality because most of the solvents disappear – or are at least of negligible concentration. However, ventilation with air causes other problems, since the wrapping often comprises oxidizable compounds which are then transformed to the aforementioned aldehydic substances (see chapter 4.2.2 *GC/MS Investigations*).

A similar procedure was carried out on a paper- based packaging material (sample set 2, see Table 3.1.5.2). The aeration was carried out in a cylindrical glass set-up with a volume of 113 l at ambient temperature (20-22° C). The vessel

either had a gas inlet at the bottom and an outlet on the top, or it was sealed gas-tight to prevent the samples getting into contact with the surrounding atmosphere. A rack was placed within the container on which the packaging material strips could be hung up. They were exposed to an air and nitrogen stream, respectively, for 1, 3, 7, 24 and 48 hours.

Sample set 2	
Packaging material no. **(Ventilation time in hours)**	**Specification**
9 (0h), **10** (1h), **11** (3h), **12** (7h), **13** (24h), **14** (48h)	Paper / aluminium / low density PE / Surlyn™

Table 3.1.5.2: Listing of packaging materials belonging to sample set 2. The specification is the same for all materials; they only differ in the time of exposure to an air-stream (see ventilation experiments).

Before evaluation by GC/MS or the sensor system, all packaging materials (of sample sets 1 and 2) were cut into 100 cm^2 pieces. They were placed in 20 ml headspace vials which were sealed gas-tight by a silicon/PTFE- (polytetra-fluoroethylene) septum. All GC/MS analyses of each wrapping species were carried out three times. In order to create a sensor array calibration database, 18 samples, one of each material type, were measured in a random order. Later, a further 9 samples of each packaging species were analysed to verify the sensor system's performance in terms of correct sample recognition and odour score prediction, the testing phase. For the packaging materials nos. 4, 5, 6 and 8, two different batches ("a" and "b") were available, both of which were analysed by GC/MS and the sensor system.

In addition, a mixture of specific chemical compounds (the so- called standard sample) having defined analyte concentrations was measured (in parallel with the packaging materials) to monitor the long-term stability of the sensor signals. This mixture consisted of toluene, n-octane, propan-1-ol and ethyl acetate (ratio 1:1:1:1) diluted in PEG 400 and is hereinafter called TOPE standard.

3.1.6 Evaluation of GC/MS and Sensor Array Data

GC/MS: The GC/MS data evaluation was performed by the Hewlett-Packard MSD Productivity ChemStation Software Rev. B.00.01 which enabled qualitative and semi-quantitative predictions by taking the retention time and the peak areas into account. Here, semi-quantitative means that the peak areas are given in arbitrary units; a calibration with standards to determine the concentration in ppm

was not carried out[3]. Since the concentrations were only considered comparatively, the absolute amount of a substance was not crucial. In order to identify the peaks, pure compounds were chromatographed and the NIST (National Institute of Standards & Technology, Gaithersburg, USA) mass spectrum library served as reference data bank.

Due to the relatively high film thickness (1.8 µm) of the chromatographic column (HP-VOC), a certain amount of "column bleed" at higher oven temperatures was unavoidable. Hence, at longer retention times the chromatograms showed a background which was finally subtracted (by an implemented function in the software) to result in mass spectra with only few peaks derived from the column film.

Sensor array: Before the sensor data could be used as input for a PCA (<u>P</u>rincipal <u>C</u>omponent <u>A</u>nalysis), they were pre-processed in order to eliminate influences on these values caused by drift / fluctuation. Within a measurement sequence several standards for re-calibration were also evaluated. Then for each sensor, the mean value of a particular feature (here, the signal height, i.e. signal's maximum subtracted from the baseline) upon exposure to the re-calibration samples was calculated:

$$\overline{R}_x(m_y) = \frac{1}{n}\sum_n R_x(n, m_y) \qquad\qquad \text{E3.1.6.1}$$

R_x = feature of sensor x upon exposure to a re-calibration sample, n = number of re-calibration samples, m_y = particular measurement sequence.

This procedure was performed for each, temporally different measurement sequence (y = 1, 2...), resulting in the corresponding mean values ($\overline{R}_x(m_y)$). A comparable treatment was carried out on the remaining samples. To compensate for drift / fluctuation phenomena, the ratio of the $\overline{R}_x(m_y)$ of two measurement cycles was calculated:

$$f_x(m_y, m_{y'}) = \frac{\overline{R}_x(m_y)}{\overline{R}_x(m_{y'})} \quad y' > y \qquad\qquad \text{E3.1.6.2}$$

---

[3] It is possible that within one sample equilibration step a complete volatilisation into the headspace will not occur. It could be demonstrated that although the heating temperature during sample equilibration was much higher than the boiling points of the substances to be detected, only about 50% of the particular compound was liberated into the headspace. A much used technique for determining the concentration of substances from headspace analysis is based on <u>m</u>ultiple <u>h</u>eadspace <u>e</u>xtraction (MHE, for details see [*Kol 97*]).

The individual sensor response values upon exposure to a "real" sample of the measurement sequence $m_{y'}$ are then multiplied by the corresponding $f_x(m_y, m_{y'})$.

A graphical, simplified depiction of this procedure is given in Figs. 3.1.6.1 and 3.1.6.2. There, a formal distinction between two cases is made; in the first case – which resembles more the application of oil spoilage- the system / sensors are calibrated by the exposure to two different standards (step 1 at day x). As an example, one of the standards (marked with an asterisk at a concentration of about 500) might be the fresh, unspoiled corn oil and the other one (marked with a reversed triangle at a concentration of about 1500) corresponds to the oil doped with 100 ppm pentanal. Subsequently, an unknown sample is measured (step 2 at day y). According to the calibration carried out at day x, the predicted concentration would be ≈ 1300. In order to prove if this prediction is true, a further (re-) calibration is performed (step 3 at day y). Obviously, in comparison with the first calibration, the sensor responses changed (the possible reasons are not discussed here, see chapter 2.3 *Sensor Drift-Evaluation and Compensation*). Based on the re-calibration the concentration of the unknown sample is now predicted to be about 800 (step 4).
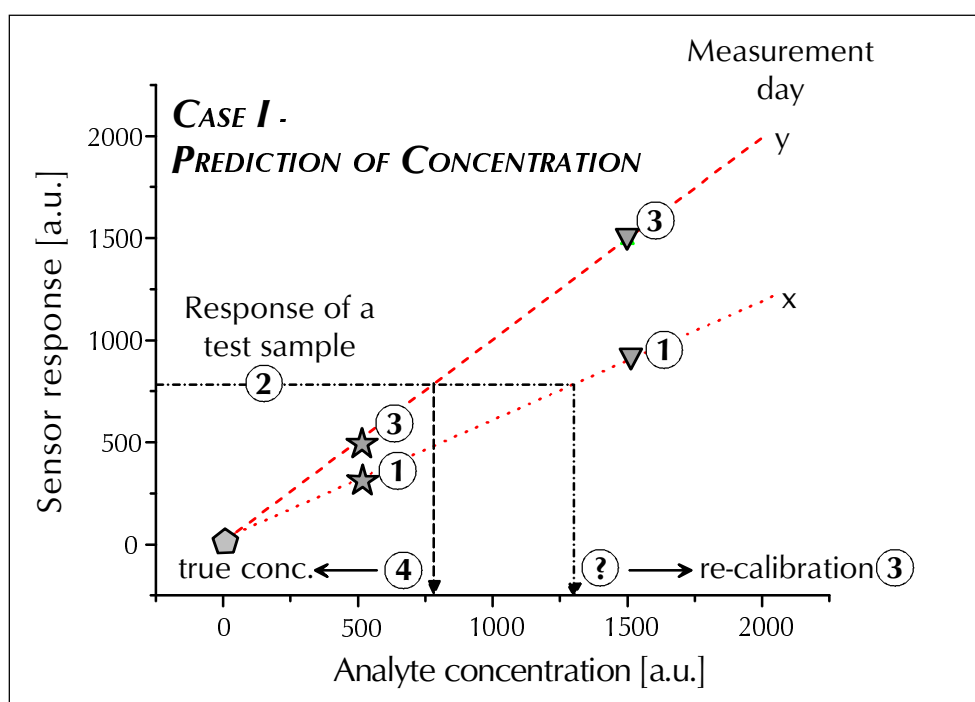
Fig. 3.1.6.1: Re-calibration to predict true concentrations.

In the second case, re-calibration has to be done for a slightly different use which is more related to the packaging material application. The first procedure is again the calibration of the system / sensors at the beginning of the investigations

(step 1 at day x). In this example, the TOPE standard might be represented by the upright triangle (concentration of 500) and a particular packaging material sample by the square (concentration of 1500). If the test sample, i.e. a sample with exactly the same specification, printing etc., in a later measurement causes another (higher) sensor response (step 2 at day y), the question arises whether is sample is a real outlier or if the deviation is based on an error within the measurement procedure. The re-calibration (step 3 at day y) with the TOPE standard determines the new calibration curve. Note that the re-calibration was performed with the TOPE standard only. If the test sample lies within the confidence bands (e.g. 95%) determined by the re-calibration, it will not be considered an outlier. Especially in the packaging material application this problem has often to be solved, since packaging with an odour score lower than 2.5 (which is related to a particular sensor response) are used to wrap the foodstuff and materials with odour scores > 2.5 (outliers) are rejected.
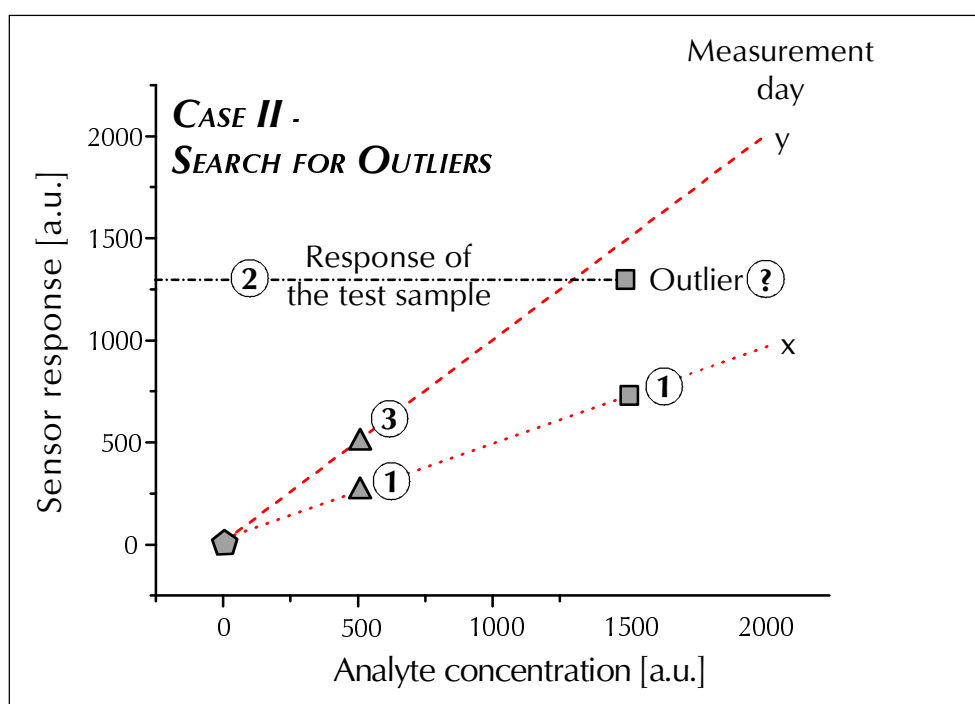
Fig. 3.1.6.2: Re-calibration to search for outliers.

The two cases discussed in Figs. 3.1.6.1 and 3.1.6.2 are –strictly speaking- only valid if the sensors respond linearly to concentration changes because the whole mathematical procedure behind is also based on linear methods. Therefore, the use of MOXs might introduce a systematic error into the calibration since the concentration dependency of MOXs is usually described by a power law. This error can be minimised if the standards used for re-calibration are as similar as possible to the samples investigated (see e.g. Table 4.1.2.1).

The corrected gas sensor array data were subsequently evaluated by a PCA as a standard pattern recognition algorithm [*Hol 95*, *Ekl 99*], implemented in the MOSES software (Version 4.32, AppliedSensor, Reutlingen, Germany). The correlation between sensor array data and human sensory assessments has been carried out using the software package "The Unscrambler" (Version 7.01, Camo, Trondheim, Norway).

Any multivariate analysis (e.g. PCA, PCR) has to comprise some validation to assure that its results can be extrapolated to new data. This requires two independent procedures in the computation of each model component (principal component, PC); the calibration and the validation, each with its own set of samples, training and test samples, respectively. In the first step a calibration is performed where a model is fitted to the available data in order to achieve the best possible description. Then a validation is executed to obtain an insight into how well the model would describe future samples. For this purpose the test samples are applied to the calibrated model in order to predict new values for those samples. The predicted values are then compared to the "true" ones. This yields a prediction residual that can be used to compute a validation residual variance (hereinafter called VRV) or a root mean square error of prediction (RMSEP). The latter represents the average uncertainty that can be expected when predicting Y-values for new samples, expressed in the same units as the Y-variable. The general equation to calculate the RMSE is given in the chapter *Results and Discussion*. This quantity is valid provided that the new samples are similar to the ones used for calibration, otherwise the prediction error might be much higher. The same holds for the VRV which is normally used to find the optimum number of model components (principal components, PC). If the VRV has a minimum value the optimum number of PCs is found and the lowest prediction error can be expected.

3.2 Miniaturised Gas Sensor System

3.2.1 Wafer Cleaning Procedures and Silanisation

The complete wetting of the area to coat was a fundamental requirement. Therefore, in order to obtain homogeneous, smooth layers a pre-treatment of the substrate's surface by silanisation was carried out. The cleaning of the silicon based substrates was essential to subsequent silanisation experiments. This holds for all studies of various polymers before examination of their behaviour on a particular surface.

The very first cleaning step consisted of a 15 min ultrasonic treatment, the substrates being placed in acetone. Then, two different methods were tested, one

of which was based on a treatment with "Piranha-solution" (mixture of H_2SO_4 and H_2O_2, volume ratio 3:1). The wafers were placed in this solution and an ultrasonic treatment of 15 min followed. Finally, the substrates were rinsed with deionised water and dried under nitrogen. Obviously, the "Piranha-solution" is together with the ultrasonic treatment too much of an aggressive approach as it caused the roughness of some wafer surfaces to increase dramatically (see chapter 4.3.2 *Polymer Morphology and Silanisation*).

The second, and more gentle, cleaning procedure was based on oxygen plasma impact. After the aforementioned purification with acetone, the dried substrates were placed in an oxygen plasma incinerator (100-E Plasma System, Technics Plasma GmbH, Kirchheim bei München, Germany) for 2 min; the O_2-pressure was 0.8 bar and the power 300 W. SEM investigations confirm that the topography of the surface itself is not affected. A schematic drawing of both procedures is shown in Fig. 3.2.1.1.
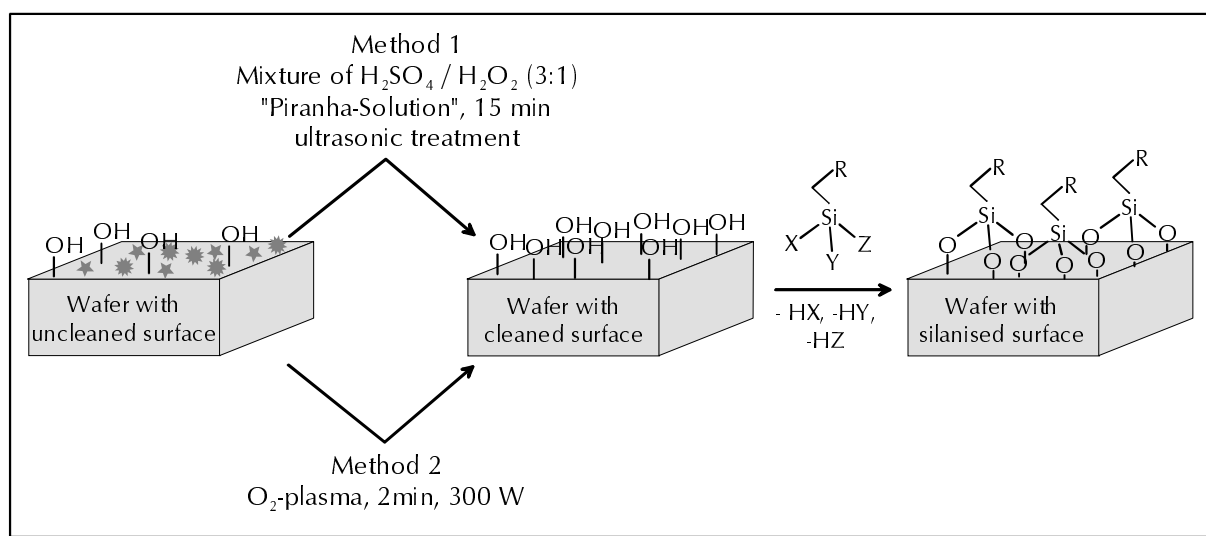
Fig. 3.2.1.1: Silanisation procedure of wafer substrates (the ligands X, Y and Z of the silane can be $-OCH_3$, $-OC_2H_5$ and $-Cl$).

After the cleaning step (method 2 preferred), the wafers were placed in a solution of 20 µl silanisation agent and 4 ml toluene and shaken gently for 30 min. Finally, the wafers were rinsed with pure toluene and dried in a N_2-stream [*Her 97*].

Preliminary tests should demonstrate that:

- Silanisation is possible without destruction of or change in the wafer's surface. The roughness should not be increased by the silanisation procedure.
- A given silanisation agent provides the same surface conditions, independent of the original substrate.
- A variety of silanisation agents covers a huge range of different surface polarities.

The following substances were chosen as silanisation agents[4]; their chemical structures are shown in Fig. 3.2.1.2:

- Trichloroctadecylsilane (TCOS)
- 3-Aminopropylmethyldiethoxysilane (APMDS)
- 3-Cyanopropyltrichlorosilane (CPTS)
- (3-Glycidoxypropyl-)trimethoxysilane (GOPTS)
- (Dichloromethyl-)trichlorosilane (DCMTCS)
- (3,3,3-Trifluoropropyl-)trichlorosilane (TFPTCS);

To check the polarity of the substrates surface contact angle measurements (static mode) with a system from KSV Ltd. (CAM 200) were performed. Water was used as the wetting liquid.

---

[4] The silanisation agents were purchased from Merck GmbH, Darmstadt (Germany) and ABCR GmbH & Co. KG, Karlsruhe (Germany).
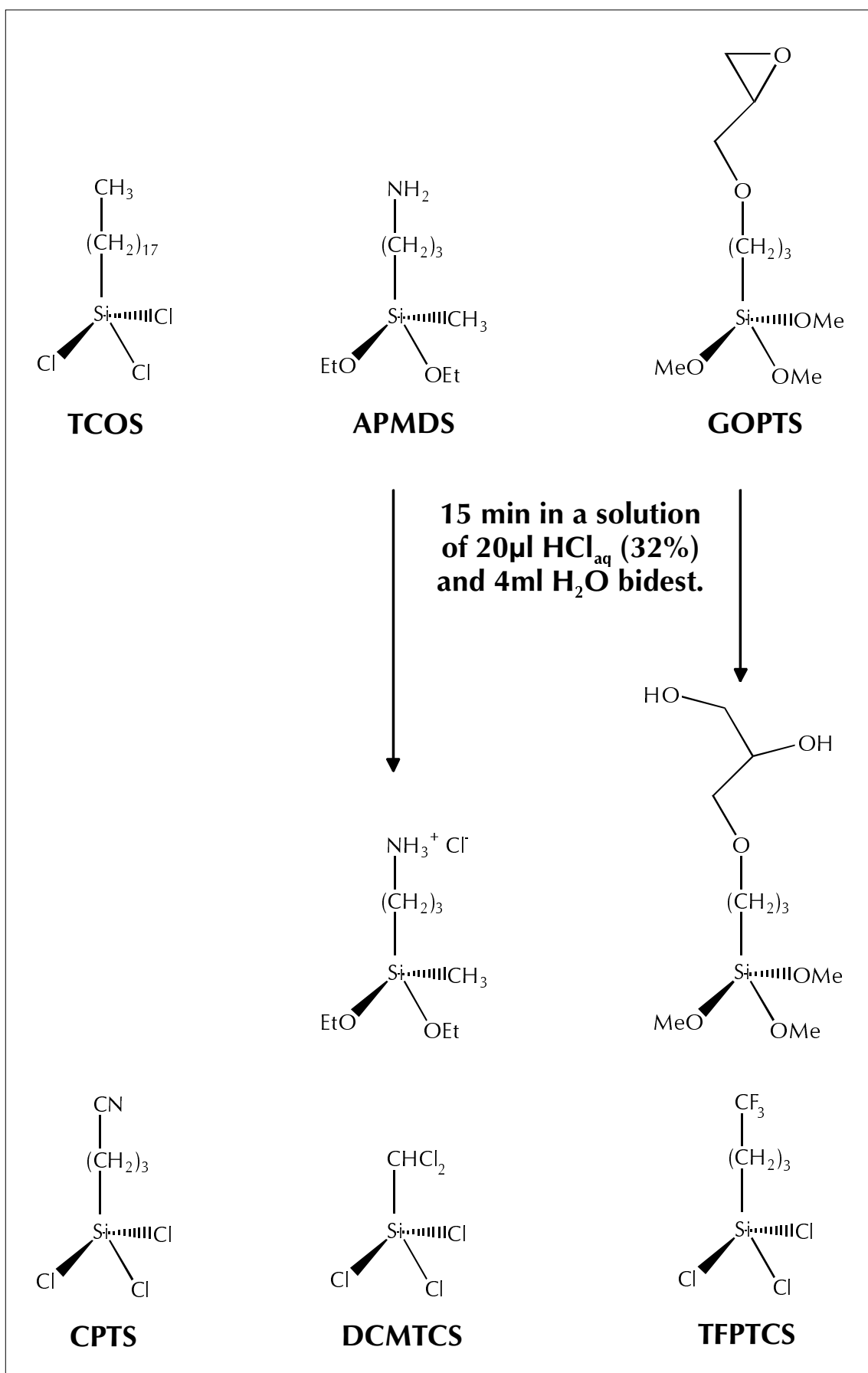
Fig. 3.2.1.2: Chemical structures of the silanisation agents used.

3.2.2 Chemically Sensitive Layers

The coating materials of the microsensor arrays housed in the hand-held device were selected according to the following requirements; different sensitivity towards various analytes (as far as is known from the literature), long-term stability (i.e. no polymer shrinkage or even irreversible change in structure) and formation of homogeneous layers after deposition on the sensing areas of the micro-structures. In total, 16 polymers (listed alphabetically in Table 3.2.2.1) were investigated:

Name	Abbreviation
Ethylcellulose	EC
Poly-(acrylonitrile-co-butadiene)	PANB
Poly-(3-aminopropyl-)methylsiloxane	PAPMS
Poly-(3-cyanopropyl-)methylsiloxane	PCPMS
Poly-(3-cyanopropyl-)phenylsiloxane	PCPPS
Polydimethylsiloxane	PDMS
Polyepichlorohydrine	PECH
Polyetherurethane	PEUT
Polyethylenimine	PEI
Polyisobutylene	PIB
Polymethyloctadecylsiloxane	PMODS
Polymethyloctylsiloxane	PMOS
Polymethyltetradecylsiloxane	PMTDS
Poly-(3,3,3-trifluoropropyl-)methylsiloxane	PTFPMS
Polysulfone	PSU
Polyvinylpyrrolidone	PVP

Table 3.2.2.1: Polymers investigated as sensing layers for microsensors.

Before deposition the polymers were dissolved in a mixture of chloroform and perchloroethylene (ratio 1:1). The concentration was 10 mg of polymer per 1 ml of this mixture.

3.2.3 Deposition Techniques

The successful deposition of chemically sensitive layers is dependent on the following conditions:

- If the polymers are applied as a dilution in organic solvents, the tool[5] size should be slightly smaller than the surface area to be coated afterwards, because normally the deposited drop spreads on the surface.
- The solvent has to fulfil two requirements. Firstly, it should completely dissolve the polymer. In most cases, a concentration of 10 mg polymer in 1 ml solvent was used. Secondly, the evaporation of the solvent has to be slow enough to deposit the solution on the target. Otherwise, the polymer will clog parts of the tool or the amount of polymer which is placed on the substrate will be irreproducible.

A variety of tools depending on the area and the geometry of the surface to be coated was tested. Native Si was used for preliminary investigations into the wetting abilities of the polymers, the determination of layer thickness etc. For these purposes, different structures were cut on Si wafers with a wafer-saw. The dimensions of the cut areas were according to the sensing parts of the CMOS devices. The wafer cleaning was based on the O_2 plasma procedure described in chapter 3.2.1 *Wafer Cleaning Procedures and Silanisation*. The coating procedure is schematically displayed in Fig. 3.2.3.1.
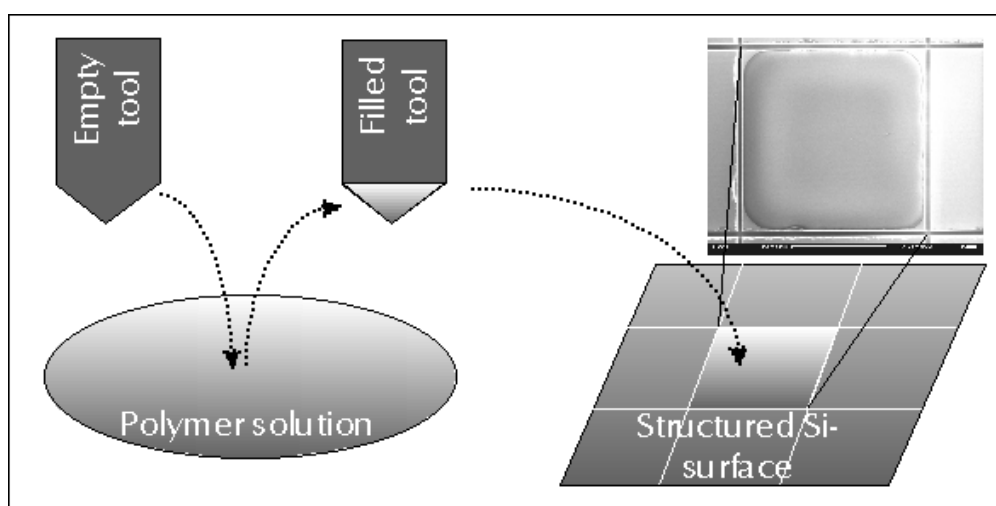
Fig. 3.2.3.1: Schematic drawing of the deposition procedure.

One type of deposition tools is based on small instruments made out of thin molybdenum film. Tools for the coating of different areas were manufactured out

---

[5] "Tool" is any component which can be used to transfer a polymer or its solution.

of molybdenum foil (thickness of 200 µm). The following table (Table 3.2.3.1) gives an overview on the available tools. The effective coating areas of the tools were derived from light microscope measurements.

Tool No.	Area [µm^2/10^3]	Tool No.	Area [µm^2/10^3]
1	734	11	188
2	916	12	260
3	498	13	91
4	21	14	40
5	591	15	301
6	440	16	416
7	115	17	505
8	281	18	1103
9	1014	19	378
10	650	20	567

Table 3.2.3.1: Inner dimensions of Mo- tools

More details on this coating mechanism cannot be given due to patent pending[6].

The first tools were prepared manually and were therefore not very reproducible regarding their size. Furthermore, their minimum feature size was limited. To circumvent these problems, further tools were produced with CNC machines of high accuracy to achieve requested precision.

As a tool material molybdenum proved to be of great rigidity which decreased the proneness to vibrations during the drop deposition. This ensures a more accurate shape of the polymer drop.

However, tools with dimensions in the range of 100 µm × 100 µm and smaller can only be obtained with difficulties by the state-of-the-art CNC machining. In order to deposit polymer drops on the relatively small cantilever beams, another, more sophisticated method -originally used in the bio-sciences- was adopted. Micropipettes made out of glass are usually employed to introduce very small amounts of liquids in cells, e.g. for fertilisation experiments. The tip opening of the

---

[6] DE-Patentanmeldung 100 14 869.7 (2000)

capillary can be varied and opening diameters of about 30 µm are easily obtainable.

The proximation of the micro-pipette towards the cantilever beam is achieved with a standard micro-manipulator which is normally used in the same experiments as discussed above. The polymer solutions are sucked up by a microinjector set-up (Narishige IM 300). Small pressures are adjustable with the instrument to press out tiny quantities of polymer solutions. The set-up is shown schematically in Fig. 3.2.3.2.
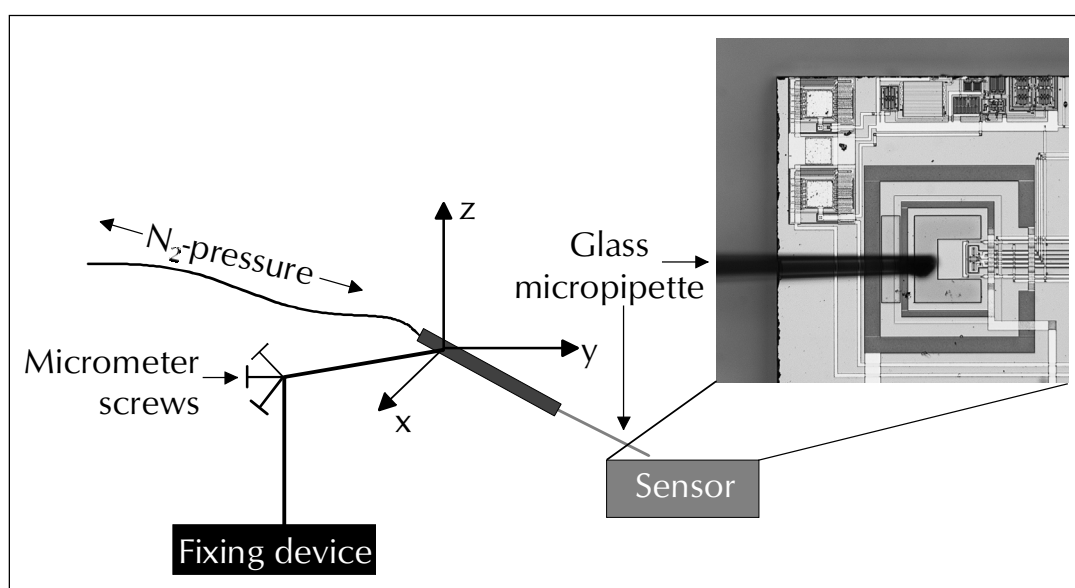
Fig. 3.2.3.2: Scheme of the glass micropipette coating set-up.

Due to their different wetting properties some polymers showed rough and inhomogeneous layers. In order to obtain closed films the wafers / chips were stored in an atmosphere saturated with dichloromethane (DCM) vapour. This procedure was carried out at room temperature for at least 5 min.

3.2.4 Optical Profilometer

In order to measure the thickness of polymer films some methods show fundamental drawbacks. Since most polymers used as chemically sensitive layers have a rather low glass temperature, i.e. at room temperature they are quite viscous, investigations with an α-stepper are ineffective; the rigid tip of the stepper penetrates into the layer and no real information of the height can be obtained. If the films are pretty thick (which is the case for our purposes) ellipsometry measurements might be erroneous because already small inhomogeneities lead to wrong results. Finally, SEM investigations can only give a vague impression of the layer thickness, whereas the mapping of the topography is very helpful.

For these reasons the following method which benefits from the phenomenon of the chromatic aberration of lenses was employed. The sample is irradiated with focussed white light. Based on the reflected light, the sensor calculates the structure of the surface topography. Thus, line scans (2-dimensional) and contour determinations (3-dimensional) are possible.

The height (z-direction) can be measured up to 300 μm, and the local, vertical resolving power is approximately 10 nm, whereas the lateral resolution is determined by the size of the light spot, for which $\varnothing \approx$ 1-2 μm. In order to achieve a sufficient reflectivity, on some polymers layers –especially in the case of those with a slightly rough surface topography- a sputtered gold film of about 50 nm was deposited.

The MicroProf™ optical sensor uses a method that is based on chromatic aberration, i.e. the wavelength dependent refractive index of lenses. A lens system having high chromatic aberration disperses the white light finally resulting in point foci of different colours and heights. If focussed light impinges on a surface, a maximum reflection can be observed (in contrast to unfocussed light). The reflected light is guided through the same optical system and a fibre-optic cable into a miniaturised spectrometer (for scheme see Fig. 3.2.4.1):
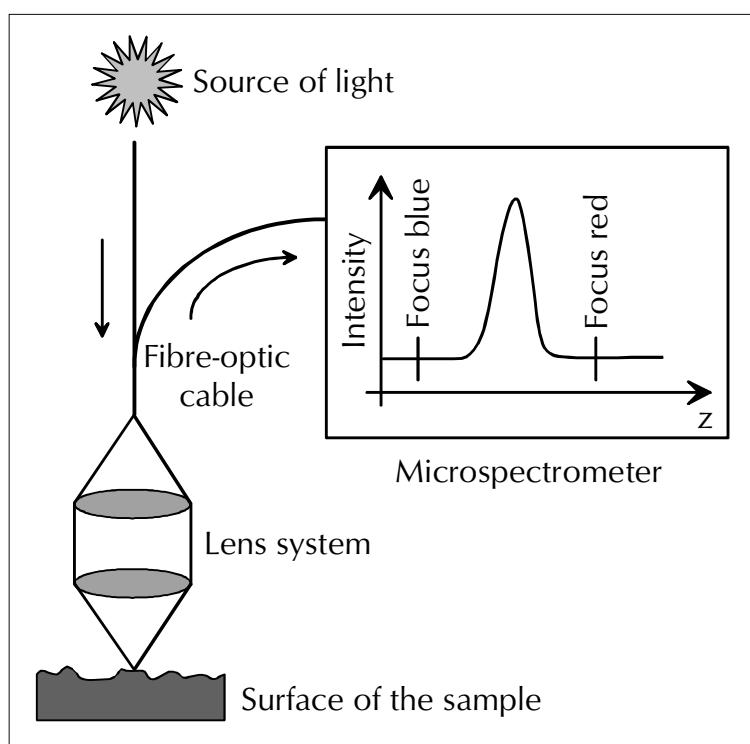
Fig. 3.2.4.1: Schematic drawing of the optical sensor.

As a result, the wavelength (colour) of the reflected light gives, on comparison with a previous calibration the distance between the sensor and the surface to be

analysed (see Fig. 3.2.4.2). Subsequent evaluation of the intensities leads to line scans or more complex topographic pictures.
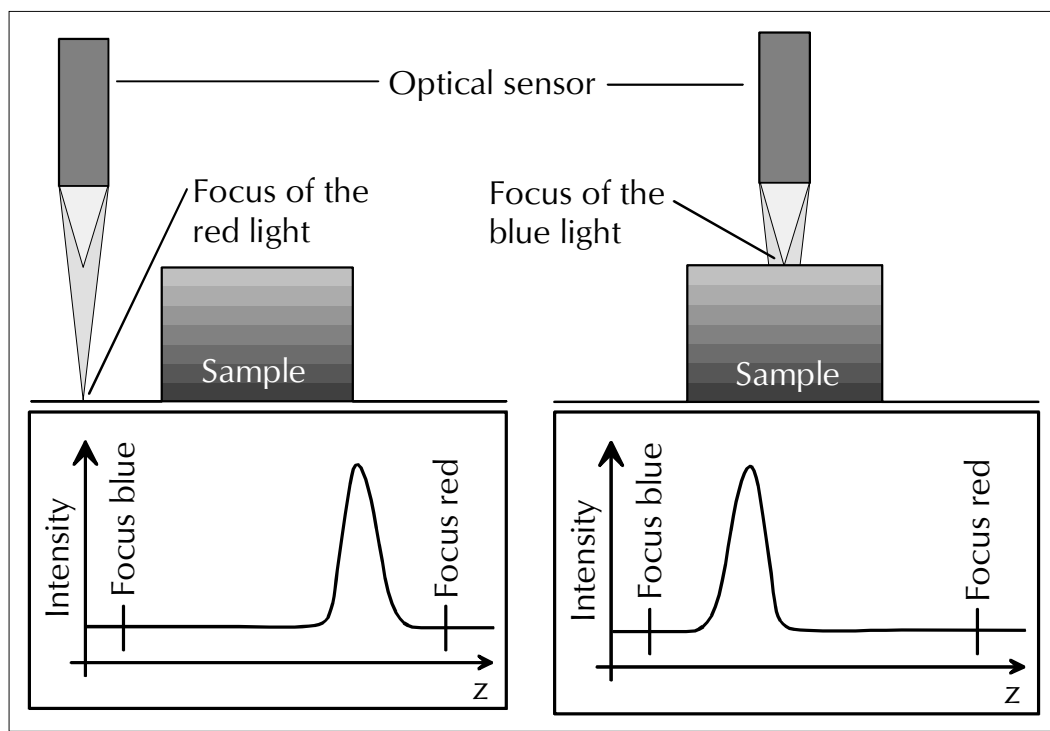
Fig. 3.2.4.2: Data acquisition with the optical sensor; different intensity values are obtained depending on the wavelength (colour) of the light which is focussed on the surface.

3.2.5 Volatile Organic Compounds - Determination of Partition Coefficients

The measurements focussed on ten different analytes: acetonitrile, butan-1-ol, chloroform, cyclohexane, 1,2-dichlorethane, ethanol, n-hexane, n-octane, propan-2-ol and toluene.

The determination of the individual partition coefficients $K_{Analyte/Polymer}$ was based on QCM-measurements ($f_{0, QCM}$ = 30 MHz) applying varying VOC concentrations with the help of a "Tübingen-specific" gas-mixing station [*Ulm 99*]. The polymers were deposited on the quartzes by an air-brush [*Ulm 99*]. The layer thickness was approximately 20 kHz for all polymers. As a result of the concentration dependent frequency shifts, the sensor sensitivity was obtained ($S_{QCM, i} = \Delta f/\Delta c$ [Hz/ppm]) which subsequently served as input for the equation E3.2.5.1 [*Hie 96*]:

$$K = \frac{\Delta f_{Analyte}[Hz] \cdot \rho_{Polymer}[g/ml] \cdot R[J/K \cdot mol] \cdot T[K] \cdot 10^7}{\Delta f_{Polymer}[Hz] \cdot M_{Analyte}[g/\ mol] \cdot 0.98 \cdot p_{Analyte}[ppmPa]} \qquad \text{E3.2.5.1}$$

3.3 References

[*Ekl 99*]: T. Eklöv, P. Mårtensson, I. Lundström, Anal. Chim. Acta 381 (1999) 221.

[*Her 97*]: M. Herold, Modifikation von SiO_2-Oberflächen und ihre Charakterisierung durch Spektrale Ellipsometrie und FK-NMR-Spektroskopie, Diploma thesis, University of Tübingen, Tübingen (1997).

[*Hie 96*]: A. Hierlemann, Massensensitive Detektion flüchtiger organischer Substanzen mit modifizierten Polysiloxanen, Ph.D. thesis, University of Tübingen, Tübingen (1996).

[*Hol 95*]: M. Holmberg, F. Winquist, I. Lundström, J. W. Gardner, E. L. Hines, Sens. Actuators B 26-27 (1995) 246.

[*Kol 97*]: B. Kolb, L.S. Ettre, Static headspace-gas chromatography: theory and practice, Wiley-VCH, Inc., New York, 1997, pp. 174-190.

[*Mit 98*]: J. Mitrovics, H. Ulmer, U. Weimar, W. Göpel, Modular sensor system for gas sensing and odour monitoring: the MOSES concept, Acc. Chem. Res. 31 (1998) 307-315.

[*Nes 98*]: Nestlé Research Center Lausanne, Glossary of terms used to describe off-flavours released by packaging materials, General study No. 2/94-e (2nd edition), R&D/QS Packaging FCh/JRu, October 1998. The sniff test is built on DIN 10955.

[*Ulm 99*]: H.E. Ulmer, Hybride modulare Sensorsysteme für die Gasanalytik und Olfaktometrie, Ph.D. thesis, University of Tübingen, Tübingen (1999).

4 RESULTS AND DISCUSSION

4.1 Artificial Ageing of Corn Oil

4.1.1 GC/MS Investigations

GC/MS was used to trace all changes in the headspace composition which occurred during the period of ageing. Moreover, an identification of newly appearing substances was possible.

As mentioned in the chapter *Experimental* a portion of the original oil was stored at $-20°$ C in a freezer. From time to time samples were taken from this portion and were analysed by GC/MS. The following figures show two chromatograms of headspace analyses, the first one of a sample from the very beginning of the whole measurement period (Fig. 4.1.1.1) and the second of a sample being stored for 100 days (Fig. 4.1.1.2).
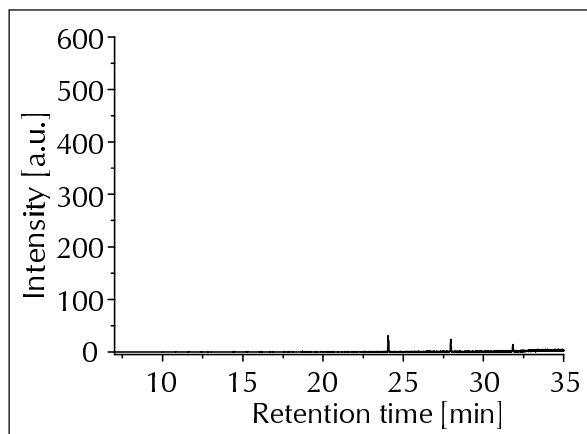
Fig. 4.1.1.1: Chromatogram of freshly opened, deodorised corn oil.
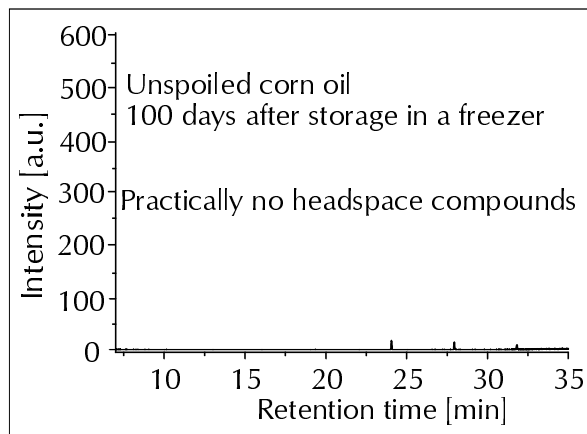
Fig. 4.1.1.2: Chromatogram of deodorised corn oil after 100 days storage at $-20°$ C.

Both figures show that the corn oil could be stored without any change in the headspace's composition. This important prerequisite enables its use as a stable standard to be applied for drift compensation. The very small peaks present in the graphs are attributed to polysiloxane derivatives released from the injector septum. Since these impurities occurred reproducibly, a simple subtraction from other chromatograms was possible and thus, these peaks were eliminated.

The artificial ageing caused by UV light could be monitored after an induction phase of a couple of weeks. Figs. 4.1.1.3 and 4.1.1.4 display the chromatograms of two oil samples in the middle and at the end of the measurement period. The results of the identification are listed in Table 4.1.1.1 giving also a rough overview of the distribution of the individual compounds present in the headspace.
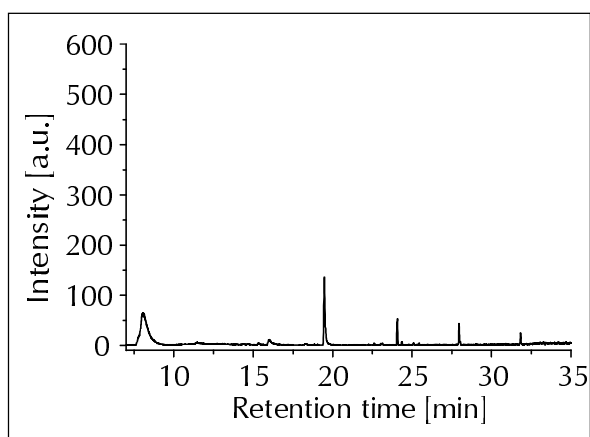
*Fig. 4.1.1.3: Chromatogram of artificially spoiled corn oil **after 56 days** of irradiation.*
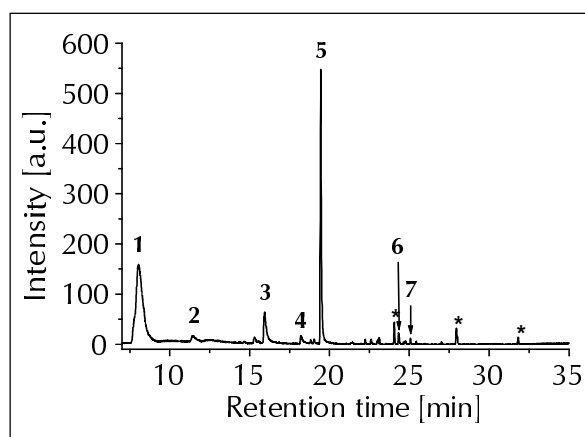
*Fig. 4.1.1.4: Chromatogram of artificially spoiled corn oil **after 100 days** of irradiation. The peaks marked with * could be attributed to the afore-mentioned polysiloxane derivatives.*

Retention time [min]	Proportion of the total amount of volatiles in the headspace [%]	Compound (corresponding number in Fig. 4.1.1.4)
8.05	49.6	Pentane (1)
11.47	1.5	2-Methylpent-1-ene (2)
15.99	12.8	Pentanal (3)
18.31	2.3	Pentan-1-ol (4)
19.47	29.6	Hexanal (5)
24.35	0.7	(E)-Hept-2-enal (6)
25.09	0.5	2-Pentylfuran (7)

Table 4.1.1.1: Substances identified in the headspace of a corn oil sample artificially aged for 100 days.

In the chapter *Basics and Survey* it was already reported that the oxidation of linoleate by $^1O_2$ leads to the formation of four isomeric hydroperoxides. The 2-(E)-heptenal originates from the isomer with the HOO- group at position no. 12. Fig. 4.1.1.5 below shows the most possible reaction pathway for its formation.

Frankel et al. [Fra 82] discovered that during the oxidation of unsaturated lipids many secondary products such as hydroperoxy epoxide and hydroperoxy cyclic peroxides are generated. The proposed decomposition pathway of 13-hydroxyperoxy-10,12-cyclic peroxide of linoleate is described in Fig. 4.1.1.6. The

degradation leads to pentane, hexanal and 2-(E)-heptenal. As shown by *Morrison et al.* [*Mor 81*] the production of pentane could be successfully correlated with flavour scores (assessed by panellists) or the peroxide value of oxidised oils containing linoleate.
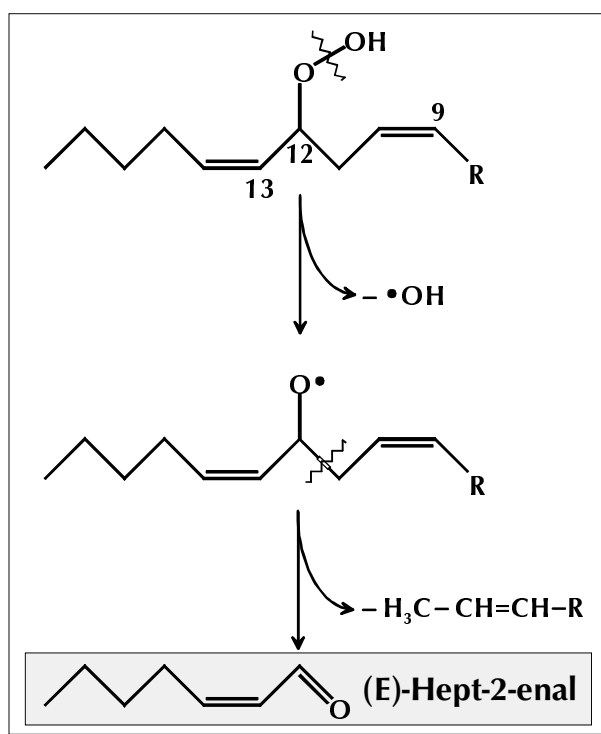
Fig. 4.1.1.5: Reaction pathway for the formation of (E)-hept-2-enal by decomposition of linoleate 12-hydroperoxide [Koc 96].
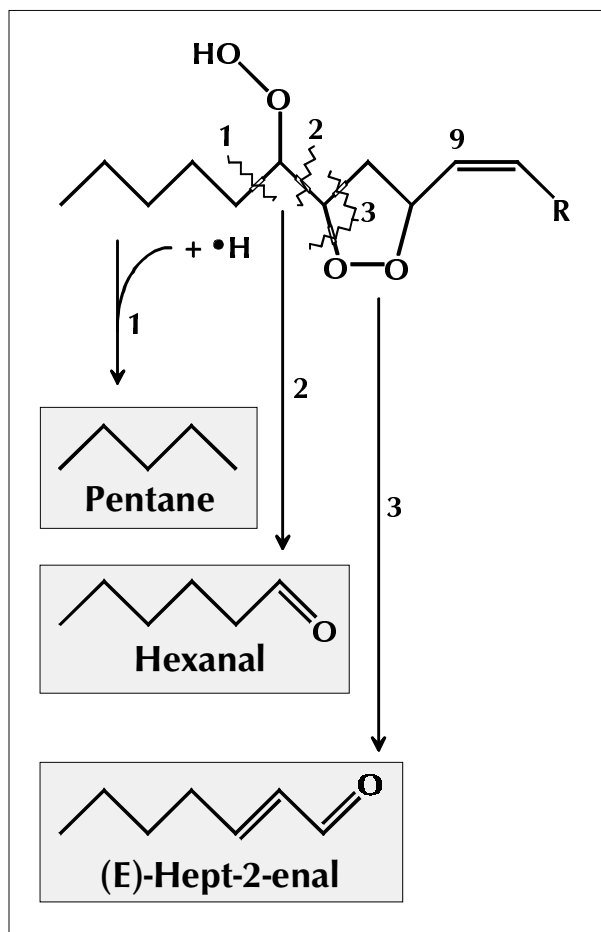
Fig. 4.1.1.6: Reaction pathway for the formation of pentane, hexanal and (E)-hept-2-enal by decomposition of 13-hydroperoxy-10,12-cyclic peroxide of linoleate [Koc 96].

The development of alkan-1-ols during storage does not essentially cause a defect in the taint of a product. One of the reasons for this is the relatively high odour threshold of alcohols in comparison with aldehydes. In addition, many alcohols contribute to the desirable odours of fruits and vegetables. The simultaneous formation of pentan-1-ol, hexanal and pentanal originating from the 13-hydroperoxy-Δ9,11-linoleate can be explained by the reaction scheme shown in Fig. 4.1.1.7.

In the 1970s and 1980s *Ho et al.* [*Ho 78*] and *Chang et al.* [*Cha 83*] reported furan derivatives appearing as off-flavour compounds in soy bean oil. *Ho* presented a pathway based on the degradation of 10-hydroperoxy-Δ8,12-linoleate. An alternative formation of 2-pentylfuran involving singlet oxygen and a hydroperoxy cyclic peroxide has been suggested by *Frankel* [*Fra 83*]. Within the reaction a cyclic peroxide is generated by concerted cyclisation of the conjugated diene system in the 9-hydroperoxy linoleate and singlet oxygen. In a subsequent

step the cyclic molecule is decomposed into pentylfuraldehyde and then to pentylfuran liberating formaldehyde.

The presence of 2-methylpent-1-ene could be explained by an isomeric change of another alkane or alkene induced by the UV irradiation. A simple conversion from n-pentane to 2-methylpent-1-ene is very unlikely and since no signification concentrations of other hydrocarbons (except n-pentane) could be detected, an unequivocal statement is not possible.
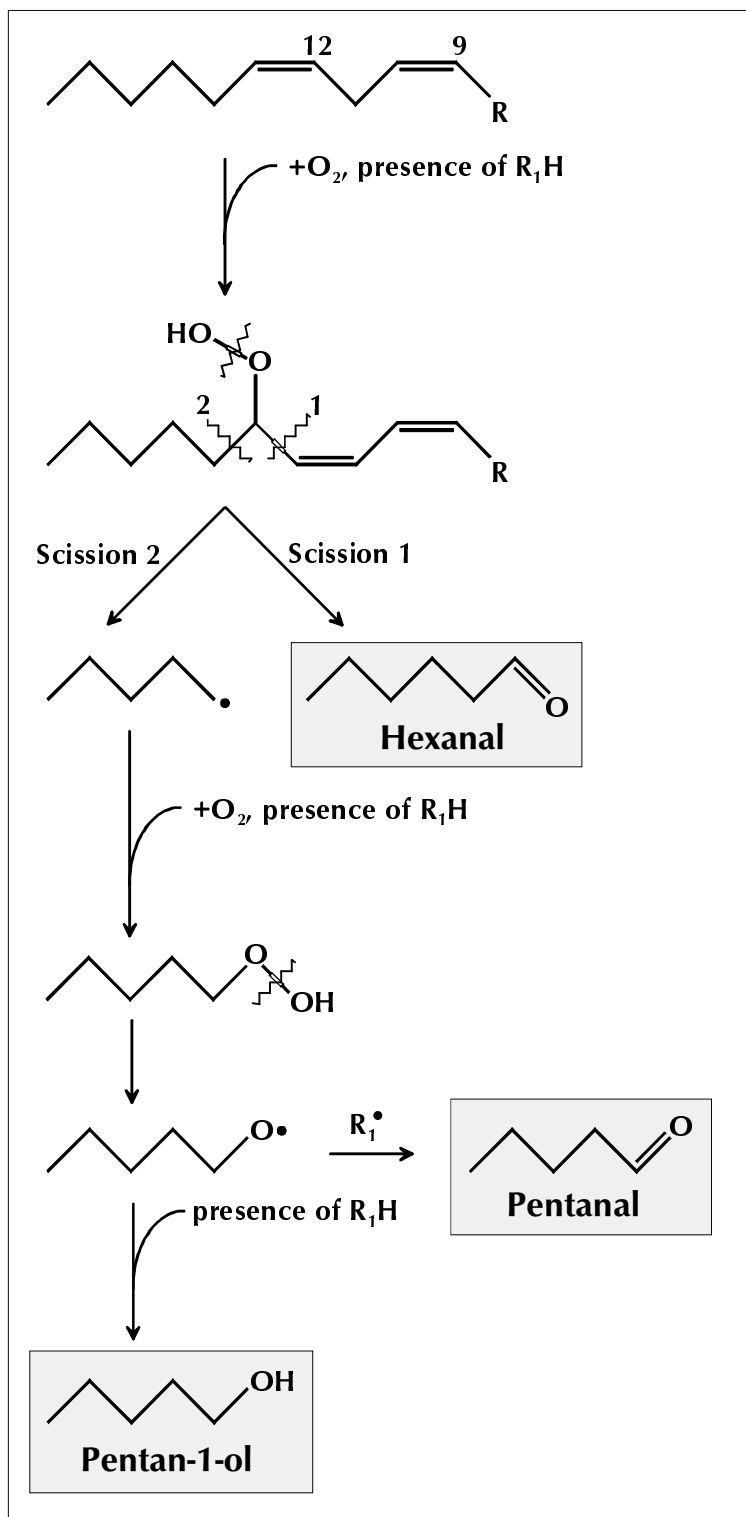
Fig. 4.1.1.7: Reaction pathway for the formation of pentan-1-ol, pentanal and hexanal by decomposition of linoleate 13-hydroperoxide [Koc 96].

4.1.2 Sensor Array Investigations

In parallel to the GC/MS-analyses, comparative measurements were performed with the MOSES II sensor system consisting of eight QCMs and eight MOXs.

Thus, each individual sample is characterised by 16 transient response curves from which a particular feature vector was extracted; the difference between the signal's maximum and its baseline was selected as being the most "valuable" feature which then served as input for the subsequent data analysis.

As mentioned in the chapter *Experimental* two different data sets were created. The first one is considered as the training data set containing measurements of oil samples (and standards) being investigated on the same day as the sampling took place. On each sampling day, additional samples were shelved and stored in the freezer until the end of the entire measurement period. After their analysis these samples built the test data set.

The following figures show the scores plots of PCA for the training data. Fig. 4.1.2.1 displays the results of samples which were not fluctuation/drift-corrected.
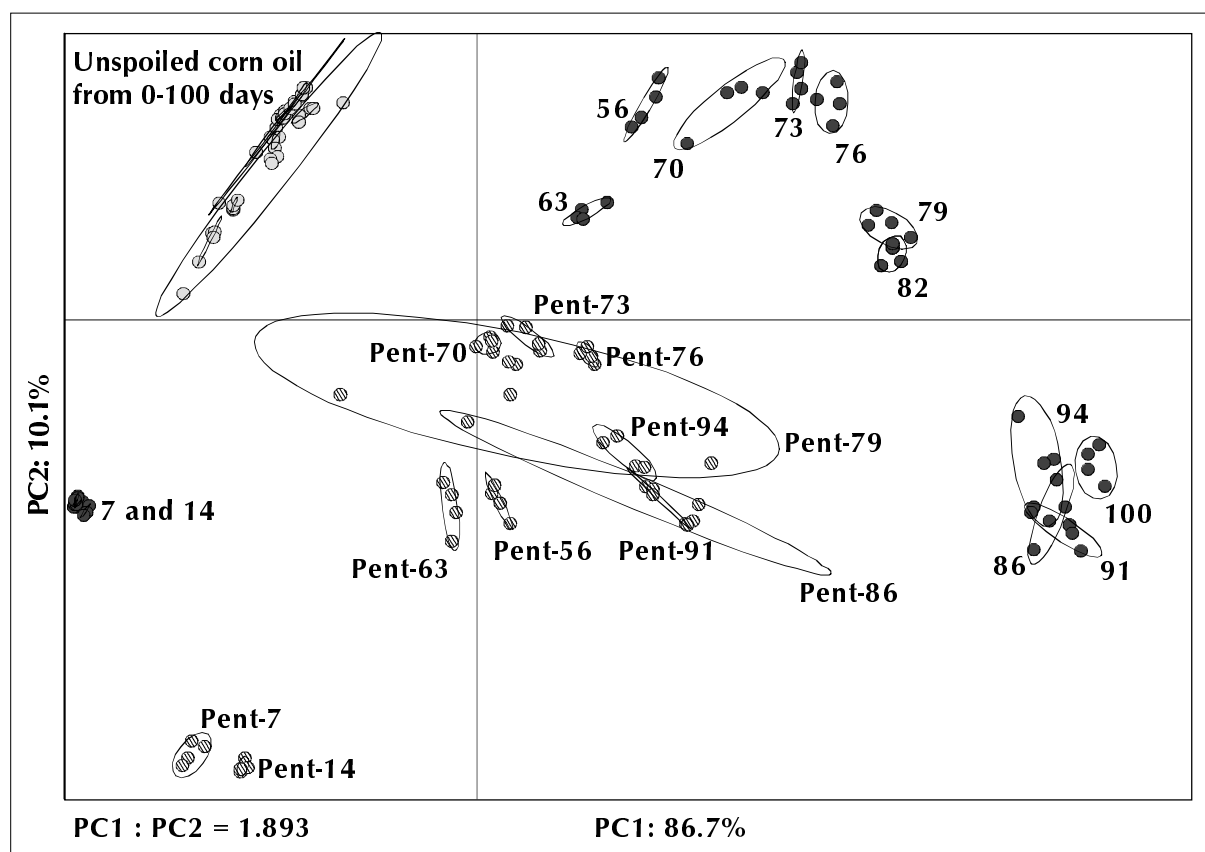
Fig. 4.1.2.1: Scores plot of a PCA of the training data set (including the standards, called Pent-x, where x denotes the measurement day) **without re-calibration**. *An individual measurement is marked by a symbol. The figure at each ellipse represents the time of artificial ageing in days. All samples belonging to the unspoiled corn oil are shown in the left upper corner.*

Obviously, the fluctuations in the sensor responses from different measurement days have a negative effect on the discriminating power (indicated by the overlapping ellipses). It has to be pointed out that the PCA as an unsupervised procedure for qualitative analysis discriminates the individual samples (represented in Fig. 4.1.2.1 as circles) on the basis of the maximum variance criterion. The ellipses drawn on the scores plot are supplementary, added for reasons of clearness; the corresponding attributions of the classes is the input of the operator and not a result of the PCA.

A clear trend showing the ageing process of the corn oil samples is hardly recognisable. Moreover, a large scattering of the pentanal standard samples can be observed. The variation within the individual pentanal samples probably has two reasons: Firstly, the sensors show fluctuations / drift in their response upon exposure to the same concentration of an analyte (assuming that the concentration is indeed really constant). Secondly, by independent GC/MS experiments of the standards it could be proven that the amount of analyte interacting with the sensor varies even though the standards were prepared in the same manner. This indicates irreproducible preparation of the standards and/or errors in the headspace sampling. Taking all these sources of error into consideration, the sensor fluctuations and the preparation of the standards cause the most serious problems. The long-term behaviour of the MOXs upon exposure to the 100 ppm pentanal standards is exemplarily depicted in Fig. 4.1.2.2. In most cases the error bars of the MOXs on a particular measurement day are smaller than the fluctuations between those days. However, on some days the deviations amongst the samples for re-calibration are considerably high. These observations indicate the complexity in the evaluation of fluctuation and drift phenomena, respectively.
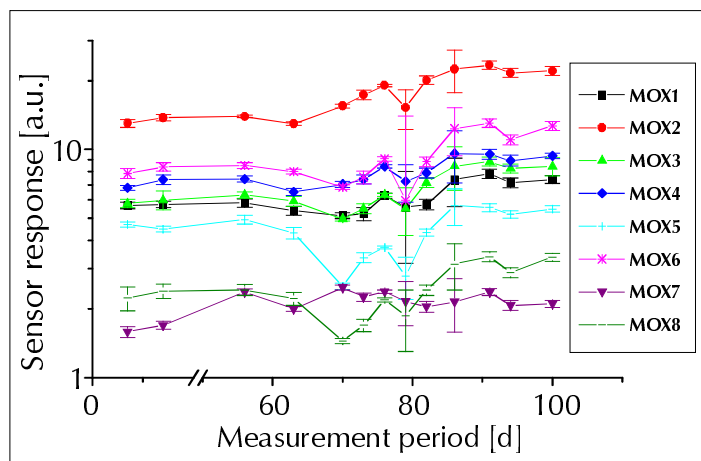
Fig. 4.1.2.2: Responses of MOXs upon exposure to a standard containing 100 ppm pentanal diluted in corn oil. The error bars represent the standard deviation of four individual samples investigated on each particular measurement day.

The influence of the fluctuation / drift correction is investigated by comparing all samples with the values of the pentanal standard (Fig. 4.1.2.3). In comparison with Fig. 4.1.2.1, a clear improvement in the discrimination between different sample classes can be seen. Moreover, the ageing process can precisely be followed looking at the individual clusters with an increased ageing time from the left to the right.
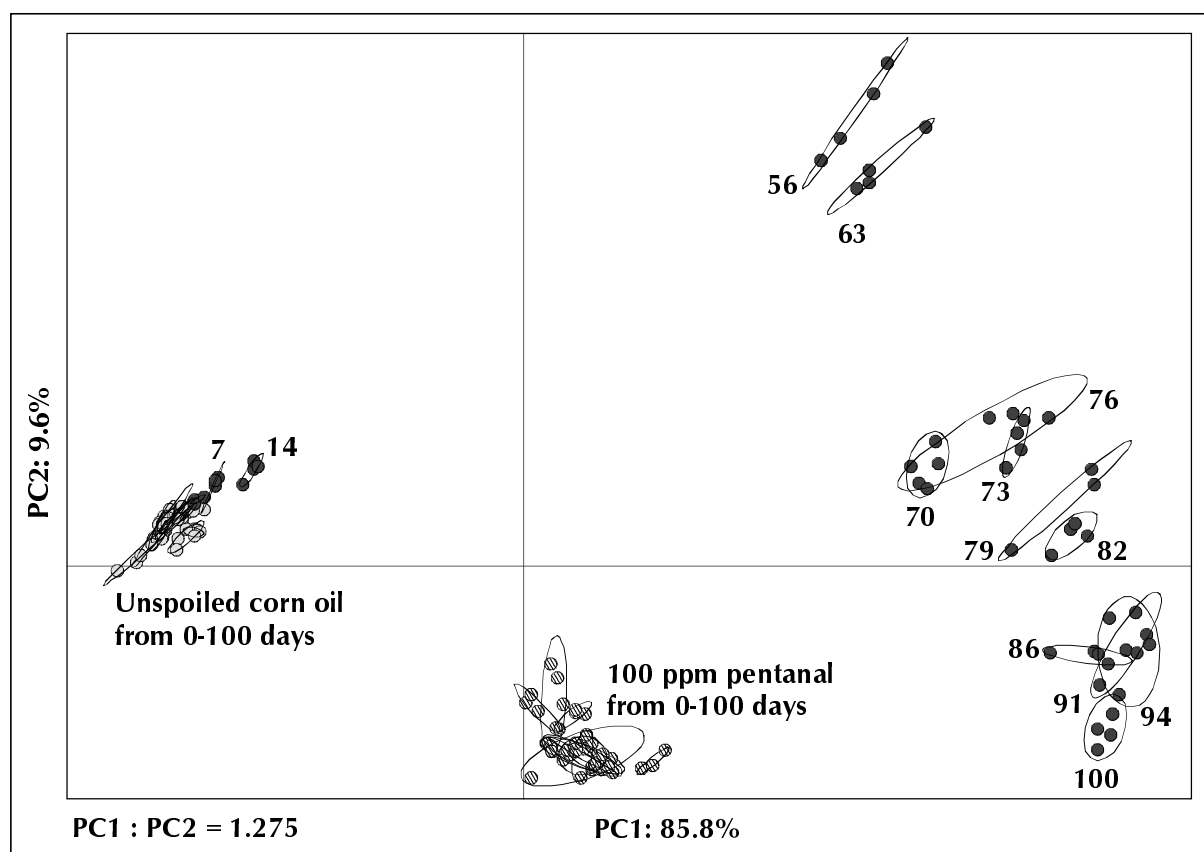
Fig. 4.1.2.3: Scores plot of a PCA of the training data set (including the standards, 100 ppm pentanal) **with re-calibration***. An individual measurement is marked by a symbol. All samples are compared to the 100 ppm pentanal standards. The figure at each ellipse represents the time of artificial ageing in days. All samples belonging to the unspoiled corn oil are shown on the left hand side.*

After evaluating the training data by means of a PCA, these data served as input for a model of a PCR. Based on this model, test data (from those samples which had been stored in a freezer until the end of the measurement period) were checked by the calibration model and the prediction of test sample age was carried out. The necessity for re-calibration can clearly be recognised looking at Figs. 4.1.2.4 - 4.1.2.5; they display the predicted values of the sensor system (y-axis, Prediction by MOSES) versus the true values (x-axis, Time of ageing). As a measure for the prediction ability of the system, the RMSE was calculated for each regression, i.e. without re-calibration, re-calibration with fresh, unspoiled corn oil and re-calibration with corn oil doped with 100 ppm pentanal. The particular RMSEs are given in Table 4.1.2.1.

	Re-calibration		
	Without (see Fig. 4.1.2.4)	*With fresh, unspoiled corn oil (see Fig. 4.1.2.5)*	*With fresh corn oil doped with 100 ppm pentanal (see Fig. 4.1.2.6)*
RMSE [d]	16.5	7.1	3.3

Table 4.1.2.1: RMSEs for three different prediction models of the age of deteriorated corn oil samples.
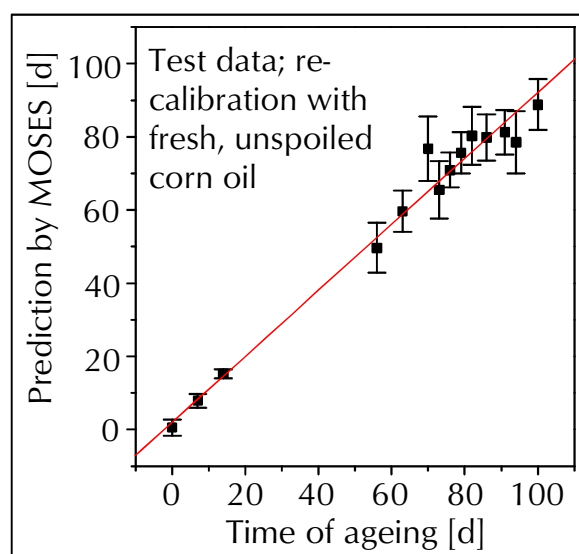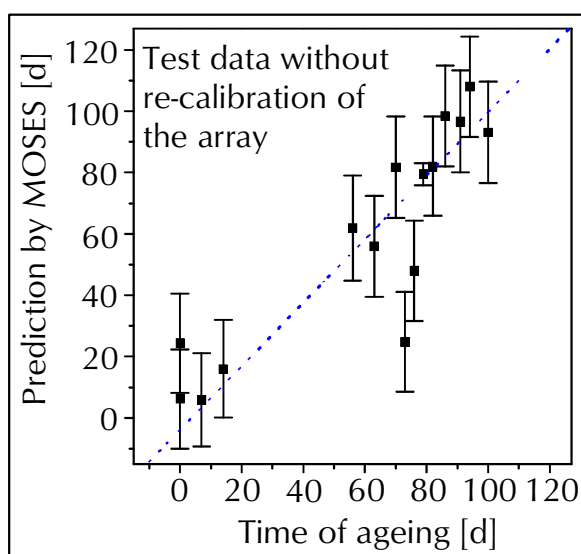
Fig. 4.1.2.4: Prediction of the age of corn oil samples by means of a PCR; the samples were not compared to any standard.

Fig. 4.1.2.5: Prediction of the age of corn oil samples by means of a PCR; the samples were compared[1] to fresh, unspoiled corn oil standards.

---

[1] The term "compared" means that between the individual values of the sensor responses upon exposure to a spoiled oil sample and the values upon exposure to a standard a ratio was calculated (according to Eq. E3.1.6.2). The terms "compared", "calibrated" and "re-calibrated" are often used synonymously in the literature.
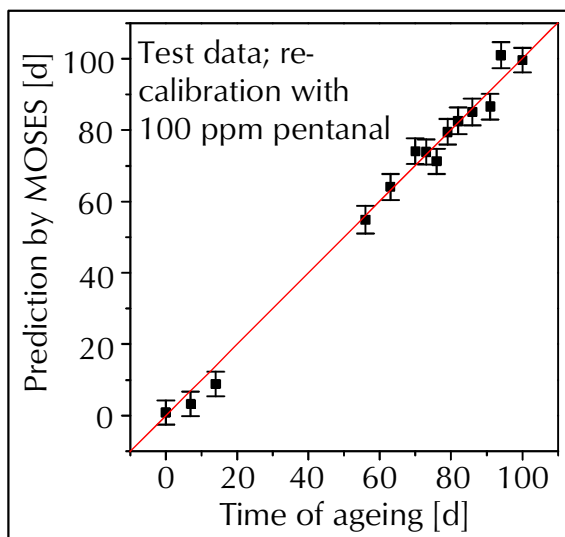
Fig. 4.1.2.6: Prediction of the age of corn oil samples by means of a PCR; the samples were compared to the 100 ppm pentanal standards.

As indicated by the RMSE, the re-calibration was most successful with the 100 ppm pentanal containing standards. The error is five times lower (with regard to a non-re-calibrated model) and two times lower (with regard to the model based on the re-calibration with fresh corn oil). A careful look at Figs. 4.1.2.5 and 4.1.2.6 reveals however, that at the beginning of the ageing process fresh, unspoiled corn oil is more appropriate for re-calibration (the error bars are smaller) in comparison with the results obtained with the pentanal doped standards. This observation supports the aforementioned assumption that the headspace composition of the standard used for re-calibration should mimic the headspace of the samples to be investigated as much as possible. In contrast to this outcome, the pentanal standards are more suited for the re-calibration of oil samples with a longer time of ageing. This is in accordance with the GC/MS results, where besides n-pentane large amounts of pentanal and hexanal could be identified. In conclusion it can be stated that a precise prediction of a sample's attribute (e.g. age, off-flavour content etc.) with a sensor system is strongly dependent on the nature of the re-calibration standards. Especially in all applications where product changes have to be followed on a long-term scale, the standards have to be adapted accordingly.

4.2 Packaging Materials

4.2.1 Odour Evaluation by Human Sensory Panel

For the olfactory check the samples are stored in an air-tight receptacle at 80° C for 1 hour. After reaching equilibrium between the solid and the gaseous phase the packaging odour is assessed by a panel of 6-10 well-trained persons (odour panel of the Centre de Recherche Nestlé, CRN).

Scale for odour scores: From 0 (no difference from a given reference) to 4 (very strong difference from the reference). Within the scope of the first sensory evaluation, eight packaging materials were selected (sample set 1 (samples nos. 1-8), see Table 4.2.1.1), all of them had different printings; in some cases the sample's specification was the same. Obviously, the whole odour score range from 0 to 4 was not covered by the chosen samples, but since the investigated foils were taken out randomly from production, a controlled selection is not possible. Remembering the quality standard, the materials should have an odour score which is lower than 2.5; only sample no. 3 had an unacceptable smell. The other seven wrapping foils would have been used to pack the chocolate since their odour scores fulfil the requirements.

Sample set 1								
Packaging material no.	1	2	3	4	5	6	7	8
Panellists	Individual odour scores							
Alain	2	2	2	1	2	2	2	2
Chantal	2	2	3	1	2	3	2	3
Jaime	1	2	2	1	1	1	2	2
Monika	2	1	3	1	1	3	2	2
Piero	1	2	2	1	2	2	1	3
Yves	2	1	4	0	1	3	2	2
Median	2	2	2.5	1	1.5	2.5	2	2
Mean score and standard deviation	1.7 ± 0.5	1.7 ± 0.5	2.7 ± 0.8	0.8 ± 0.4	1.5 ± 0.5	2.3 ± 0.8	1.8 ± 0.4	2.3 ± 0.5
Taint description	Painting Solvent Caoutchouc	Varnish Acrylic Solvent Latex	PE Solvent Slip agent Caoutchouc Rubber Sour milk	‾‾‾‾‾	Caoutchouc Rubber Cold seal	Solvent Latex Wax Inks Painty Acid acetic	Caoutchouc Slip agent Sour milk Pharmacy	Caoutchouc Rubber Cold seal Painting Varnish

Table 4.2.1.1: Overview of the sniff test results for different packaging materials belonging to sample set 1. The scores range from 0-4 (in arbitrary units). The odour evaluation was performed by the sensory panel of the Nestlé Research Centre [Rui 01].

The odour scores assigned by the human sensory panel do not correspond to the total amount of volatiles in the headspace (these results are given in chapter 4.2.2 *GC/MS Investigations*). The total amount of volatiles represents the summation of all peak areas within a chromatogram that has emerged from GC/MS analyses. Samples like no. 5 have been appraised by a relatively low odour score (1.5) which is in agreement with the relatively low concentration of

outgassing analytes (348 arbitrary units). In comparison with this, sample no. 6 had a 0.8 higher odour score whereas the total amount of volatiles was about 2 times lower. Although samples no. 5 and 6 had the same specification this phenomenon is not too surprising. This outcome is mainly based on the fact that the appearing substances (more details are presented in chapter 4.2.2 *GC/MS Investigations*) cover a wide range of odour thresholds and odour activity values which means that high concentrations of a compound do not necessarily entail an intensive odour impression. In some cases a correlation between a high odour score and a high concentration of volatiles can be found (e.g. sample no. 3), but looking at Tables 4.2.1.1 and 4.2.2.4 it is evident that for other materials such an easy correlation is not possible. GC-sniffing experiments revealed for instance that the sniffing person perceived a certain smell and no peak could be found in the chromatogram.

In connection with the sample aeration described before applied to eliminate malodours, a certain packaging material was selected (the specification is shown in Table 3.1.5.2). The chosen foil was exposed to an air stream for five different time durations. Table 4.2.1.2 shows the results of the sensory panel assessment:

Sample set 2						
Packaging material no.	**9** (0h)	**10** (1h)	**11** (3h)	**12** (7h)	**13** (24h)	**14** (48h)
Panellists	Individual odour scores					
Alain	3	2	3	3	2	2
Chantal	3	3	3	3	2	2
Jaime	4	3	3	2	2	2
Lionel	2	3	1	3	2	1
Monika	3	3	3	2	1	1
Tuan	3	3	2	2	2	1
Yves	3	3	3	3	2	0
Median	**3**	**3**	**3**	**3**	**2**	**1**
Mean score and standard deviation	**3 ± 0.6**	**2.9 ± 0.4**	**2.6 ± 0.8**	**2.6 ± 0.5**	**1.9 ± 0.4**	**1.3 ± 0.8**
Taint description	Slip agent (4)	Slip agent (4)	Slip agent (3)	Slip agent (4)	Slip agent (3)	Slip agent (2)
	Wax	Wax	Wax	Wax		
	Burnt wax	Burnt wax		Burnt wax		Burnt wax
	Solvent	Solvent	Solvent		Solvent	
	PE odour	PE odour	PE odour	PE odour		
	Styrene	Styrene	Styrene		Styrene	
	Fatty	Fatty				
	Rancid	Rancid		Rancid	Rancid	
	Acrid		Acrid			

Table 4.2.1.2: Overview of the sniff test results for different packaging materials belonging to sample set 2. The scores range from 0-4 (in arbitrary units). The odour evaluation was performed by the sensory panel of the Nestlé Research Centre [Rui 01]. The figures in brackets below the term "slip agent" give a semiquantitative measure for this particular taint.

Compared with the experiments carried out with sample set 1, one major difference can clearly be seen. As all samples (in sample set 2) are the same –they just differ in the aeration time- a declining odour score by aeration is correlated with the decrease in the total amount of volatiles. In the following chapter *4.2.2 GC/MS Investigations* it will be pointed out in more detail that not all of the off-odours occurring disappear in this procedure because the gas used (air or nitrogen) has a great influence on their concentration. A comparison with EN data is carried our in chapter 4.2.3 *Odour Prediction by the Modular Sensor System (MOSES II)*. The odour evaluation of the sample sets 1 and 2 was only done for the calibration phase. Since the packaging foils were sealed gas-tight before they were investigated in the validation phase, it can be assumed that the odour score did not change dramatically during storage. As a general remark it can be stated that the human sensory evaluations lead to very coherent results if only the mean values of the odour description by the individual panel members are taken into consideration. A deeper examination shows, however, that the standard deviation of the above mentioned results is remarkably high. This in turn is significant for assessments done by human beings which are naturally subjective.

Most polyolefin films release a typical rancid odour which can be associated with burnt wax. This is generally attributed to slip agents used to enhance the frictional properties of the laminate. These additives include fatty acid amides.

Off-flavours result from thermal degradation and oxidation of the amides and the impurities they contain. Although such residual odours cannot be completely avoided in practice, the risk of tainting can be minimised by moderating the temperature of lamination and sealing.

The thermal degradation and oxidation of polyethylene itself may also give rise to substances which contribute to the overall PE-odour. In the literature, 2,2,4,6,6-pentamethylheptane is mentioned as being mainly responsible for this smell.

4.2.2 GC/MS Investigations

Within this chapter not all of the chromatograms of the investigated samples will be presented. Rather the idea is to give an overview displaying a selection of typical results.

The chromatogram of sample no. 2 is shown in Fig. 4.2.2.1.
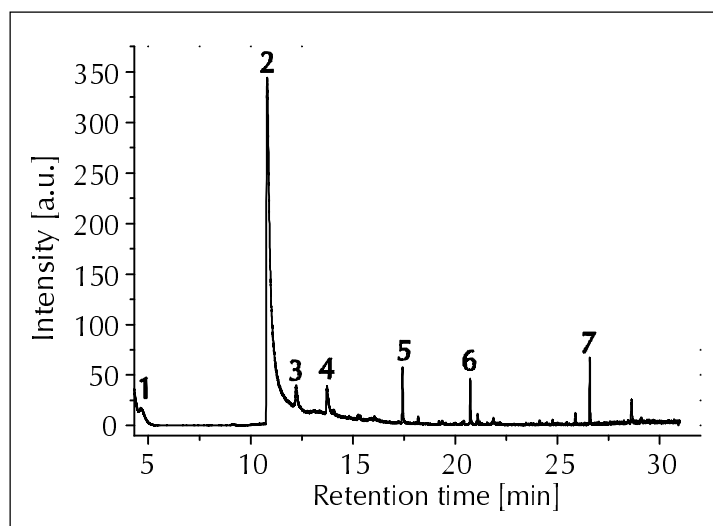
Fig. 4.2.2.1: Chromatogram of packaging material sample no. 2.

The chromatogram is dominated by the ethyl acetate peak which contributes to 85% of the total amount of all headspace components. 2-Methylprop-1-ene, cyclohexane, n-propyl acetate, butan-2-one, 2-ethylhexan-1-ol and hexanedioic acid diethyl ester can be considered as other main analytes (see Table 4.2.2.1).

Retention time [min]	Compound
4.65	2-Methylprop-1-ene (1)
10.81	Ethyl acetate (2)
12.22	Cyclohexane (3)
13.71	n-Propyl acetate (4)
17.44	Butan-2-one (5)
20.75	2-Ethylhexan-1-ol (6)
26.60	Hexandioic acid diethyl ester (7)

Table 4.2.2.1: Peak identification of the chromatogram displayed in Fig. 4.2.2.1; the figures in brackets correspond with those in the chromatogram.

The high ethyl acetate concentration results from its use as a solvent during the package processing; it probably originates from printing inks and varnishes. The same holds also for the residual cyclohexane. Since propyl derivatives are formed as by-products in the industrial synthesis of ethyl acetate, it also appears in the headspace analysed. The occurrence of 2-ethylhexan-1-ol in packaging materials is rather common; the oxidation of this alcohol leads to 1-hepten-3-one to which a

"musty" tainting can be attributed whereas the odour impact of ethyl acetate is often characterised as "fruity" [*Tic 96*]. A conclusive explanation for the presence of the hexanedioic acid diethyl ester cannot be given so far.

As previously described, for some packaging materials two batches were available. In order to demonstrate how these batches can vary concerning their headspace composition, the chromatograms of packaging material no. 4 (batch a and b) are discussed in more detail. Obviously, in the chromatogram of sample no. 4, batch a, (see Fig. 4.2.2.2) 2-methylprop-1-ene is the dominating analyte in the sample's headspace (50%).
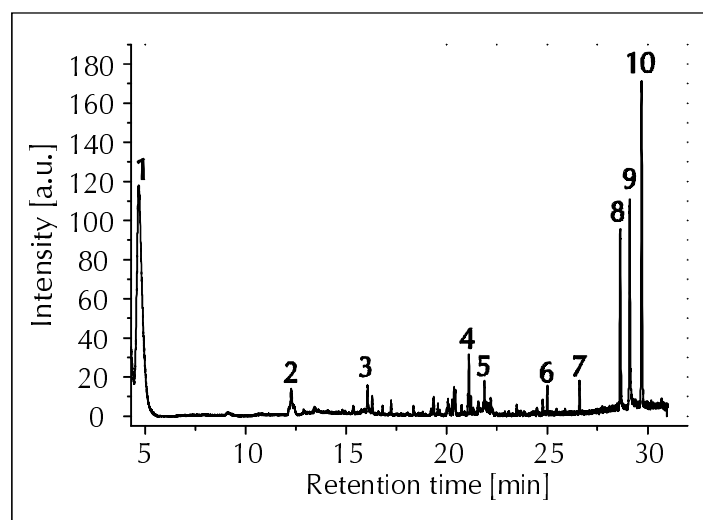
Fig. 4.2.2.2: Chromatogram of packaging material sample no. 4, batch a.

The whole chromatogram reveals at least ten compounds of considerable importance (see Table 4.2.2.2).

Retention time [min]	Compound
4.65	2-Methylprop-1-ene (1)
12.22	Cyclohexane (2)
16.05	Hexanal (3)
21.08	3,3-Dimethylhexane (4)
21.87	Not identified (5)
25.02	Not identified (6)
26.64	Tetradecane (7)
28.63	Not identified (8)
29.10	Not identified (9)
29.70	Phenylisoquinoline * (10)

*Table 4.2.2.2: Peak identification of the chromatogram displayed in Fig. 4.2.2.2; the figures in brackets correspond to those in the chromatogram; the exact structures of the compounds marked with * are not clear.*

The peak at 4.65 min could be identified as 2-methylprop-1-ene (isobutene). Its release is probably based on the fact that residual monomer has been encapsulated in the polymer backbone since oriented polypropylene (OPP) is one integral part of the packaging material. Due to the low boiling point of isobutene (-6.9° C) it is in some cases already evaporated from the wrapping foils. An alternative explanation to the appearance of 2-methylprop-1-ene might be the decomposition of oligo- or polymers during the sample conditioning in the oven of the headspace sampler or during the GC/MS analysis. To a small degree cyclohexane (compound no. 2) is again present in the sample's headspace. Hexanal (compound no. 3) can be considered as a frequently appearing off-flavour in various packaging materials (mainly based on paper or cardboard materials). Even small quantities can cause odour impressions which are commonly qualified by the descriptors "green" and "grassy" suggesting the typical smell of freshly cut green grass. Some of the analyte peaks in the retention time range between 20 and 30 min. could not be clearly identified. The fragmentation patterns of the compounds labelled nos. 5, 6, 8 and 9 indicated an ordinary hydrocarbon backbone, but the total structure is still unknown. The exact position of the phenyl group within the phenylisoquinoline molecule is not determined so far; also its origin remains unanswered looking at potential sources within the packaging material production process.

Although the specification and the printing of the samples shown in Figs. 4.2.2.2 (no. 4, batch a) and 4.2.2.3 (no. 4, batch b) are identical, the headspace composition is completely different. Not only the qualitative difference is worth mentioning, but also the higher peak intensities in Fig. 4.2.2.3 (one order of magnitude) have to be taken into consideration.
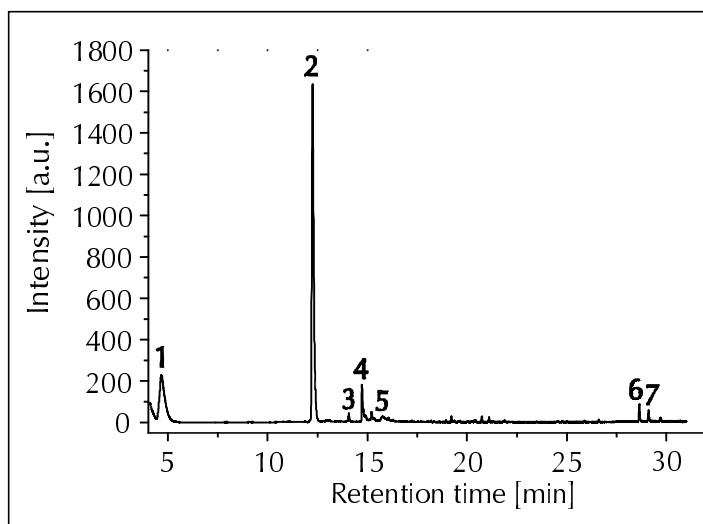
Fig. 4.2.2.3: Chromatogram of packaging material sample no. 4, batch b.

The headspace of sample no. 4, batch b, mainly comprises cyclohexane (62% of the total amount of volatiles) which was found in batch a only as a minor compound. All relevant components are listed in Table 4.2.2.3.

Retention time [min]	Compound
4.65	2-Methylprop-1-ene (1)
12.22	Cyclohexane (2)
14.08	Methylcyclohexane (3)
14.73	1-Ethoxypropan-2-ol (4)
15.72	Pentan-2,4-dione (5)
28.63	Not identified (6)
29.10	Not identified (7)

Table 4.2.2.3: Peak identification of the chromatogram displayed in Fig. 4.2.2.3; the figures in brackets correspond with those in the chromatogram.

Interestingly, two other substances could be detected being well known for their characteristic odours; compound no. 4 was identified as 1-ethoxypropan-2-ol and peak no 5 could be attributed to pentan-2,4-dione. The ether alcohol 1-ethoxypropan-2-ol serves as a solvent in heliography and flexography inks and causes a "sweetish" odour. A "camphorated" flavour can be imparted to printed films by pentan-2,4-dione (also called acetylacetone). This substance is released from titanium acetylacetone, an adhesion promoter for gravure inks. The GC/MS investigations of two different batches of the same wrapping material clearly demonstrate the complexity and the huge possible variation making simple correlation between different analytical methods quite difficult. The chromatograms of the other packaging materials (nos. 1, 3, 5, 6, 7 and 8) are not displayed. In general, these samples have the same major headspace components in varying concentrations: 2-methylprop-1-ene, cyclohexane, methylcyclohexane, pentan-2,4-dione, 2-ethylhexan-1-ol, 1-ethoxypropan-2-ol and very small amounts of 1-methoxypropan-2-ol, toluene and isomeric xylenes.

The following table displays an overview of the total amounts of volatiles released from the packaging material samples nos. 1-8.

Packaging material no.	Samples used for calibration (training data)	Samples used for validation (test data)
	Total amount of volatiles in the headspace determined by GC/MS [a.u./10^3]	Total amount of volatiles in the headspace determined by GC/MS [a.u./10^3]
1	1550	1524
2	623	589
3	6993	6985
4	402	410
5	348	324
6	153	168
7	2621	2618
8	195	175

Table 4.2.2.4: The total amount of volatiles present in the sample's headspace (samples nos. 1-8) is the sum of all peak areas appearing in the chromatogram. The given values are mean values of three individual measurements.

One goal of the GC/MS measurements was to monitor the solvent release during aeration of the samples in a laboratory hood. Moreover, the compounds having the greatest influence on the odour impression should be identified.

A much more complex headspace composition could be found for the packaging material belonging to sample set 2. Here, more than seventy compounds were detected in the headspace of the analysed packaging material shown in Fig. 4.2.2.4 (packaging material no. 9). The aeration was carried out in a special set-up (see experimental section) in which the samples could be hung up in a defined gas stream. The result of the peak identification is given in Table 4.2.2.5.
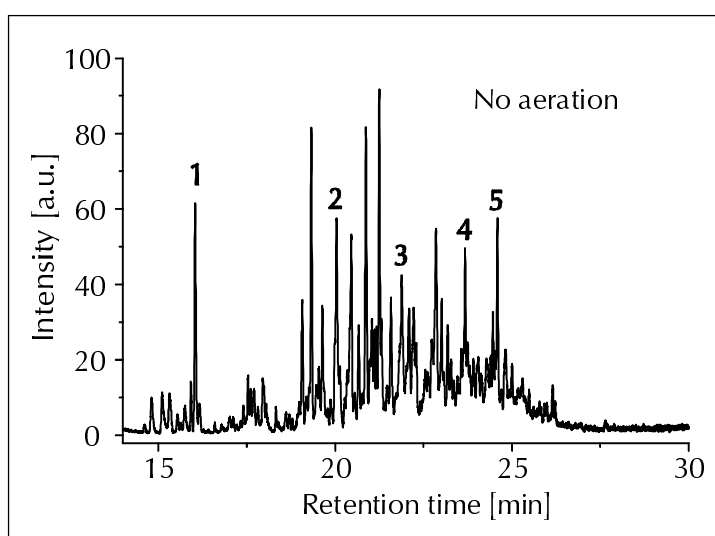
Fig. 4.2.2.4: Chromatogram of packaging material sample no. 9 without aeration in the laboratory hood.

Retention time [min]	Compound
14.81	Branched HC[2]
15.10	Pentan-1-ol
15.54	Butanoic acid
16.04	Hexanal (1)
19.08	n-Heptane or n-octane derivative[3]
19.32	Branched HC
19.64	n-Octane derivative
19.90	Phenol
20.03	Trimethyloctane (2) *
20.46	Branched HC
20.87	3-Methyldecane
21.25	n-Heptane derivative
21.31	Methyldecane *
21.58	Trimethyldecane *
21.89	Decahydronaphthalene (3)
22.85	Decahydro-2-methylnaphthalene
23.68	2,6-Dimethylundecane (4)
24.59	Trimethyldodecane (5) *

*Table 4.2.2.5: Peak identification of the chromatogram displayed in Fig. 4.2.2.4; the figures in brackets correspond to those in the chromatogram; the exact structures of the compounds marked * are not clear.*

Compared to all other chromatograms described above, the huge amount of different outgassing analytes is noteworthy. Although the chromatogram in Fig. 4.2.2.4 consists of more than 70 peaks, in the Table above only 17 different compounds are listed. Most of the analytes are linear or branched, aliphatic hydrocarbons. Probably, they are remaining by-products of the polymer synthesis. Five substances have been randomly selected to monitor the effect of two methods of aeration; the ventilation was done by air or nitrogen. The selected compounds have been; hexanal, trimethyloctane, decahydronaphthalene, 2,6-

---

[2] HC: Hydrocarbon
[3] Derivative: Backbone of the corresponding compound and alternating side groups

dimethylundecane and trimethyldodecane. With the standard GC method only part of the peaks could be clearly separated. Thus a subsequent mass spectrometer analysis and the identification of the compound remains very difficult in some cases. The main problem is the low structural difference between the branched hydrocarbons which makes correct discrimination very difficult. For the remaining unidentified peaks the library search leads to ambiguous results. Furthermore, chain-like hydrocarbons are not usually attributed to the characteristic "slip agent" odour (see Table 4.2.1.2).

The chromatogram of a sample measured after 48 h of aeration (sample no. 14) in the laboratory hood (Fig. 4.2.2.5) reveals two phenomena when compared with Fig. 4.2.2.4. Firstly, the amounts of nearly all components decrease considerably. Secondly, the concentration of hexanal (retention time 16.04 min) increases with time. These GC/MS results are in agreement with the human odour panel evaluations: Lower intensity of "slip-agent" smell after aeration; the rancid taint is still present (see chapter 4.2.1 *Odour Evaluation by Human Sensory Panel*).
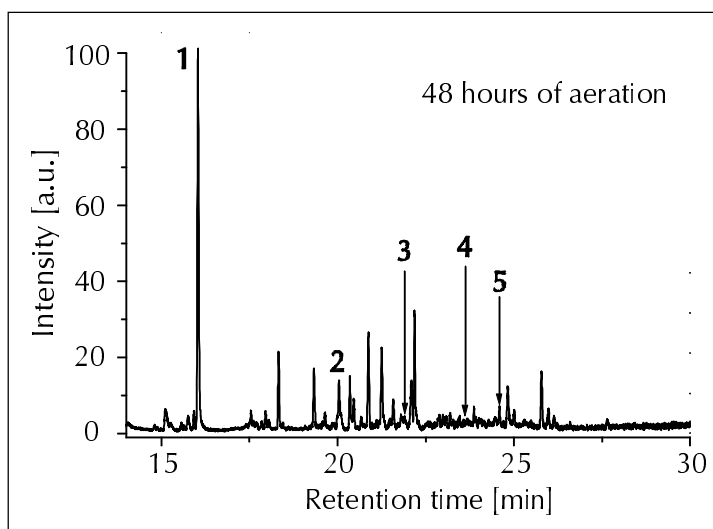
Fig. 4.2.2.5: Chromatogram of packaging material no. 14 with 48 h aeration in the laboratory hood.

The diagrams in Figs. 4.2.2.6 and 4.2.2.8 point out the influence of the nature of the gas which is chosen for the aeration.
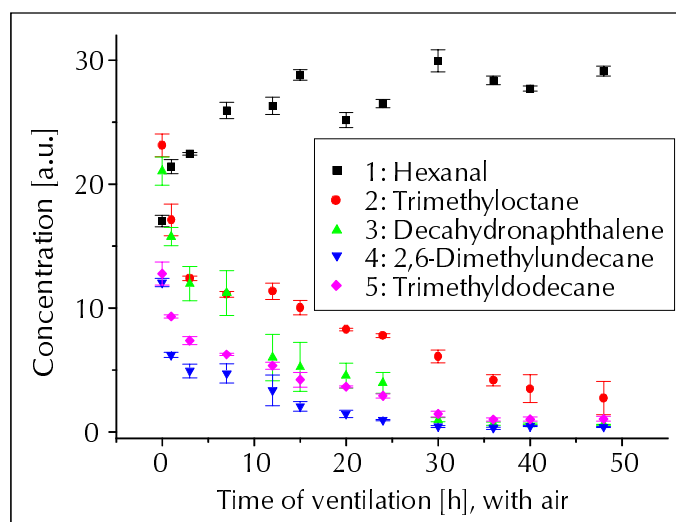
Fig. 4.2.2.6: **Ventilation** *of packaging material sample set 2 (samples nos. 9-14)* **with air** *(80% nitrogen, 20% oxygen). The samples were aerated for 0, 1, 3, 7, 12, 15, 20, 24, 30, 36 40 and 48 hours (x-axis). The y-axis represents the concentration (and peak area) of the individual analytes in arbitrary units measured by GC/MS. The error bars represent the standard deviation (± 1 sd) of three measurements.*

The data represented in Fig. 4.2.2.6 (ventilation with air) in comparison with Fig. 4.2.2.8 reveal two main differences. Firstly, the hexanal concentration increases over the time; it seems to reach a constant value for longer aeration times (more than 20 h). Secondly, the exponential decay of the four hydrocarbons is lower and compounds like trimethlyoctane still have a considerable concentration after 48 h although the gas flow was kept constant for both the aeration with pure nitrogen and air. Since the ventilation of the samples with air is more related to the actual procedure under "real-life" conditions, the sampling intervals have been shortened in order to monitor the concentration trend of the individual analytes more precisely. The increase of the hexanal concentration can be explained by looking in more detail at the specification of sample set 2 (samples nos. 9-14). One part of the material consists of paper which can be produced from two different qualities of pulp. Mechanical pulp contains, in addition to cellulose, most of the lignin and other components of wood such as resin and mineral compounds; chemical pulp comprises essentially cellulose fibres. For both, a broad range of off-odours including numerous aldehydes (mainly pentanal, hexanal and heptanal), as well as esters and alcohols can be detected which specifically originate from pulp. Under natural circumstances they arise from the oxidation of lipids and other components of resin. Another potential source of the release of off-odours having a carbonyl groups is related to lithographic printing (offset printing). Lithographic inks consist of pigments

dispersed in resin solutions, themselves dissolved in a solvent composed of vegetable and mineral oils. Often malodours are formed from the vegetable oils during the drying process which also involves an oxidation. The oxidation starts from unsaturated fatty acids leading to the conjugation of double bonds, the formation of peroxides and finally the occurrence of volatile aldehydes, ketones and carboxylic acids [*Tic 96, Sch 81, Ull 87*].

The following table displays an overview of the total amounts of volatiles released from the packaging material samples nos. 9-14 (ventilation with air).

Packaging material No.	Samples used for calibration (training data)	Samples used for validation (test data)
	Total amount of volatiles in the headspace determined by GC/MS [a.u./10^3]	Total amount of volatiles in the headspace determined by GC/MS [a.u./10^3]
9	607	591
10	497	441
11	457	385
12	329	292
13	160	145
14	108	95

Table 4.2.2.6: The total amount of volatiles present in the sample's headspace (samples nos. 9-14) is the sum of all peak areas appearing in the chromatogram. The given values are mean values of three individual measurements.

The values in Table 4.2.2.6 indicate that parts of the compounds originally present in the packaging materials volatilise during storage. This phenomenon was also confirmed by independent GC/MS measurements. The corresponding results are shown in Fig. 4.2.2.7:
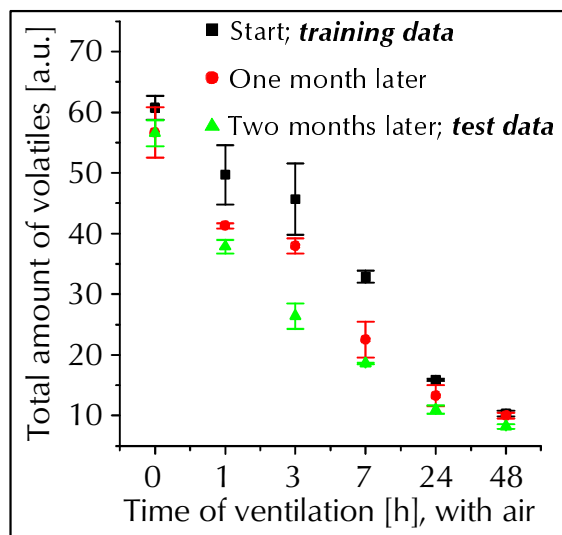
Fig. 4.2.2.7: Change in the total amount of volatiles (of samples belonging to sample set 2) during storage determined by GC/MS. The given values are mean values of three individual measurements. The error bars represent the standard deviation (± 1 sd) of these measurements.

The diagram reveals the problem of a defined storage. Within the 1st measurement cycle (training data, black squares) the total amount of volatiles is at a maximum. The test data are represented by the 3rd measurement cycle (green triangles); a considerable concentration change is observed. For this reason a re-evaluation by the human odour panel would have been very useful. However, due to logistic problems a second investigation by the CRN was not possible.

Fig. 4.2.2.8 shows the exponential concentration decay of the five aforementioned analytes after an aeration with nitrogen. Each data point represents the mean value of three individually measured samples; the error bars give the standard deviation which is in some cases, especially for low aeration times, remarkably high. This is an indication of the heterogeneous distribution of the particular analytes among the individual packaging samples. An aeration of 48h leads to a negligible concentration of trimethyloctane, decahydro-naphthalene, 2,6-dimethylundecane and trimethyldodecane in the headspace. Only hexanal still appears at 48 h of aeration, to an amount that is relatively constant for even longer aeration times. In comparison with Fig. 4.2.2.6, the influence of the purge gas on the headspace composition is evident. The chemically inert nitrogen does not cause oxidation or other kinds of degradation processes increasing the concentration of already existing analytes or leading to new compounds which might cause off-flavours. Especially for paper- / cardboard-based packaging materials that readily undergo such oxidation processes (see chapter 2.1.2.2 *Paper Packaging*) the use of pure N_2 is recommended.
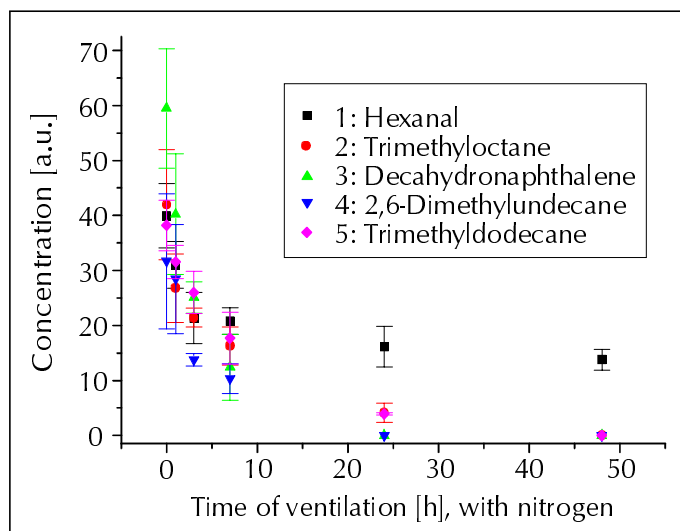
Fig. 4.2.2.8: **Ventilation** *of packaging material sample set 2 (samples nos. 9-14)* **with pure nitrogen***. The samples have been aerated for 0, 1, 3, 7, 24 and 48 hours (x-axis). The y-axis represents the concentration (and peak area) of the individual analytes in arbitrary units measured by GC/MS. The error bars represent the standard deviation (± 1 sd) of three measurements.*

As a general remark it can be stated that the variations in the headspace composition of different packaging materials (based on GC/MS analyses) can also be explained by the discrimination of the sensor array data after a principal component analysis (different clusters in the scores plot, see chapter 4.2.3 *Odour Prediction by the Modular Sensor System (MOSES II)*).

4.2.3   Odour Prediction by the Modular Sensor System (MOSES II)

As described in the chapter *Experimental* the samples were also measured in parallel by the sensor system MOSES II.

The first attempt of the sensor array measurements focussed on the system's ability to distinguish between different kinds of packaging materials with respect to their specification, i.e. the individual materials the foils consist of. This is an essential prerequisite in order to use the sensor array for the odour prediction of a variety of packaging. To verify this purpose all samples belonging to the sample sets 1 - 2 were examined by MOSES II. Moreover, from some of the packaging species (samples nos. 4, 5, 6 and 8) two different production batches were available which have also been measured. Whenever two different batches of one sample have been investigated, the packaging's structure, the printing and the supplier are absolutely identical. What differs is the date of production. Normally, the time between the production of different batches is several months. A

selection of the results (only including parts of sample set 1) is displayed in Fig. 4.2.3.1 which shows the scores plot of a principal component analysis (PCA) of sensor data.
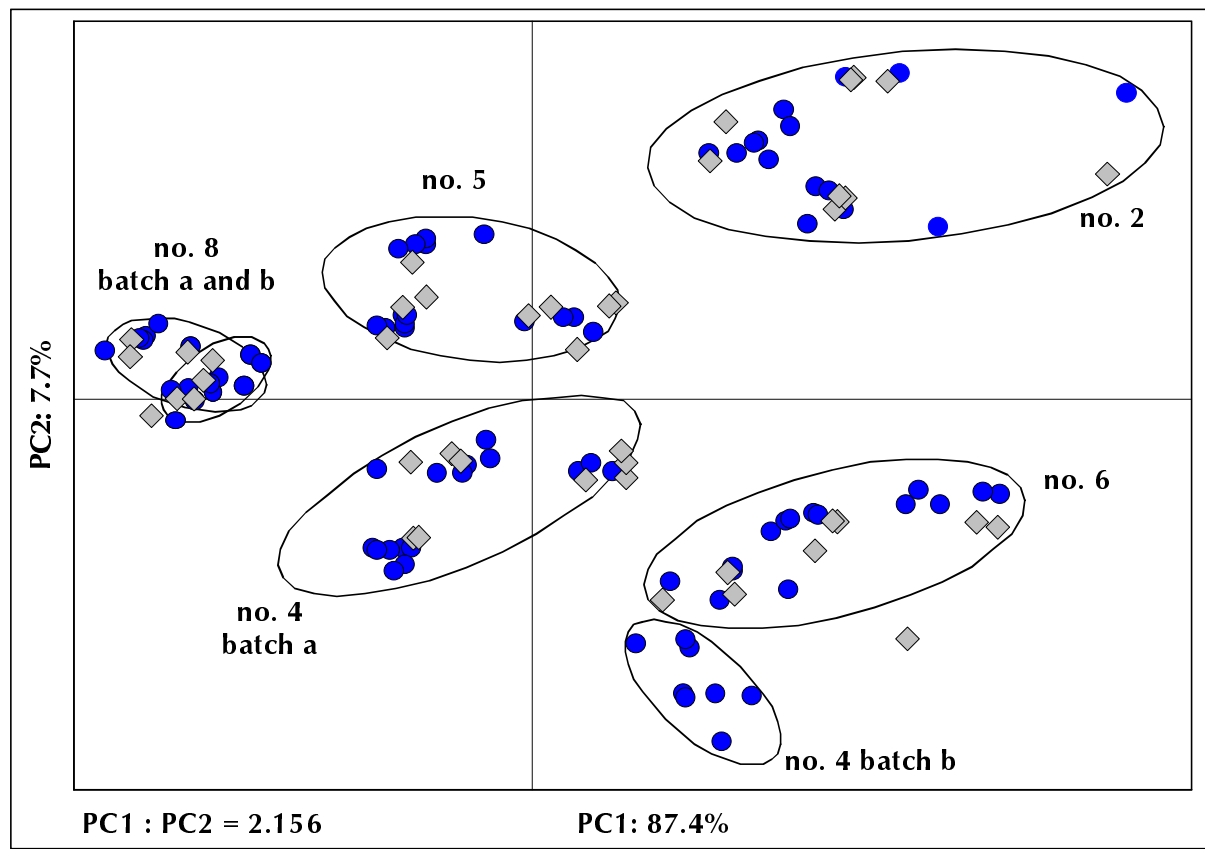
Fig. 4.2.3.1: Scores plot of a principal component analysis (PCA) derived from sensor array data. An individual measurement is marked by a symbol; the calibration data are represented by black circles, the test data are labelled as grey diamonds. The number of the samples investigated is according to Table 3.5.1 (see chapter 3.5 Sample Preparation of the Packaging Materials). From samples nos. 4 and 8 two independent batches b are additionally depicted; for the batches b no test data were collected since they were not considered for the correlation between the panel and the sensor array.

For reasons of clarity the data from the samples nos. 1, 3 and 7 are not depicted in Fig. 4.2.3.1. The sensor data consist of the responses of eight QCMs and eight MOXs. The feature which served as input for the PCA and PCR was the height of the individual response curves, i.e. the baseline was subtracted from the maximum of the signal of all samples investigated (see Fig. 4.2.3.2). Each individual measurement is represented by a circle (calibration) or diamond (validation) respectively. The ratio of PC 1 to PC 2 expresses the scaling between the two axis, i.e. one centimetre along the direction of PC 1 is equal to 2.156 centimetres along PC 2. Together with the percentage of explained variation of each PC this ratio gives a further measure of the PC's importance. For the

calibration of the system (training phase) 18 samples of each packaging material were used. Thus, the whole calibration database which is built up from 14 individual sample types comprised 252 single measurements. As a first outcome it can be stated that the sensor array is able to differentiate between the diverse sample specifications. This result is really based on the different compound patterns which can already be seen from the individual chromatograms i.e. the discrimination is not related to varying total amounts of volatiles. The latter problem can be overcome to a large extent if the sensor data are normalised. The performance is even better taking into account that not only samples of different specifications could be separated, but also samples belonging to the same kind of material (samples nos. 5 and 6). In some cases (see sample no. 8) the individual batches are in the same cluster. This result could also be confirmed by GC/MS where both batches had the same qualitative and quantitative composition. Moreover, the batch-to-batch change could be monitored as is shown for samples no. 4. As already discussed in the chapter 4.2.2 *GC/MS Investigations* this differentiation is based on the large variation in their chromatograms.
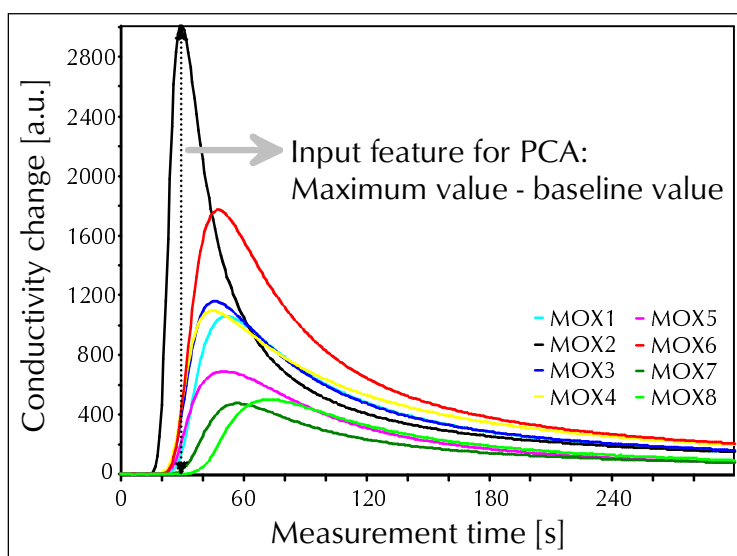
*Fig. 4.2.3.2: Measurement curves of eight MOXs upon exposure
to a packaging material sample. The input feature for the PCA is
the baseline value subtracted from the maximum of the signal.*

The second, and for practical reasons, more important result is the reproducibility of the analyses described above. Therefore, two months after the calibration database was created, 9 of the same (but not identical!) samples were re-examined. The data from these investigations are also shown in Fig. 4.2.3.1 and are labelled as grey diamonds. Since none of the test data were misclassified the

intention to use such a system as a tool for quality control over longer periods with only a few additional expenditures for re-calibration is strongly supported.

Nevertheless, the performance of a sensor system in predicting the odour of a material can better be proven if using the principal component regression (PCR) as a quantitative method. This approach is compulsory for achieving a correlation between the human sensory tests and the sensor system's output. Although a linear regression is applied as a link between human and technical noses (another method is described in [*Dol 01*]), it has to be stressed that the perceived intensity of an odour is not linearly related to a large range of its concentration [*Ros 96*]. Actually, a sigmoidal relationship seems to express the biological olfaction in a more appropriate manner [*Pan 81*]. This sigmoidal curve is characterised by a threshold below which an odour cannot be observed and a saturation at which concentration changes of the odorous compounds cannot be distinguished (see Fig. 2.1.1). Assuming that the odour perception of the human panel is in the range between the two turning points of the sigmoidal curve, a linear model can be used in a first approximation. Therefore, the correlation between the human evaluation and the prediction of MOSES is based on a principal component regression (PCR) which has been carried out separately for sample set 1 and 2.

One of the main interests of the gas sensor system is in its use for the odour prediction of unknown samples. Therefore, calibration data (derived from a defined sample set) and the odour scores of the human panel served as input for the prediction model. Since PCR is a linear technique, it is most successful when sensor responses are known to be linear. PCR can produce over optimistic results if prediction accuracy is based only on data used to generate the PCs (here the so-called training data) [*Jur 00*]. This problem can be eased by using a leave-one-out cross-validation procedure with the training data. However, a better way to verify the predictive ability of a model is to use independent test samples. Both approaches, the test set validation as well as the cross-validation, led to comparable results. The regression model and the prediction of unknown samples were based on three PCs; they explain 95.1% of the total variance of sample set 1 and 97% of sample set 2.

Since the whole data set (training and testing data) is very large, a real test set validation was applied (Figs. 4.2.3.4 and 4.2.3.7) to check the model's validity. Each data point depicted in Figs. 4.2.3.3 (regression of the calibration data of sample set 1) and 4.2.3.5 (regression of the calibration data of sample set 2) represents a mean value of the sensory assessments of the panellists and 18 individual sensor array measurements. The errors bars show the corresponding standard deviation (± 1 sd). As the number of test data was only half in comparison with the training data the means displayed in Figs. 4.2.3.4 (validation

of sample set 1) and 4.2.3.7 (validation of sample set 2) are based on nine electronic nose measurements.

The calibration with sample set 1 which is displayed in Fig. 4.2.3.3 led to a very good agreement with the hypothetical perfect correlation (thin dotted line, bisector of the 90° angle); the linear fit of the data points is given by the dashed line. The error bars demonstrate how difficult it is to define a precise odour value. Although the members of the sensory panel are well trained persons the uncertainty in the assessment is remarkable. As a measure of the quality of the predicted values (output of the sensor array) compared with the true values (human assessment), the RMSEs (RMSEC for the calibration samples and RMSEP for the test samples) were calculated. They have the same units as the measurement data and were computed according to the following equation:

$$RMSE = \sqrt{\frac{1}{n}\sum_{i=1}^{n}(\hat{y}_i - y_i)^2} \qquad \text{E4.2.3.1}[4]$$

$\hat{y}_i$ = predicted value, y_i = measured value ("true"),

n = number of data points used for the linear fit

The RMSEC of the calibration of sample set 1 is 0.14 which indicates the good quality of the model on which the subsequent prediction of test data is based. The value of the correlation coefficient R = 0.97 is near the maximum of 1. This holds for the slope of the linear fit m_f = 0.87 as well.

More interesting than the calibration itself is the result of the validation phase in which the same types of samples were measured again in order to predict the odour value based on the calibration model that was established two months before (see Fig. 4.2.3.4). The correlation coefficient R reveals only a minor difference (ΔR = 0.03) and the slope of the linear fit is even slightly better (m_f = 0.88). However, the RMSEP of the validation now has a value of 0.26 which is almost double the RMSEP for the calibration. It has to be mentioned that for the test phase no additional human sensory evaluation was performed, i.e. the odour scores which have already been attributed to the calibration samples were used again.

---

[4] Another type of error is expressed by: $rel.RMSE = \sqrt{\sum_{i=1}^{n}\frac{(\hat{y}_i - y_i)^2}{y_i^2}}$. This error should preferentially be applied if the concentrations of the samples investigated span a range of several magnitudes (e.g. from 50 ppb to 50 ppm).
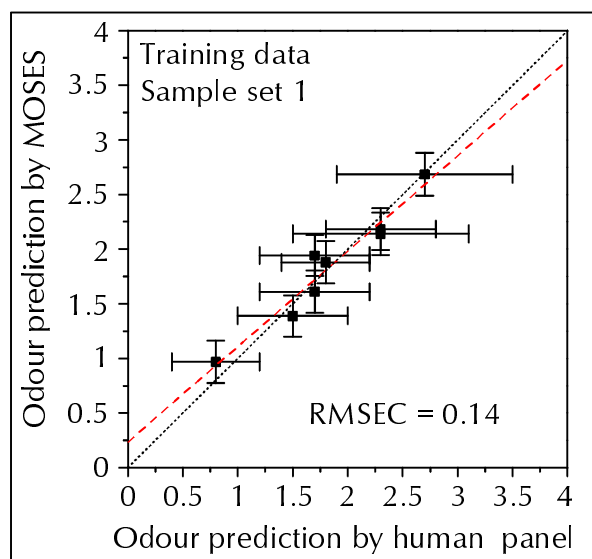
*Fig. 4.2.3.3: PCR (**training data**) showing the correlation between the odour evaluation by the human sensory panel and the odour prediction by MOSES. This calibration model is based on 144 individual measurements of sample set 1. Each data point in the diagram corresponds to the mean value of 18 individual electronic nose measurements and the sensory evaluations of the panellists; the error bars represent the standard deviation (± 1 sd). The RMSEC is a measure of the quality of the predicted values compared with the true values (see Eq E4.2.3.1)*
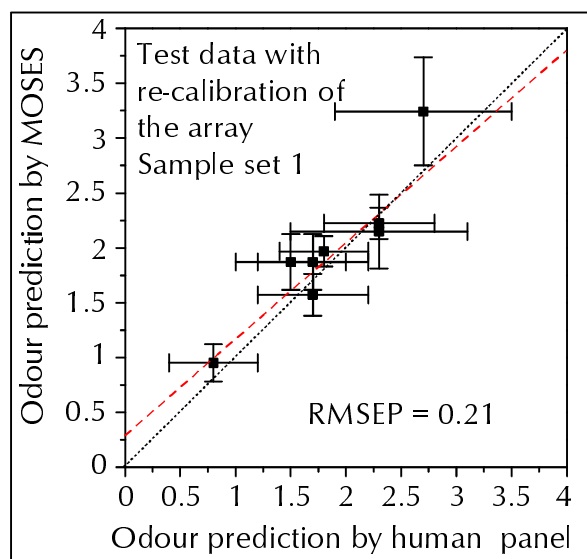
*Fig. 4.2.3.4: PCR (**test data**) showing the correlation between the odour evaluation by the human sensory panel and the odour prediction by MOSES. This prediction is based on 144 individual measurements of sample set 1. The calibration shown in Fig. 4.2.3.3 served as a model. Each data point in the diagram corresponds to the mean value of nine individual electronic nose measurements and the sensory evaluations of the panellists; the error bars represent the standard deviation (± 1 sd). The RMSEP is a measure of the quality of the predicted values compared with the true values (see Eq E4.2.3.1).*

A comparable result can be found for the measurements carried out on sample set 2. The calibration model is plotted in Fig. 4.2.3.5. The individual data points obtained are very close to the dotted line having a slope m of 1; there is only a marginal discrepancy Δ of 0.06. The RMSEC of 0.10 signifies that the calibration model is a very useful basis for a further validation step. This also holds for the value of R which is in high accordance with the optimum value. The corresponding coefficients for the test data became worse as can be seen in Fig. 4.2.3.7. In particular, the RMSEP of the MOSES odour prediction rises to a value of 0.21. The increase in the length of the error bars representing the standard deviation (± 1 sd) of nine individual predictions is in accordance with the augmented RMSEP. For the calibration model the error bars for the assessment by the human panel were much higher compared to those of the sensor array. In the

case of the validation carried out with the test data they are in the same order of magnitude. The necessity for re-calibration can clearly be seen by looking at Fig. 4.2.3.6 which displays the prediction results without re-calibration. In this case the RMSEP increases making a precise prediction even more difficult. A detailed discussion on the long-term stability of sensor arrays which is a crucial point if dealing with re-calibration strategies, is presented in chapter 4.2.4 *Long-term Investigations, Sensor Response Fluctuations and Re-calibration.*
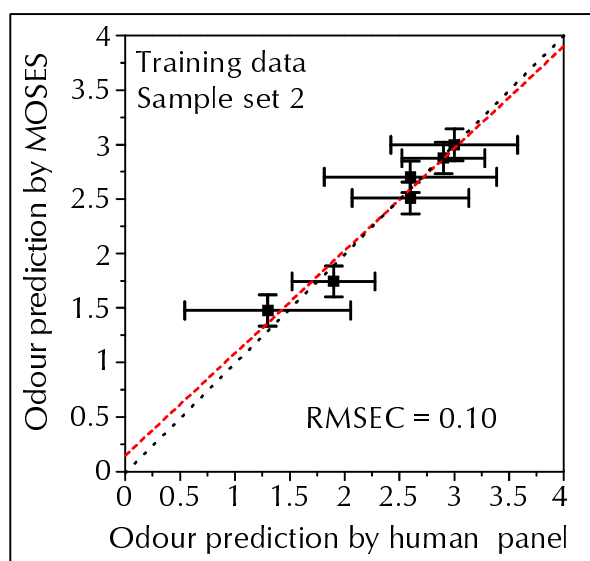
*Fig. 4.2.3.5: PCR (**training data**) depicting the correlation between the odour evaluation by the human sensory panel and the odour prediction by MOSES. This calibration model is based on 108 individual measurements of sample set 2. Each data point in the diagram corresponds to the mean value of 18 individual electronic nose measurements and the sensory evaluations of the panellists; the error bars represent the standard deviation (± 1 sd). The RMSEC is a measure of the quality of the predicted values compared with the true values (see Eq E4.2.3.1).*
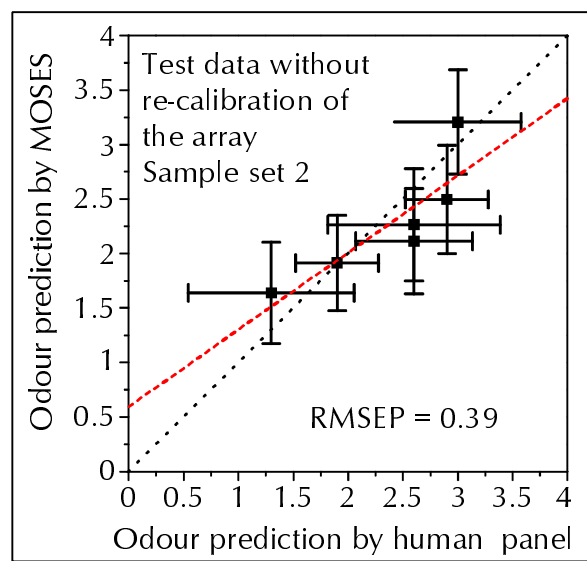
*Fig. 4.2.3.6: PCR (**test data, without re-calibration**) depicting the correlation between the odour evaluation by the human sensory panel and the odour prediction by MOSES. This prediction is based on 108 individual measurements of sample set 2. The calibration shown in Fig. 4.2.3.5 served as a model. Each data point in the diagram corresponds to the mean value of nine individual electronic nose measurements and the sensory evaluations of the panellists; the error bars represent the standard deviation (± 1 sd). The RMSEP is a measure of the quality of the predicted values compared with the true values (see Eq E4.2.3.1).*
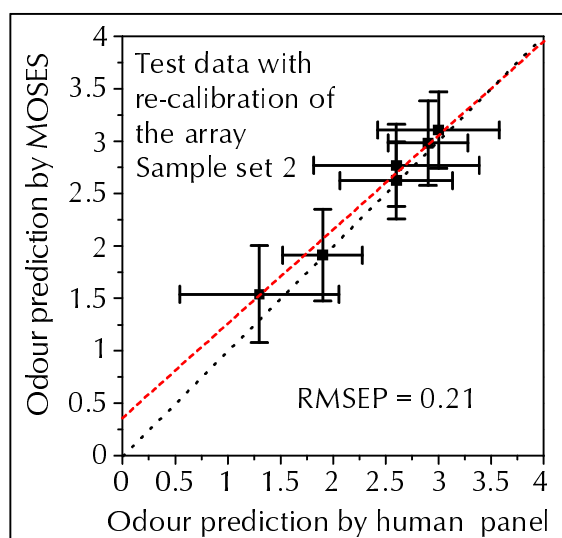
*Fig. 4.2.3.7: PCR (**test data with re-calibration**) displaying the correlation between the odour evaluation by the human sensory panel and the odour prediction by MOSES. This prediction is based on 108 individual measurements of sample set 2. The calibration shown in Fig. 4.2.3.5 served as a model. Each data point in the diagram corresponds to the mean value of nine individual electronic nose measurements and the sensory evaluations of the panellists; the error bars represent the standard deviation (± 1 sd). The RMSEP is a measure of the quality of the predicted values compared with the true values (see Eq E4.2.3.1).*

An important aspect in the establishment of a reliable calibration model is the use of appropriate samples for training, covering the whole range of variation expected in future samples. If such calibration models are based on "real-life" samples this task is even more difficult to realise because extremes (in our case samples to which an odour score of "0" or "4" would be attributed) do in general rarely occur. This circumstance has the following consequences. Firstly, only algorithms like PCR which enable extrapolation are useful. Secondly, the model is based on samples with a relatively low variation and thus prediction errors increase even though a linear evaluation algorithm is applied.

Furthermore, the GC/MS investigations pointed out that the samples could not be stored without any release of remaining solvents and/or off-odours between the creation of the training and –two months later- the test data set (see Fig. 4.2.2.7). The augmentation of the RMSEP may also be related to the fact that the samples were examined by the sensory panel only before the establishment of the training data set. Therefore, in all five diagrams (Figs. 4.2.3.3 - 4.2.3.7) the standard deviation for the human odour prediction is the same. One might

assume that after the decrease in the total amount of volatiles present in the headspace the sensory analysis may be different too.

4.2.4 Long-term Investigations, Sensor Response Fluctuations and Re-calibration

The need for re-calibration of sensor arrays becomes evident when looking at the sensor signals upon exposure to a re-calibration standard (constant concentration of a mixture of toluene, n-octane, propan-1-ol and ethyl acetate, ratio 1:1:1:1) over a period of six months (Figs. 4.2.4.1 - 4.2.4.2). Although the concentration of the re-calibration standard should be constant the sensor responses show fluctuations which are higher in the case of MOXs (standard deviation is 7.9% of the mean value) compared with QCMs (standard deviation is 2.8% of the mean value). The reasons for these fluctuations will be discussed in more detail later.
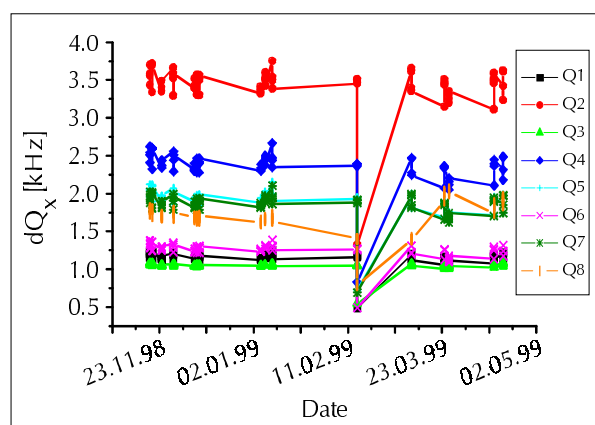
Fig. 4.2.4.1: Sensor responses (signal height) of QCMs (dQ_x) upon exposure to a re-calibration standard over a period of half a year; raw data recorded in Tübingen.
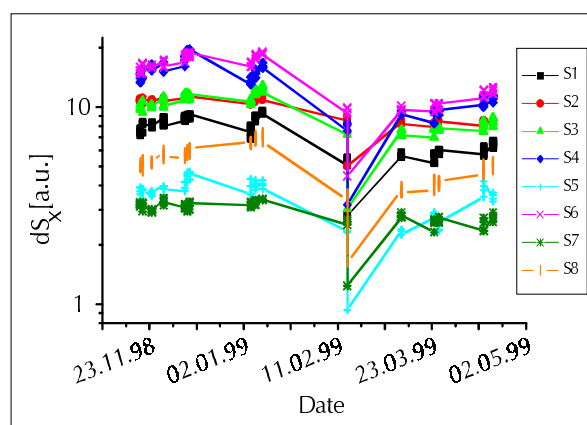
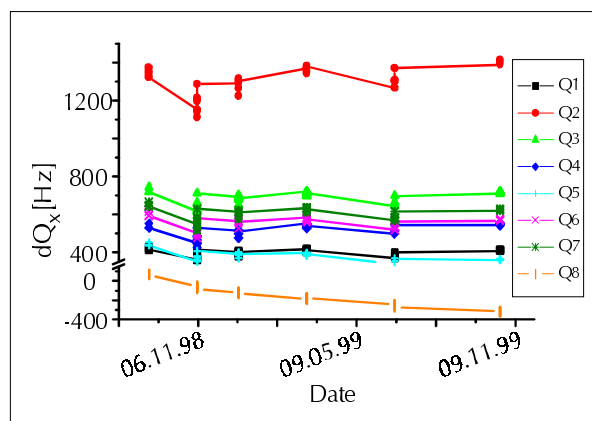*Fig. 4.2.4.2: Sensor responses (signal height) of MOXs (dS_x) upon exposure to a re-calibration standard over a period of half a year; raw data recorded in Tübingen.*

The figures displaying the raw data of QCM and MOX sensor responses (from the arrays located at Tübingen) can generally be described to have a rather small scatter in the individual samples (on a certain measurement day) and low deviations over the whole measurement period. Obviously, on February 15, 1999 one re-calibration sample has to be considered as a complete outlier which influenced both the Q_x and S_x in the same manner.

In order to minimise the systematic error that naturally occurs in the sample preparation, sample conditioning and sample up-take (route from the headspace vial to the sensor system's inlet), the following mathematical operation was applied to the aforementioned raw data. On each measurement day, eight re-

calibration samples were investigated together with actual samples in the same run. Thereupon, the mean value of each sensor after exposure to the eight re-calibration samples was calculated.

$$d\overline{Q}_x = \frac{1}{8}\sum_{y=1}^{n} dQ_x \qquad\qquad \text{E4.2.4.1}$$

$d\overline{Q}_x =$ mean value of each individual QCM, x = 1-8, n = 8

$$d\overline{S}_x = \frac{1}{8}\sum_{y=1}^{n} dS_x \qquad\qquad \text{E4.2.4.2}$$

$d\overline{S}_x =$ mean value of each individual MOX, x = 1-8, n = 8

Subsequently, for a particular measurement day a mean value of all sensor responses (QCMs and MOXs have been considered separately) was determined:

$$d\tilde{Q}_{date} = \frac{1}{8}\sum_{x=1}^{n} d\overline{Q}_x \qquad\qquad \text{E4.2.4.3}$$

$d\tilde{Q}_{date} =$ mean value of the individual QCM mean values, x = 1-8

$$d\tilde{S}_{date} = \frac{1}{8}\sum_{x=1}^{n} d\overline{S}_x \qquad\qquad \text{E4.2.4.4}$$

$d\tilde{S}_{date} =$ mean value of the individual MOX mean values, x = 1-8

This mean value ($d\tilde{Q}_{date}$ and $d\tilde{S}_{date}$) was divided by the value for each individual sensor ($d\overline{Q}_x$ and $d\overline{S}_x$) resulting in the relative values of frequency shift and conductivity change, respectively, which are presented in the following diagrams (Figs. 4.2.4.3 and 4.2.4.4):

$$rd\overline{Q}_x = \frac{d\tilde{Q}_{date}}{d\overline{Q}_x} \qquad\qquad \text{E4.2.4.5}$$

$rd\overline{Q}_x =$ measurement data, shown in Fig. 4.2.4.3.

$$rd\overline{S}_x = \frac{d\tilde{S}_{date}}{d\overline{S}_x} \qquad\qquad \text{E4.2.4.6}$$

$rd\overline{S}_x =$ measurement data, shown in Fig. 4.2.4.4.

The same procedure was carried out for the standard deviations (represented by the error bars).
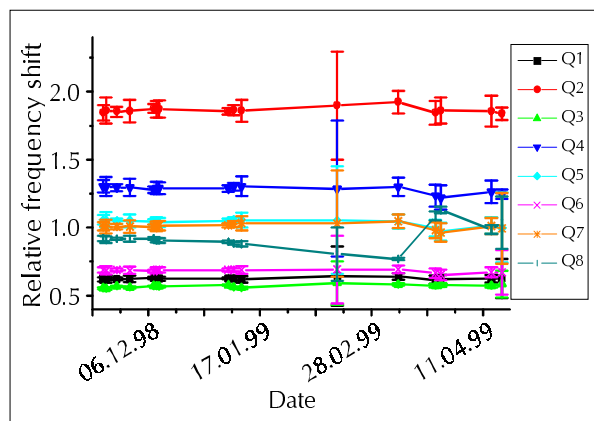
Fig. 4.2.4.3: Relative sensor responses of QCMs ($rd\overline{Q}_x$) upon exposure to a re-calibration standard; data recorded in Tübingen.
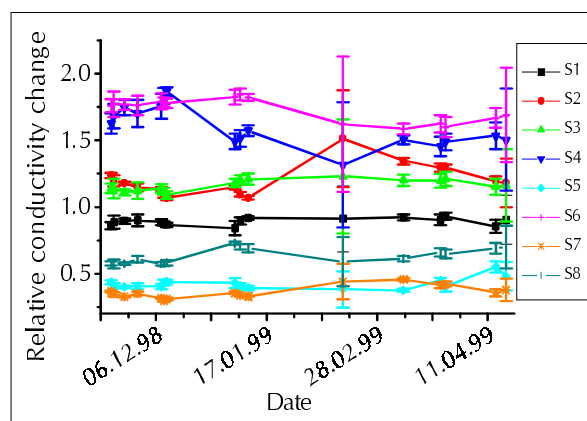
Fig. 4.2.4.4: Relative sensor responses of MOXs ($rd\overline{S}_x$) upon exposure to a re-calibration standard; data recorded in Tübingen.

The previously described mathematical operation led to a smoothing of the curves. Considering the small error bars (neglecting the outlier mentioned above) the QCMs reveal a very satisfying long-term stability. For the MOXs it is obvious that the sensors respond differently to the headspace of a re-calibration sample. If the curves were parallel, the conclusion could be made that all of them would have been exposed to a diverse concentration as intended, e.g. if the concentration is lower than expected, the responses of all MOXs would show a decrease. However, since some of the graphs intersect this assumption cannot be made. More probably, the MOXs display statistical fluctuations which are not coherent with the sampling of the re-calibration sample or the headspace composition of the standard itself.

Without an appropriate re-calibration procedure the odour prediction of samples worsens when measured several months after the calibration data's recording (see Figs. 4.2.3.6 and 4.2.3.7).

Figs. 4.2.4.1 - 4.2.4.4 demonstrate that the responses of most sensors have the same temporal behaviour. Thus, there has to be a common effect which influences the sensors in the same manner. This holds especially for the raw data where a correlation is even more obvious. Therefore, the correlation coefficients $r_{xy}(\tau)$ (see chapter 2.3 *Sensor Drift - Evaluation and Compensation*) were determined for both the types of individual sensors, Q_x and S_x.

A positive correlation coefficient $r_{xy}(\tau)$ indicates a positive relation between the two variables, i.e. when one increases, the other also has the tendency to increase. The closer to +1, the stronger is this relation. Negative correlation indicates a negative relation between the two variables (sensors), i.e. when one

increases the other has the tendency to decrease. The closer to –1, the stronger is this relation.

One has to keep in mind that in the case of x=y the correlation coefficient $r_{xy}(\tau)$ becomes $r_{xy}(\tau) \equiv 1$. Therefore, the afterimages displaying the correlation coefficients show this phenomenon if the response data of a certain sensor are correlated with themselves. In the following figures the y-axis is denoted "correlation coefficient", in fact the empirical cross-correlation coefficient $r_{xy}(\tau)$ is meant (to avoid confusion with the empirical autocorrelation coefficient $r_{xx}(\tau)$).
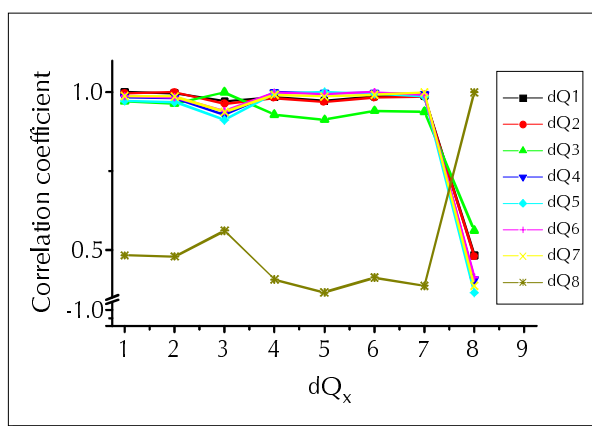
Fig. 4.2.4.5: Correlation coefficients $r_{xy}(\tau)$ of dQ_x; data recorded in Tübingen.
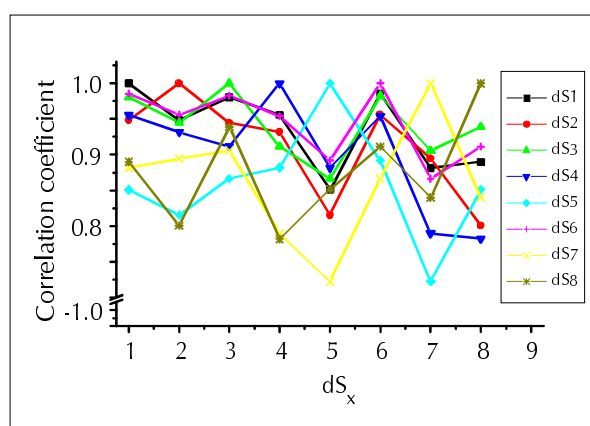
Fig. 4.2.4.6: Correlation coefficients $r_{xy}(\tau)$ of dS_x; data recorded in Tübingen.

Fig. 4.2.4.5 shows how strongly the responses of the individual QCMs are correlated; the values of r reach the maximum of 1 for almost all QCMs. Sensor Q_8 reveals exceptional behaviour, although its correlation coefficient is also positive the absolute value is only half of Q_{1-7}. In simpler terms, a concentration change of the re-calibration sample's headspace has the same influence on Q_{1-7}, whereas Q_8 is less affected. With the goal of finding suitable re-calibration strategies, the characteristics of Q_{1-7} seem to be more desirable; the same mathematical algorithm can be applied to all sensors neglecting small errors which derive from the fact that the r_{xy}'s are slightly different. Moreover, the high correlation between the sensors Q_{1-7} also indicate the stability of their responses upon exposure to the TOPE standard over time.

The correlation coefficients of the MOXs exhibit a comparable tendency (see Fig. 4.2.4.6). All of them have values higher than 0.7, but the scattering within the range 0.7 to 1.0 is higher than that for the QCMs. This is a sign for the individual behaviour of the MOXs towards the same analytes / concentrations. This makes the re-calibration procedure more demanding. It also has to be taken into consideration that MOXs do not normally respond linearly to concentration changes in the headspace.

In addition to the long-term investigations carried out over six months at the IPC (see Figs. 4.2.4.1 and 4.2.4.2), the same aforementioned re-calibration standard has been applied to another MOSES instrument located at Nestlé. Both set-ups consist of the same set of sensors. The whole period comprised one year, the procedure being repeated every two months. The results are displayed in Figs. 4.2.4.7 and 4.2.4.8.

Fig. 4.2.4.7: Sensor responses (signal height) of QCMs (dQ_x) upon exposure to a re-calibration standard over a period of one year; raw data recorded at Nestlé [Vis 01].
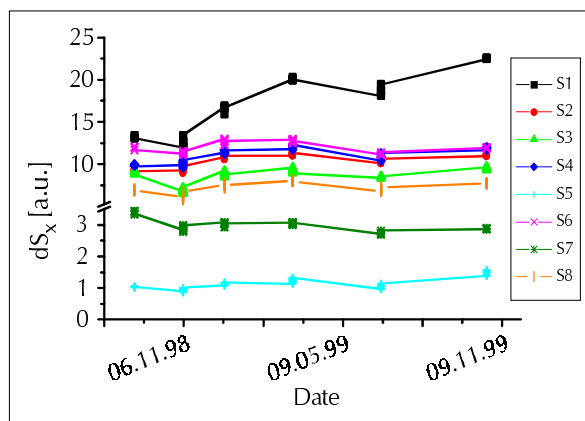
Fig. 4.2.4.8: Sensor responses (signal height) of MOXs (dS_x) upon exposure to a re-calibration standard over a period of one year; raw data recorded at Nestlé [Vis 01].

The two figures above (Figs. 4.2.4.7 - 4.2.4.8) show clearly that the sensors are highly correlated with respect to their sensor response upon exposure to the re-calibration standard. This holds for the QCMs as well as for the MOXs. Apart from one QCM which revealed a real drift over the measurement period (Q_8), all the other sensors only showed response fluctuations (without any constant increase or decrease in the signal). The scattering of the sensor responses on a particular measurement day is very small. Compared with the same kind of data which have been obtained with the system located in Tübingen (see Fig. 4.2.4.1) these results are remarkable indicating high accuracy in the re-calibration sample's preparation. Since at both locations the same headspace sampler (with identical measurement parameters) was used, instrumental error is unlikely. The long-term behaviour of S_1 is still a matter of debate. The diagrams showing the correlation coefficients of the data in Figs. 4.2.4.7 and 4.2.4.8 are given below (Figs. 4.2.4.9 and 4.2.4.10).
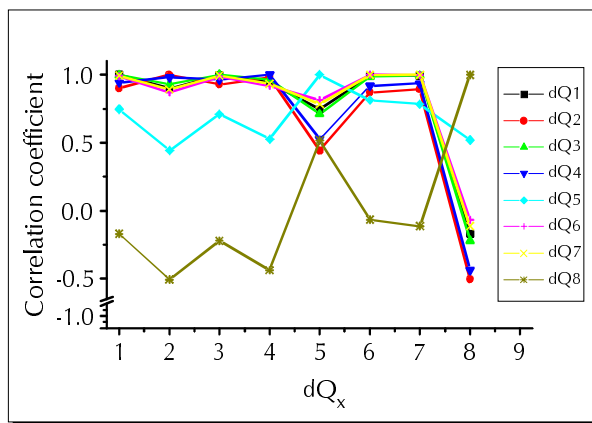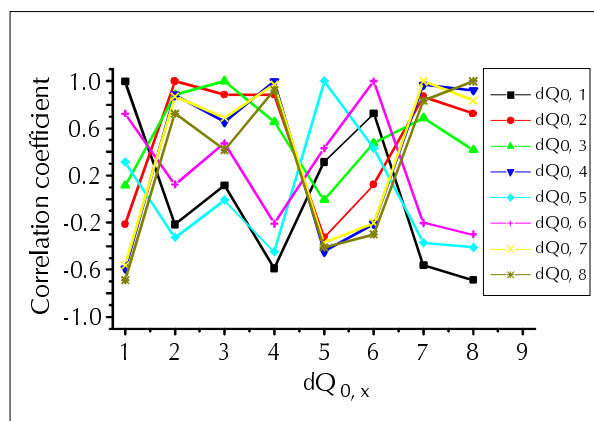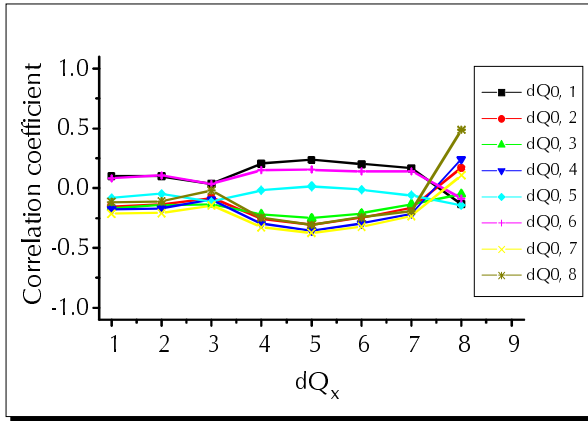
Fig. 4.2.4.9: Correlation coefficients $r_{xy}(\tau)$ of dQ_x; data recorded at Nestlé.
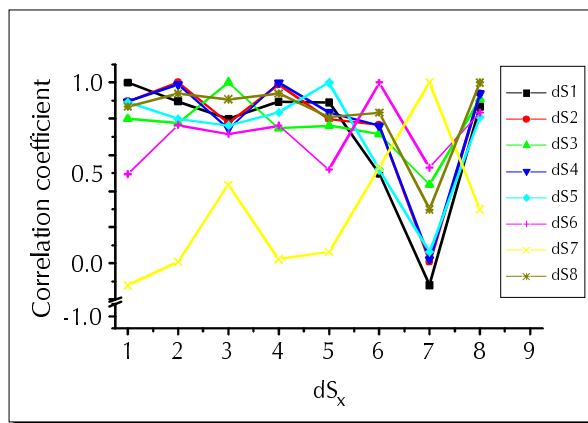
Fig. 4.2.4.10: Correlation coefficients $r_{xy}(\tau)$ of dS_x; data recorded at Nestlé.

With regard to the results obtained for the data recorded in Tübingen (see Fig. 4.2.4.5) the correlation coefficients presented in Fig. 4.2.4.9 show slight deviations; it is again the sensor Q_8 which has a value of $r_{xy}(\tau)$ being completely different to those of the other QCMs. Moreover, in this case the coefficient explaining the correlation between Q_8 and $Q_{1, 2, 3, 4, 6, 7}$ is negative. This signifies that if changes in the headspace lead to an increase in the response of Q_8, all the other sensors show a contrary behaviour (or vice versa).

For the MOXs there is also one sensor (S_7) which showed an inverse performance to the others. Again the scatter of the absolute values is higher than for the QCMs that were exposed to the same headspace at the same time. In contrast to the phenomenon observed in the case of the microbalances (here the sensor Q_8 with a real drift also had an entirely different correlation coefficient) this behaviour cannot be stated for S_7; although its response (dS_7) over a period of one year seems to be coherent with those of $S_{2-6, 8}$ the correlation coefficient indicates divergence. Since the values are rather small the assumption can be made that there is hardly any correlation. The possible reasons for this phenomenon are manifold:

- The preparation of the re-calibration standard is highly dependent on the operator's accuracy. Although a pipette (Eppendorf, Multipette™ plus) was used to introduce the organic solvents into the polyethylene glycol (PEG 400) matrix, there are still errors caused by the pipette itself or the individual operator which have to be considered.
- As proved by independent GC/MS investigations the error resulting from faulty sample uptake by the headspace sampler is negligible.
- Small humidity changes may also affect the sensor responses. However, this effect cannot be too dominant as in this case the QCMs should show the

same behaviour as the MOXs (since polymer-coated quartz resonators are very sensitive to humidity changes).

In addition to the evaluation of the correlation among sensors of the same transduction principle the correlation coefficients' determination was also extended to study the relation between different sensor types (QCMs and MOXs). Therefore, not only the signal height (baseline subtracted from the maximum value, hereinafter called dQ_x and dS_x, respectively) but also the response values upon exposure to synthetic air (baselines, hereinafter called $dQ_{0, x}$ and $S_{0, x}$, respectively) have been examined in detail. Thus, several combinations of the data given above were studied in order to find the reasons for the phenomenological observations. The following four figures represent the time dependent "zero air" values $dQ_{0, x}$ and $S_{0, x}$ of QCMs and MOXs for the arrays used in Tübingen (Figs. 4.2.4.11 and 4.2.4.12) and at Nestlé (Figs. 4.2.4.18 and 4.2.4.19). The $dQ_{0, x}$ responses for the first measurement day were set to 0; the values for the subsequent days are displayed with respect to this starting point.
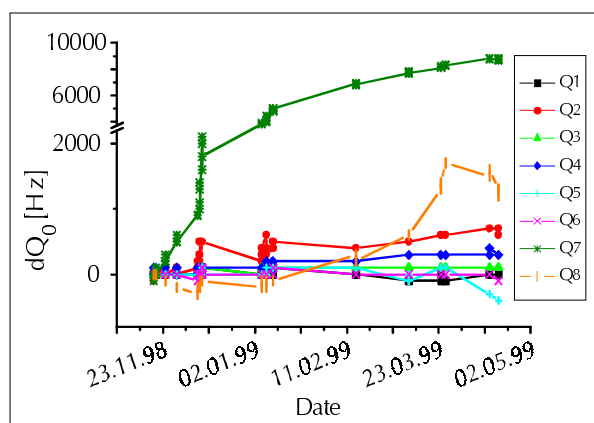
Fig. 4.2.4.11: dQ_0 responses of QCMs recorded over half a year in Tübingen.
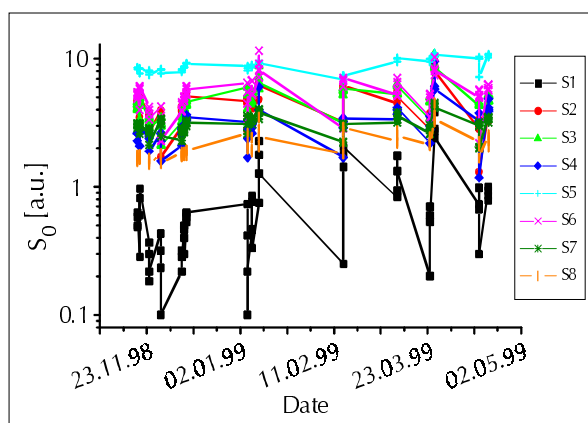
Fig. 4.2.4.12: S_0 responses of MOXs recorded over half a year in Tübingen.

Although the responses of Q_7 upon exposure to the re-calibration samples (dQ_7, see Fig. 4.2.4.1) are very stable, the monitoring of its baseline over the same period exhibits deviation. The curve for Q_7 ($dQ_{0, 7}$) shows the largest baseline shift of all QCMs with respect to the first measurement day. Nevertheless, this drift seems to have no influence on the sensor's sensitivity. Compared with Q_7 the other quartzes reveal fluctuations which are only in the order of some hundred Hz. Moreover, it is remarkable that the baseline scattering on a certain measurement day does not exceed 100 Hz (even for Q_7).

In contrast to the QCMs the metal oxide sensor responses for the individual re-calibration samples deviate considerably. However, their variations seem to have

a common origin which is also demonstrated by the high values of the correlation coefficients. The scattering itself appears to be statistical.
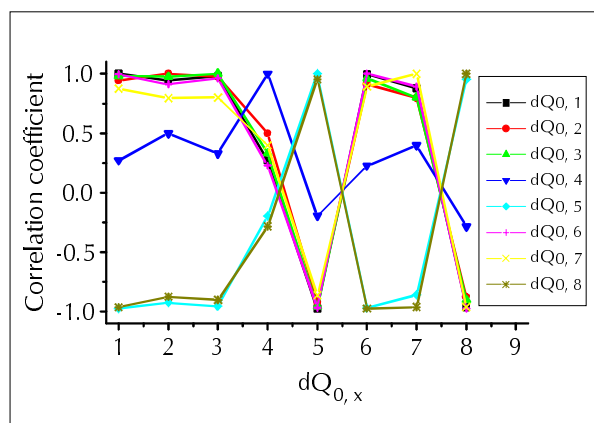

Fig. 4.2.4.13: Correlation coefficients $r_{xy}(\tau)$ of $dQ_{0,x}$; data recorded in Tübingen.
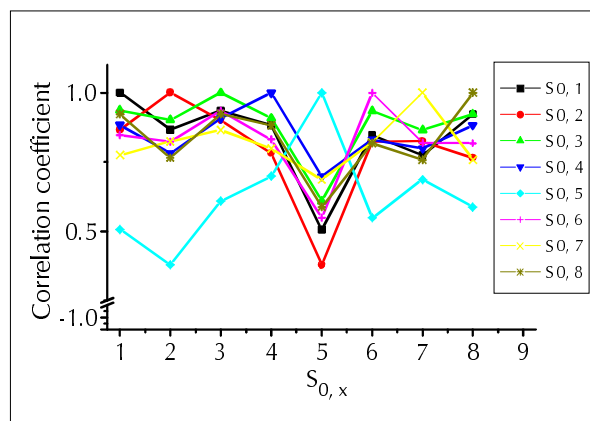
Fig. 4.2.4.14: Correlation coefficients $r_{xy}(\tau)$ of $S_{0,x}$; data recorded in Tübingen.

The values of the correlation coefficients of $dQ_{0,x}$ span nearly the whole potential range between $-1 \leq r_{xy}(\tau) \leq 1$. The fact that negative and positive coefficients were obtained for all QCMs indicates the existence of different causes of the $dQ_{0,x}$ changes. A careful look, however, shows a common tendency to two groups of QCMs. To one of them belong the sensors $Q_{2-4,7,8}$, to the other $Q_{1,5,6}$.

Although the MOXs were exposed simultaneously to the same synthetic air, their correlation coefficients $r_{xy}(\tau)$ are all positive having quite high values between 0.75 and 1.0. Thus, there seems to be a common effect to which seven of the eight sensors respond comparably. Only sensor S_5 exhibits behaviour distinct from the others, although its correlation coefficient is also positive indicating a corporate trend.

To answer the question if changes in the sensor's baseline over time ($dQ_{0,x}$ and $S_{0,x}$) have an influence on its response upon exposure to a defined gas concentration, the correlation coefficients between dQ_x and $dQ_{0,x}$ as well as dS_x and $S_{0,x}$ were determined. The results are displayed in Figs. 4.2.4.15 and 4.2.4.16.
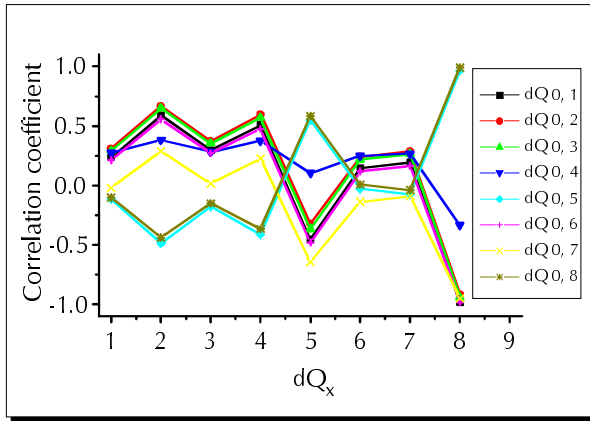
Fig. 4.2.4.15: Correlation coefficients $r_{xy}(\tau)$ of dQ_x vs. $dQ_{0,x}$; data recorded in Tübingen.
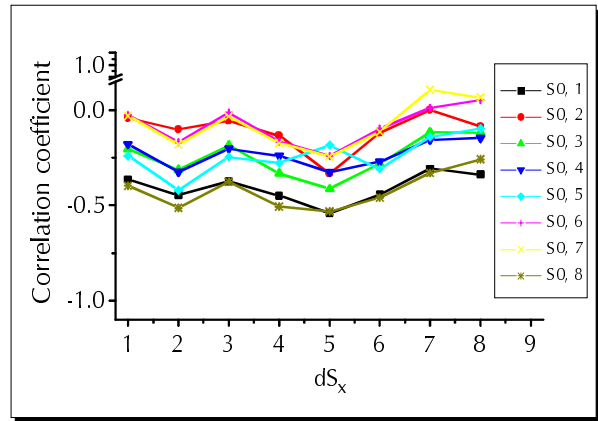
Fig. 4.2.4.16: Correlation coefficients $r_{xy}(\tau)$ of dS_x vs. $S_{0,x}$; data recorded in Tübingen.

In the case of the QCMs it can be stated that due to the small values of $r_{xy}(\tau)$ changes in the baseline only have minor impacts on dQ_x. Thus, knowledge of $dQ_{0,x}$ will probably not provide any information on the subsequent sensor's response. However, the already described correlation of $dQ_{0,x}$ fluctuations (see Fig. 4.2.4.13) leading to a classification of two groups of QCMs, also persists in the present plot.

The curves for the individual MOXs shown in Fig. 4.2.4.16 run very much in parallel; this means for instance that sensors like S_2 and S_7 have for $S_{1,\,3\text{-}6,\,8}$ the least negative values of $r_{xy}(\tau)$ whereas the sensors S_1 and S_8 have in nearly all cases the most negative values. As a joint feature the negative algebraic sign for almost each sensor is worth noting. This characteristic signifies that the baseline shift and the corresponding sensor response with respect to analyte exposure comport antithetically. If the correlation coefficient is very small (e.g. for S_2 and S_7), changes in the baseline cannot be correlated with any other dS_x, not even with its own. On the other hand sensors like S_1 and S_8 having constant negative values for the additional MOXs might be potential candidates to predict the dS_x behaviour by taking their baseline fluctuations into account.
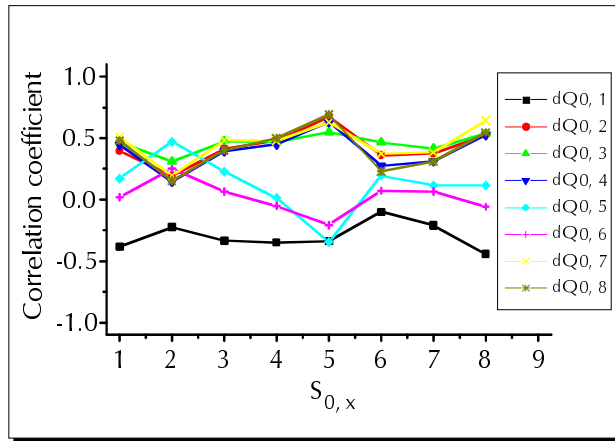
Fig. 4.2.4.17: Correlation coefficients $r_{xy}(\tau)$ of $S_{0,x}$ vs. $dQ_{0,x}$; data recorded in Tübingen.

High positive correlation coefficients $r_{xy}(\tau)$ would demonstrate that the microbalances and the metal oxide sensors react to changes in the "background" gas in a very similar way. However, from Fig.4.2.4.17 such a behaviour cannot be seen. The majority of all values is located in the range between 0 and 0.5. Once again, the almost identical behaviour of the QCMs $Q_{2-4, 7, 8}$ is very obvious (compare Figs. 4.2.4.13 and 4.2.4.15).

The following paragraph deals with the sensor data which have been found at Nestlé.
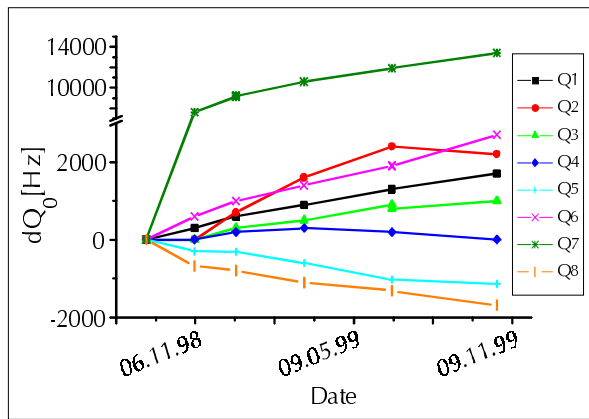
Fig. 4.2.4.18: dQ_0 responses of QCMs recorded over one year at Nestlé [Vis 01].
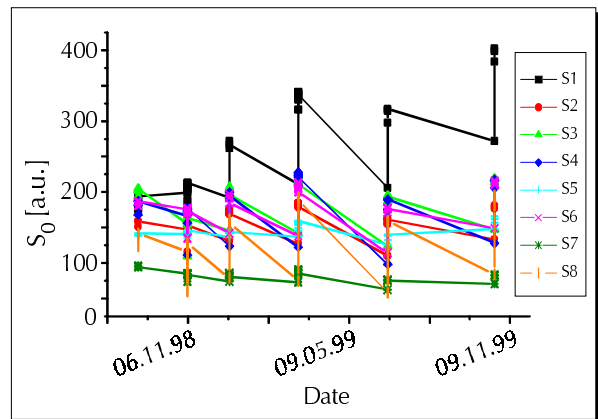
Fig. 4.2.4.19: S_0 responses of MOXs recorded over one year at Nestlé [Vis 01].

The baseline shifts of the QCMs being part of the MOSES system located at Nestlé are very remarkable (see Fig. 4.2.4.18). All of them follow a linear trend which can also be described as a real drift phenomenon. The changes occur in two directions, positive and negative shifts of $Q_{0,x}$ (the quartz' frequency upon exposure to synthetic air). Over the period of one year seven QCMs have a drift

of 2000 Hz at maximum. Here, sensor Q_7 shows exceptional behaviour revealing a baseline change of 13000 Hz at the end of the investigations. The scattering which might result from the individual re-calibration samples on a certain measurement day is extremely small.

As expected the MOXs are more sensitive to changes in the background gas (synthetic air) resulting in larger deviations in $S_{0,x}$. Fig. 4.2.4.19 displays in a very clear manner how the baseline is influenced regularly by only one sample whereas the others led to rather stable sensor signals. This phenomenon will be discussed in more detail in the chapter 4.2.5 *Re-calibration Strategies*. Apart from this consistent outlier, the long-term stabilities of the $S_{0,x}$ averages are satisfying and they do not indicate any drift.

Fig. 4.2.4.20: Correlation coefficients $r_{xy}(\tau)$ of $dQ_{0,x}$; data recorded at Nestlé.
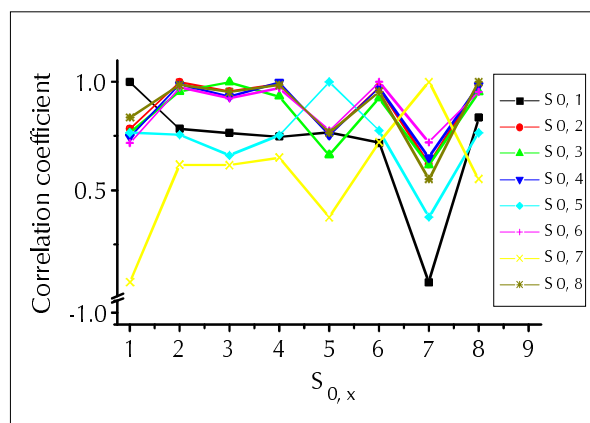
Fig. 4.2.4.21: Correlation coefficients $r_{xy}(\tau)$ of $S_{0,x}$; data recorded at Nestlé.

Disregarding the correlation coefficient $r_{xy}(\tau)$ for the baseline value of sensor Q_4, Fig. 4.2.4.20 demonstrates an unequivocal result; the whole QCM array can be divided into two groups. To group I belong $Q_{1-3, 6, 7}$ and to group II the sensors $Q_{5, 8}$. For sensors of the same group the correlation coefficient's value is almost +1, whereas for the QCMs of the opposite group the value is in the region of –1 (and vice versa). With regard to Fig. 4.2.4.18 this observation can be explained conclusively; there the sensors $Q_{5, 8}$ (group II) showed a negative drift of their baseline in contrast to the sensors of group I displaying a positive drift. Q_4 shows independent behaviour and seems not be highly correlated with the baseline responses of the other sensors.

In Fig. 4.2.4.21 five metal oxide sensors again behave very similarly, namely $S_{2-4, 6, 8}$. Their coefficients are in general high ($r_{xy}(\tau) \geq 0.7$). Among all sensors negative values are an exception; r is only negative for the S_1/S_7 pair.

Fig. 4.2.4.22: Correlation coefficients $r_{xy}(\tau)$ of dQ_x vs. $dQ_{0,x}$; data recorded at Nestlé.
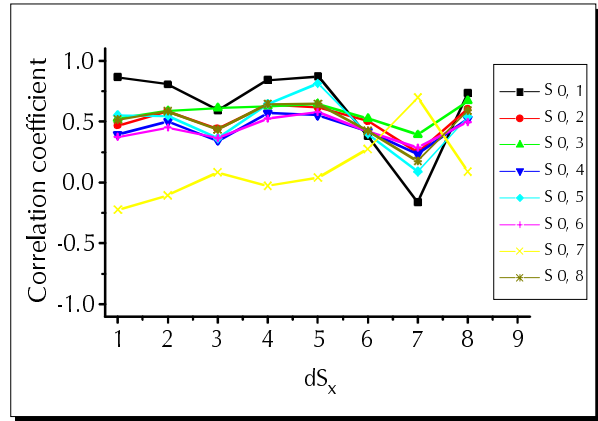
Fig. 4.2.4.23: Correlation coefficients $r_{xy}(\tau)$ of dS_x vs. $S_{0,x}$; data recorded at Nestlé.

In accordance with Fig. 4.2.4.20 the plot in Fig. 4.2.4.22 shows a comparable result. Correlation between the sensor responses upon exposure to a re-calibration sample (x-axis) and the baseline responses of sensors belonging to the same group (for classification see the paragraph above) led to positive $r_{xy}(\tau)$-values. If the dQ_x of a sensor is correlated with the $dQ_{0,x}$ of a sensor being part of the opposite group the correlation coefficient is negative. For instance, the value of dQ_2 is positively correlated with $dQ_{0, 1\text{-}4, 6, 7}$ whereas negative values are obtained if the correlation is carried out with $dQ_{0, 5, 8}$. Compared to the corresponding data which have been gained after the evaluation of the array located in Tübingen (see Fig. 4.2.4.15) it can be stated that the absolute values of r are larger for the QCMs used by Nestlé.
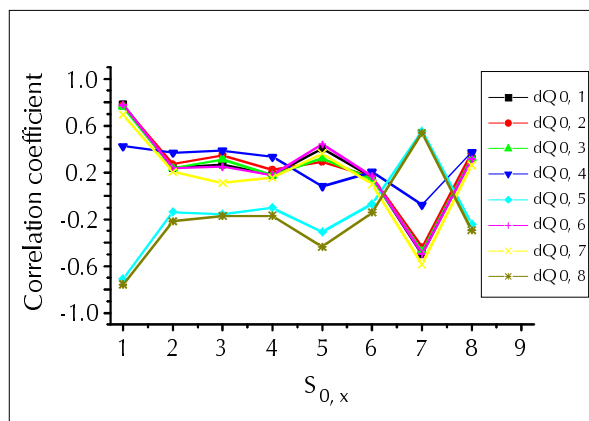
Fig. 4.2.4.24: Correlation coefficients $r_{xy}(\tau)$ of $S_{0,x}$ vs. $dQ_{0,x}$; data recorded at Nestlé.

Fig. 4.2.4.24 only shows significant correlation coefficients (between the baseline shifts of MOXs and QCMs) for the metal oxide sensor S_1. Its response

changes upon exposure to synthetic air correlate positively with the QCMs of group I and negatively with those of group II.

As mentioned in chapter 2.3 *Sensor Drift - Evaluation and Compensation*, the correlation of sensor data within a time series can be evaluated by inspecting the autocorrelation function. The $r_{yy}(\tau)$ for all sensors of both sensor systems (located at Nestlé and in Tübingen) were determined; the autocorrelation functions showed in all cases a statistical, random behaviour indicating that the sensor data were uncorrelated. To give an example, Fig. 4.2.4.25 displays the autocorrelation function of a QCM; the corresponding functions for the other sensors look similar. In only one case, a clear sign for a drifting sensor could be found. As depicted in Fig. 4.2.4.26, the QCM Q_8 of the array installed at Nestlé showed a steadily decreasing $r_{yy}(\tau)$-value (except for the last four values). From 32 sensors, Q_8 was the single one exhibiting a real drift. A first hint of this is already evident from Fig. 4.2.4.7.
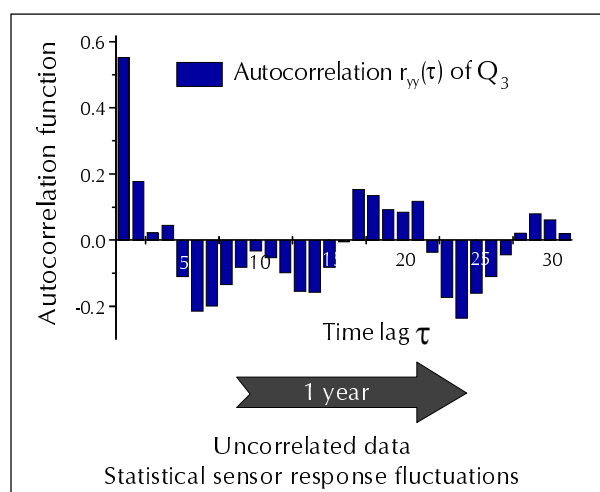
Fig. 4.2.4.25: Autocorrelation function of Q_3 of the array installed at Nestlé.
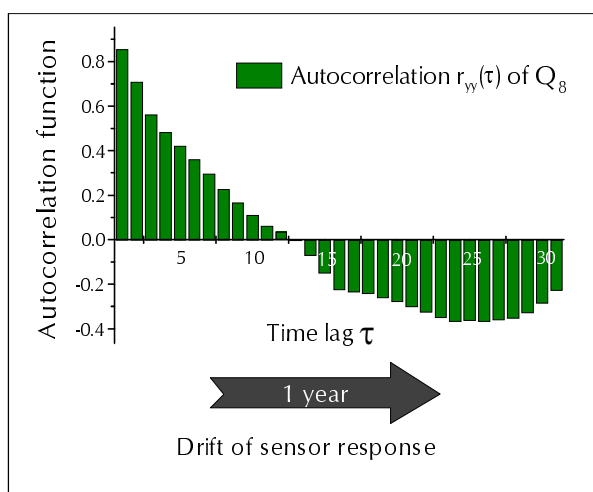
Fig. 4.2.4.26: Autocorrelation function of Q_8 of the array installed at Nestlé.

The results which were obtained for the cross-correlation coefficients $r_{xy}(\tau)$ of the QCM sensor responses of the Nestlé array (see Fig. 4.2.4.9) confirm the corresponding autocorrelation functions discussed above. Although the individual sensor signals show statistical fluctuations upon exposure to a re-calibration sample over a longer time period, they are still (cross-) correlated on a particular measurement day. Therefore, the prediction of the sensor response of a particular Q_x should be possible on the basis of the response of Q_y. This prediction works well if the two QCMs being correlated have a $r_{xy}(\tau)$-value that is only slightly less than +1. As an example, in Fig. 4.2.4.27 the predicted response values of Q_1 are plotted against the measured frequency shifts of Q_3. The RMSE in this case

amounts to only 0.7%. The analogous prediction errors of the predicted sensor response on the basis of the shift of Q_3 are listed in Table 4.2.4.1. The values are considerably small (between 1.7 and 3.7%) indicating the high precision of the prediction ability. In contrast to these results it is hardly possible to give a reliable prediction of a sensor's response on the basis of a drifting sensor. As already mentioned in Fig. 4.2.4.26, the QCM Q_8 revealed a significant response drift over the period of one year. Hence, such a sensor cannot be used to predict other frequency shifts (see Fig. 4.2.4.28).
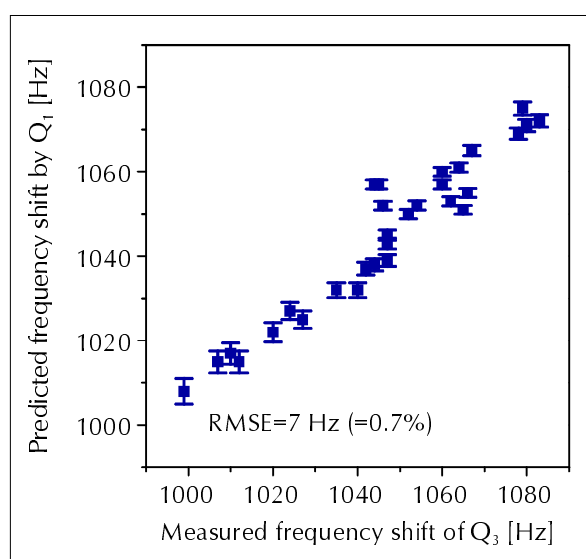
Fig. 4.2.4.27: Prediction of the frequency shift of Q_1 on the basis of the response of Q_3 upon exposure to a re-calibration sample. Q_3 is a non-drifting sensor.
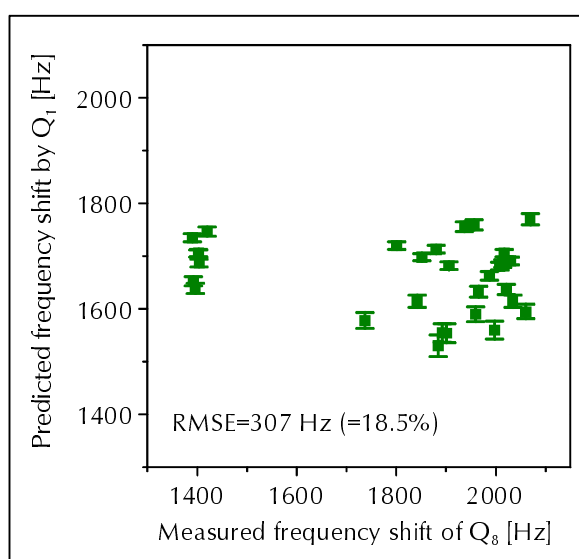
Fig. 4.2.4.28: Prediction of the frequency shift of Q_1 on the basis of the response of Q_8 upon exposure to a re-calibration sample. Q_8 is a drifting sensor.

Sensor	Q_2	Q_4	Q_5	Q_5	Q_7
RMSE [Hz]	40	58	71	31	31
Rel. RMSE [%]	2.4	2.5	3.7	2.5	1.7

Table 4.2.4.1: Prediction errors of sensor responses (RMSE and rel. RMSE, respectively).

4.2.5 Re-calibration Strategies

In order to compensate for the influence of sensor fluctuations or drift effects on PCA and PCR evaluations an appropriate re-calibration strategy is essential. Several investigations showed that only application-related re-calibration procedures lead to satisfying results concerning the differentiation of varying samples or the prediction of certain attributes (e.g. odour score). The re-calibration samples have to fulfil two prerequisites: The headspace should have a

similar composition to the samples being investigated. In addition, the headspace component concentrations should be in the same range; this becomes especially important for MOXs since they display a non-linear analyte concentration sensor response behaviour.

Not only the type of re-calibration samples is relevant but also the position of these samples within a whole sample run (including re-calibration and "normal" sample) is an issue if reliable results are to be obtained. Therefore, the number of those samples needed for a reliable re-calibration and their distribution among all the other vials were investigated.

The approach of Tübingen was different compared with the way in which Nestlé was performing the re-calibration. In Tübingen the vials used as standards were distributed randomly among the other (packaging material) samples. In contrast, at Nestlé all of them were positioned at the beginning of each measurement sequence. Figs. 4.2.5.1 and 4.2.5.2 display the baseline values $S_{0, MOX}$ of both MOXs arrays on a particular day.
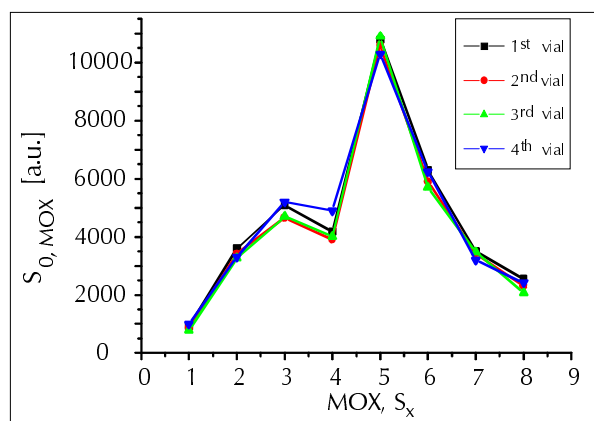
Fig. 4.2.5.1: S_0 of MOXs before exposure to a re-calibration standard; the **standards** were **distributed randomly** within a sample run; strategy at **Tübingen**.
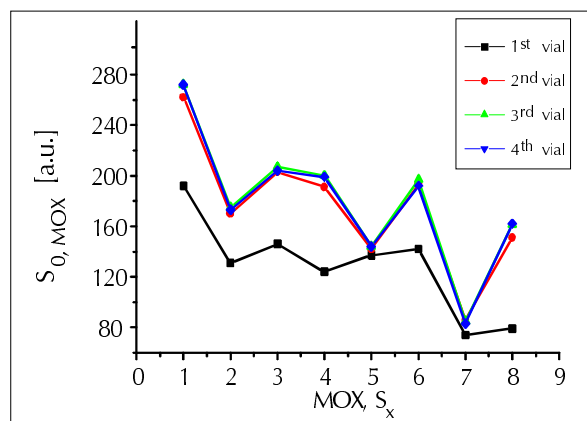
Fig. 4.2.5.2: S_0 of MOXs before exposure to a re-calibration standard; the **standards** were measured **at the beginning** of a sample run; strategy at **Nestlé**.

The fact that the individual $S_{0, MOX}$ values for the two arrays are quite different is not surprising; the reason for this behaviour might be the specific histories of each array. For Nestlé, it is much more important that after exposing the sensors to the first vial, the S_0 values increase and then remain stable for all subsequent vials containing a standard. This is a clear indication of a pre-conditioning effect of the SnO_2 material. Although no significant dependency of the sensor signals (i.e. the height of the measurement curve) upon exposure to the re-calibration samples could be observed, it cannot be excluded that for other standards and headspace compositions, this baseline shift might have an impact. Therefore, it is explicitly

advised to distribute the standards randomly or evenly among the measurement sequence. If, for practical reasons, the re-calibration samples have to be positioned at the beginning, at least the sensor responses to the first vial should be omitted. Taking this into account both re-calibration strategies led to a successful use of the algorithm in order to improve PCA and PCR results.

In contrast to the MOXs, such a baseline shift could not be observed for the QCMs. This demonstrates that "memory" and conditioning effects (generally speaking the sensor's history) play an inferior role for this kind of transducer.

The extensive investigations on edible oils and packaging materials with sensor systems demonstrated the complexity when measuring "real-life" samples. The response pattern of the arrays can be influenced by several causes: the provenience of the samples, the sample preparation before measurement, the sampling system, the sensors (sensor arrays) and the data treatment.

The results presented in this work emphasise the importance to have representative samples for calibration. Errors in the prediction of test samples occur among other things due to variations between the samples used for calibration and testing (which is often unavoidable if using "real-life" samples). In addition, the individual sensors are not absolutely stable regarding their response upon exposure to standards applied for re-calibration. Real drift phenomena were hardly observed, instead (statistical) fluctuations were recorded. The latter, however, had also to be handle in order to obtain reliable predictions.

Since an already existing sensor system always has to be adapted to a particular application, the aforementioned points influencing the whole performance of an analysis vary in their relevance. The MOSES II systems used are established set-ups which proved to be very suitable for assessing quality parameters important for foodstuff or other materials involved in food industry.

New developments in the field of chemical gas sensors concentrate on the miniaturisation of the devices, i.e. tiny sensors, electronics on chip, small housing, simplified sampling unit etc. In other words, the sensor systems became portable with the constraint that their performance is still lower in comparison to (immobile) laboratory set-ups. The miniaturisation of each of the parts listed before holds newly upcoming problems. One of them is the deposition of chemically sensitive layers and this topic will be discussed in the following chapter.

4.3 Miniaturised Gas Sensor System

A major task in the miniaturisation of the sensor system focussed on the coating procedure of sensor surfaces with dimensions in the range of 150 to 800 μm. As chemically sensitive layers, polymers play the dominant role in all three kinds of transducers; the cantilevers, the calorimetric sensors and the capacitors. The use of polymers is a crucial requirement since the power consumption of the whole set-up should be as low as possible (this requirement could hardly be fulfilled if using e.g. MOXs).

The selection of appropriate polymers is govern by two main criteria:

- **Sensitivity** of the polymer towards different VOCs.
- **Wetting ability** of the polymer on the substrate resulting in smooth and homogeneous layers.

The first point is more important if QCMs are used as transducers. Sensors based on optical transduction principles require homogeneous layer, i.e. the dielectric constant has to be the same throughout the entire film. Within this work, the search for polymers aimed at both criteria. However, the investigations on the wetting abilities played a more dominant role.

In order to gain an impression of the preferential sorption of organic volatiles into sensitive layers QCM measurements were carried out to determine the corresponding partition coefficients.

The deposition of the coatings should be carried out automatically resulting in reproducible properties of the sensing layers (e.g. lateral dimensions, thickness). Firstly, a new deposition technique has to be established in order to avoid the main drawbacks of the air-brush method which is commonly used to coat QCMs (experimental results will be discussed later on). In some cases, a modification of the surface properties is necessary to create homogeneous and smooth layers. To change these properties the silanisation of the surface is a technique which eventually improves the layer characteristics on a certain substrate. After a selection of silanisation agents and sensitive layers, preliminary tests were performed to link the different substrates / transducers and layers in a combinatorial manner.

4.3.1 Determination of Partition Coefficients

In a first test series, four QCMs (fundamental frequency f_0 = 30 MHz) have been exposed to ten different organic solvents of various polarities and polarizabilities. The following polymers were chosen for the preliminary tests; PDMS, PEUT, EC and PECH. The layer thickness was approximately 20 kHz for all

polymers. The measurement chamber was kept at a constant temperature of 25° C. The results are exemplarily displayed below in two radial diagrams (one representing the K-values for PDMS, Fig. 4.3.1.1, the other for PECH, Fig. 4.3.1.2).
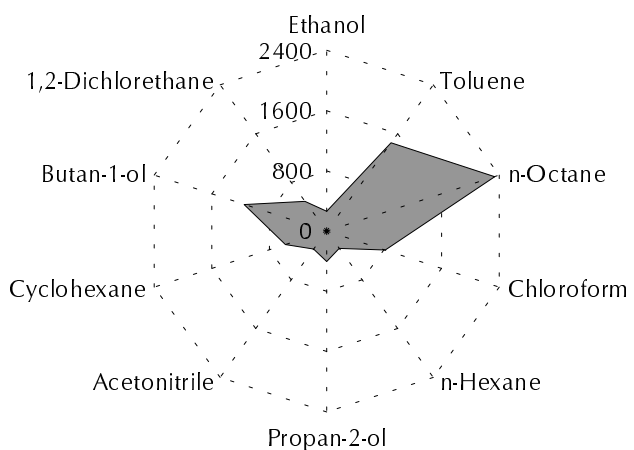
Fig. 4.3.1.1: Polar plot representing the partition coefficients of VOCs in PDMS.
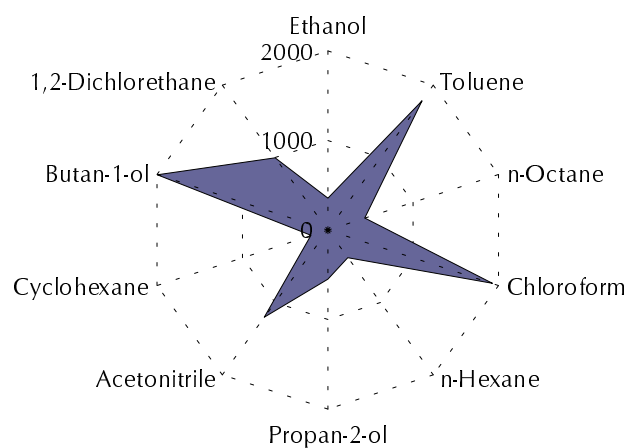
Fig. 4.3.1.2: Polar plot representing the partition coefficients of VOCs in PECH.

On overview on all K-values (all polymer / analyte-combinations) is given in Table 4.3.1.1. The values have been determined according to Eq. E3.2.5.1.

	Partition coefficient for			
	PDMS	**PEUT**	**EC**	**PECH**
Ethanol	264	935	2248	357
Toluene	1451	2494	4497	1786
n-Octane	2340	1383	3238	432
Chloroform	814	1684	992	1930
n-Hexane	282	667	343	382
Propan-2-ol	404	1434	2216	548
Acetonitrile	296	700	1081	1203
Cyclohexane	578	512	879	196
1-Butan-1-ol	1148	5426	9583	1999
1,2-Dichlorethane	491	1306	2392	998

Table 4.3.1.1: Values of partition coefficients at 25° C.

As can be seen from the table above, there is a high affinity (resulting in high partition coefficient values) of non-polar solvents for non-polar polymers (e.g. n-

octane and PDMS) as well as of polar analytes for polar polymers (e.g. butan-1-ol and PEUT). The remarkably high partition coefficient values for butan-1-ol in PEUT, EC and PECH may result from a phenomenon which could already be observed in test measurements with capacitance sensors (see [*Kra 00*]). Although a constant concentration of butan-1-ol was achieved by the flow rig, temperature changes in the measurement chamber reveal extraordinary behaviour for this analyte. Since the partition coefficient K is temperature dependent normally a decrease in K should be observed if the temperature of the chamber is increased; this holds for all investigated compounds except butan-1-ol. Here, a maximum butan-1-ol concentration is noted in the range of 20-25°C. At temperatures below 20°C the actual concentration might be reduced by the formation of dimers or by adsorption on the walls of the chamber. Above 25°C these phenomena disappear and the analyte shows the expected temperature dependency. The lowest K-values were obtained for the nonpolar n-hexane and cyclohexane; even in PDMS they are remarkably small.

4.3.2 Polymer Morphology and Silanisation

The layer topography of four different polymers, namely PDMS, PEUT, EC and PCPMS, was investigated by SEM (scanning electron microscopy). The coatings were deposited by an air-brush; a dilution of the polymers in dichloromethane was sprayed onto the Si wafers. Figs. 4.3.3.1 - 4.3.3.6 reveal that for non-polar polymers like PDMS the surface is rather smooth and independent of the chemical composition of the substrate, i.e. oxide or nitride layer.

More polar polymers such as polyetherurethane (PEUT), ethylcellulose (EC) and polyepichlorohydrine (PECH) show rough and, in some cases, non homogeneous layers (Figs. 4.3.3.2 - 4.3.3.6). Therefore, pretreatment of the substrate's surface by silanisation was carried out to obtain a defined and closed surface.

Preliminary tests should demonstrate three points:

- A silanisation is possible without destruction or change in the wafer's surface. The roughness should not be increased by the silanisation procedure.
- A given silanisation agent should provide the same surface conditions independent of the original substrate.
- A variety of silanisation agents should cover a huge range of different surface polarities.

In the scheme shown in chapter 3.2.1 *Wafer Cleaning Procedures and Silanisation*, the preparation is briefly described. The first cleaning method of the

surface is based on an ultrasonic treatment with a mixture of H_2SO_4 / H_2O_2. Obviously, this so-called "Piranha solution" is together with the ultrasonic treatment too much of an aggressive approach as it caused the roughness of some wafer surfaces to increase dramatically which confirms Fig. 4.3.2.1.
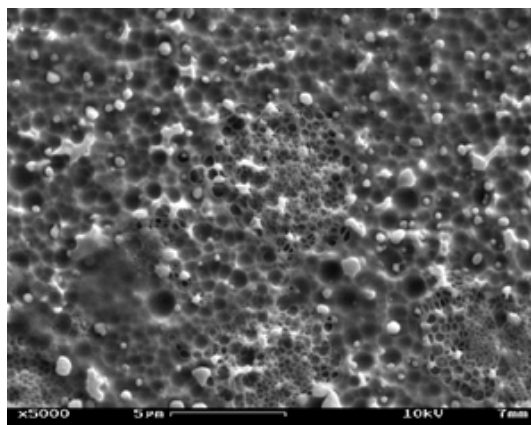
Fig. 4.3.2.1: SEM picture of a native Si surface after treatment with "Piranha solution".

Thinking about already processed sensors, this "Piranha method" would destroy the whole chip. Therefore, a second, more gentle pretreatment was applied to eliminate the surface impurities; it comprises an exposure to O_2 plasma. SEM investigations confirm that the topography of the surface itself is not affected.

As a first result of the contact angle measurements it can be stated that the surfaces of the wafers (directly after the O_2 plasma treatment) are very polar leading to a complete spreading of the water drop (no contact angle could be measured). Furthermore, with the same silanisation agent the same contact angles (considering the error ranges) can be achieved independently of the substrate. For this reason the investigations carried out with GOPTS and APMDS were performed only using a M2+Pass layer[5].

The silanisation with the very non-polar TCOS resulted in the largest contact angle. As anticipated, the hydrophobic end chains (C_{18}-rest) decrease the wettability of water to a large extend. Unfortunately, the polarity differences of the other compounds were not as large as expected. For this reason, APMDS and GOPTS silanised wafers were treated with an HCl solution aiming at the formation of more polar end groups (thus leading to smaller contact angles). Although a decrease in the angles can be observed the effect is still too small. The results of the contact angle measurements are summarised in Table 4.3.2.1

---

[5] "M2+Pass" denotes a surface layer of the substrate (see list of abbreviations).

	Without silanisation agent (directly after O$_2$ plasma treatment)	TCOS [°]	APMDS [°]	APMDS and HCl treatment [°]	CPTS [°]	GOPTS [°]	GOPTS and HCl treatment [°]	DCMTCS [°]	TFPTCS [°]
IMOX	Complete wetting	107.07 ±1.37	54.27 ±8.05	n. i.	48.45 ±3.25	n. i.	n. i.	n. i.	n. i.
M2+Pass	Complete wetting	107.21 ±1.85	53.18 ±3.19	45.32 ±3.79	52.48 ±3.12	53.46 ±2.75	46.75 ±1.35	60.16 ±1.92	70.70 ±0.93
Nitride	Complete wetting	105.73 ±0.86	59.44 ±7.50	n. i.	52.06 ±2.84	n. i.	n. i.	n. i.	n. i.

Table 4.3.2.1: Contact angle values for distilled water on differently silanised wafers. "n. i." = not investigated. "IMOX", "M2+Pass" and "Nitride" denote different surface layers of the substrate (see list of abbreviations).

In order to mimic the actual experimental conditions in a more appropriate manner, the contact angle measurements were repeated using a mixture of chloroform (CHCl$_3$) and perchlorethylene (C$_2$Cl$_4$) –which is the mixture used finally to dissolve the polymers in- in a ratio of 1:1 as a wetting agent. The reason for the use of this solvent mixture will be discussed in the chapter "Coating Techniques". The results are shown in Table 4.3.2.2; the experiments carried out with water already reveal that there is no dependency of the contact angle on the substrate, thus for the investigations with CHCl$_3$ / C$_2$Cl$_4$ only the M2+pass wafers were used. Compared with water, the mixture of both chlorinated HCs wets nearly all surfaces independent of their silanisation layer. Therefore, these results are not that valuable and cannot be interpreted in the sense of a measurable value of the surface properties.

	Without silanisation agent (directly after O₂ plasma treatment)	TCOS [°]	APMDS [°]	APMDS and HCl treatment [°]	CPTS [°]	GOPTS [°]	GOPTS and HCl treatment [°]	DCMTCS [°]	TFPTCS [°]
M2+Pass	Complete wetting	28,63 ±3,01	Complete wetting	n. i.	Complete wetting	Complete wetting	n. i.	Complete wetting	27,54 ±2,20

Table 4.3.2.2:Contact angle values for a mixture of CHCl₃ and C₂Cl₄ (ratio 1:1) on differently silanised wafers. "n. i." = not investigated. "M2+Pass" denotes a particular surface layer of the substrate (see list of abbreviations).

4.3.3 Coating Techniques

As already mentioned in the introduction the air-brush technique does not seem to be the most suitable way to deposit the sensitive layers. There are two main drawbacks which are unavoidable in using this technique:

- The polymer solution has to be very dilute (danger of plugging the air-brush system). Thus, thick films (5-10µm) are hardly achieved reproducibly.
- The aerosol droplets lead to relatively rough and heterogeneous surfaces. Maybe an "after-treatment" in a convenient solvent vapour will reduce the roughness (smoothing effect); pores in the coating film might be closed.

The silanisation of the wafer surfaces with the aim to obtain closed and smooth polymer coatings and the subsequent deposition of the sensing materials by air-brush was not successful in all cases as shown in Figs. 4.3.3.1 - 4.3.3.6.
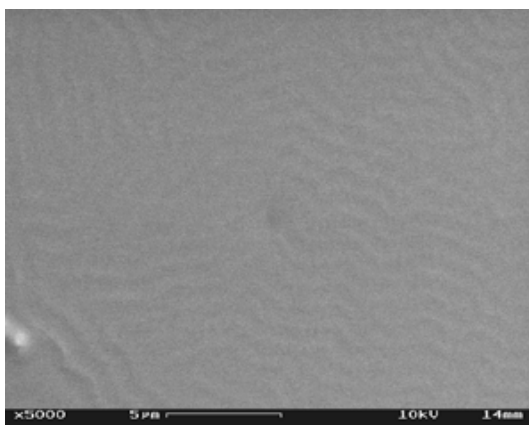
Fig. 4.3.3.1: PDMS on native Si.
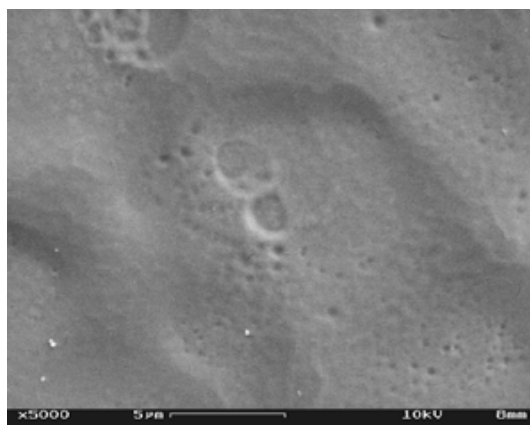
Fig. 4.3.3.2: PEUT on native Si.
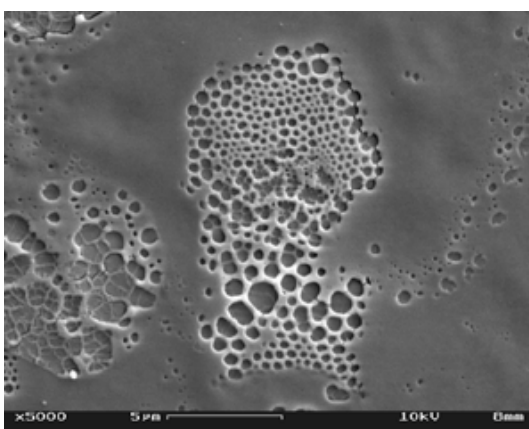
Fig. 4.3.3.3: EC on native Si.
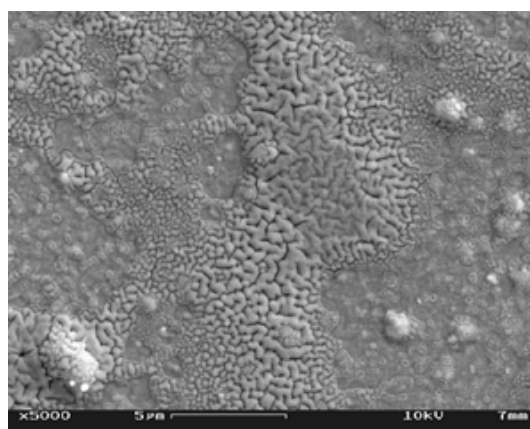
Fig. 4.3.3.4: PECH on native Si.
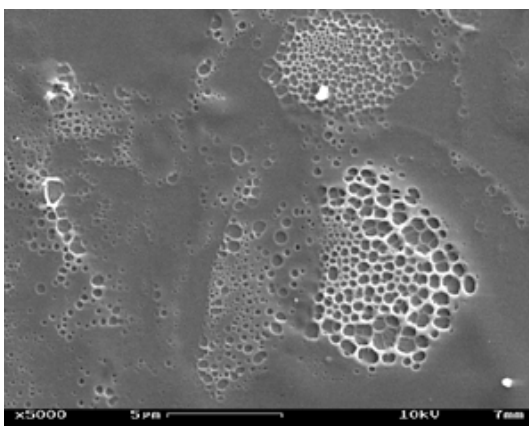
Fig. 4.3.3.5: EC on Si silanised with GOPTS.
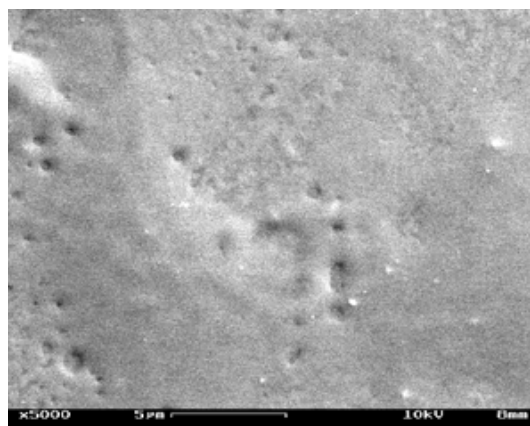
Fig. 4.3.3.6: PECH on Si silanised with GOPTS.

While PDMS can be deposited by an air-brush resulting in rather smooth, closed and homogeneous films; PEUT (at least in part), EC and PECH turned out to belong to the group of "problematic polymers". In order to improve the wettability of these "problematic polymers", the Si substrates were treated with different silanisation agents (see chapter 4.3.2 *Polymer Morphology and*

Silanisation). Looking at Figs. 4.3.3.5 and 4.3.3.6, it is quite obvious that silanisation leads only to a very slight amelioration. Similar results were obtained for all combinations of the polymers PEUT, EC and PECH with the differently silanised surfaces.

The most obvious reasons for this are probably related to the fact that the deposition by air-brush is a rather "crude" technique; the polymer solution reaches the surface in the form of small drops with a very high speed and the deposition itself takes place "explosively". In addition, the coating of micro-processed devices with dimensions in the µm-range requires shadow masks to assure that only the sensing element of the whole unit is covered with polymer [*Kol 99*]. The possibility of forming a sensitive layer by spin coating is only appropriate for blank silicon wafers without any kind of electronics; completely bonded devices cannot be coated by applying this technique. For all these reasons, the idea arose to deposit the polymers by a new approach which was originally based on facilities used to bond and handle micro-electronics.

The ordinary bonder allows the deposition of polymer solutions onto micro-structures in an easy way. The new tools to transfer the polymer from a "reservoir" onto the device's surface consisted of two different set-ups. In a first attempt, manually fabricated tools with feature sizes down to 600 µm were attached to the bonder and served as manipulators. They were subsequently dipped in polymer solutions to load the tools. The tool then transferred the defined amount of solution to the device where it was then deposited very precisely on capacitor structures. The coated capacitors were characterised [*Kra 00*] and some of the results are given in Figs. 4.3.3.7 and 4.3.3.8.
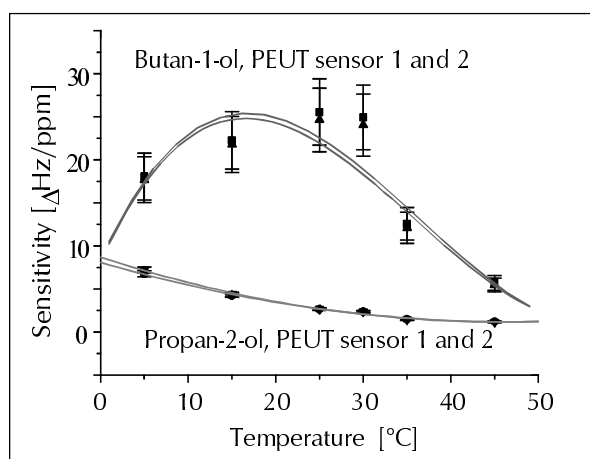
Fig. 4.3.3.7: Temperature dependency of the sensitivity of PEUT-coated capacitors for propan-2-ol and butan-1-ol [Kra 00].
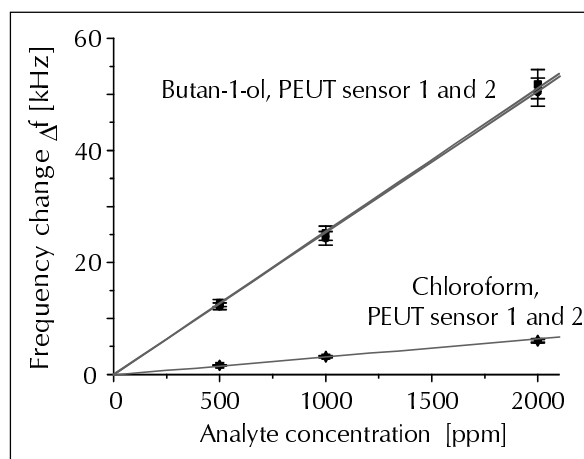
Fig. 4.3.3.8: Frequency change of PEUT-coated capacitors upon exposure to chloroform and butan-1-ol [Kra 00].

The tool's movement was easy to follow with the aid of a microscope. Hence, a more precise approach was possible which is crucial for addressing defined positions on substrate surfaces.

A large series of different organic solvents (and their mixtures) were tested to meet two main requirements: Firstly, all polymers under investigation should be soluble in the solvents / mixtures. Secondly, the evaporation of the solvent while the polymer solution was moved from the reservoir to the device should be as slow as possible. Unfortunately, low boiling solvents (e.g. dichloromethane) which have excellent solvent abilities evaporate so fast that a reproducible deposition of the polymer was hardly realisable. A mixture of chloroform and perchloroethylene (ratio 1:1) fulfilled the above mentioned prerequisites in the most suitable way.

The drop-deposition seemed to be more complex if compared to the air-brush technique, but its advantages are manifold:

- An automation of the whole procedure is possible
- No shadow masks are required
- Low polymer and solvent consumption
- Very exact and accurate polymer deposition (see Fig. 4.3.3.15)

The shape of the polymer drops depend not only on the tool geometry (varying tool size etc.) but also "geometrical effects" of the substrate have an influence. If the wafer is "unstructured" which means that the surface is not cut, the drops keep the original shape of the tool. As an example the next figure (Fig. 4.3.3.9) shows a wafer (1 cm × 1 cm) on which 16 PDMS polymer drops have been deposited and a further photo (Fig. 4.3.3.10) displays a magnified view of a single drop.
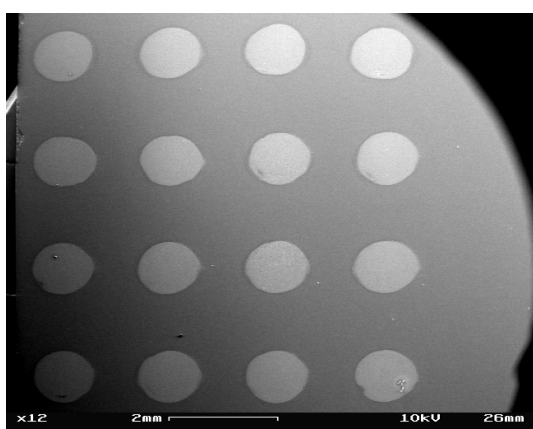
Fig. 4.3.3.9: SEM picture of a Si wafer with PDMS drops.
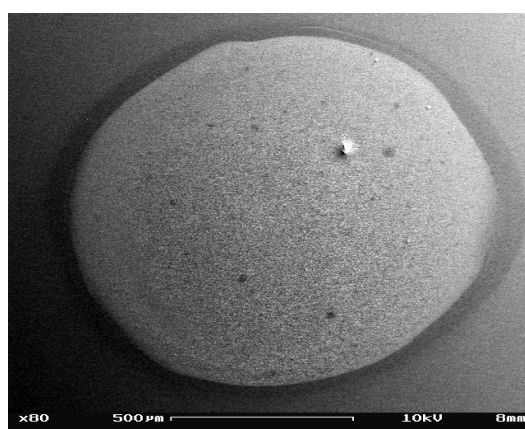
Fig. 4.3.3.10: SEM picture of a PDMS drop on native Si.

The software package "Global-Lab" (Data Translation, Marlboro, USA) provides a rather simple technique to evaluate certain characteristics (features) of the drops, namely:

- The area (the area of the particle, excluding holes)
- The axis ratio (a value between 0.0 and 1.0 computed by minor axis / major axis)
- The perimeter (the length around the outside of the particle)
- The roundness (a value between 0.0 and 1.0 indicating how closely the shape of the particle resembles a circle; this is computed by 4π x area / perimeter^2

In order to achieve reliable statistical statements, the four polymers PDMS, PEUT, EC and PCPMS were selected and from each of them 90 polymer drops were placed on five wafers (16 drops on each). For each wafer, drop features such as area, roundness etc. were determined and a standard deviation of the mean value was calculated (represented by the error bars). The following diagrams (Fig. 4.3.3.11 - 4.3.3.14) present the results that have been obtained for PDMS, PEUT, EC and PCPMS:
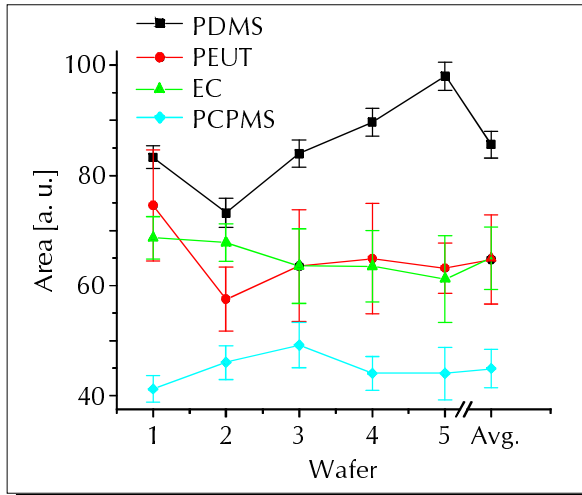
Fig. 4.3.3.11: Areas of polymer drops. Avg. = average value of the five wafers.
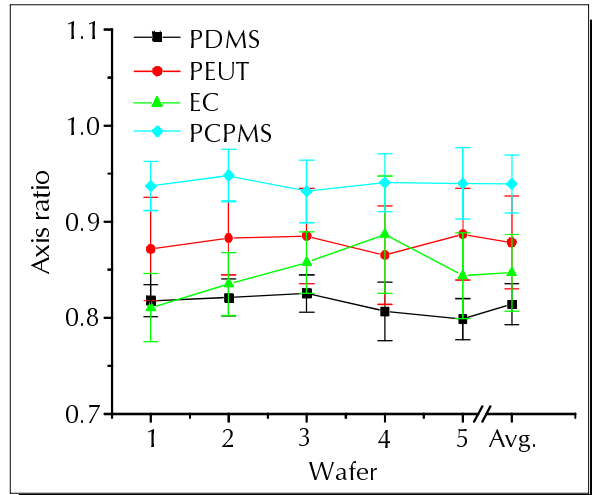
Fig. 4.3.3.12: Axis ratios of polymer drops. Avg. = average value of the five wafers.
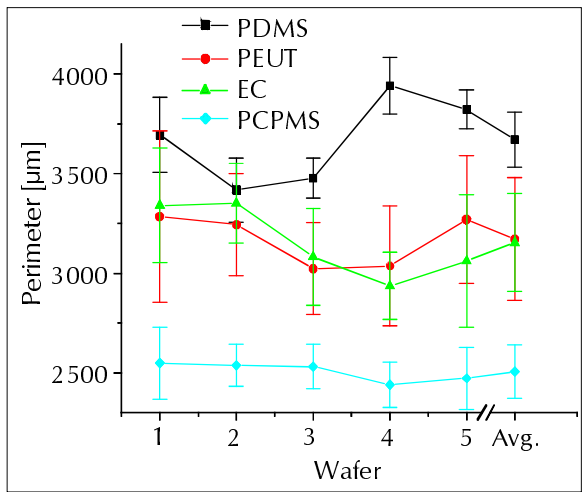
Fig. 4.3.3.13: Roundness of polymer drops. Avg. = average value of the five wafers.
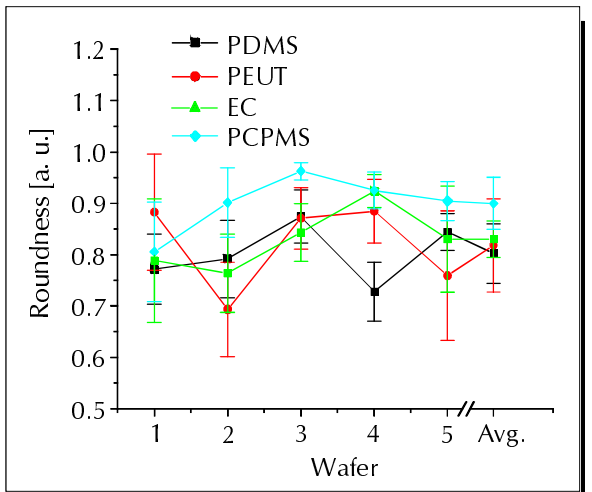
Fig. 4.3.3.14: Perimeters of polymer drops. Avg. = average value of the five wafers.

Firstly, it has to be mentioned that for the deposition of PCPMS a different manually fabricated tool was used which had a smaller feature size. This aspect demonstrates very clearly the weakness of this technique of producing tools. Although the tools were made in the same way deviations in certain parameters (e.g. diameter size) have to be considered resulting in varying drop characteristics.

The behaviour of the polymer drops is presented in Table 4.3.3.1 according to the Figs. 4.3.3.11 - 4.3.3.14:

	Max. deviation of the area from the mean value [%]	Max. deviation of the axis ratio from the mean value [%]	Max. deviation of the roundness from the mean value [%]	Max. deviation of the perimeter from the mean value [%]
PDMS	15	2	10	7
PEUT	15	2	15	5
EC	6	5	11	7
PCPMS	9	1	10	3

Table 4.3.3.1: Maximum deviation of selected drop features from the corresponding mean values.

The large scatter of the features "area" and "roundness" is very remarkable and for our purposes too high. Unambiguous explanations for these deviations cannot be given so far since the individual values scatter statistically. A time dependent decrease which would indicate a plugging of the tool cannot be stated. Looking at the absolute values of the four features (see Figs. 4.3.3.11 - 4.3.3.14) a similar behaviour of PEUT and EC can be observed. The reason for the outstanding PCPMS results is related to the use of a replaced tool.

In order to avoid two previously mentioned shortcomings of the manual tool preparation another approach was envisaged. For our purposes a molybdenum foil having a thickness of 200 μm was crafted by machine resulting in tools which differed in their dimensions (see chapter 3.2.3 *Deposition Techniques*).

Deviations in the diameter are possible since the lateral spread is governed by the wetting ability of the sensitive layer. On the other hand, a clear convergence of the coating film towards a given surface shape can be stated. Some wafer surfaces have been cut into little squares of 800 μm × 800 μm and subsequently a polymer drop has been applied; Fig. 4.3.3.15 demonstrates how the polymer reaches the pre-set borders.
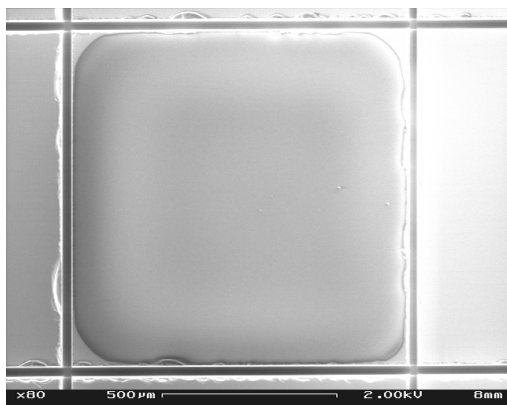
Fig. 4.3.3.15: Deposited polymer drop (PDMS) on structured silicon wafer (800 µm × 800 µm).

Although the polymer deposition is carried out in a very gentle way, the problems which have already been observed using the air-brush technique still partially persist. Again, polymers like EC and PECH form rather rough and, in the case of PECH, inhomogeneous layers. Therefore, the approach to modify the surface by silanisation was resumed.

After the silanisation of the wafers, polymers were deposited to check if the surface modification leads to an improvement in the layer properties (especially topography). The results which are briefly described in the tables below (see Tables 4.3.3.2 - 4.3.3.5) were obtained using Si wafers with a native oxide layer. They have been prepared differently:

- O_2 plasma without subsequent silanisation
- O_2 plasma and silanisation with TCOS
- O_2 plasma and silanisation with APMDS
- O_2 plasma and silanisation with CPTS. This preparation failed due to spoilage of the silanisation agent or its hydrolysis during the silanisation procedure (on the SEM pictures white particles can clearly be seen, e.g. Fig. 4.3.3.16).
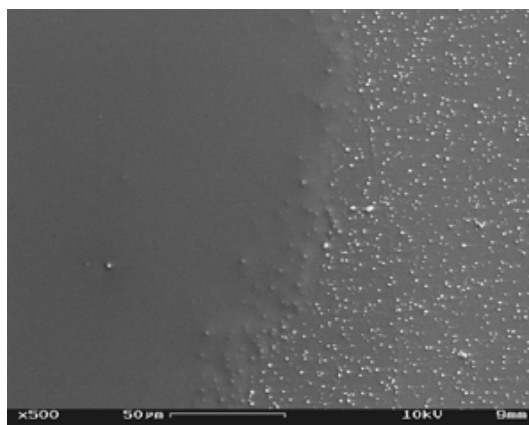
Fig. 4.3.3.16: PDMS (left hand side)
on CPTS silanised wafer.

On each wafer several drops of the same polymer were applied in order to gain statistical information. The results are briefly summarised in Tables 4.3.3.2-4.3.3.5.

PDMS:

Treatment	Comments
O_2 plasma	Homogeneous layer, thicker drops seem to have residual solvents encapsulated $\rightarrow$ cracks within the layer due to evaporation before the SEM measurement.
O_2 plasma, silanisation with TCOS	Although the wafers are silanised with TCOS, the polymer drops do not form homogeneous layers. The shape of the drops is not at all reproducible, the wetting is insufficient.
O_2 plasma, silanisation with APMDS	Homogeneous layer, variations in the drop height, thicker drops seem to have residual solvents encapsulated $\rightarrow$ cracks within the layer due to evaporation before the SEM measurement.

Table 4.3.3.2: Results of the SEM measurements of PDMS on differently modified wafer surfaces.

PEUT

Treatment	Comments
O_2 plasma	Smooth and homogeneous layer, most of the droplets have a reproducible shape, low variation of the drop's height (inner area is higher than the outer sphere) $\rightarrow$ "chromatographic effect"[6].
O_2 plasma, silanisation with TCOS	Strong "chromatographic effect", low reproducibility of the drop sizes, layers are smooth but they are only in part homogeneous.
O_2 plasma, silanisation with APMDS	Smooth layer, variations in the drop height.

Table 4.3.3.3: Results of the SEM measurements of PEUT on differently modified wafer surfaces.

EC

Treatment	Comments
O_2 plasma	Homogeneous and smooth layer, hardly any "chromatographic effect", low variations in the height of individual drops.
O_2 plasma, silanisation with TCOS	Low reproducibility of the drops; some are homogeneous, others show a contraction of the polymer, all of them are smooth.
O_2 plasma, silanisation with APMDS	Smooth layer, variations in the drop height.

Table 4.3.3.4: Results of the SEM measurements of EC on differently modified wafer surfaces.

---

[6] By "chromatographic effect" it is meant that immediately after placing a polymer solution droplet on the surface it starts to spread on the substrate. Thereby, the individual compositions of the solutions are partly separated due to different effective capillary forces.

PECH

Treatment	Comments
O_2 plasma	Rough topography of the drop surfaces, the layer is possibly not completely covering the substrate.
O_2 plasma, silanisation with TCOS	Rough topography of the drop surfaces, drops seem to have residual solvents encapsulated $\rightarrow$ cracks within the layer due to evaporation before the SEM measurement, very strong "chromatographic effect" and very insufficient wetting.
O_2 plasma, silanisation with APMDS	PECH behaviour is not satisfactory: Form and topography seem to be independent of the silanisation agent, the layer is even more brittle.

Table 4.3.3.5: Results of the SEM measurements of PECH on differently modified wafer surfaces.

4.3.4 Automated Coating and Polymer / Surface Screening

After the promising results which have been obtained by using the bonder, an x,y,z – table was configured to deposit a large quantity of polymer drops on wafer substrates. The set-up was positioned in the clean room (see Fig. 4.3.4.1) to avoid contamination of the pre-treated surfaces.
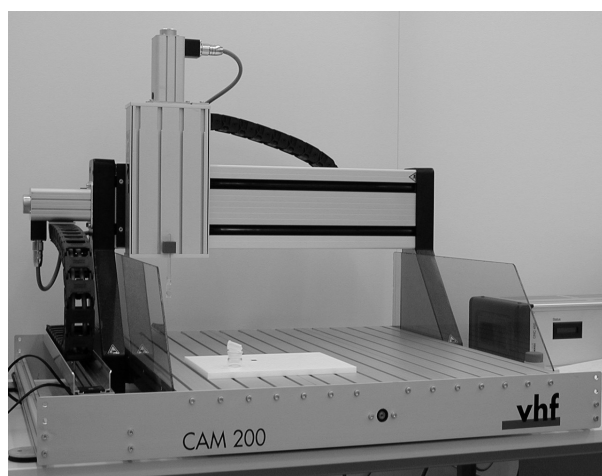
Fig. 4.3.4.1: x,y,z-table for automated polymer drop deposition

This instrumentation serves as a basis for a subsequent screening procedure with the aim to find appropriate surfaces and coating materials. Altogether six different surface treatments, i.e. O_2-cleaning with or without silansiation will be combined with individual coating materials.

In a first run, wafers (preliminarily cleaned in the O_2 plasma) were coated with the 16 polymers listed in Table 3.2.2.1 in the chapter 3.2.2 *Chemically Sensitive Layers*.

The main goal was to figure out how precise and reproducible droplets can be applied with the x,y,z-table. According to the specification given by the manufacturer, the resolution of height and also in lateral dimensions is 10 μm. Fig. 4.3.4.2 displays for instance the standard pattern of polymer droplets; in this case PEUT was used:
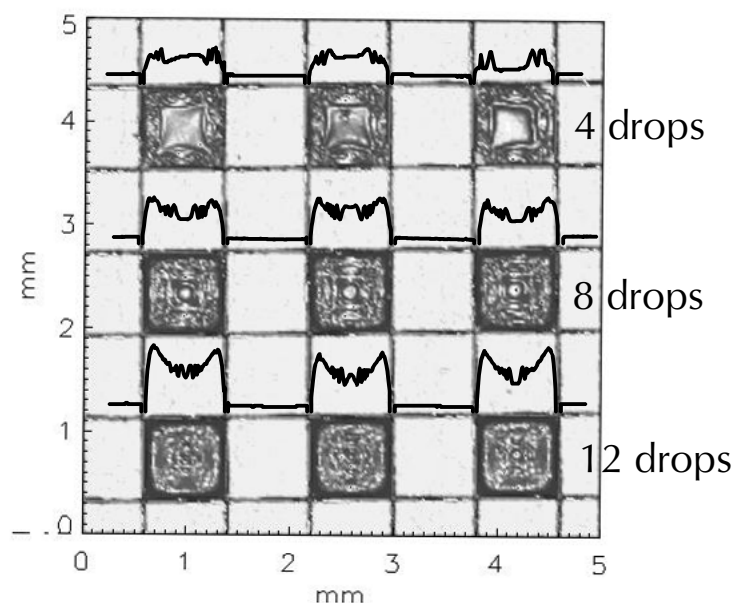
Fig. 4.3.4.2: Top view on a Si wafer symmetrically coated with PEUT; the upper row consists of fourfold droplets, the row in the middle of eightfold and the last row of twelvefold droplets. Above each row the line scans of the profilometer measurements are depicted (the scaling on the left hand side does not indicate the height of the droplets!).

4.3.5 Topography Investigations

A very fast and exact method to determine the height of deposited organic layers (like polymers) is based on the profilometer principle as described in chapter 3.2.4 *Optical Profilometer*. The different transduction principles which are foreseen for the Körber-μ-Nose require varying thicknesses of the sensitive

materials. Especially for capacitors a complete coverage of the field lines is necessary. Thus, polymer films thicker than 5 µm are needed. Besides an increase in the concentration of the polymer solution required to deposit a multiple drop, deposition should increase the thickness at the selected position. In principle, the profilometer investigations give three main pieces of information:

- The profile (shape) of the deposited layer (2-dimensional scan mode)
- The drop topography (3-dimensional mode)
- The layer's height
- The reproducibility of the technique

The following diagrams show the results for selected polymers on a native Si surface:
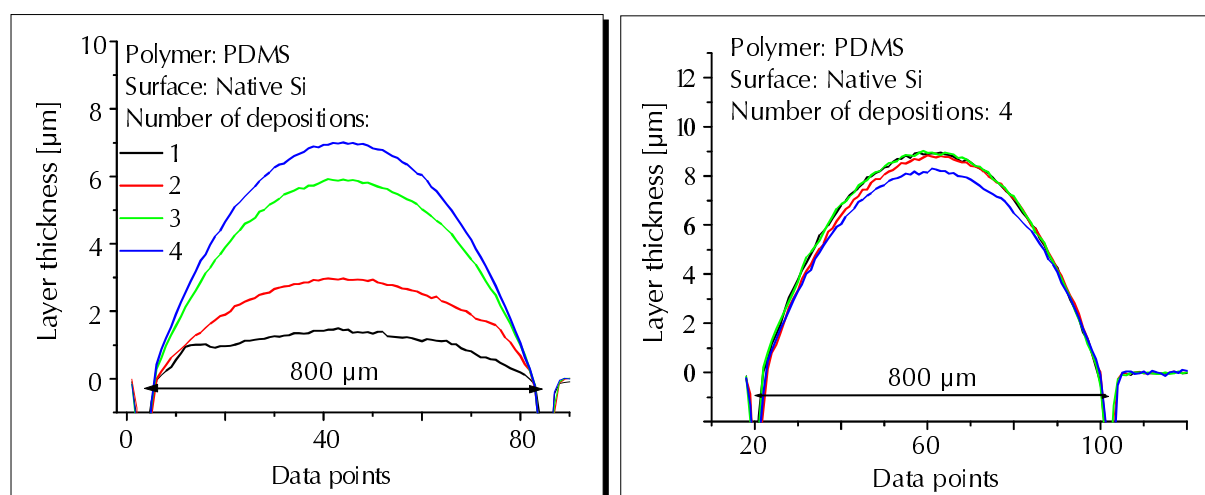
Fig. 4.3.5.1: Dependency of the PDMS layer thickness on the number of depositions. Each line represents the mean of four repeats.

Fig. 4.3.5.2: Layer thickness of PDMS, four-fold deposition. Four repeats.

It has to be mentioned that the x-axis only represents the number of data points. A dimension scale (800 µm) is given within the diagram. Thus, the real relations between height and width are different to those shown above. The diagrams (Figs. 4.3.5.1 - 4.3.5.2) reveal that for PDMS this method is very convincing. The smaller the number of depositions the higher is the scatter in the thickness of the individual repetitions. If the number of depositions is ≥ 2 the same results can be obtained reproducibly. With a threefold or fourfold deposition a thickness of more than 5 µm was achieved which is regarded to be enough for the capacitance sensors. In addition, an almost linear increase in the

drop volume and the number of depositions is found (see Fig. 4.3.5.3). The drop height increases by about 2 µm per deposition:
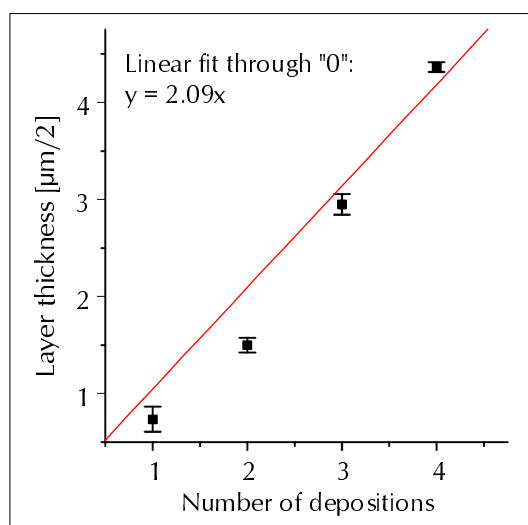
Fig. 4.3.5.3: Functional behaviour of the number of PDMS drop depositions with the increase in drop height (notice the scaling of the y-axis, the actual height is indeed double, see also calculated slope).

The light microscope pictures below (Figs. 4.3.5.4 and 4.3.5.5) show the result of a method to make the coating more homogeneous and smooth. The PDMS drop was deposited with the help of tool no. 16 (550 × 550 µm) on a native Si surface which was structured in squares of 800 × 800µm. The Newton's rings indicate a wavy outer sphere of the drop which means that the film thickness varies considerably at the periphery. In order to have a more even layer the wafer was stored in a dichloromethane (DCM) atmosphere for some minutes. As a result points can be made: Firstly, the drop moves to the square's corner covering the given area more completely. Secondly, the Newton's rings disappear corresponding to a smoother film topography.
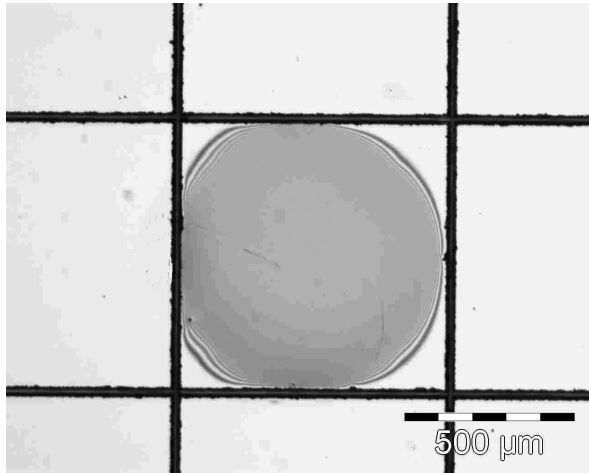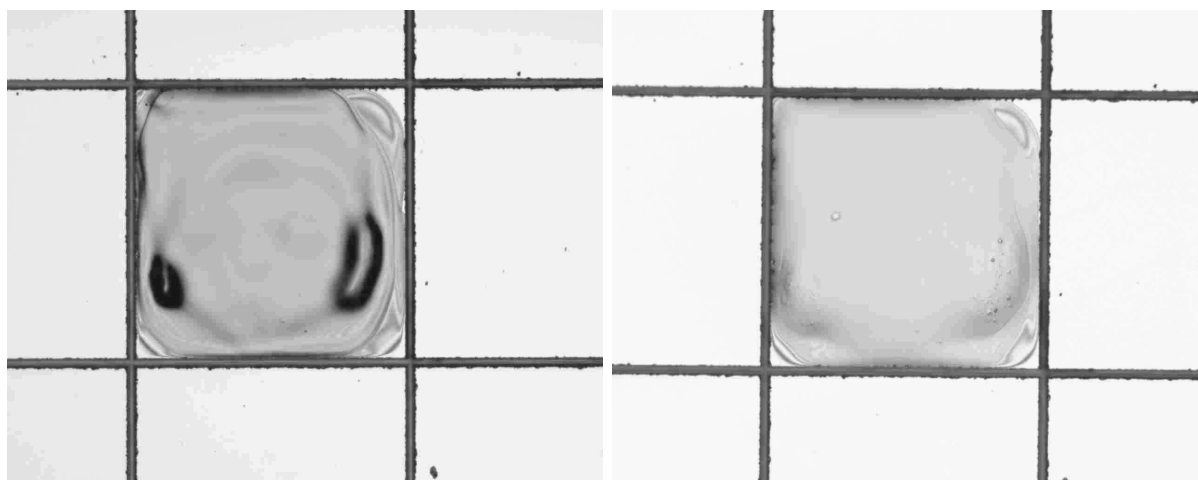
Fig. 4.3.5.4: PDMS drop; fourfold deposition; before DCM post-treatment.
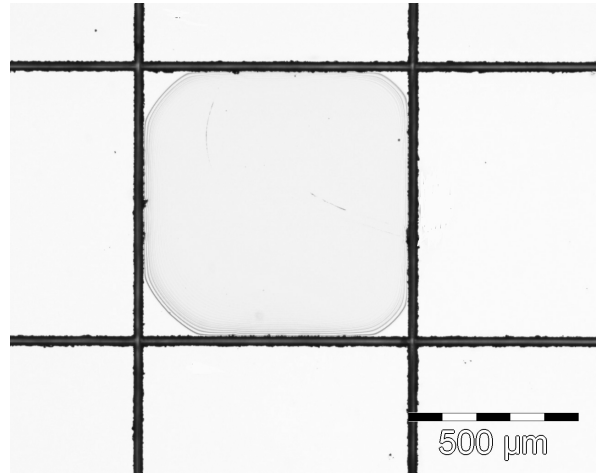
Fig. 4.3.5.5: PDMS drop; fourfold deposition; after DCM post-treatment.

Since the desired height of more than 5 µm can be attained, two other problems were broached; the automation of the coating procedure and the achievement of a large drop height. The following figure (Fig. 4.3.5.6) depicts the result of an automated deposition. The lateral and z-dimensions are highly reproducible. Again, using a new tool no. 16, almost the same dependency of the number of depositions and the corresponding drop height can be observed (compare with Fig. 4.3.5.1); one single drop leads to an increase in height of ≈ 2 µm. This linearity is valid for the large range of h = 2-23 µm.
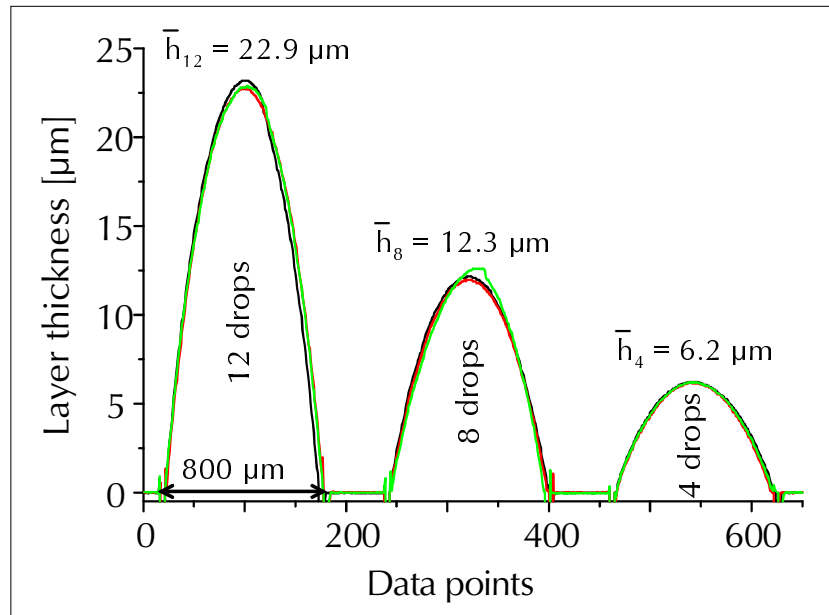
Fig. 4.3.5.6: Dependency of the PDMS layer thickness on the number of depositions (three repeats).

The previous results are confirmed by further profilometer measurements. As an example Fig. 4.3.5.7 displays a PDMS drop (twelvefold deposition) after DCM curing. The drop surface is very smooth, homogeneous and the polymer wets the whole area to be coated:
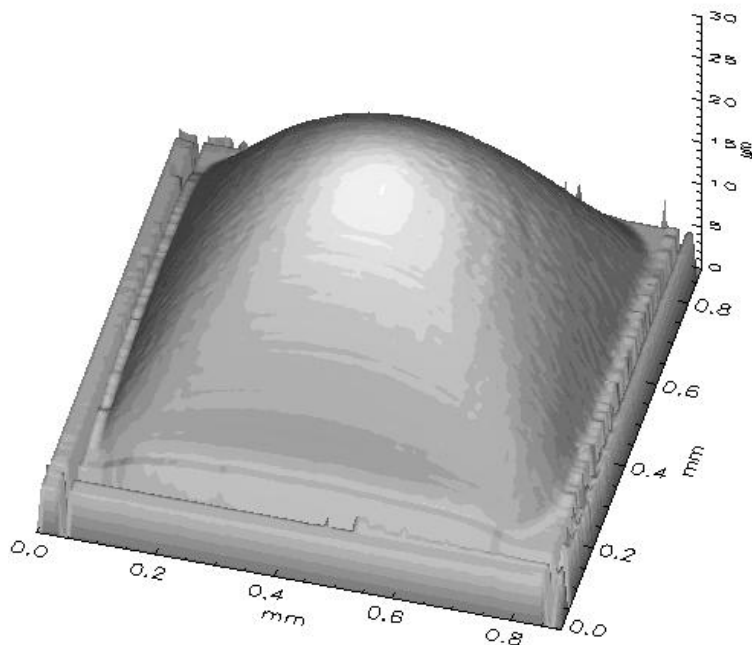
Fig. 4.3.5.7: 3-dimensional picture of a PDMS drop.

The second, extensively studied polymer is PEUT. The results which have been obtained for PEUT are very comparable to those of PDMS. Although all polymer solutions had the same concentration, the thickness of a fourfold PEUT drop deposition is about 4 µm lower than in the case of PDMS. The reproducibility is still satisfying (especially for threefold and fourfold deposition) and the polymer surface's topography is rather smooth. The spike in Fig. 4.3.5.8 is probably an artefact resulting from a diffuse reflection of the thin gold layer which has to be sputtered onto the polymer in order to achieve a higher reflection intensity. Moreover, for a smaller number of depositions the polymer surface itself is rougher, but this could not explain the sharp spikes.
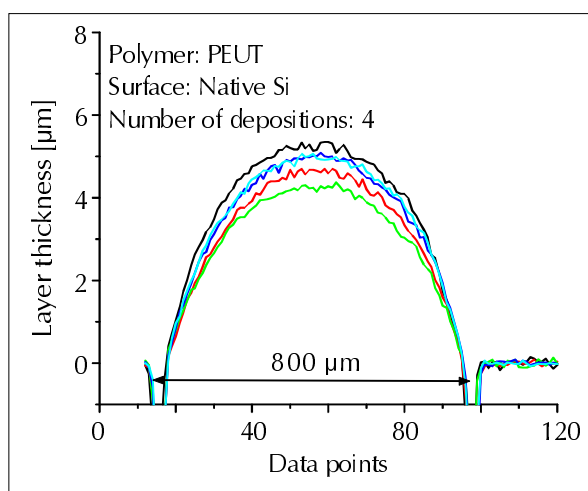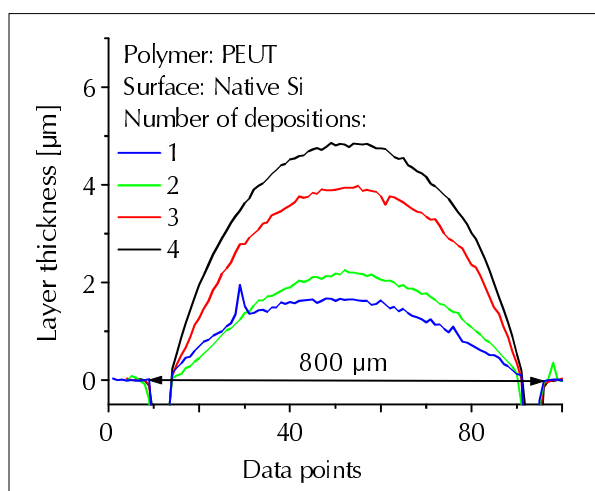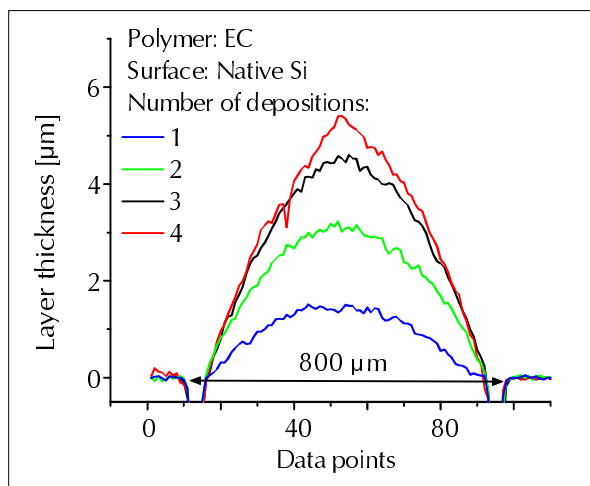
Fig. 4.3.5.8: Dependency of the PEUT layer thickness on the number of depositions. Each line represents the mean of four repeats.

*Fig. 4.3.5.9: Layer thickness of PEUT, four-fold deposition. Four repeats.*

The layer thickness is linearly correlated with the number of drop depositions whereas for PEUT the height is increased by a factor of 1.24 (according to the linear fit) by applying an additional drop (see Fig. 4.3.5.10).
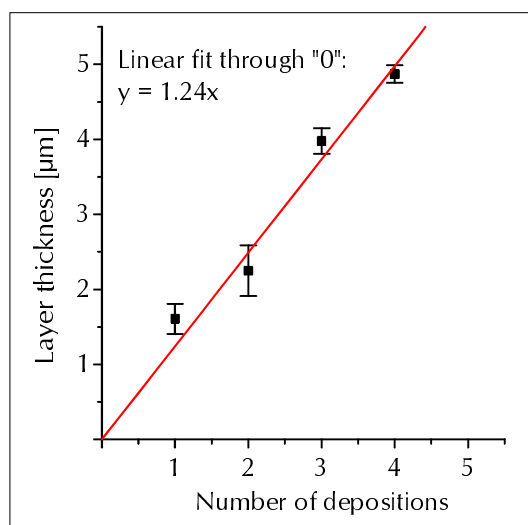
Fig. 4.3.5.10: Functional behaviour of the number of PEUT drop depositions with the increase in drop height.

The topography of the polymer surface can be smoothed if the layers are stored for a couple of minutes in a DCM atmosphere. As it will be shown later, this does not necessarily give an improvement for all polymers (see Fig. 4.3.5.38). PEUT, however, belongs to the group of layers where this post-treatment is successful. Fig. 4.3.5.11 indicates that same parts of the polymer layer (darker parts) are considerably higher than those neighbouring the edges of the pre-

structured Si wafer. The curing with DCM reduces this inequality in height (see Fig. 4.3.5.12).
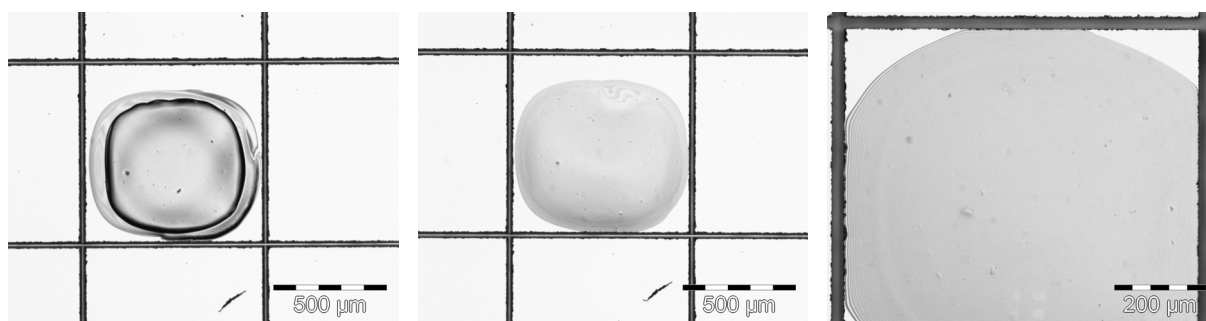

Fig. 4.3.5.11: PEUT drop; fourfold deposition; before DCM post-treatment.

Fig. 4.3.5.12: PEUT drop; fourfold deposition; after DCM post-treatment.

For ethylcellulose (EC) two observations are notable. First of all, there is a larger scatter amongst the repetitions of a certain number of depositions. In some cases (see Fig. 4.3.5.14) the difference between the lowest and the highest layer thickness is 2.2 µm (for the same number of depositions). In addition, the polymer surface's roughness increases in comparison with PDMS and PEUT. This profilometer result cannot directly be confirmed by a simple look at the corresponding light microscope pictures (Figs. 4.3.5.16 - 4.3.5.18). Again it emerged that maximum drop heights of more than 5 µm can only be achieved with at least four depositions (see Fig. 4.3.5.13).

Fig. 4.3.5.13: Dependency of the EC layer thickness on the number of depositions. Each line represents the mean of four repeats.
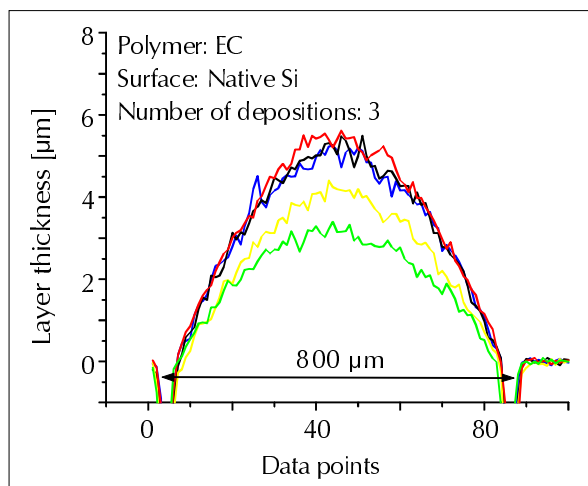
Fig. 4.3.5.14: Layer thickness of EC, triple deposition. Five repeats.

In turn, a linear functional behaviour between the number of depositions and the layer thickness can be seen (see Fig. 4.3.5.15). A comparison with the polymers discussed before reveals that the error bars increase by a factor of two.
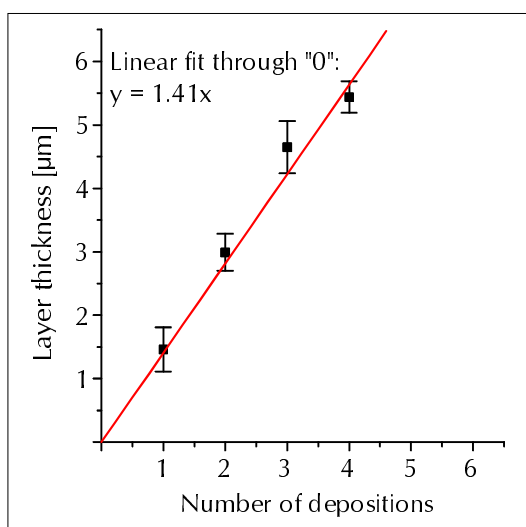
Fig. 4.3.5.15: Functional behaviour of the number of EC drop depositions with the increase in drop height.

Fig. 4.3.5.16: EC drop; fourfold deposition; before DCM post-treatment.

Fig. 4.3.5.17: EC drop; fourfold deposition; after DCM post-treatment.

Fig. 4.3.5.18: EC drop; fourfold deposition; after DCM post-treatment.

The light microscope pictures above (Figs. 4.3.5.17 - 4.3.5.18) present EC polymer drops which resulted from a fourfold deposition. Without a DCM post-treatment the drops themselves kept the tool's shape to a large extent, but each drop has a hemline. The treatment with DCM led to a smoothing of the height difference between the "inner" and "outer" sphere of the drop.

One of the most problematic polymers –with the aim of obtaining closed and smooth layers- is PECH. The material shows an extreme tendency to lump; examining macroscopic PECH-pieces, this property is already obvious because due to its rubbery-like behaviour it is very difficult to cut the polymer grains into small slices. Fig. 4.3.5.20 gives evidence of the low wetting ability and hence, the limited trend to produce uniform layers. This is also confirmed by the profilometer investigations which could not be finally unequivocally evaluated (see Fig. 4.3.5.19). They demonstrate how irregularly the surface is covered. As expressed in Fig. 4.3.5.21, the curing in a DCM atmosphere led to a considerable improvement of the layer properties, but it still did not meet the requirements. Small cavities remained even after several hours of curing.
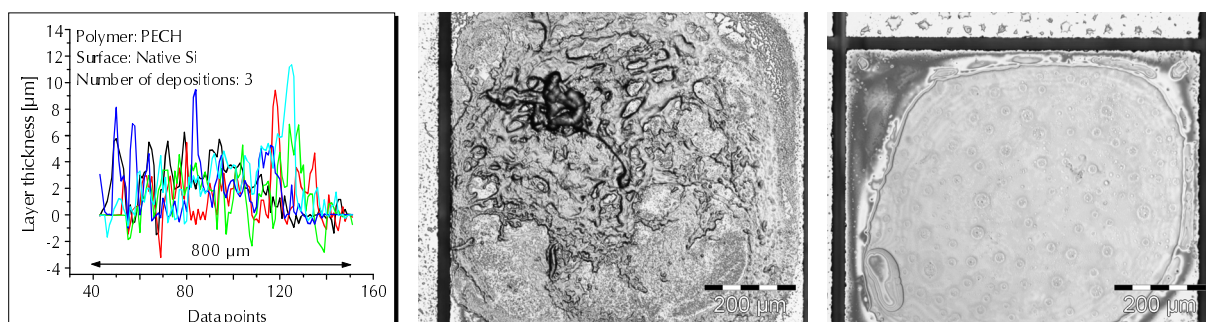
Fig. 4.3.5.19: Layer thickness of PECH, threefold deposition. Five repeats.

Fig. 4.3.5.20: PECH drop; fivefold deposition; before DCM post-treatment.

Fig. 4.3.5.21: PECH drop; fivefold deposition; after DCM post-treatment.

Another characteristic behaviour is observed for PCPPS. A low number of droplet depositions (approx. 4-6) led to the formation of small, isolated globules (see Fig. 4.3.5.22). With an increase in the number of coating steps, the drops start to merge and they create larger "polymer agglomerations"; nevertheless, the surface is not uniformly covered (see. Fig. 4.3.5.23). These phenomena indicate two things: Firstly, the interaction between the PCPPS-droplets compensates for the polymer's tendency to spread on the surface. Secondly, the low adhesion forces lead to considerable mobility of the globules. This is nicely shown by Fig. 4.3.5.24; here a single drop is formed which necessarily implies that polymer from the outer parts moved into the centre. Similarly to examples discussed before, PCPPS layers also show a much higher wettability after exposure to DCM vapour. Most probably, the DCM is adsorbed on the substrate in a preliminary step and thus, its surface tension is decreased. In addition, DCM is absorbed by the polymer forming a more or less viscous solution. This kind of dilution augments its mobility and finally, as displayed in Fig. 4.3.5.25, a larger area is homogeneously covered.
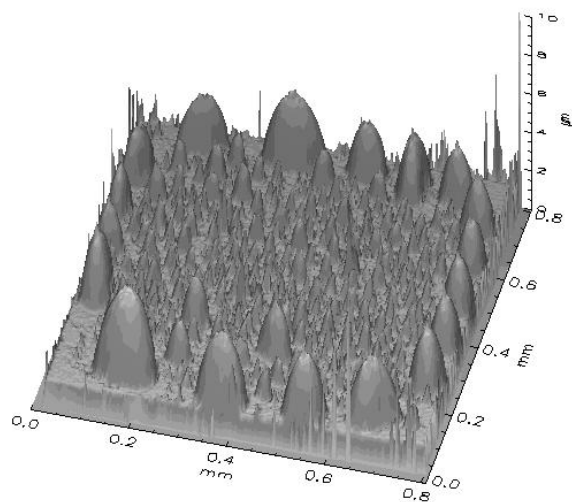
Fig. 4.3.5.22: PCPPS droplets; fourfold deposition; before DCM post-treatment (maximum value of the z-axis scaling is 10 µm).
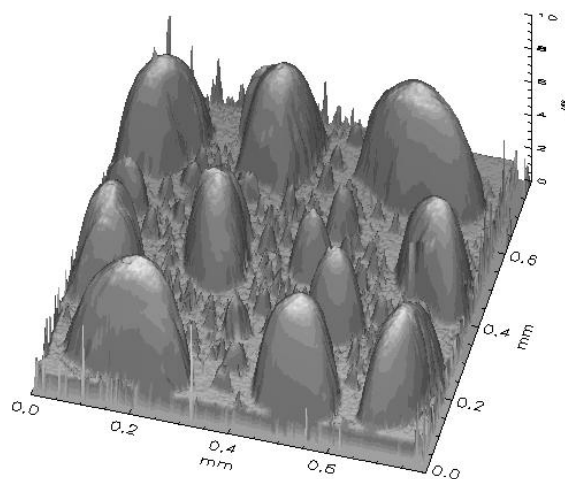
Fig. 4.3.5.23: PCPPS droplets; twelvefold deposition; before DCM post-treatment (maximum value of the z-axis scaling is 10 µm).
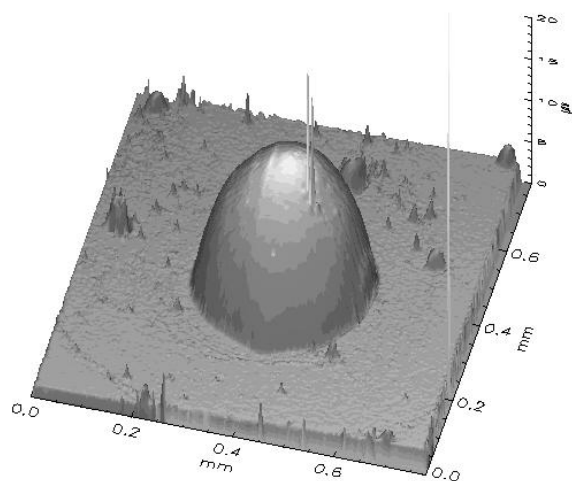

Fig. 4.3.5.24: PCPPS drop; twentyfold deposition; before DCM post-treatment (maximum value of the z-axis scaling is 20 µm).
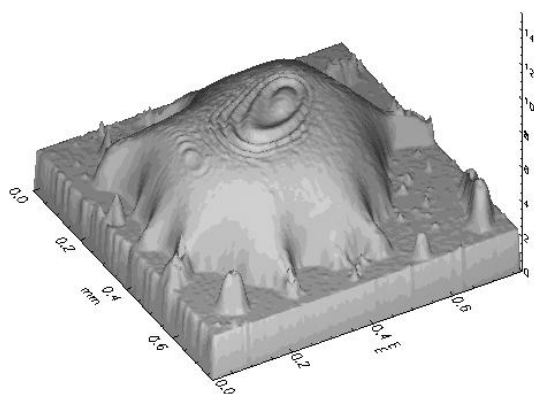

Fig. 4.3.5.25: PCPPS drop; twelvefold deposition; after DCM post-treatment (maximum value of the z-axis scaling is 15 µm).

Although PCPPS and PCPMS are very alike from the chemical point of view (PCPMS has instead of phenyl groups a methyl group), their wetting behaviour is quite different. Before the layers are cured with DCM, they are not very smooth but they did at least reveal no cavities (see Figs. 4.3.5.26 and 4.3.5.27).
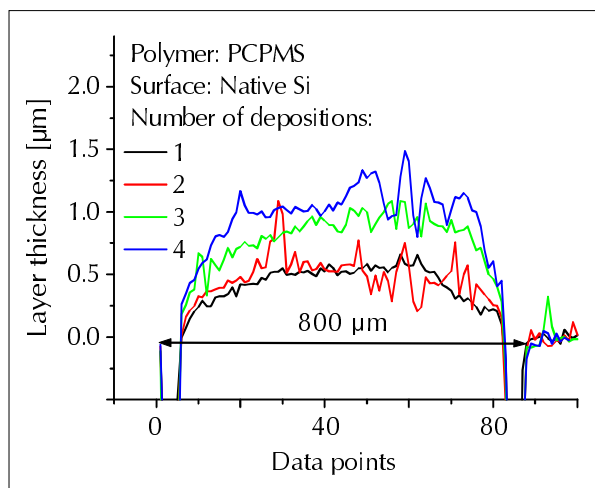
Fig. 4.3.5.26: Dependency of the PCPMS layer thickness on the number of depositions. Each line represents the mean of four repeats.
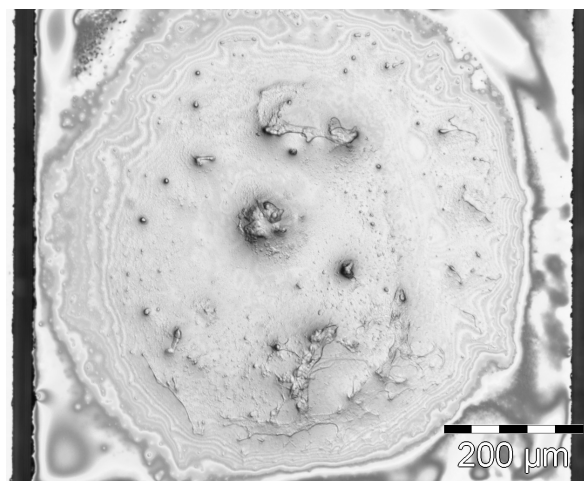

Fig. 4.3.5.27: PCPMS drop; fourfold deposition; before DCM post-treatment.

Within the curing procedure PCPMS proved to have an extreme mobility. Only after a few minutes in the DCM atmosphere, the polymer reaches the chinks of the structured wafer. Due to this high mobility, parts of the polymer may flow into these small channels which would also explain the low layer thicknesses. This is a critical point because the migration of the whole polymer layer will afterwards certainly lead to drift effects of the sensor responses upon exposure to VOCs.
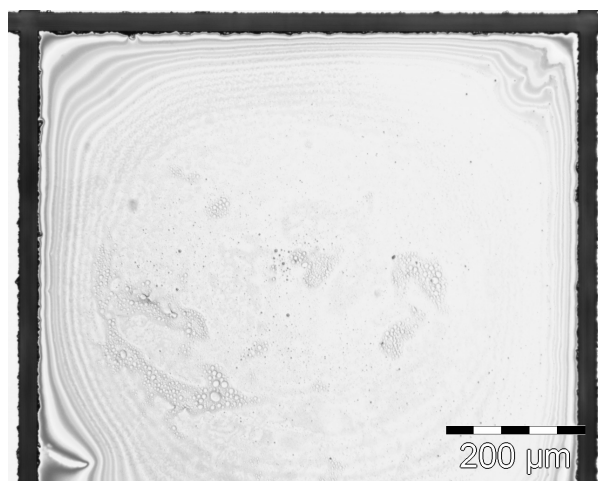
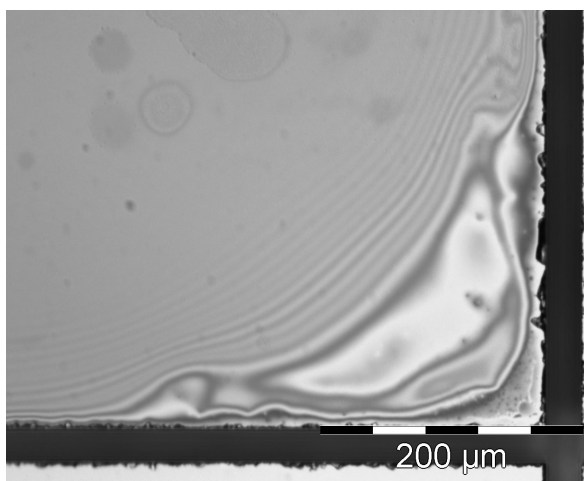Fig. 4.3.5.28: PCPMS drop; fourfold deposition; after DCM post-treatment.

Fig. 4.3.5.29: PCPMS drop; fourfold deposition; after DCM post-treatment.

A very remarkable wetting behaviour could be observed for PMODS. The placement of this polymer on structured Si wafers led to ring-shaped layers with layer heights along the chinks being considerably higher than in the inner part of

the area to be coated. Moreover, the layer's surface is rough with some encapsulated holes. The 2- and 3-dimensional profilometer measurements are displayed in Figs. 4.3.5.30 - 4.3.5.32; they are in accordance with the microscopic investigations (see Fig. 4.3.5.33). The existing differences in layer thickness between the outer and the inner part of the droplet could almost be equalised by storing the coated substrate in a DCM atmosphere as demonstrated in Fig. 4.3.5.31.
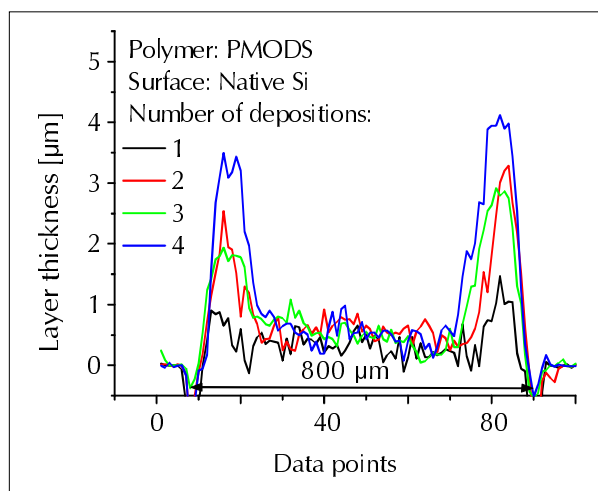

Fig. 4.3.5.30: Dependency of the PMODS layer thickness on the number of depositions. Each line represents the mean of four repeats.
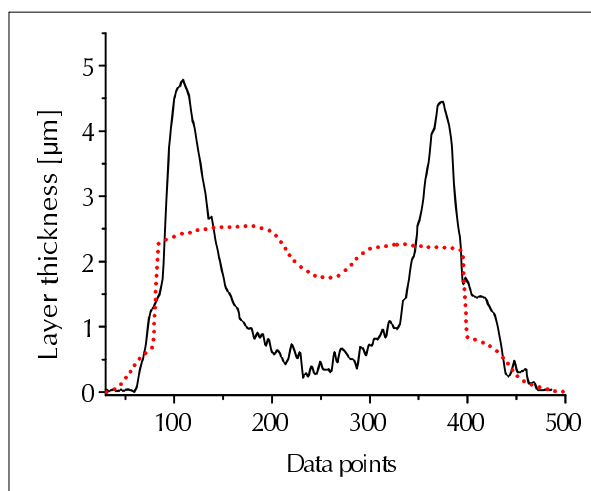
Fig. 4.3.5.31: Equalising effect on the profile of the PMODS layer during the storage in a DCM atmosphere; the dotted line represents the profile after the DCM treatment.
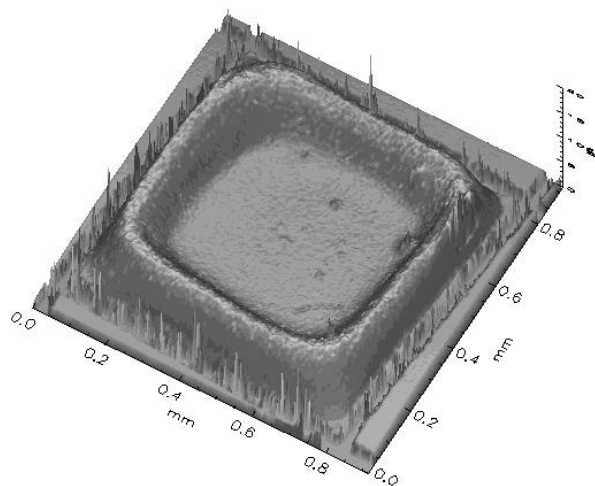
Fig. 4.3.5.32: PMODS drop; fivefold deposition; before DCM post-treatment (maximum value of the z-axis scaling is 20 µm).
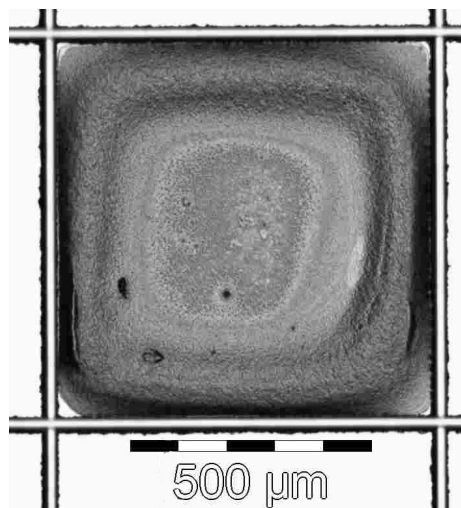
Fig. 4.3.5.33: PMODS drop; fivefold deposition; before DCM post-treatment.

The difference between PMODS, PMTDS and PMOS is in the variation of the length of the aliphatic side groups: PMODS has C_{18}-chains, PMTDS C_{14}-side groups and PMOS C_8-chains. One would attribute to all of them a non-polar character and thus, PMTDS and PMOS are expected to behave in a similar manner as PMODS. But as indicated by Figs. 4.3.5.34 and 4.3.5.35 they reveal a very unsatisfying wetting of the substrate.
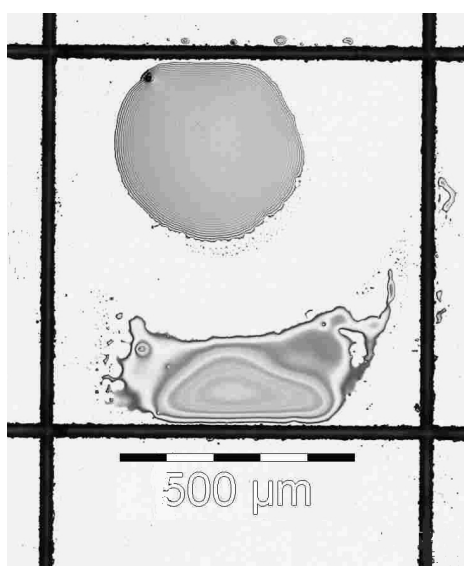

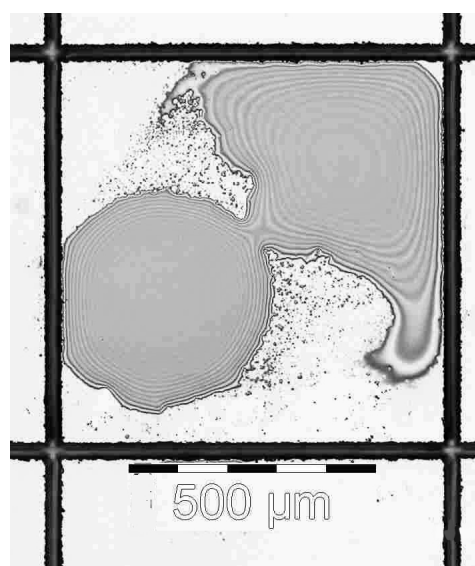*Fig. 4.3.5.34: PMTS drop; fourfold deposition; after DCM post-treatment.*

Fig. 4.3.5.35: PMOS drop; fivefold deposition; after DCM post-treatment.

Concerning the shape of the deposited polymer drops, PMODS is very similar to PANB. Although the chemical structure of PANB with the polar acrylonitrile units is very different from the non-polar PMODS with the long aliphatic side groups, both form ring-shaped polymer droplets after deposition and before curing in a DCM atmosphere (Fig. 4.3.5.36). The storage in a DCM-containing vapour has the same effect on the PANB ring as already observed for PMODS: after several minutes (the curing time is also dependent on the layer thickness) the whole area foreseen is homogeneously covered (Fig. 4.3.5.37):
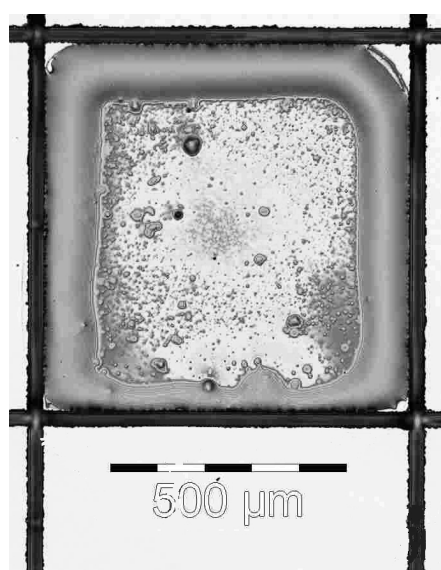

Fig. 4.3.5.36: PANB drop; fivefold deposition; before DCM post-treatment.
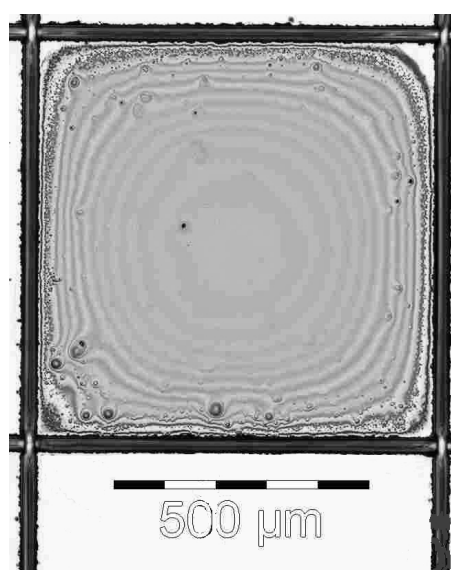
Fig. 4.3.5.37: PANB drop; fivefold deposition; after DCM post-treatment.

Several polymers need necessarily to be cured after their placement on the Si substrate in order to obtain closed layers. This holds for: PEI, PIB, PSU and PVP.

In contrast, the curing of PAPMS in a DCM atmosphere should be avoided. As shown by Fig. 4.3.5.38, the presence of DCM leads to a dramatic increase in the polymer's mobility. Consequently, the previous, properly deposited layer, spread along the chinks of the pre-structured wafer.
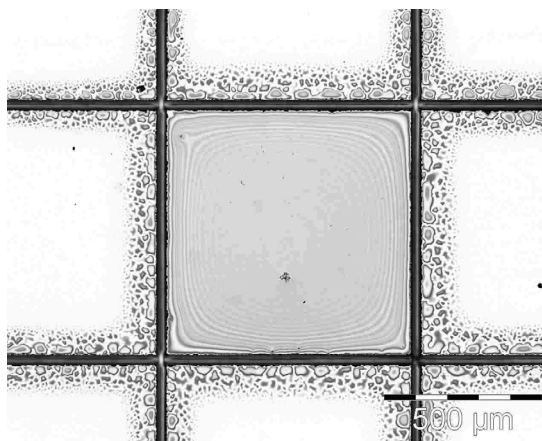
Fig. 4.3.5.38: PAPMS drop; fourfold deposition; after DCM post-treatment.

From the point of view of the surface wetting, PFTS turned out to be entirely inappropriate. Due to the fluorinated propyl group of this polymer it can be recognised as a non-stick coating such as Teflon. Therefore, only small droplets are formed after the deposition which do not spread onto large areas after curing (as for example PCPPS).

4.3.6 Polymers on Sensors

After the extensive polymer screening among the most promising materials a preliminary selection was carried out in order to coat bonded sensors. At the very beginning the deposition on sensors was focussed on PDMS, PEUT, EC, PECH and PANB. The first four polymers were used as sensitive materials for capacitors; the characterisation of these devices upon exposure to ten different analytes, varying temperature etc. is documented in [*Kra 00*]. PANB, PDMS and PEUT were also placed on thermopiles of particular sizes of the sensing areas (see Figs. 4.3.6.1, 4.3.6.2 and 4.3.6.3, respectively). For PANB the maximum layer height was 5.3 µm and in the cases of PDMS and PEUT thicknesses of 3.4 µm and 3.2 µm were determined.
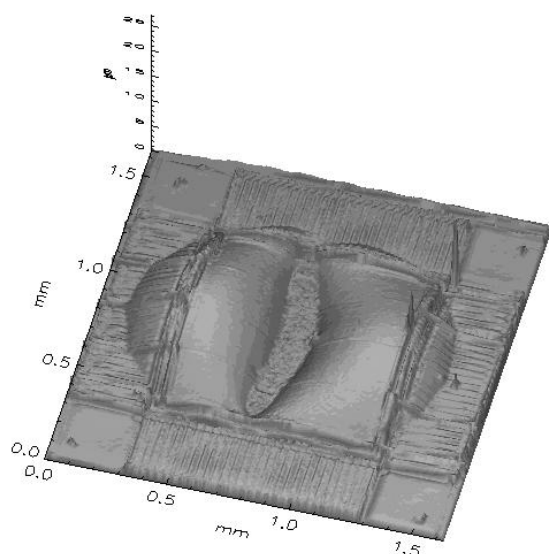
Fig. 4.3.6.1: PANB on a thermopile; only the sensing area with dimensions of 325 × 325 µm is displayed.
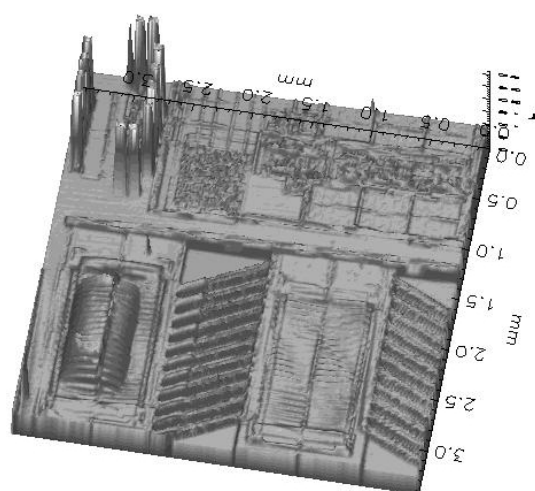
Fig. 4.3.6.2: PDMS on a thermopile; both the sensing membrane with the PDMS coating (left) and the uncoated reference membrane (right) are shown. The upper part of the picture reveals the chip's electronics. The dimensions of the membranes are 700 × 1500 µm.

The very accurate positioning of the polymer is clearly demonstrated in Fig. 4.3.6.3. Here, the PEUT film covers only the inner ("hot") junctions of the calorimetric sensor, whereas the outer ("cold") junctions remain uncoated. This is exactly how the polymer layer has to be placed. With this sensor, measurements were carried out exposing it to toluene and ethanol in varying concentrations; the results are presented in [*Fra 01*].

Fig. 4.3.6.3: *PEUT layer on the sensing membrane of a calorimetric sensor (dimensions 750 × 1500 µm).*

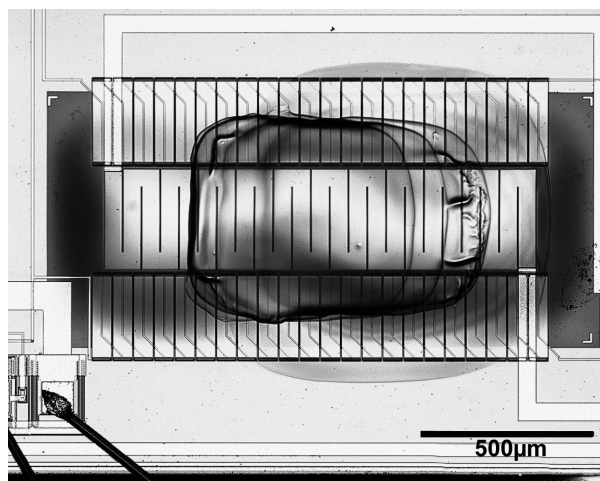Fig. 4.3.6.4: *PEUT layer on a **cracked**, sensing membrane of a calorimetric sensor (dimensions 750 × 1500 µm).*

In this particular case, no appropriate tool, i.e. corresponding to the size of the membrane, was available. Therefore, in order to achieve the required polymer thickness, a multiple deposition with a smaller tool was performed. In total, six drops were placed onto the sensing part.

In contrast to the deposition of polymer drops on Si wafers, the placement on sensors with very thin membranes is a critical issue. Hence, any direct contact between the tool and the membrane has to be avoided. As shown in Fig. 4.3.6.4, the membrane easily cracks at the transition between the etched part and the bulk wafer. Since the coating procedure is almost the last step before the sensor chip is finally packaged, its destruction at this stage should be prevented.

Cantilevers as the third kind of transducers which are also used on the SMC were coated by applying the micropipette technique. The main benefit of this approach is the very precise positioning of the drops and herewith associated the small drop size; diameters of the droplets down to 50 µm can be achieved (see Fig. 4.3.6.5). If several single drops are deposited, they easily form a unique layer after the curing step (see Fig. 4.3.6.6). Generally, it can be stated that all those polymers with rather low glass transition temperatures, i.e. which are viscous at room temperature, are more suitable when using a micropipette. Due to the small opening of the glass capillary (in the range of 30 µm), the problem of clogged tips sometimes occurs. After demonstrating that this technique is very suitable to coat cantilevers, further measurements focussing on gas tests (i.e. VOC detection) have to follow.
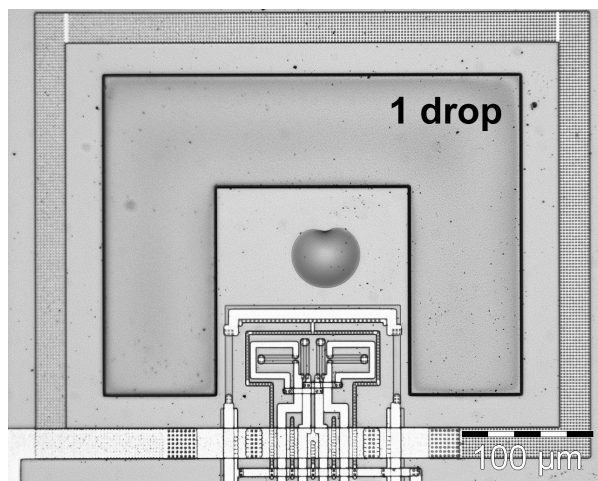
Fig. 4.3.6.5: PDMS droplet on a resonating cantilever.
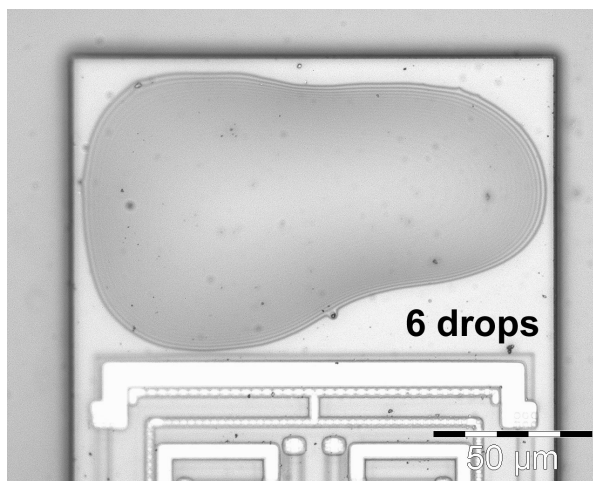
Fig. 4.3.6.6: PDMS layer on a resonating cantilever.

The studies on various polymers as sensitive coatings revealed that different techniques have to be applied in order to fulfil the main requirements. These are namely: Polymer deposition on completely bonded sensors (this requirement excludes spin-coating), an automation should be possible and even very small areas (like the cantilever beams) have to be coated precisely.

In the next step all three transducers –cantilever, calorimetric and capacitance sensor- will be integrated on one single chip, the so-called standard micronose chip (SMC). Nine differently coated SMCs will then be the sensing part of the portable hand-held device.

4.4 References

[*Cha 83*]: S.S. Chang, G.-H. Tang, J. Tang, Q.Z. Jin, H. Shi, J.T. Carlin, C.T. Ho, Isolation and identification of 2-pentenylfurans in the reversion of soy bean oil, J. Am. Oil Chem. Soc. 60 (1983) 553-557.

[*Dol 01*]: B.J. Dolemann, N.S. Lewis, Comparison of odour detection thresholds and odour discriminabilities of a conducting polymer composite electronic nose versus mammalian olfaction, Sens. Actuators B 72 (2001) 41-50.

[*Ein 97*]: J.W. Einax, H.W. Zwanziger, S. Geiß, Chemometrics in environmental analysis, Wiley-VCH, Weinheim, 1997.

[*Fra 82*]: E.N. Frankel, W.E. Neff, E. Selke, D. Weisleder, Photosensitised oxidation of methyl linoleate: Secondary and volatile thermal decomposition products, Lipids 17 (1982) 11-18.

[*Fra 83*]: E.N. Frankel, Volatile lipid oxidation products, Prog. Lipid Res. 22 (1983) 1-33.

[*Fra 01*]: M. Frank, N. Kerness, S. Raible, C. Hagleitner, U. Weimar, H. Baltes, New coating procedure for CMOS chemical microsensors, ISOEN 01, Washington, 2001, accepted.

[*Ho 78*]: C.T. Ho, M.S. Smagula, S.S. Chang, The synthesis of 2-(1-pentenyl)furan and its relationship to the reversion of soy bean oil, J. Am. Oil Chem. Soc. 55 (1978) 233-237.

[*Jur 00*]: P.C. Jurs, G.A. Bakken, H.E. McClelland, Computational methods for the analysis of chemical sensor array data from volatile analytes, Chem. Rev. 100 (2000) 2649-2678.

[*Koc 96*]: S.P. Kochhar, Oxidative pathways to the formation of off-flavours, in: Food taints and off-flavours, M.J. Saxby (Ed.), Blackie Academic & Professional (Chapman & Hall), London, 1996, pp. 168-225.

[*Kol 99*]: A. Koll, A. Kummer, O. Brand, H. Baltes, Discrimination of volatile organic compounds using CMOS chemical microsensors with thickness adjusted polymer coating, Proc. of SPIE Smart Structures and Materials 3673 (1999) 308-317.

[*Kra 00*]: G. Krause, Charakterisierung integrierter, kapazitiver CMOS-Sensoren in Mikrosystemtechnik zur Gasanalyse, Diploma thesis, University of Tübingen, Tübingen, 2000.

[*Mor 81*]: W.H. Morrison, B.G. Lyon, J.A. Robertson, Correlation of gas liquid chromatographic volatiles with flavour intensity scores of stored sunflower oils, J. Am. Oil Chem. Soc. 58 (1981) 23-27.

[*Ott 99*]: M. Otto, Chemometrics – Statistics and computer application in analytical chemistry, Wiley-VCH, Weinheim, 1999.

[*Pan 81*]: R.M. Pangborn, A critical review of threshold, intensity and descriptive analyses in flavour research, in: Flavour'81, Proceedings of the 3rd Weurmann Symposium '81, München, P. Schreier (Ed.), Verlag Walter de Gruyter, Berlin, 1981.

[*Ros 96*]: K.J. Rossiter, Structure-odour relationships, Chem. Rev. 96 (1996) 3201-3240.

[*Rui 01*]: Human sensory panel data were kindly provided by J. Ruiz, Centre de Recherche Nestlé, Vers-chez-les-Blanc, Switzerland.

[*Sch 81*]: P. Schieberle, W. Grosch, Model experiments about the formation of volatile carbonyl compounds, J. Am. Oil Chem. Soc. 58 (1981) 602-607.

[*Tic 96*]: P. Tice, Packaging materials as a source of taints, in: Food taints and off-flavours, M.J. Saxby (Ed.), Blackie Academic & Professional (Chapman & Hall), London, 1996, pp. 226-263.

[*Ull 87*]: F. Ullrich, W. Grosch, Identification of the most intense volatile flavour compounds formed during autoxidation of linoleic acid, Z. Lebensm. Unters. Forsch. 184 (1987) 277-282.

[*Vis 01*]: Sensor data derived from the MOSES set-up at Nestlé were kindly provided by P. Visani, Centre de Recherche Nestlé, Vers-chez-les-Blanc, Switzerland.

5 CONCLUSIONS AND OUTLOOK

5.1 Conclusions

The main focus of the present work consisted in the application specific use of gas sensor systems. Two industrially relevant subjects -the quality assessment of vegetable oil and of packaging material- were extensively investigated. In both cases, the long-term stability of the sensor responses and the compensation for drift / fluctuations were crucial issues. Simultaneous measurements with GC/MS and evaluations by human sensory panels were carried out in order to obtain complementary information on the investigated samples. The corresponding conclusions are presented in chapters 5.1.1 and 5.1.2.

Based on the very convincing results which were achieved with the rather "stationary" MOSES II system (being a typical laboratory apparatus), the development of a portable, hand-held device was a natural consequence. Here, the basic idea is to detect problems related to VOCs and off-odours already at their initiation point. The second part of this thesis reports on new coating procedures for chemical microsenors which are used in the aforementioned portable system (for conclusions see chapter 5.1.3).

5.1.1 Vegetable oil

The spoilage of vegetable oils could be monitored with both GC/MS and the sensor system. Most of the occurring analytes in the sample headspaces were identified. Their presence is in agreement with previous investigations carried out on the degradation of edible oils. Besides the expected aldehydes such as pentanal and hexanal also n-pentane was detected. The latter is primarily formed due to the use of UV-light which was applied in order to speed-up the deterioration process. Both methods –GC/MS and sensor system- confirmed that at the very beginning an induction phase is the dominating time parameter. Until the end of the third week no significant change in the headspace could be observed.

Taking only the raw data of the sensor responses (MOXs and QCMs) into account, neither a meaningful PCA, nor a reasonable PCR were obtained. Therefore, the raw data were mathematically correlated with the response fluctuations of the sensors upon exposure to re-calibration samples. Looking at the corresponding scores plots, the success of the procedure is obvious. Here, in the case of the corrected data, the temporal variance of the samples could clearly be traced. This output indicated that a subsequent PCR will also lead to convincing results. Since within the spoilage process the headspace composition changed, i.e. the amount of analytes increased, the samples used for re-calibration

had to be adapted accordingly to obtain more precise prediction results. The latter was manifestly shown by the varying and improved RMSEs in dependency on the re-calibration standard.

5.1.2 Packaging Materials

The investigations on packaging materials revealed a huge variety of different VOCs which can be present in the headspace. However, it has to be emphasised that not all of them are considered to cause a malodour. The odour assessments by human sensory panels provided odour attributes (qualitative descriptors) and odour scores being a measure for the odour intensity to a certain extent. Remarkably, the deviations in the scores among the individual panel members were rather large and hence, taking this uncertainties into account, a precise quantitative odour description by humans was difficult.

GC/MS measurements pointed out that the natural scatter in the headspace of the same packaging material can be very large. In some cases the headspace composition varied considerably depending on the date of production. Since the investigated materials were "real-life" samples, one also has to cope with this variance when applying sensor systems for quality control purposes.

The ventilation of packaging materials in a gas stream in order to release unwanted off-odours did not necessarily ameliorate their quality. Tests with ordinary air and nitrogen turned out that in the presence of oxygen additional, undesired degradation processes were initiated in which the formation of new potential malodours was involved.

In accordance with the results acquired by GC/MS, the evaluation of the sensor system's output led to the same conclusion; if packaging materials have different headspace compositions, then they also can be discriminated by the sensor arrays. However, as mentioned before, the same packaging material (concerning its specification, printing etc.) can show various outgassing of VOCs.

The long-term investigations which were carried out on two different sensor systems showed in general the same trend. The computation of the autocorrelation functions proved for both set-ups (and their sensors) that no real drift of the sensor responses occurred. Only to one QCM -among 32 sensors in total- the term "drift" could be attributed. The cross-correlation coefficients exhibited in turn that changes in the sensor responses had mostly a common source such as inaccurately adjusted concentrations of the re-calibration samples. Moreover, the effect of drift / fluctuation phenomena on the performance of the sensor systems to differentiate (qualitatively and quantitatively) between various samples was also dependent on the features extracted from the raw data which served as input for subsequent multivariate analyses. For instance, although the

baseline of a sensor is drifting, the signal height upon exposure to a known VOC concentration can still be stable.

The correlation between the evaluations of the human sensory panels and the data derived from sensor systems were successful. As shown by several PCRs, a reliable statement on the correct prediction of quality attributes was based on independent data sets for the training and the validation. Naturally, the RMSEs are much smaller when only taking the training data into account. In addition, the prediction results improve if the samples used for the training cover the whole range of all possibly occurring odour scores.

5.1.3 Miniaturised Gas Sensor System

The screening of various polymers to be used as sensitive layers turned out that two basic principles[1] govern their selection for this special purpose. One prerequisite is their sensitivity towards different VOCs. The determination of the individual partition coefficients has demonstrated that the response patterns of the polymers are significantly diverse.

For most of the polymers the spray coating (air-brush) technique is inappropriate since no smooth and homogeneous layers were obtained. A pre-treatment of the substrates by silanisation led to no significant improvement of the topography.

Preliminary tests with manually produced microtools showed that this approach is in principle suitable to transfer and deposit small amounts of polymers in a precise manner. Here, the most critical parameter was the reproducible manufacturing of the tools. Therefore, with the help of CNC machining, other microtools made out of molybdenum were fabricated. With these manipulators the screening of several polymers –with the aim to determine their surface wetting behaviour- was carried out. The automated set-up allowed the coating of already bonded and housed sensors. The deposition of polymers could be carried out with high precision and reproducibility; the adjustment of particular layer thicknesses was possible.

The deposition method based on the micropipette is extremely useful to place polymers on cantilever beams because all of the state-of-the-art approaches do not allow to coat such small areas. However, it is still an issue to improve the accuracy of the obtained layer thicknesses.

---

[1] Of course, there are definitely more than two properties which make a polymer a suitable sensitive layer.

Most of the polymers had very individual wetting properties which could not be correlated with their chemical structure (e.g. polarity of the side groups). This made a forecast on their suitability as sensitive materials almost impossible.

5.2 Outlook

The promising results in the field of vegetable oils and packaging materials encourage to install these sensor systems on the factory floor. Since the tests which have been carried out under laboratory conditions were very successful, the systems have now to prove their ability to serve as at-line or on-line instrumentation. For these purposes, reproducible sampling without headspace-samplers or thermodesorption units (being still the state-of-the-art) becomes a very important issue.

The sensors themselves already reveal a satisfying long-term stability. However, in many cases problems in quality prediction occur due to faulty sampling. As long as this problem persists, the calibration of sensor systems will be unavoidable. The search for easy-to-handle re-calibration samples might not appear to be too exciting, but the better the re-calibration procedure, the better the prediction results. Gaseous re-calibration standards filled in a gas cylinder would be very useful. However, not all desired analyte mixtures can be supplied in this way.

Looking at the limits of detection, miniaturised, polymer-coated CMOS-sensors already demonstrated their high performance. The three transducers will then be located on one chip in the hand-held sensor system. After assembly of the whole set-up, i.e. housed and packaged sensor chips, microcontroller, sampling, and gas flow unit, preliminary tests in the lab and subsequent "real-life" measurements have to be carried out.

The software controlling the automated polymer deposition has to be adapted to the design of the SMC. Some parameters of the micropipette technique have to be optimised (in particular with respect to achieve a higher reproducibility of the droplet's size). A further challenge is the automation of the deposition with the micropipette.

ABBREVIATIONS

A

AEDA	Aroma extract dilution analysis
AFM	Atomic force microscopy
APMDS	3-Aminopropylmethyl-diethoxysilane
ASSS	Application-specific sensor system
a.u.	Arbitrary unit

C

CHARM	Combined hedonic aroma response measurement
CMOS	Complementary metal oxide semiconductor
CNC	Computer numeric control
CPTS	3-Cyanopropyltrichloro-silane
CRN	Centre de Recherche Nestlé

D

DCM	Dichloromethane
DCMTCS	(Dichloromethyl-)trichloro-silane

E

EC	Ethylcellulose
EDTA	Ethylene diamine tetraacetic acid
EN	Electronic Nose
ETH	Eidgenössisch Technische Hochschule (Zürich)

F, G, H

FTIR	Fourier transform infrared (spectroscopy)
GC	Gas chromatograph(y)
GC/MS	Gas chromatography / mass spectrometry
GOPTS	(3-Glycidoxypropyl-)tri-methoxysilane
HCs	Hydrocarbons
HSS	Headspace sampler / sampling

I, L, M

IMOX	Intermetal oxide
IPC	Institute of Physical Chemistry at the University of Tübingen
LOD	Limit of detection
M2 + Pass	Passivation on top of the second metalisation layer
met	Metalized
MHE	Multiple headspace extraction
MOSES	Modular sensor system
MOX	Metal oxide sensor
MS	Mass spectrometry
MSD	Mass selective detector

N, O

NIR	Near infrared (spectroscopy)
NIST	National Institute of Standards & Technology
Nitride	Nitride passivation layer
OAV	Odour activity value
OPP	Oriented polypropylene

P

PANB	Poly-(acrylonitrile-co-butadiene)
PAPMS	Poly-(3-aminopropyl-)-methylsiloxane

PC	Principal component		RMSEP	Root mean square error of prediction
PCA	Principal component analysis		sd	Standard deviation
PCPMS	Poly-(3-cyanopropyl-)-methylsiloxane		SEM	Scanning electron microscopy
			Sens	Sensitiser
PCPPS	Poly-(3-cyanopropyl-)-phenylsiloxane		SIM	Selected ion monitoring
			SMC	Standard micronose chip
PCR	Principal component regression			

T, U, V

PDMS	Polydimethylsiloxane
PE	Polyethylene
PECH	Polyepichlorohydrine
PEG	Polyethylene glycol
PEI	Polyethylenimine
PEUT	Polyetherurethane
PIB	Polyisobutylene
PMODS	Polymethyloctadecyl-siloxane
PMOS	Polymethyloctylsiloxane
PMTDS	Polymethyltetradecyl-siloxane
PP	Polypropylene
ppm	Parts per million
ppt	Parts per trillion
PSU	Polysulfone
PTFPMS	Poly-(3,3,3-trifluoropropyl-)-methylsiloxane
PVP	Polyvinylpyrrolidone

TCOS	Trichloroctadecylsilane
TFPTCS	(3,3,3-Trifluoropropyl-)tri-chlorosilane
UV	Ultra violet (light)
VOC	Volatile organic compounds
VRV	Validation residual variance

Q, R, S

QCM	Quartz crystal microbalance
QDA	Quantitative descriptive analysis
RIE	Reactive ion etching
RMSE	Root mean square error
RMSEC	Root mean square error of calibration

SYMBOLS

A, C

aq.	Dissolved in water
C	Matrix containing concentration information
c_a	Concentration of an analyte in the gaseous phase
ΔC	Change in concentration

E

ε_{drift}	Parameter contributing to the sensor signal by drift
ε_{eff}	Effective dielectric constant of polymer / analyte system
ε_{noise}	Parameter expressing the electronic noise of a set-up
ε_{poly}	Dielectric constant of polymer layer
ε_r	Relative dielectric constant
E1	Single electrode of interdigitated capacitor
E2	Double electrode of interdigitated capacitor

F, G, H

f	Frequency
f_0	Fundamental frequency
Δf	Change in frequency
G	Gravimetric sensitivity
ΔG	Free (Gibbs) Enthalpy change
h_{eff}	Effective polymer thickness after analyte absorption
$\overline{h}_x$	Average height after x depositions
ΔH	Enthalpy change

L, K, M

λ	Wavelength
K	Partition coefficient
M	Molecular weight
$M_{analyte}$	Molecular weight of analyte
m_f	Slope of linear fit curve
m_y	Measurement sequence y
m/z	Mass per ionic charge

N, O, P

n	Number of re-calibration samples
n	Number of data points used for linear fit
P	Matrix containing regrssion coefficients
$p_{analyte}$	Vapour pressure of analyte

Q, R, S

Q_x	Quartz crystal microbalance sensor numbered x
$d\tilde{Q}_{date}$	Mean value of the individual QCM response values at a particular day
dQ_x	Sensor response (signal height) of QCM numbered x
$d\overline{Q}_x$	Mean value of individual QCM responses
$rd\overline{Q}_x$	Relative QCM responses at a particular day
R	Regression coefficient
R	Gas constant
R_x	Feature of sensor x upon exposure to a re-calibration sample

ΔR	Difference of regression coefficients
ρ_{poly}	Density of polymer
$r_{xy}(\tau)$	Cross-correlation coefficient of two sensors x and y at a time lag τ
$r_{yy}(\tau)$	Autocorrelation coefficient of a sensor y at a time lag τ
S_a	Swelling coefficient
$S_{measured}$	Observed sensor signal
S_{truth}	"True" sensor signal
S_x	Metal oxide sensor numbered x
$d\tilde{S}_{date}$	Mean value of the individual MOX response values at a particular day
dS_x	Sensor response (signal height) of MOX numbered x
$d\bar{S}_x$	Mean value of individual MOX responses
$rd\bar{S}_x$	Relative MOX responses at a particular day

T, U, V

T	Temperature [K]
τ	Time lag
θ	Contact angle [°]
ΔU_{thermo}	Thermovoltage
V_{eff}	Volume fraction
V_{poly}	Polymer volume

X, Y

X	Matrix containing sensor response information
$\hat{y}_i$	Predicted value
y_i	Measured ("true") value

PUBLICATIONS

Parts of this work have been previously published or presented.

Full papers

- M. Frank, T. Hermle, H. Ulmer, J. Mitrovics, U. Weimar, W. Göpel, Quality tests of electronic noses: the influence of sample dilution and sensor drifts on the pattern recognition for selected case studies, Sens. Actuators B 65 (2000) 88-90.
- M. Frank, H. Ulmer, J. Ruiz, P. Visani, U. Weimar, Complementary analytical measurements based upon gas chromatography-mass spectrometry, sensor system and human sensory panel: a case study dealing with packaging materials, Anal. Chim. Acta 431 (2001) 11-29.
- S. Montag, M. Frank, H. Ulmer, D. Wernet, W. Göpel, H.-G. Rammensee, "Electronic nose" detects major histocompatibility complex-dependent pre- and postrenal odor components, submitted to PNAS.

Posters and Presentations

- M. Frank, U. Weimar, W. Göpel, Rancidity investigations on edible oils: a comparison of headspace analysis using an electronic nose and gas chromatography / mass spectrometry (GC/MS), Presentation at the 5th International Symposium on Olfaction and Electronic Nose (ISOEN 98), September 27-30, 1998, Baltimore, USA.
- M. Frank, U. Weimar, J. Ruiz, P. Visani, W. Göpel, Application of a hybrid modular sensor system for the quality control of packaging materials, Presentation at the 9th International Trade Fair and Conference on Sensors, Transducers & Systems (Sensor 99), May 18-20, 1999, Nuremberg, Germany, Conf. Proc. Vol. 1, pp. 497-501.
- R. Emele, M. Frank, U. Weimar, W. Göpel, Determination of low off-odour compound concentrations using sensor arrays and a purge & trap unit, Poster at the 9th International Trade Fair and Conference on Sensors, Transducers & Systems (Sensor 99), May 18-20, 1999, Nuremberg, Germany, Conf. Proc. Vol. 2, pp. 605-609.
- M. Frank, Modular sensor systems in the food industry: Recent case studies including comparative chemistry approaches, Presentation at the conference on developments in electronic noses, December 1, 1999, Leatherhead, UK.

- M. Frank, U. Weimar, J. Ruiz, P. Visani, W. Göpel, Application of a hybrid modular sensor system for the quality control of packaging materials, Poster at the 4. Dresdner Sensor-Symposium, December 6-8, 1999, Dresden, Germany, Book of abstracts, pp. 73-74.
- M. Frank, S. Hahn, P. Visani, N. Bârsan, U. Weimar, Long-term investigations on sensor arrays: The necessity for re-calibration, Presentation at the 7th International Symposium on Olfaction and Electronic Nose (ISOEN 2000), July 20-24, 2000, Brighton, UK.
- S. Hahn, M. Frank, U. Weimar, Rancidity investigation on olive oil: A comparison of multiple headspace analysis using an electronic nose and GC/MS, Presentation at the 7th International Symposium on Olfaction and Electronic Nose (ISOEN 2000), July 20-24, 2000, Brighton, UK.
- S. Montag, M. Frank, H. Ulmer, D. Wernet, H.-G. Rammensee, Detection of MHC-dependent odor components, Poster at the 7th International Symposium on Olfaction and Electronic Nose (ISOEN 2000), July 20-24, 2000, Brighton, UK.
- H. Ulmer, J. Mitrovics, M. Frank, U. Weimar, Electronic noses in the food industry: Possibilities and Limitations, Presentation at the Fraunhofer IPA Technologie-Forum F 59, November 8, 2000, Stuttgart, Germany, Book of abstracts, pp. 47-54.
- M. Frank, J. Claußen, N. Kerness, S. Raible, C. Hagleitner, U. Weimar, H. Baltes, New coating procedure for CMOS chemical microsensors, Poster at the 8th International Symposium on Olfaction and Electronic Nose (ISOEN 2001), March 25-30, 2001, Washington D.C., USA.

ACKNOWLEDGEMENTS

First of all it is a pleasure to thank Prof. Dr. Drs. h.c. Wolfgang Göpel for giving me the great opportunity to do a Ph.D. at the Institute of Physical and Theoretical Chemistry (IPC) at the University of Tübingen. The professional environment and the enthusiastic ambience maintained in his research group, was the basis of making this work possible. He motivated and encouraged me at any stage of my thesis and all the work performed in "related topics". This thesis is a tribute to Wolfgang Göpel who made Tübingen to a central point in the research fields of chemical sensors and "electronic noses".

I would like to thank Prof. Dr. Christiane Ziegler for her spontaneous readiness to continue as my advisor after the accidental death of Prof. Göpel. As my examiner she provided many suggestions to improve the quality of this thesis and assisted whenever needed.

I wish to thank Prof. Dr. Henry Baltes from the ETH Zurich for his willingness to serve as a co-examiner for this thesis and for the possibility to use the technical equipment of his research group. I took much pleasure in all the KÖRBER-project meetings and the common conference dinners with discussions on all "non-chemical-sensor topics".

My greatest thanks go to Dr. Udo Weimar. He is in fact *the* leading head of the "chemical sensor group" who spends almost all his energy in keeping the things running. For me, Udo Weimar personifies most of the support, guidance and advice throughout all our common work. He is a big motivator and he always put me back on track if something went in the wrong direction. Furthermore, I would like to thank him for his critical proof-reading of this thesis. Being part of one of his "Jungs" was a great pleasure.

A big "thank you" goes to Dr. Nicolae Bârsan and Dr. Stefan Raible for contributing new ideas, improvements and fruitful discussions within the sensor coating business; both proved to be really excellent colleagues.

I am deeply indebted to all my colleagues of the "Weimar group" for their help, the lively discussions (not only on scientific subjects) and all the fun we had together. In particular, I would like to thank my office mate Christopher Fietzek for sharing the pleasant times in the lab; our chats spanned the whole range of our daily lives.
The same holds for Stefan Strathmann ("Mr. NOSE") with whom I participated in many conferences, schools and trade fairs. His bohemian character I enjoyed very much.

LISTE DER AKADEMISCHEN LEHRER

Meine akademischen Lehrer waren:

K. Albert, J.-M. Basset, E. Bayer, M. Brendle, D. Christen, H. Eckstein, G. Gauglitz, W. Göpel, G. Häfelinger, H.P. Hagenmaier, M. Hanack, D. Hoffmann, V. Hoffmann, G. Jung, S. Kemmler-Sack, W. Koch, B. Koppenhöfer, D. Krug, N. Kuhn, E. Lindner, H. Mayer, H.-J. Meyer, H. Mongeot, U. Nagel, W. Nakel, H. Oberhammer, D. Oelkrug, H. Pauschmann, G. Pausewang, H. Pommer, G. Reinhardt, K.-D. Schierbaum, V. Schurig, E. Schweda, F.F. Seelig, H.-U. Siehl, B. Speiser, H. Stegmann, J. Strähle, W. Voelter, H.-D. Wiemhöfer, K.-P. Zeller, C. Ziegler.

CURRICULUM VITAE

Michael Frank

Born January 27, 1972, in Göppingen, Germany

Citizen of Germany

07/1998 - present	Work on Ph.D. thesis and related topics at the Institute of Physical and Theoretical Chemistry at the University of Tübingen, directed by Prof. W. Göpel and Prof. C. Ziegler, Title: "Multi-Sensor Systems for VOC: Recalibration and Coating Procedures"
07/1998	Diploma in Chemistry at the University of Tübingen
12/1997 – 06/1998	Work on diploma thesis directed by Prof. W. Göpel, Title: "Vergleichende Messungen an Lebensmittel-proben mit Verfahren der Analytischen Chemie und der Gassensorik"
09/1995 – 04/1996	Stay abroad at the University Claude Bernard de Lyon, France, Laboratoire des Multimatériaux et Interfaces directed by Prof. H. Mongeot and at the Ecole Supérieure Chimie, Eléctronique, Physique de Lyon, Laboratoire de Chimie Organométallique de Surface, directed by Prof. J.-M. Basset
10/1994	Vordiplom in Chemistry
10/1992 – 07/1998	Student of Chemistry at the University of Tübingen
09/1991 – 10/1992	Alternative civilian service at the intensive-care unit of the Klinik am Eichert, Göppingen, Germany
06/1991	Abitur
09/1982 – 06/1991	Werner-Heisenberg-Gymnasium, Göppingen, Germany
09/1978 – 07/1982	Primary School, Dürnau, Germany

LEBENSLAUF

Michael Frank

Geboren am 27.01.1972 in Göppingen
Staatsangehörigkeit: Bundesrepublik Deutschland

Schulausbildung

09/1978 – 07/1982	Grundschule in Dürnau
09/1982 – 06/1991	Werner-Heisenberg-Gymnasium in Göppingen
06/1991	Abitur

Zivildienst

09/1991 – 10/1992	Versorgungsdienst der Intensivstation der Klinik am Eichert in Göppingen

Studium

10/1992 – 07/1998	Studium der Chemie an der Eberhard-Karls-Universität in Tübingen
10/1994	Abschluß der Diplomvorprüfungen
09/1995 – 04/1996	Auslandsaufenthalt an der Université Claude Bernard de Lyon, Frankreich, im Laboratoire des Multimatériaux et Interfaces von Prof. H. Mongeot und an der Ecole Supérieure Chimie, Eléctronique, Physique de Lyon, im Laboratoire de Chimie Organométallique de Surface, von Prof. J.-M. Basset
10/1997	Diplomhauptprüfungen
12/1997 – 06/1998	Diplomarbeit unter Anleitung von Prof. W. Göpel mit dem Titel: „Vergleichende Messungen an Lebensmittelproben mit Verfahren der Analytischen Chemie und der Gassensorik"

Promotion

Seit 07/1998	Wissenschaftlicher Angestellter am Institut für Physikalische und Theoretische Chemie und Anfertigung der Dissertation unter Anleitung von Prof. W. Göpel und Prof. C. Ziegler mit dem Titel: „Multi-Sensor Systems for VOC: Recalibration and Coating Procedures", „Multisensorsysteme für VOC: Rekalibrierung und Beschichtungstechniken"